AN EVALUATION OF REANALYSIS PRODUCTS FOR ALASKA TO FACILITATE CLIMATE IMPACT STUDIES

By

Rick T. Lader

RECOMMENDED:

_____
Dr. John E. Walsh

_____
Dr. Igor V. Polyakov

_____
Dr. T. Scott Rupp

_____
Dr. Uma S. Bhatt
Advisory Committee Chair

_____
Dr. Uma S. Bhatt, Chair
Department of Atmospheric Sciences

APPROVED:

_____
Dr. Paul W. Layer
Dean, College of Natural Science and Mathematics

_____
Dr. John C. Eichelberger
Dean of the Graduate School

_____
Date

AN EVALUATION OF REANALYSIS PRODUCTS FOR ALASKA TO FACILITATE CLIMATE IMPACT STUDIES

A

THESIS

Presented to the Faculty

of the University of Alaska Fairbanks

in Partial Fulfillment of the Requirements

for the Degree of

MASTER OF SCIENCE

By

Rick T. Lader, B.S.

Fairbanks, Alaska

August 2014

Abstract

Alaska is experiencing effects of global climate change due, in large part, to the positive feedback mechanisms associated with polar amplification. The major risk factors include loss of sea ice, glaciers, thawing permafrost, increased wildfires, and ocean acidification. Reanalyses, which are weather forecast models that assimilate observations, are integral to understanding mechanisms of Alaska's past climate and to help calibrate future modeling efforts. This study evaluates five reanalyses using monthly gridded datasets of temperature, precipitation, and snow-water equivalent, as well as daily station data of maximum and minimum temperature, precipitation, and snow depth across six climate regions in Alaska, and at eight stations from 1979-2009. The reanalyses evaluated in this study include the: NCEP-NCAR Reanalysis (NCEP-R1), North American Regional Reanalysis (NARR), Climate Forecast System Reanalysis (CFSR), ERA-Interim, and Modern-Era Retrospective Analysis for Research and Applications (MERRA). MERRA was the top-performing reanalysis for the station-based assessment, has the lowest statewide precipitation bias, and is the most reliable model for snow-water equivalent. NARR and ERA-Interim have the lowest near-surface air temperature biases across Alaska. The quality of reanalysis data varies by region, season, and variable. This thesis provides guidance for reanalysis users to make informed decisions.

Table of Contents

List of Figures

List of Tables

Acknowledgments

There are many people to thank for their contributions to this project. I would like to begin with my advisor, Uma Bhatt, for her guidance, perspective, and countless hours spent providing comments and recommendations. Thank you to my committee members, John Walsh, Scott Rupp, and Igor Polyakov for their support, suggestions, and expert knowledge. Thank you to the faculty in the Department of Atmospheric Sciences at UAF, Nicole Molders, Ken Sassen, Xiangdong Zhang, Bill Simpson, and Javier Fochesatto for providing me with different insights on how the reanalysis products can be used. Thank you to Rick Thoman at the National Weather Service Office in Fairbanks for his perspective from an operational standpoint, and to Barbara Day for making sure I completed all of my necessary paperwork on time.

This work was made possible through financial support from the Alaska Climate Science Center, funded by Cooperative Agreement Number G10AC00588 from the United States Geological Survey. Its contents are solely the responsibility of the author and do not necessarily represent the official views of the USGS. This includes support to present a poster, "A comparison of reanalysis products for Alaska to facilitate impact studies" at the 4th World Climate Research Programme International Conference on Reanalyses, held from 7-11 May 2012 in Silver Spring, Maryland. More recently, support was provided to present a poster, "Evaluating daily reanalysis temperature and precipitation for Alaska" at an Extreme Temperature and Precipitation Workshop, held in Berkeley, California from 20-23 August 2013.

This project could not have been completed without the support from my friends and fellow students, Greg Deemer, Erin Gleason, Peter Bieniek, David Fee, Taryn Lopez, Derek Starkenburg, Mike Madden, and Mike Pirhalla for entertaining conversation, collaboration, and the opportunity to step away from the desk from time to time. Thank you to my parents for

supporting me from day one and for the many phone conversations I have had with them since moving across the continent. Thank you to John Burr and Ruth Gronquist for their advice and sense of humor that is second to none. I also want to thank their flat-coated retriever, Mojo Sam, for giving me daily reminders that the most important thing to do is to start each day with a good breakfast, preferably at 5 am, but no later than 6:30 am. Lastly, I thank Erika Burr for her companionship and a listening ear at the end of each day.

Chapter 1 Alaska's climate and modeling needs

1.1 Alaska's changing climate

Alaska is at the forefront of global climate change. Alaska has warmed more, and is warming at a faster rate than any other region in the United States because of its Arctic location. In the past 60 years, the average annual surface air temperature in Alaska has warmed 1.7˚C (3°F) and temperatures are projected to increase by as much as 5.6˚C (10˚F) by the end of the 21st century (Chapin et al. 2014). This enhanced warming relative to the rest of the globe has been coined 'polar amplification' and it is characterized by positive feedback mechanisms in the climate system (Bekryaev et al. 2010). The most common of these is the ice-albedo feedback, which shows that reduced ice leads to increased solar absorption at the surface, higher temperatures, and finally, more melting of ice.

Climate change in Alaska centers on rapid loss of sea ice, glacial ice, thawing permafrost, increased wildfires, and ocean acidification. There are numerous interactions that will occur due to these contributing factors, but perhaps the most important effect is that of global sea level rise. Coastal Alaska communities are already being forced to adapt to the effects of rising sea levels (Fig. 1.1.1), and this is projected to be a common theme among more southerly latitudes with time, which will include major metropolitan centers. The future is not wholly bleak, however, because the web of interactions will undoubtedly promote new areas of growth. For example, based on air temperatures in Fairbanks there has been a 45% increase in growing season length since the beginning of the last century (Wendler and Shulski 2009), but this increase is substantially smaller for Interior Alaska based on multiple climate stations due to micrometeorological variations. Future climate projections suggest that the growing season length will increase over the next century (Chapin et al. 2014).

FIG. 1.1.1 One effect of the reduction in Alaska sea ice is that storm surges that used to be buffered by the ice are now causing more shoreline damage. Photos show infrastructure damage from coastal erosion in Tuntuliak (top) and Shishmaref, Alaska (bottom). (Photo credits: (top) Alaska Department of Environmental Conservation; (bottom) Ned Rozell).

With the magnitude of change that is occurring and is expected to occur, it is necessary to model past and future climate scenarios with the best observational data available. For Alaska, this is problematic. There are only 20 first-order surface weather stations that are routinely maintained by National Weather Service personnel across the entire state (Fig. 1.1.2). There are many other cooperative stations, but these are typically insufficient for climate research because of a too-short time record, or incompleteness. Of the 'usable data', much of it can be unreliable. A large percentage of the precipitation that falls across Alaska is snow, which is difficult to

measure accurately, particularly in windy conditions (Yang et al. 1998). Satellite data has greatly enriched Alaska's observational archive, but even satellites often have problems because of Alaska's high latitude. Niu and Pinker (2011) found a mismatch between satellite-based measurements of surface shortwave radiation compared to ground observations, which was attributed to melting of snow and ice and low solar elevations. This data insufficiency necessitates the need for reliable climate modeling and simulation based on the limited data that Alaska has.

Reanalysis models help to bridge this data gap. Reanalysis is a type of weather forecasting that produces high-spatiotemporal gridded meteorological data by assimilating past observations into a physically consistent forecast model. Each analysis cycle begins by using the previous forecast as a background field or 'first guess'. The background field is then interpolated to the location of an assimilated observation and the difference between this estimate and the value of the observation is the analysis increment (Kalnay 2003). The analysis increment is added onto the background field with appropriate weighting measures and a new analysis is produced. The reanalysis output is primarily used for 1) climate studies, and 2) providing initial states and boundary conditions for regional downscaling and other types of modeling.

The model physics of reanalyses are held constant to try and avoid artificial climate trends. Yet because the observing systems used in the data assimilation change with time, these false climate shifts still occur. For example, the advent of the modern satellite era in 1979 represents a major change in data assimilation. Prior to this, mainly surface data, and vertical soundings from a limited number of stations were used to help construct the analysis. Afterwards the data assimilation was able to capture a global snapshot of the atmosphere within each new cycle. For this reason, it is generally not good practice to use reanalysis data to detect climate

trends. However, one way to make trend analysis more feasible is to check the reanalysis output with and without a new observing system (Bengtsson et al. 2004). A complete description of the reanalyses used for this study follows in Chapter 2.

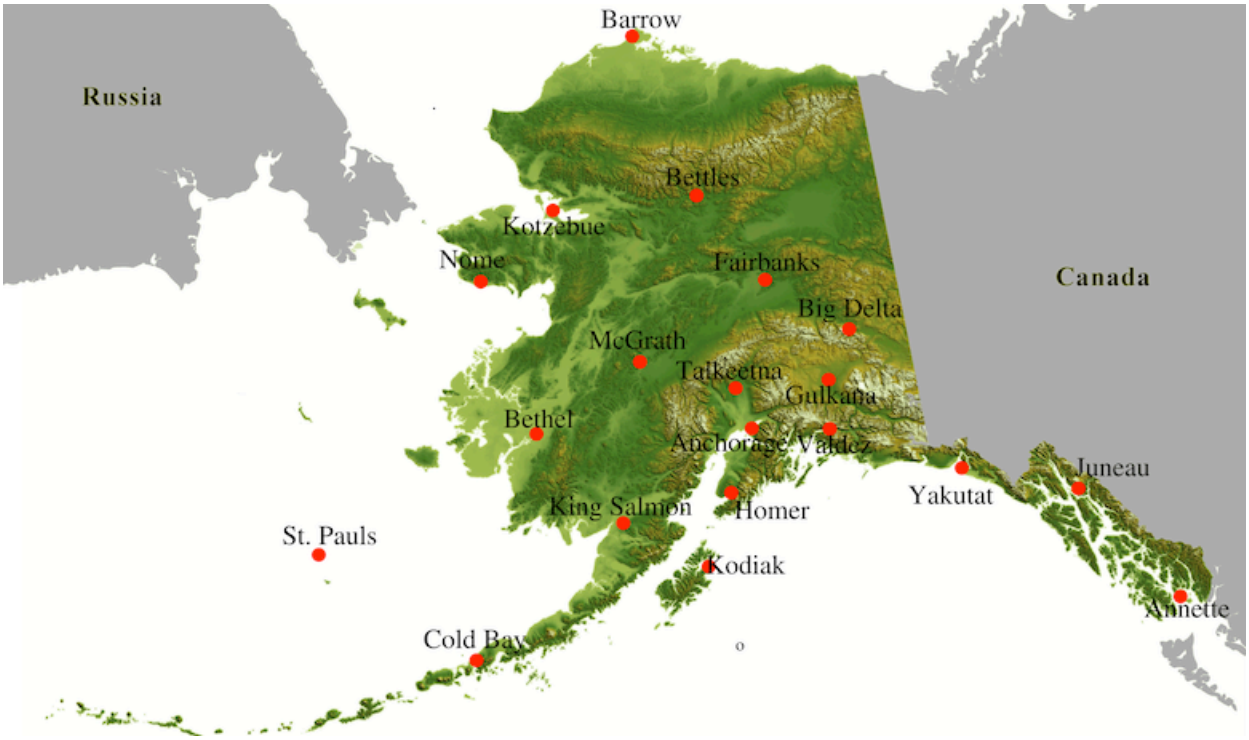

FIG. 1.1.2 Station map of the 20 first-order weather stations in Alaska (Image credit: Alaska Climate Research Center).

1.2 Previous usage of reanalysis for Alaska

A primary example illustrating the use of reanalysis datasets is in investigations of global teleconnection patterns. The Pacific Decadal Oscillation (PDO) is a key driver of Alaska's climate variability and is characterized by sea surface temperature (SST) anomalies in the North Pacific. The warm phase of the PDO is associated with higher than normal SSTs in the Gulf of Alaska, causing above-normal precipitation along the southern coast, but below-normal precipitation for the mountain-blocked interior (Mantua et al. 1997). Mills and Walsh (2013)

used pressure and temperature data from the National Centers for Environmental Prediction-National Center for Atmospheric Research (NCEP-NCAR) reanalysis (Kalnay et al. 1996) to link the PDO with downstream atmospheric signals for North America. Other Alaska-relevant studies have used NCEP-NCAR reanalysis data to study the impacts of the Aleutian Low (Rodionov et al. 2005; Pickart et al. 2009; Shulski et al. 2010), and El Niño (Bieniek et al. 2011).

Reanalysis provides initial and boundary conditions to help drive regional forecast models. Francis and Atkinson (2012) initialized a wave model in the southeast Chukchi Sea with data from the North American Regional Reanalysis (NARR) (Mesinger et al. 2006). This study documented the synoptic conditions necessary for significant wave heights to occur and stressed the potential impact that rapidly decreasing sea ice could have on coastal erosion and inland flooding. The sea ice can act as a buffer that tends to dampen waves. In a separate but related study, NARR was used to develop a wind-field climatology and an understanding of extreme wind events in the Chukchi-Beaufort Sea region (Stegall and Zhang 2012).

Mernild et al. (2014) used forcing data from the Modern-Era Retrospective Analysis for Research and Applications (MERRA) (Bosilovich et al. 2008) to show that the largest contribution to sea-level rise from melting glaciers and ice caps in the northern hemisphere (excluding Greenland) is from Alaska. Beyond the implications of sea-level rise due to glacial runoff are the impacts to Alaska's fisheries where there is a delicate biochemical balance that enables certain populations to thrive and causes others to fail.

Precipitation is projected to increase in Alaska during all seasons; however, it is possible that soil moisture will decrease due to enhanced evapotranspiration from higher temperatures and increased drainage from thawing permafrost (Chapin et al. 2014). Drier landscapes will promote changing wildfire patterns that pose challenges for terrestrial ecosystems and human health.

Rupp et al. (2007) simulated boreal fire dynamics using multiple datasets, including the NCEP-R1. They found that using the reanalysis data did not allow for an accurate simulation of annual burned area because the model was too cold and wet. This finding suggests that while reanalysis datasets are extraordinarily useful in Alaska, they are also prone to error. Reanalysis estimates are not equal to observations and an understanding of how these models operate is necessary.

1.3 Project goals

Alaska is the most data-sparse region in the United States, yet is dealing with the largest impacts from climate change. Reanalyses provide an invaluable service to the climate community; however, each model has its own strengths and weaknesses. The relatively low amount of data that is assimilated into the reanalyses at far northern latitudes makes the output datasets more dependent on the background forecast model. An understanding of each reanalysis – the data assimilation, the forecast model, and the changes to the observing systems involved – is essential prior to selecting the best available dataset for an end user's application.

To address these needs, this study evaluates essential meteorological variables from five reanalyses for Alaska on both daily and monthly scales over a 31-year period from 1979-2009. These include: 2-m air temperature (monthly mean (T2M), daily maximum (T_{max}) and daily minimum (T_{min})), precipitation (PRCP) (monthly and daily), snow-water equivalent (SWE) (monthly), and snow depth (SNDP) (daily). Descriptions of all meteorological surface observations (Section 2.1), reanalyses used (Section 2.2), and known data quality issues that relate to these variables (Section 2.3) are described in Chapter 2.

Statewide maps of reanalysis model bias, and standard deviation (Std. Dev.) for the monthly data follow in Chapter 3. These maps of T2M (Section 3.3), PRCP (Section 3.4), and

SWE (Section 3.5) are presented in seasonal form. It is important to note that the standard seasons have been adjusted to the following: winter (November-March), spring (April-May), summer (June-August), and autumn (September-October). Each variable subsection concludes with a statistical table that quantifies model mean, bias, and standard deviation across six climate zones in Alaska.

An evaluation of daily time series of maximum temperature, minimum temperature, precipitation, and snow depth at eight stations across Alaska follows in Chapter 4. These include: Barrow (PABE) (Section 4.2), Nome (PAOM) (Section 4.3), Bethel (PABE) (Section 4.4), McGrath (PAMC) (Section 4.5), Fairbanks (PAFA) (Section 4.6), King Salmon (PAKN) (Section 4.7), Anchorage (PANC) (Section 4.8), and Juneau (PAJN) (Section 4.9). Each section includes figures of the daily-averaged annual cycle, standard deviation, bias, and root-mean-square error (RMSE) for all four variables. These are followed by climate extreme indices of Annual Extreme Warm Days, Annual Extreme Cold Days, Annual Extreme Precipitation Days, and Growing Season Length with appropriate threshold values indicated. The entire time series for each variable is included next to assist data users that are only interested in a segment of the 31 years used in this study.

Chapter 5 begins with a synthesis of the key results (Section 5.1), and follows with user guidance in the form of frequently asked questions (FAQs) (Section 5.2). Information on how to access the daily and monthly time series that were used to construct each of the figures is provided along with a description of the data format (Section 5.3). This study concludes with a brief summary in Chapter 6.

Chapter 2 Meteorological surface observations and reanalysis data

2.1 Meteorological surface observations

2.1.1 Surface data

Station data for the eight Alaska locations analyzed in this study (Sections 4.2-4.9) comes from the National Climatic Data Center (NCDC) Global Surface Summary of Day (GSOD) product. The GSOD reports daily data according to Greenwich Mean Time (GMT, 0000Z – 2359Z), which is temporally consistent with the reanalysis output. In contrast, the Global Historical Climatology Network (GHCN) station data are reported from local midnight to midnight. It was found that there is a notable difference when computing daily and monthly statistics while using GSOD data as opposed to local midnight-to-midnight. Daily maximum and minimum temperature is provided to the nearest 0.056˚C (0.1°F), precipitation amount to the nearest 0.254 mm (0.01 in.), and snow depth to the nearest 0.254 mm (0.1 in.) A more comprehensive description of this data is available online (ftp://ftp.ncdc.noaa.gov/pub/data/gsod/readme.txt).

2.1.2 Gridded temperature and precipitation verification datasets

Hill et al. (2014) developed a high-resolution (2 km) gridded dataset of monthly 2-m air temperature and precipitation that encompasses all of Alaska from 1961-2009. They acquired station data from 150 sites for temperature and 200 sites for precipitation and applied a Delta downscaling method (Hayhoe 2010) to create their gridded fields. The temperature anomaly field was interpolated and then combined with climatology, which was based on the Precipitation-elevations Regressions on Independent Slopes Model (PRISM) data (Daly et al. 1994). Rather than using absolute anomalies for precipitation, they computed proportional anomalies relative to

the PRISM climatology to avoid negative precipitation values. In this study, the temperature (Section 3.3) and precipitation (Section 3.4) products of the reanalyses are compared to Hill et al. (2014) from 1979-2009.

2.1.3 Gridded snow verification dataset

Luojus et al. (2013) developed a global snow-water equivalent (SWE) dataset (GlobSnow v.2.0) with a spatial resolution of 25 km that covers the period from 1979 to present. Brightness temperatures from three satellites – Scanning Multichannel Microwave Radiometer (SMMR), Special Sensor Microwave/Imager (SSM/I), and Advanced Microwave Scanning Radiometer (AMSR-E) – are used to help construct the snow depth field, which subsequently is converted to SWE. No SWE information is provided for mountainous grid cells, which includes much of southern Alaska. In this study (Section 3.5), the SWE products of the reanalyses are compared to GlobSnow v.2.0 from 1980-2009.

2.2 Reanalysis models and topography

2.2.1 NCEP-NCAR Reanalysis

The NCEP-NCAR reanalysis (hereafter NCEP-R1) was developed in the mid-1990s to support climate studies by using a frozen state-of-the-art data assimilation, analysis and forecast system. NCEP-R1 uses a global spectral model with T62 (210 km) horizontal resolution and has 28 vertical sigma levels (Kalnay et al. 1996). Model output is available from 1948 to present at up to 6-hourly temporal resolution. Three-dimensional variational (3DVAR) data assimilation is performed using spectral statistical interpolation (SSI) (Parrish and Derber 1992) to create the analysis fields. 3DVAR assimilates only those observations that are available at an analysis time.

The 2-m temperature fields, including the monthly means, daily maxima and daily minima are considered class B variables. This classification indicates that the temperature variables are influenced both directly by assimilated observations (satellite retrievals and radiosondes) and the atmospheric model. Precipitation rate and water equivalent of accumulated snow depth are class C variables, which means that these quantities are entirely derived by the model. The class C variables are deemed less reliable because they are not constrained by observations.

2.2.2 North American Regional Reanalysis

The NCEP North American Regional Reanalysis (NARR) was developed in 2003 to improve upon the existing global reanalyses and to provide users with a more detailed and accurate land hydrology dataset over the domain of North America (Mesinger et al. 2006). NARR uses the Eta model that was operational at NCEP as of September 2000 and is coupled to the four-layer Noah land surface model (Ek et al. 2003). NARR has a spatial resolution of 32 km with 45 vertical levels and outputs variable information from 1979 to present at up to 3-hourly time intervals.

NARR does not assimilate 2-m temperature observations because these were found to fit poorly with rawinsonde data. For Canada, rain-gauge observations were assimilated to aid the precipitation analysis prior to December 2002; afterwards the hydrologic fields are entirely model derived. For Alaska, and the adjacent ocean surfaces north of 42.5°N, no precipitation observations are assimilated for the entire period. The NARR SWE product is constrained by the 47-km resolution Snow depth analysis (daily) of the U.S. Air Force Weather Agency (SNODEP) (Kopp and Kiess 1996) by considering a 5:1 snow to liquid ratio.

2.2.3 Climate Forecast System Reanalysis

NCEP released the Climate Forecast System Reanalysis (CFSR) in 2010 as an upgrade to its pre-existing global and regional reanalyses (Saha et al. 2010). In addition to its use for climate studies, the initial states of CFSR are used for sub-seasonal forecasting as part of the Climate Forecast System version 2 (CFS-2) project. CFSR uses the operational Global Forecast System (GFS) atmospheric model of 2003, with T362 (about 38 km) horizontal resolution and 64 vertical levels that are a hybrid of sigma and pressure coordinates. CFSR is coupled to ocean, land, and sea-ice models to produce globally gridded data from 1979 to present. 3DVAR data assimilation with Gridpoint Statistical Interpolation (GSI) (Kleist et al. 2009) is used for the analyses. GSI treats background errors between analyses and observations using physical space whereas SSI uses spectral space.

The 2-m temperature fields in CFSR are derived primarily from satellite radiances and radiosonde information; no station observations of 2-m temperature are assimilated. The precipitation analysis is generated using a combination of the pentad dataset of the Climate Prediction Center Merged Analysis of Precipitation (CMAP) (Xie and Arkin 1997) and the Climate Prediction Center (CPC) daily gauge analysis. However, because there are few gauge observations for Alaska, the precipitation analysis there is more heavily weighted toward the model's 6-hourly forecast field. The snow depth analyses assimilate daily SNODEP grids for the entire period and National Environmental Satellite, Data and Information Service (NESDIS) Interactive Multisensor Snow and Ice Mapping System (IMS) fields (Helfrich et al. 2007) beginning in February 1997. Reanalyzed snow depth in CFSR gets converted to SWE using a 10:1 ratio except in cases when the first-guess deviates from the analysis by a factor of 2 or more.

2.2.4 ERA-Interim Reanalysis

The ECMWF released its ERA-Interim reanalysis in 2009 to improve upon ERA-40 and set the stage for the next generation reanalysis that will encompass the entire 20th century (Dee et al. 2011). The forecast model of ERA-Interim (Integrated Forecast System (IFS) release Cy31r2) is comprised of atmosphere, ocean, and land model components, and was used operationally at the end of 2006. ERA-Interim uses a spectral T255 (79 km) model that operates with 12-hourly analysis cycles, producing gridded data from 1979 to present. ERA-Interim employs four-dimensional variational data assimilation (4DVAR), which takes into account the time of an observation that occurs within the analysis window. The forecast model makes a first-guess for each observation in 4D before it gets assimilated and appropriate quality control measures are conducted.

Synoptic land station reports of 2-m temperature are assimilated and directly influence the analysis. Precipitation is a model-derived field that combines surface observations of temperature and humidity along with radiosonde data. The land component of the forecast system produces SWE, snow density, and snow depth estimates. The final snow depth field is subsequently generated using a Cressman analysis of station snow depth and IMS snow cover.

2.2.5 Modern-Era Retrospective Analysis for Research and Applications

The National Aeronautic and Space Administration (NASA) released its Modern-Era Retrospective Analysis for Research and Applications (MERRA) in 2008, which produces meteorological data from 1979 to present (Bosilovich et al. 2008; Rienecker et al. 2011). MERRA utilizes the Goddard Earth Observing Satellite atmospheric model version 5.2.0 and data assimilation system (GEOS-5 DAS). The spatial resolution of variable output is 1/2°

latitude x 2/3° longitude (nominally 65 km) and there are 72 vertical levels. 3DVAR data assimilation is conducted using GSI, in which an Incremental Analysis Update (IAU) is applied during the correction phase of the reanalysis. This technique limits drastic changes from one analysis cycle to the next by introducing smaller updates and creates a smoother product. MERRA employs the Catchment Land Surface Model (Koster et al. 2000) and produces hourly output.

Neither 2-m temperature, nor gauge precipitation, nor snow measurements are directly assimilated into MERRA, which enables the use of these surface observations for independent validation to assess the quality of the analyzed fields. However, MERRA assimilates instantaneous SSM/I rain-rate observations.

2.2.6 Model topography

Table 2.1.1 lists the station height of the 8 locations in this study and the model height of the nearest corresponding land grid cell for each station. The model values represent an average terrain height for the land within each cell, which is generally higher than the actual stations. Figure 2.1.1 shows the model terrain height for each reanalysis. It is readily apparent how the higher resolution grids (e.g. NARR, and CFSR) are better able to resolve the mountainous regions, such as the Brooks Range and the Alaska Range.

a) NCEP-R1 topography

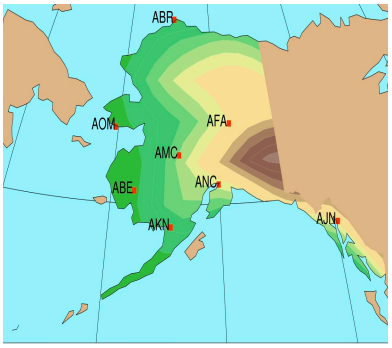

b) CFSR topography

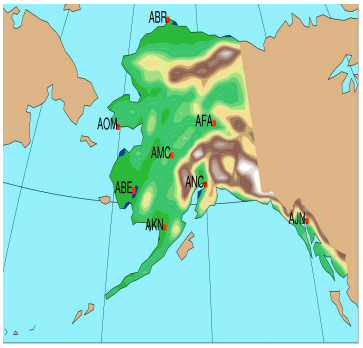

c) NARR topography

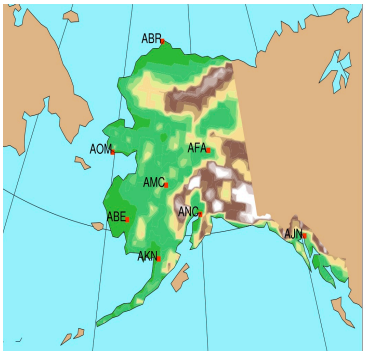

d) ERA-Interim topography

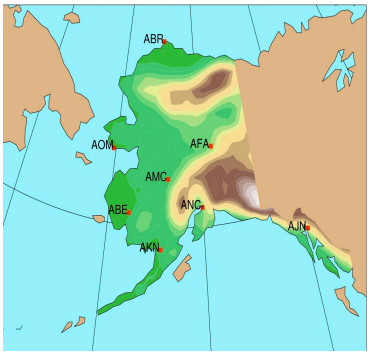

e) MERRA topography

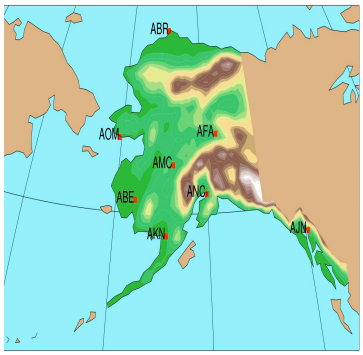

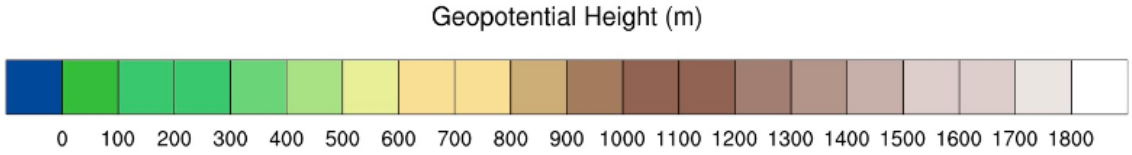

FIG. 2.1.1 Reanalysis topography with approximate spatial resolution in parentheses is a) NCEP-R1 (210 km) b) CFSR (38 km), c) NARR (32 km), d) ERA-Interim (79 km), and e) MERRA (65 km).

Table 2.1.1 Altitude (m). The altitudes for the reanalyses corresponding to the nearest land grid cell to each station (see Section 1.3 for key to station codes) used in this study.

	STATION	NCEP-R1	CFSR	NARR	ERA-I	MERRA
PABE	9	350	5	20	13	5
PAOM	4	102	235	487	43	48
PABE	31	85	15	0	49	10
PAMC	102	324	188	186	276	190
PAFA	132	571	239	186	487	316
PAKN	20	160	45	115	158	58
PANC	37	771	149	63	473	97
PAJN	5	502	464	115	249	125

2.3 Known dataset problems

A goal of atmospheric reanalysis is to produce gridded climate data using a consistent data assimilation and analysis/forecast system. In the interest of incorporating the best available datasets, however, there are inevitably false climate shifts in the time series that result from changes in the assimilated observing systems. The advancement into the modern satellite era in 1979 represents a primary example of how observing systems change with time. This problem is avoided in this study by choosing 1979-2009 as the study period. Other problems relate to intrinsic model bias, observational quality and the quality control of suspect observations.

In NCEP-R1, the snow cover mask from 1973 was used every year from 1974-1994 (Kistler et al. 2001). This undoubtedly limited the variability of various snow products in NCEP-R1. Kistler et al. (2001) also note that the atmospheric model in NCEP-R1 has a cold bias due to a radiation imbalance that reflects too much shortwave radiation back to space at the top of the atmosphere and allows too much longwave radiation to escape. This strong cold bias in NCEP-R1 stands out in a performance evaluation against five other reanalyses (Decker et al. 2012). There are also deficiencies with moisture diffusion that are present in the precipitation rate field and cause moisture convergence in high-latitude valleys, which can lead to the appearance of spectral precipitation.

NARR was originally completed at the end of 2002 and at that time it was decided that no more precipitation-gauge measurements would be assimilated over Canada as NARR continued in real time (Mesinger et al. 2006). Model precipitation in NARR is generally too high, but often gets lowered by the data assimilation (Ruane et al. 2010). This observing system change in December 2002 likely induced a spurious climate shift across Canada, and adjacent areas, such as over Alaska. More generally, because not all locations assimilate precipitation

there are nonphysical boundaries in NARR's hydrological fields. For example, NARR assimilates observations from the pentad dataset of CMAP for oceanic regions south of 42.5°N, but not to the north. There is a nonphysical boundary around this latitude as a result of assimilation blending.

CFSR has been shown to have exceptionally high precipitation values across polar regions (Cullather and Bosilovich 2011; Lindsay et al. 2014). CFSR assimilates precipitation observations, both land and satellite-based, but becomes more reliant on the model in high latitudes. All three of the next-generation global reanalyses in this study are affected by a discontinuity in 1998 with the ingest of Advanced Microwave Sounding Unit (AMSU) data. Precipitation increased following the assimilation of this new data stream.

The ERA-Interim SWE analysis is affected by permanent ice locations (e.g. alpine glaciers) because a nonphysical value of 10,000 mm is applied (Drusch et al. 2004). Additionally, the interpolation scheme causes there to be a low SWE bias in high-latitude regions where most snow depth observations are drawn from low elevation stations.

Chapter 3 A regional assessment of reanalyses for Alaska

3.1 Introduction

Atmospheric reanalysis provides an estimate of the climate that is invaluable in the observation-sparse Arctic. These datasets are among the best tools available for stakeholders that require a continuous, long time record, and robust gridded climate data. Alaska presents a modeling challenge; however, not only because of its high latitude, but also due to its topography. Two major mountain ranges – the Brooks Range, and the Alaska Range – are key features in determining Alaska's climate. Global and regional reanalyses have very coarse resolution (10s to 100s of kilometers) with respect to the elevation gradients that characterize these mountain ranges. Alaska also has over 6000 miles of shoreline that undergoes phase changes from ice to water and back as part of the seasonal cycle. Southeast Alaska is comprised of glaciers that are sub-grid scale in the reanalyses. Because of these challenges, it is necessary to conduct a careful evaluation of the reanalysis products across Alaska so users can make informed choices, particularly in data-void areas.

3.2 Methods

3.2.1 Climate divisions

Reanalysis products are compared quantitatively by partitioning the data according to Alaska climate divisions. Bieniek et al. (2012) used a cluster analysis to develop 13 climate divisions for Alaska (Fig. 3.2.1) that exhibit similar patterns of near-surface air temperature variability. These regions represent a logical and concise way to study the reanalysis products across a state with climate regimes as diverse as Alaska. Several of these divisions have been combined due to data considerations in the southern part of the state. The Central Interior,

Northeast Interior, and Southeast Interior together now make up the Interior. Bristol Bay and the Aleutians together are considered Bristol Bay. Five divisions in southern Alaska – the Northwest Gulf, Northeast Gulf, North Panhandle, Central Panhandle, and South Panhandle – were combined to form the Southeast. The North Slope, West Coast, and Cook Inlet divisions remain unchanged.

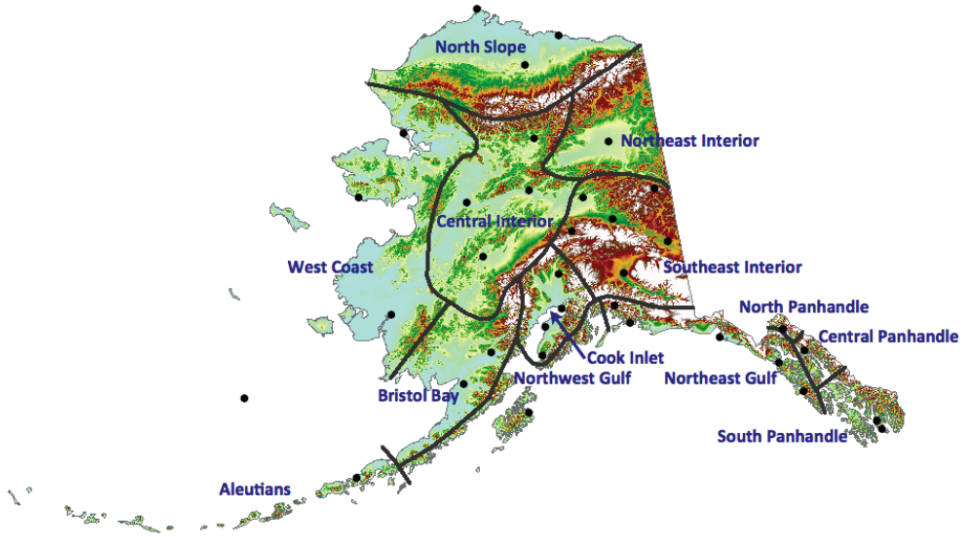

FIG. 3.2.1 Alaska climate divisions (from Bieniek et al. 2012) were calculated using cluster analysis on the meteorological stations identified in the map with black dots.

3.2.2 Reanalysis data preparation

The subsequent sections in this chapter include a comparison between monthly reanalysis products and observations of near-surface air temperature (T2M) (Section 3.3), precipitation (PRCP) (Section 3.4), and snow-water equivalent (SWE) (Section 3.5). In each section, the datasets have been re-gridded to a common 0.5˚ x 0.5˚ resolution to facilitate a direct grid-to-grid comparison. Re-gridding was done using bilinear interpolation for the rectilinear grids (NCEP-R1, CFSR, ERA-Interim, and MERRA). For NARR and the observational datasets, the 'triple2grid' function from the NCAR Command Language (NCL) was used. This function uses

a nearest-neighbor approach to spread the original data onto a rectilinear grid. Acceptable observations for this re-gridding were limited to a distance of 50 km from the new coordinates. It is possible that cells that were originally over water have affected the re-gridded coastline.

For each variable there is a six-map set of anomalies for each season followed by an analogous set for observed and modeled standard deviation. Canada and the waters adjacent to Alaska have been masked out of these figures. The seasons used are tailored for Alaska and do not follow the traditional meteorological seasons. Winter is considered as November-March; spring is April-May; summer is June-August; autumn is September-October (R. Thoman 2014, personal communication). At the end of each section is a table that provides the area-averaged mean, bias, and standard deviation for the six climate divisions employed in this study. Bias and standard deviation are computed relative to the monthly mean from the 31 yearly values. Monthly mean values are averaged to construct the seasonal values. Refer to Table 3.3.1 for regional climate statistics of 2-m temperature; Table 3.4.1 for precipitation; Table 3.5.1 for SWE. Values from the tables are used to support statements from the comparison of the spatial maps.

3.3 Comparison of reanalysis products to observed near-surface air temperatures

3.3.1 Temperature verification dataset

Hill et al. (2014) developed a high-resolution (2-km) gridded dataset of monthly 2-m air temperature that encompasses all of Alaska from 1961-2009. They acquired station data from 150 Alaskan sites and applied a Delta downscaling method (Hayhoe 2010) to create their gridded fields. In this case, the temperature anomaly field was interpolated and then combined with climatology, which was based on PRISM data (Daly et al., 1994). In this study, the 2-m air temperature products of the reanalyses are compared to Hill et al. (2014) from 1979-2009. This

data provides the most independent view of gridded temperature data for Alaska, since 2-m air temperature is usually not assimilated in the reanalysis models.

3.3.2 Near-surface air temperatures

Climatology in winter and spring in Alaska is characterized by a north-to-south temperature gradient where the Southeast is the warmest and the North Slope is the coolest part of the state (Fig. 3.3.1a,g). In summer the continental Interior has the warmest temperatures, but the latitudinal temperature gradient returns during autumn (Fig. 3.3.2a,g).

ERA-Interim has the lowest statewide bias, but NARR performs comparably well. All of the reanalyses considered estimate 2-m air temperature by interpolating between the surface and the lowest model level, except for ERA-Interim, which assimilates observations. The models have a large cold bias in the Interior during winter and spring. NCEP-R1 has a cold bias that approaches 5.0˚C in the Interior and is routinely greater than 2.0˚C throughout Alaska (Table 3.3.1). MERRA has a warm bias above 2.0˚C on the North Slope during spring that continues into summer but is of a lesser magnitude. The models generally show a warm bias along coastal locations, and the North Slope, while being too cold across the Interior. Bias estimates right along the coast are less reliable however, because maritime grid cells likely affected the re-gridding of Hill et al. (2014).

The highest variability of near-surface air temperatures in Alaska occurs during winter; in the Interior at this time, the standard deviation of 2-m temperature is around 4˚C (Fig. 3.3.3a). In spring (Fig. 3.3.3g), the variability decreases except for on the North Slope, which remains snow covered. The least variable time of year is in summer when the standard deviation falls to around

1˚C statewide (Fig. 3.3.4a). With the return of darkness and snow in autumn, the variability increases once again (Fig. 3.3.4g).

The four highest resolution models – NARR, CFSR, ERA-Interim, and MERRA – have similar standard deviations to Hill et al. (2014). NCEP-R1 shows much too high standard deviation values during summer and autumn. There is a tendency for the models to overestimate the variability during summer, but underestimate it in winter and spring. This is especially true for the southern half of Alaska. On the North Slope, the models routinely overestimate the standard deviation of 2-m temperature, regardless of season.

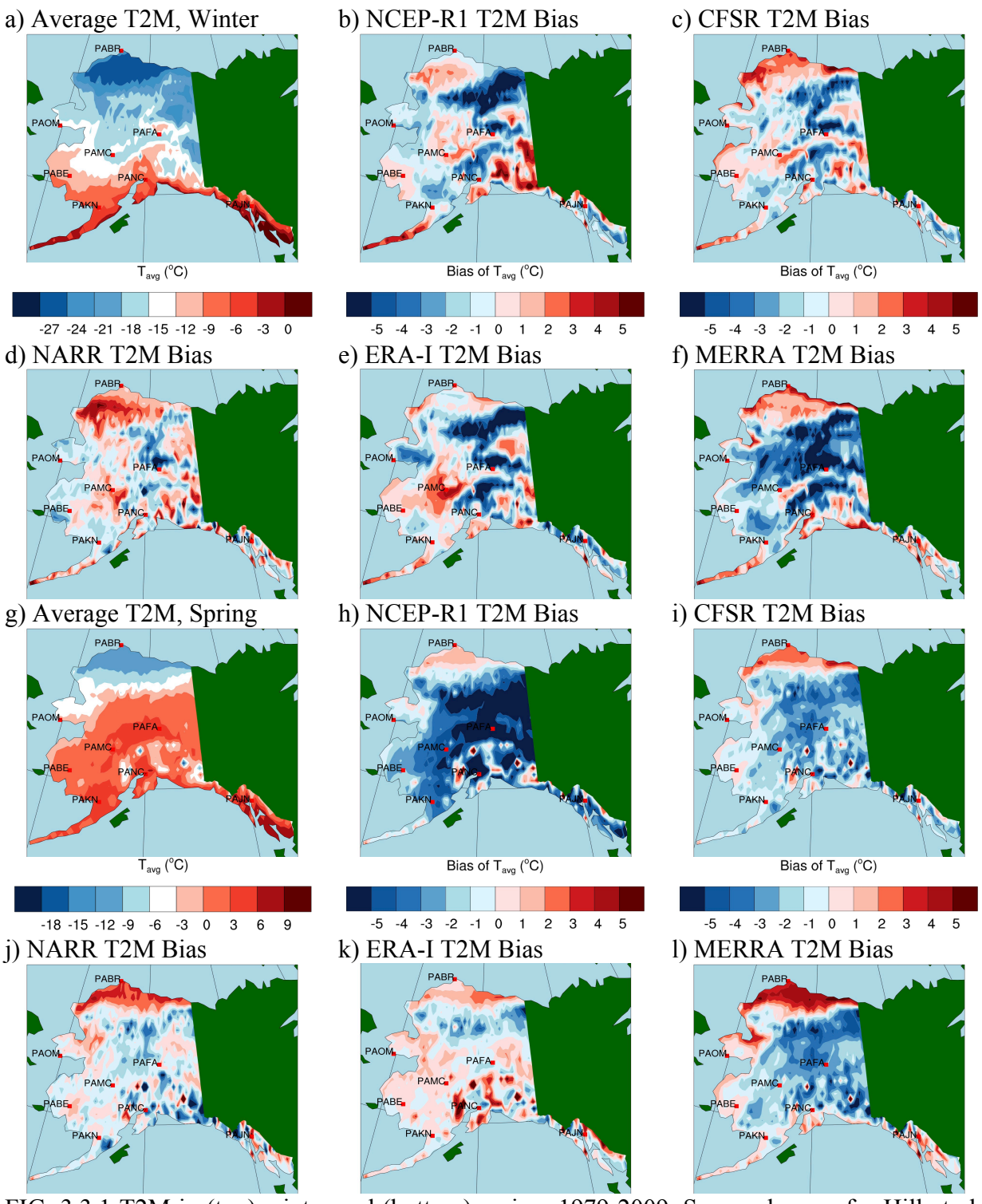

FIG. 3.3.1 T2M in (top) winter and (bottom) spring, 1979-2009. Seasonal mean for Hill et al. (2014) is in the top left (a,g), followed by model bias (b-f, h-l).

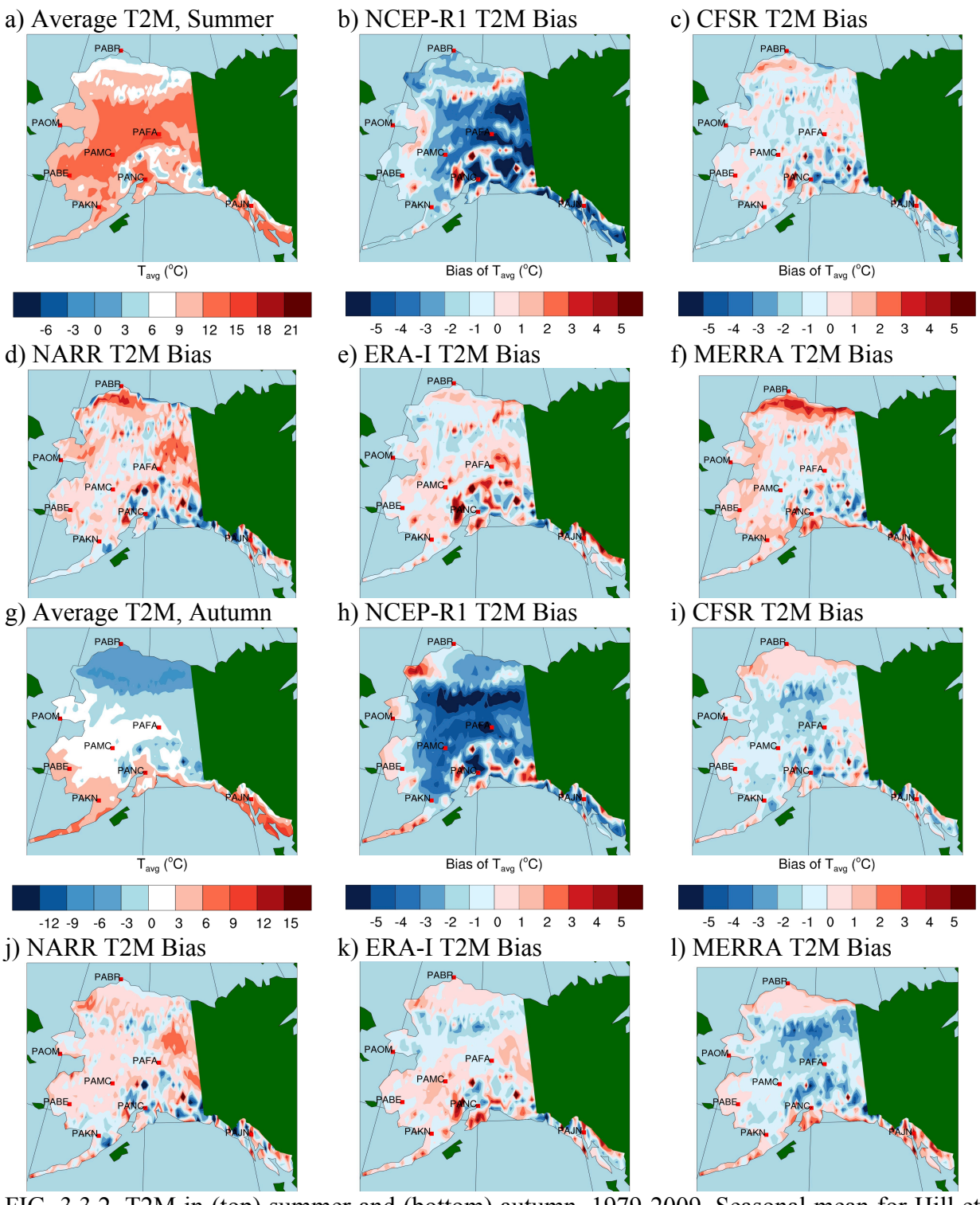

FIG. 3.3.2. T2M in (top) summer and (bottom) autumn, 1979-2009. Seasonal mean for Hill et al. (2014) is in the top left (a,g), followed by model bias (b-f, h-l).

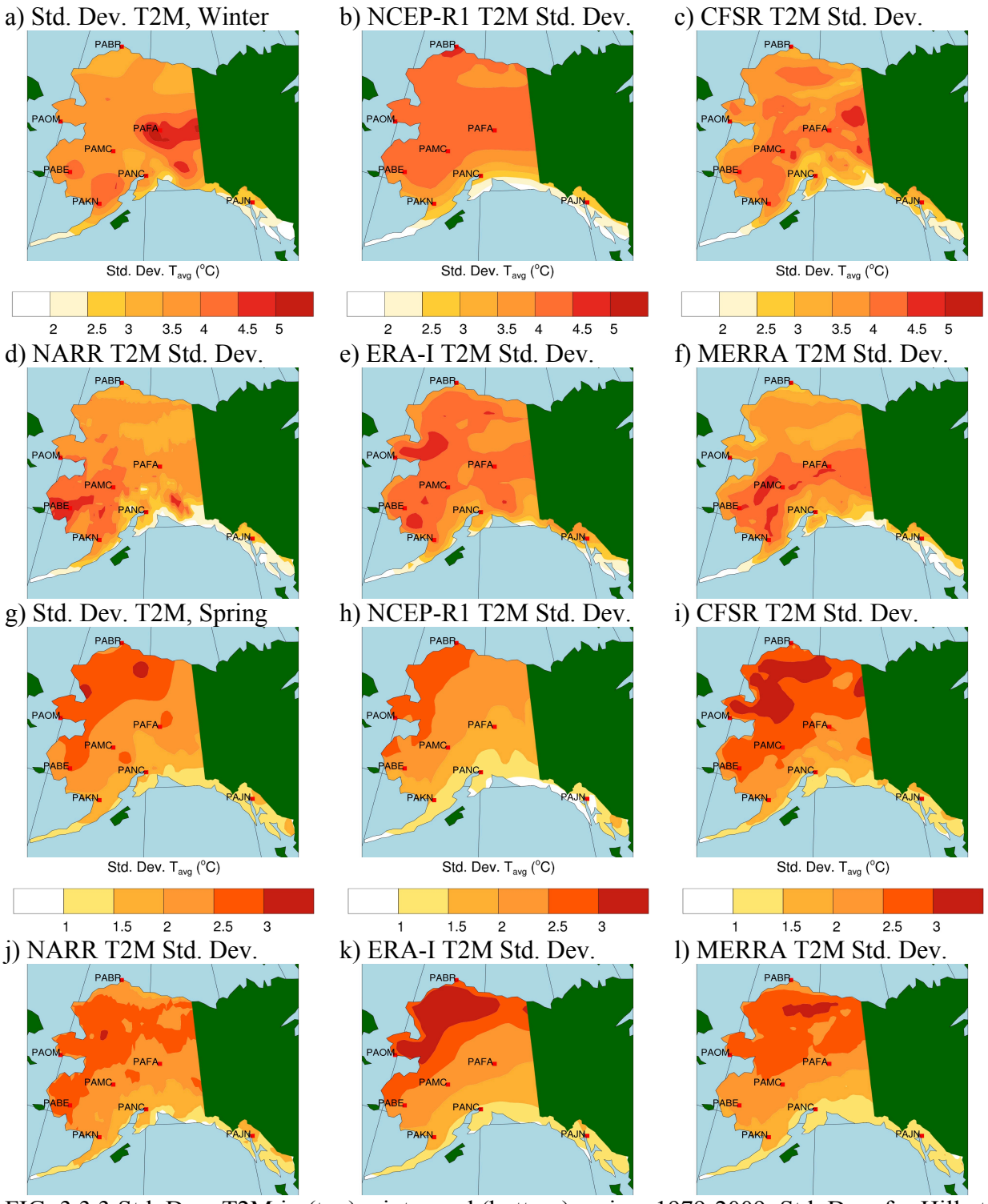

FIG. 3.3.3 Std. Dev. T2M in (top) winter and (bottom) spring, 1979-2009. Std. Dev. for Hill et al. (2014) is in the top left (a,g), followed by model Std. Dev. (b-f, h-l).

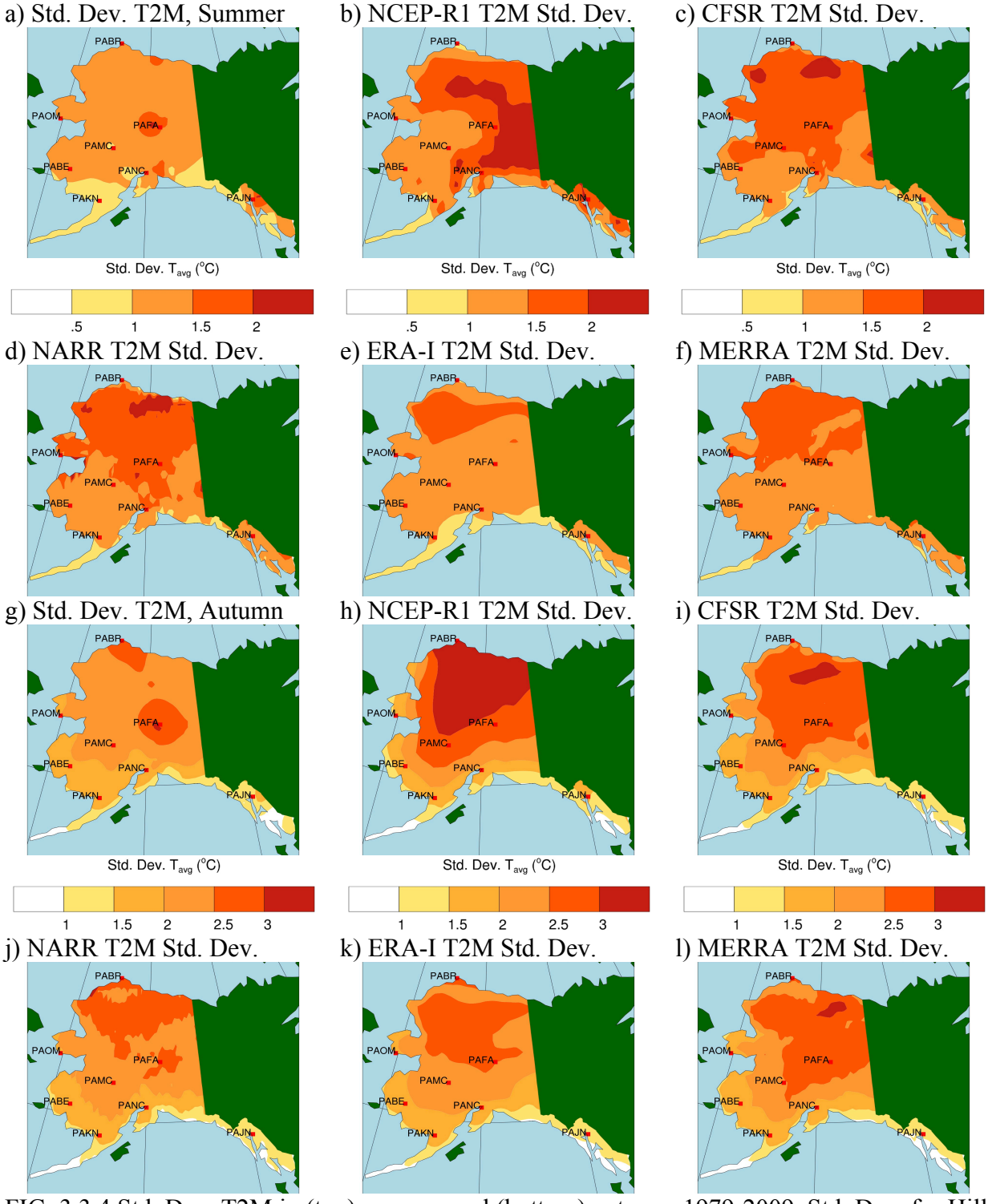

FIG. 3.3.4 Std. Dev. T2M in (top) summer and (bottom) autumn, 1979-2009. Std. Dev. for Hill et al. (2014) is in the top left (a,g), followed by model Std. Dev. (b-f, h-l).

Table 3.3.1 Monthly average temperature (T_{avg}) (˚C) by **climate division**. Bias (˚C) (warm/cold) compared to Hill et al. (2014). (HC). Standard deviation (SD) (˚C).

	WINTER			SPRING			SUMMER			AUTUMN		
N. Slope	T_{avg}	Bias	SD	T_{avg}	Bias	SD	T_{avg}	Bias	SD	T_{avg}	Bias	SD
NCEP-R1	-24.3	-0.9	4.1	-9.6	-0.5	2.5	6.5	-1.3	1.7	-6.3	-1.3	3.2
CFSR	-22.4	1.0	3.8	-8.6	0.5	2.9	7.8	0.0	1.9	-4.6	0.4	2.7
NARR	-21.6	1.8	3.5	-7.5	1.6	2.4	8.5	0.7	1.9	-4.5	0.5	2.7
ERA	-24.7	-1.3	4.1	-8.7	0.4	3.2	8.0	0.2	1.5	-4.9	0.1	2.6
MERRA	-22.6	0.8	3.5	-6.9	2.2	2.8	9.3	1.5	1.7	-4.9	0.1	2.6
HC	-23.4	N/A	3.5	-9.1	N/A	2.7	7.8	N/A	1.3	-5.0	N/A	2.4
W. Coast	T_{avg}	Bias	SD	T_{avg}	Bias	SD	T_{avg}	Bias	SD	T_{avg}	Bias	SD
NCEP-R1	-14.8	-0.8	4.2	-3.2	-1.7	2.4	10.1	-0.8	1.4	0.1	-1.2	2.2
CFSR	-13.7	0.3	3.7	-2.0	-0.5	2.7	10.6	-0.3	1.6	0.9	-0.4	2.1
NARR	-14.3	-0.3	4.1	-1.4	0.1	2.7	11.4	0.5	1.5	1.7	0.4	2.1
ERA	-14.3	-0.3	4.2	-1.3	0.2	2.8	10.8	-0.1	1.4	1.1	-0.2	2.1
MERRA	-15.0	-1.0	3.6	-1.3	0.2	2.5	11.5	0.6	1.4	1.1	-0.2	2.0
HC	-14.0	N/A	3.8	-1.5	N/A	2.6	10.9	N/A	1.2	1.3	N/A	2.0
Interior	T_{avg}	Bias	SD	T_{avg}	Bias	SD	T_{avg}	Bias	SD	T_{avg}	Bias	SD
NCEP-R1	-17.4	-1.0	4.1	-3.9	-4.8	2.0	8.9	-2.9	1.9	-4.2	-3.3	2.8
CFSR	-17.4	-1.0	3.9	-1.4	-2.3	2.6	11.4	-0.4	1.6	-1.7	-0.8	2.5
NARR	-16.5	-0.1	3.7	0.1	-0.8	2.4	12.3	0.5	1.6	-0.5	0.4	2.4
ERA	-17.5	-1.1	4.1	0.7	-0.2	2.2	12.0	0.2	1.3	-0.9	0.0	2.4
MERRA	-19.4	-3.0	3.9	-1.7	-2.6	2.3	11.6	-0.2	1.4	-2.3	-1.4	2.5
HC	-16.4	N/A	3.9	0.9	N/A	2.2	11.8	N/A	1.2	-0.9	N/A	2.3
Bristol B.	T_{avg}	Bias	SD	T_{avg}	Bias	SD	T_{avg}	Bias	SD	T_{avg}	Bias	SD
NCEP-R1	-5.9	0.1	3.0	0.3	-2.0	1.4	9.6	-0.9	1.2	3.3	-0.8	1.6
CFSR	-6.3	-0.3	3.3	1.6	-0.7	1.8	10.3	-0.2	1.1	3.6	-0.5	1.6
NARR	-6.1	-0.1	3.3	2.1	-0.2	1.8	10.5	0.0	1.0	3.9	-0.2	1.5
ERA	-5.6	0.4	3.3	2.9	0.6	1.6	11.0	0.5	0.9	4.7	0.6	1.5
MERRA	-6.7	-0.7	3.3	2.0	-0.3	1.6	11.2	0.7	1.1	4.1	0.0	1.6
HC	-6.0	N/A	3.5	2.3	N/A	1.8	10.5	N/A	0.9	4.1	N/A	1.6
C. Inlet	T_{avg}	Bias	SD	T_{avg}	Bias	SD	T_{avg}	Bias	SD	T_{avg}	Bias	SD
NCEP-R1	-9.0	-1.1	3.1	-1.6	-3.1	1.3	8.0	-1.9	1.7	0.1	-1.8	2.0
CFSR	-9.0	-1.1	2.9	0.4	-1.1	1.7	9.6	-0.3	1.4	1.3	-0.6	1.8
NARR	-8.6	-0.7	2.9	0.4	-1.1	1.7	9.1	-0.8	1.4	1.1	-0.8	1.8
ERA	-9.3	-1.4	3.5	2.5	1.0	1.5	10.9	1.0	1.1	2.4	0.5	2.0
MERRA	-9.2	-1.3	3.2	0.5	-1.0	1.5	10.5	0.6	1.2	1.6	-0.3	1.9
HC	-7.9	N/A	3.4	1.5	N/A	1.7	9.9	N/A	1.1	1.9	N/A	1.9
Southeast	T_{avg}	Bias	SD	T_{avg}	Bias	SD	T_{avg}	Bias	SD	T_{avg}	Bias	SD
NCEP-R1	-2.5	0.1	2.2	1.6	-2.5	1.1	8.4	-2.3	1.3	4.6	-1.1	1.2
CFSR	-3.0	-0.4	2.5	2.6	-1.5	1.3	9.7	-1.0	1.1	5.1	-0.6	1.2
NARR	-2.2	0.4	2.2	3.1	-1.0	1.2	9.7	-1.0	1.1	5.4	-0.3	1.1
ERA	-3.0	-0.4	2.6	4.0	-0.1	1.2	10.6	-0.1	1.0	5.8	0.1	1.1
MERRA	-1.7	0.9	2.3	4.4	0.3	1.2	11.7	1.0	1.1	6.6	0.9	1.1
HC	-2.6	N/A	2.5	4.1	N/A	1.3	10.7	N/A	1.0	5.7	N/A	1.2

3.4 Comparison of reanalysis products to observed precipitation

3.4.1 Precipitation verification dataset

Hill et al. (2014) also developed a high-resolution (2 km) gridded dataset of monthly precipitation similar to 2-m air temperature that covers Alaska over the period from 1961-2009. They compiled data from 200 Alaskan sites and following their temperature data set methodology used a Delta downscaling method to produce their final gridded product. Rather than using absolute anomalies as they did with the near-surface air temperature they instead computed proportional anomalies relative to the PRISM climatology to avoid negative precipitation values. In this study, the precipitation products of the reanalyses are compared to Hill et al. (2014) from 1979-2009.

3.4.2 Precipitation

Climatology in winter (Fig. 3.4.1a) is characterized by an extreme precipitation gradient from north to south. The Southeast averages nearly 30 cm per month while the North Slope receives little more than 1 cm. Spring (Fig. 3.4.1g) is the driest season throughout Alaska. In summer, the north-south precipitation gradient is smallest and this coincides with the wettest time of year for locations north of the Alaska Range (Fig. 3.4.2a). Autumn brings a return to drier conditions for much of Alaska, but is the wettest season for the Southeast, which averages greater than 42 cm per month (Fig. 3.4.2g).

NARR and MERRA consistently have the lowest precipitation bias. NARR does, however, show an unrealistic north-south boundary around 150˚W with too much precipitation west of this line and too little to its east (Ruane et al. 2010). This is most pronounced during summer (Fig. 3.4.2d). NCEP-R1 has a notable persistent wet bias across the Interior; in summer,

there is a swath with a monthly anomaly greater than 5 cm (Fig. 3.4.2b). CFSR has a very large precipitation bias throughout the year that is the largest in spring (Fig. 3.4.1i). Lindsay et al. (2014) noted similar characteristics for the Arctic and suggests that that this is related to the atmospheric model in CFSR. Lorenz and Kunstmann (2012) showed that CFSR and ERA-Interim often have positive daily precipitation biases of around 2 mm in the middle and high latitudes of the northern hemisphere. ERA-Interim has a positive bias across most of Alaska that is largest for the Bristol Bay region (Table 3.4.1). All of the reanalyses underestimate precipitation in the Southeast; however, CFSR and ERA-Interim have a strong dry bias that is approximately 50 percent less than the other models.

The highest precipitation variability for most of Alaska occurs during summer (Fig. 3.4.4a), although it is later in autumn for the Southeast when the monthly standard deviation can exceed 19 cm (Fig. 3.4.4g). For locations north of the Alaska Range, winter and spring have a very low standard deviation that is often below 2 cm (Fig. 3.4.3a,g).

The reanalyses tend to underestimate precipitation variability in the southern half of the state, which coincides with regions where the models have a dry bias. NARR and ERA-Interim have the best agreement with Hill et al. (2014). NCEP-R1 has very low precipitation variability across southern Alaska, which is likely due to its coarse resolution. CFSR shows high standard deviation values north of the Alaska Range, but performs better to the south. MERRA has too low precipitation variability throughout Alaska.

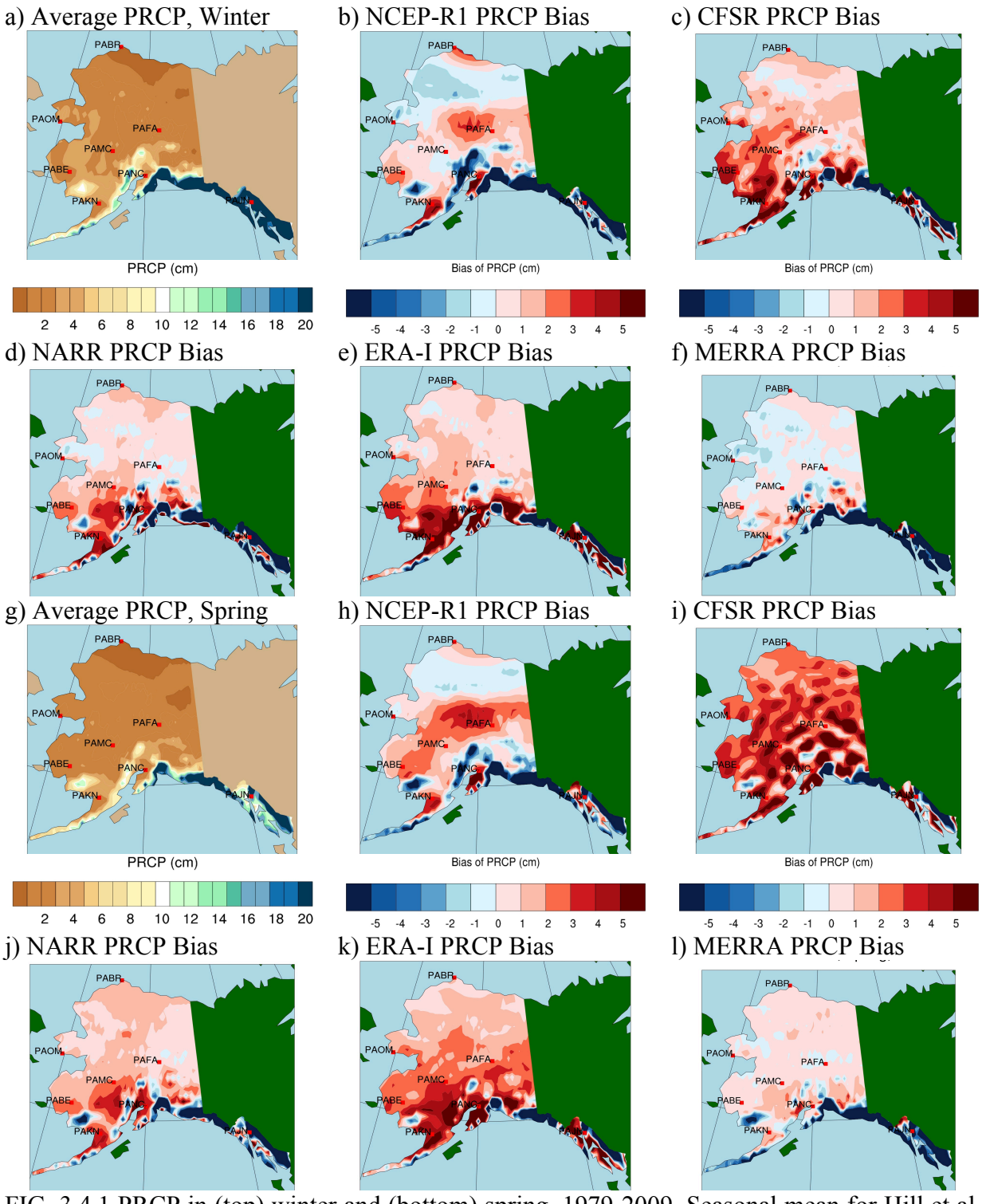

FIG. 3.4.1 PRCP in (top) winter and (bottom) spring, 1979-2009. Seasonal mean for Hill et al. (2014) is in the top left (a,g), followed by model bias (b-f, h-l).

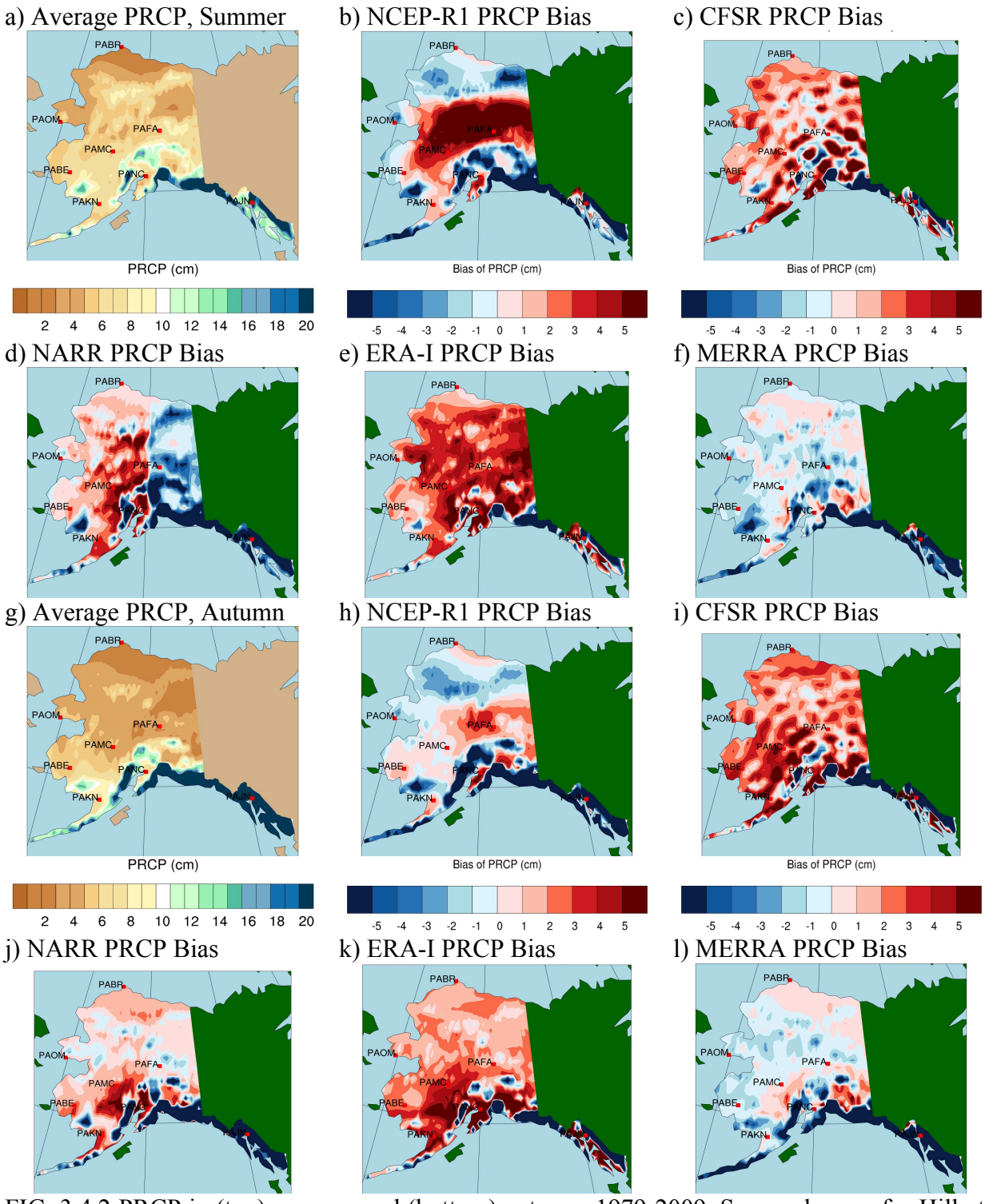

FIG. 3.4.2 PRCP in (top) summer and (bottom) autumn, 1979-2009. Seasonal mean for Hill et al. (2014) is in the top left (a,g), followed by model bias (b-f, h-l).

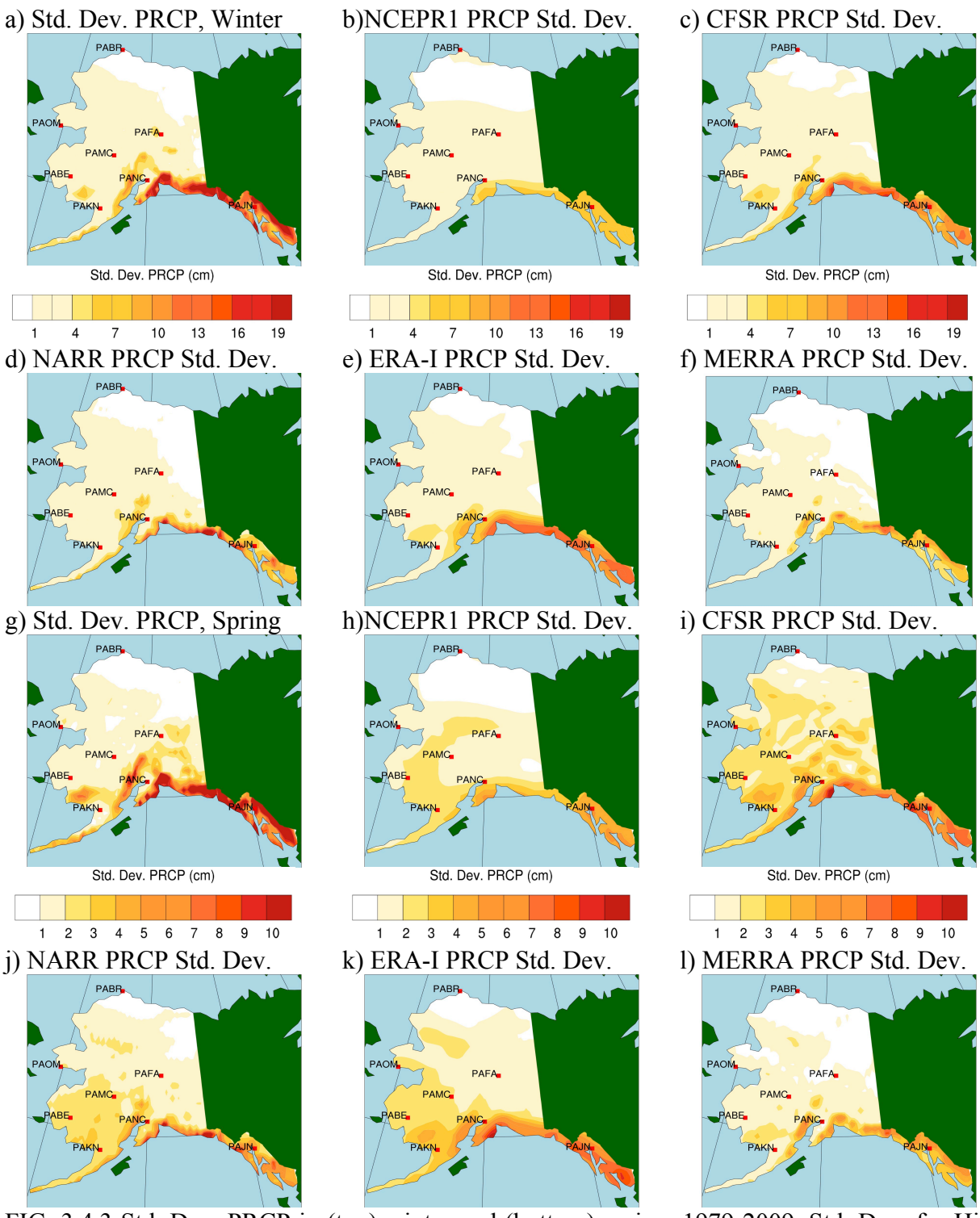

FIG. 3.4.3 Std. Dev. PRCP in (top) winter and (bottom) spring, 1979-2009. Std. Dev. for Hill et al. (2014) is in the top left (a,g), followed by model Std. Dev. (b-f, h-1).

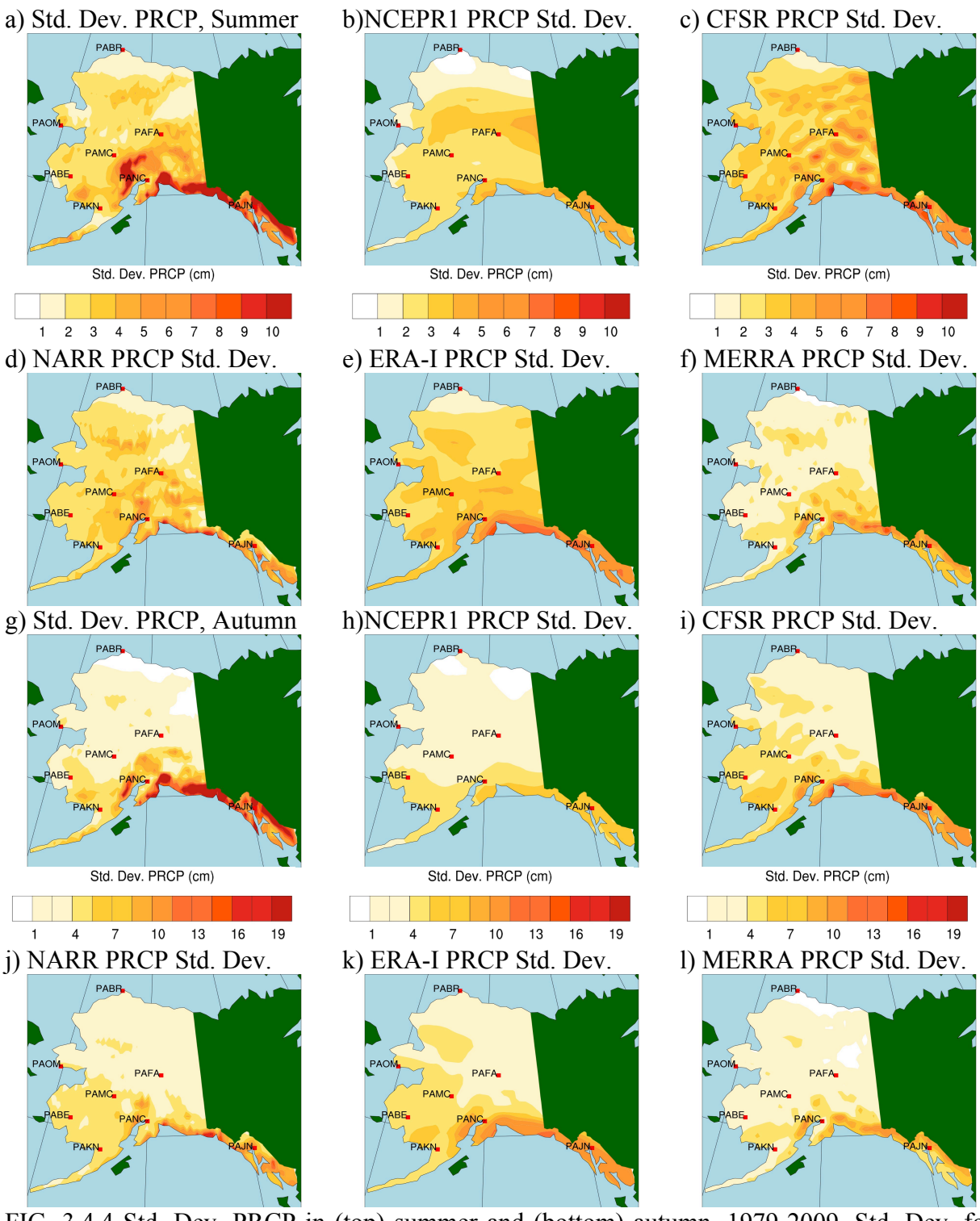

FIG. 3.4.4 Std. Dev. PRCP in (top) summer and (bottom) autumn, 1979-2009. Std. Dev. for Hill et al. (2014) is in the top left (a,g), followed by model Std. Dev. (b-f, h-1).

Table 3.4.1 Monthly average precipitation (PRCP) (cm) by **climate division**. Bias (cm) (wet/dry) compared to Hill et al. (2014) (HC). Standard deviation (SD) (cm).

	WINTER			SPRING			SUMMER			AUTUMN		
N. Slope	PCP	Bias	SD	PCP	Bias	SD	PCP	Bias	SD	PCP	Bias	SD
NCEP-R1	1.0	-0.3	0.7	1.0	0.0	0.6	2.6	-1.5	1.3	1.7	-0.9	1.1
CFSR	2.0	0.7	1.0	3.2	2.2	1.2	6.1	2.0	2.6	5.0	2.4	2.0
NARR	2.0	0.7	0.9	2.3	1.3	1.1	4.2	0.1	2.0	3.9	1.3	1.6
ERA	1.9	0.6	1.0	2.0	1.0	1.0	6.4	2.3	2.1	4.3	1.7	1.8
MERRA	1.2	-0.1	0.6	1.5	0.5	0.7	4.0	-0.1	1.5	2.7	0.1	1.2
HC	1.3	N/A	0.8	1.0	N/A	0.7	4.1	N/A	2.0	2.6	N/A	1.3
W. Coast	PCP	Bias	SD	PCP	Bias	SD	PCP	Bias	SD	PCP	Bias	SD
NCEP-R1	2.9	0.0	1.7	3.0	0.8	1.6	5.7	0.2	2.2	4.6	-0.6	2.4
CFSR	5.0	2.1	2.4	5.2	3.0	2.3	7.4	1.9	3.1	7.7	2.5	3.4
NARR	3.8	0.9	2.0	3.3	1.1	1.9	6.2	0.7	2.6	5.8	0.6	2.9
ERA	4.5	1.6	2.4	4.1	1.9	2.2	7.9	2.4	2.9	7.1	1.9	3.4
MERRA	2.7	-0.2	1.5	2.4	0.2	1.4	4.5	-1.0	1.8	4.2	-1.0	2.2
HC	2.9	N/A	1.9	2.2	N/A	1.5	5.5	N/A	2.4	5.2	N/A	2.6
Interior	PCP	Bias	SD	PCP	Bias	SD	PCP	Bias	SD	PCP	Bias	SD
NCEP-R1	3.0	0.4	1.5	3.2	1.0	1.4	9.6	2.8	2.8	4.9	-0.1	2.0
CFSR	3.8	1.2	2.0	5.6	3.4	2.1	8.6	1.8	3.6	7.2	2.2	2.8
NARR	3.0	0.4	1.6	3.1	0.9	1.6	6.2	-0.6	2.8	5.0	0.0	2.2
ERA	3.7	1.1	1.9	4.3	2.1	1.8	10.1	3.3	3.1	7.0	2.0	2.7
MERRA	2.5	-0.1	1.3	2.6	0.4	1.2	6.0	-0.8	2.1	4.5	-0.5	1.9
HC	2.6	N/A	1.9	2.2	N/A	1.6	6.8	N/A	3.1	5.0	N/A	2.7
Bristol B.	PCP	Bias	SD	PCP	Bias	SD	PCP	Bias	SD	PCP	Bias	SD
NCEP-R1	6.1	-0.7	2.7	5.2	-0.3	2.3	7.3	-1.7	2.4	8.3	-3.3	3.2
CFSR	10.1	3.3	3.9	8.5	3.0	3.2	10.5	1.5	3.4	13.4	1.8	4.7
NARR	8.3	1.5	3.3	6.6	1.1	2.8	8.8	-0.2	2.9	10.6	-1.0	3.8
ERA	10.3	3.5	4.1	8.7	3.2	3.3	10.6	1.6	3.5	13.8	2.2	4.8
MERRA	6.1	-0.7	2.6	4.8	-0.7	2.0	6.8	-2.2	2.2	8.2	-3.4	3.2
HC	6.8	N/A	3.7	5.5	N/A	3.0	9.0	N/A	4.0	11.6	N/A	4.8
C. Inlet	PCP	Bias	SD	PCP	Bias	SD	PCP	Bias	SD	PCP	Bias	SD
NCEP-R1	6.5	-3.9	3.2	5.2	-1.7	2.3	7.8	-3.3	2.7	9.3	-7.5	3.7
CFSR	11.0	0.6	5.3	9.5	2.6	3.8	12.4	1.3	4.5	16.4	-0.4	6.1
NARR	10.0	-0.4	5.1	7.6	0.7	3.3	9.5	-1.6	4.3	13.4	-3.4	5.6
ERA	12.9	2.5	6.2	10.2	3.3	4.1	13.3	2.2	4.5	18.6	1.8	6.8
MERRA	8.8	-1.6	4.4	6.4	-0.5	2.8	8.8	-2.3	3.4	12.1	-4.7	4.7
HC	10.4	N/A	7.4	6.9	N/A	5.7	11.1	N/A	6.3	16.8	N/A	8.6
Southeast	PCP	Bias	SD	PCP	Bias	SD	PCP	Bias	SD	PCP	Bias	SD
NCEP-R1	15.5	-14.0	5.6	10.5	-7.6	4.0	9.7	-8.6	3.8	19.2	-23.2	5.1
CFSR	25.5	-4.0	10.0	16.4	-1.7	6.4	16.0	-2.3	6.2	32.3	-10.1	9.4
NARR	20.8	-8.7	8.7	12.0	-6.1	5.4	8.9	-9.4	4.7	19.9	-22.5	8.1
ERA	25.9	-3.6	10.1	15.6	-2.5	6.4	14.4	-3.9	6.0	32.5	-9.9	9.4
MERRA	15.6	-13.9	6.2	9.1	-9.0	3.9	9.2	-9.1	4.0	20.1	-22.3	5.9
HC	29.5	N/A	14.0	18.1	N/A	9.2	18.3	N/A	8.5	42.4	N/A	15.0

3.5 Comparison of reanalysis products to observed snow-water equivalent

3.5.1 Snow verification dataset

The GlobSnow v.2.0 dataset (Luojus et al. 2013) is used for SWE verification in this study. For a description of this product refer to Section 2.1.3. Due to missing data across the three southernmost climate divisions – Bristol Bay, Cook Inlet, and Southeast – these have been excluded from this analysis. The SWE that appears in the figures of model bias across these regions represents analyzed SWE, and was retained to address several data quality issues. In this study, the SWE products of the reanalyses are compared to GlobSnow v2.0 from 1980-2009.

3.5.2 Snow-water equivalent

Maximum SWE throughout most of Alaska occurs during winter (Fig. 3.5.1a), but also in spring in the far northwest (Fig. 3.5.1g). By summer (Fig. 3.5.2a) the snow has melted completely except across the mountain peaks, which are not included. In autumn (Fig. 3.5.2g), snow returns to the North Slope and the Interior, while patches of the West Coast remain snowless.

The three highest resolution models – NARR, CFSR, and MERRA – have the lowest SWE bias over northern Alaska. In nearly all cases, the reanalyses show negative SWE anomalies. ERA-Interim has a negative anomaly that is frequently 50 mm or greater in winter and spring (Fig. 3.5.1e,k) (Table 3.5.1). NCEP-R1 shows similar or even larger anomalies, particularly in the Interior (Fig. 3.5.1b,h). ERA-Interim also produces unrealistic SWE values of 2000 mm or greater across the glaciated regions in the Cook Inlet and Southeast climate divisions. These locations are easiest to see in Fig. 3.5.2e by their dark red color.

Winter and spring (Fig. 3.5.3a,g) have the largest variability of SWE in Alaska with typical standard deviation values of 40-50 mm in the Interior and West Coast. In summer the statewide standard deviation of SWE is zero (Fig. 3.5.4a), however, GlobSnow v2.0 does not provide data over the mountains. Of course, the mountains do retain snow during summer, and this is important for hydrology. By autumn the highest variability is on the North Slope and in the Interior where the snowpack has returned (Fig. 3.5.4g). Consistent with the anomaly fields, the variability of SWE in NARR, CFSR, and MERRA are closest to the GlobSnow v2.0 dataset.

The reanalyses all underestimate SWE throughout Alaska. A plausible explanation for this is due to the use of in situ observations to produce the snow analyses. Most of the available stations across Alaska are at low elevation and likely receive less snowfall than the nearby mountainous locations. By interpolating from grid cells with low observed SWE to mountainous grid cells without any observations, a negative SWE bias is produced across much of Alaska in the reanalyses.

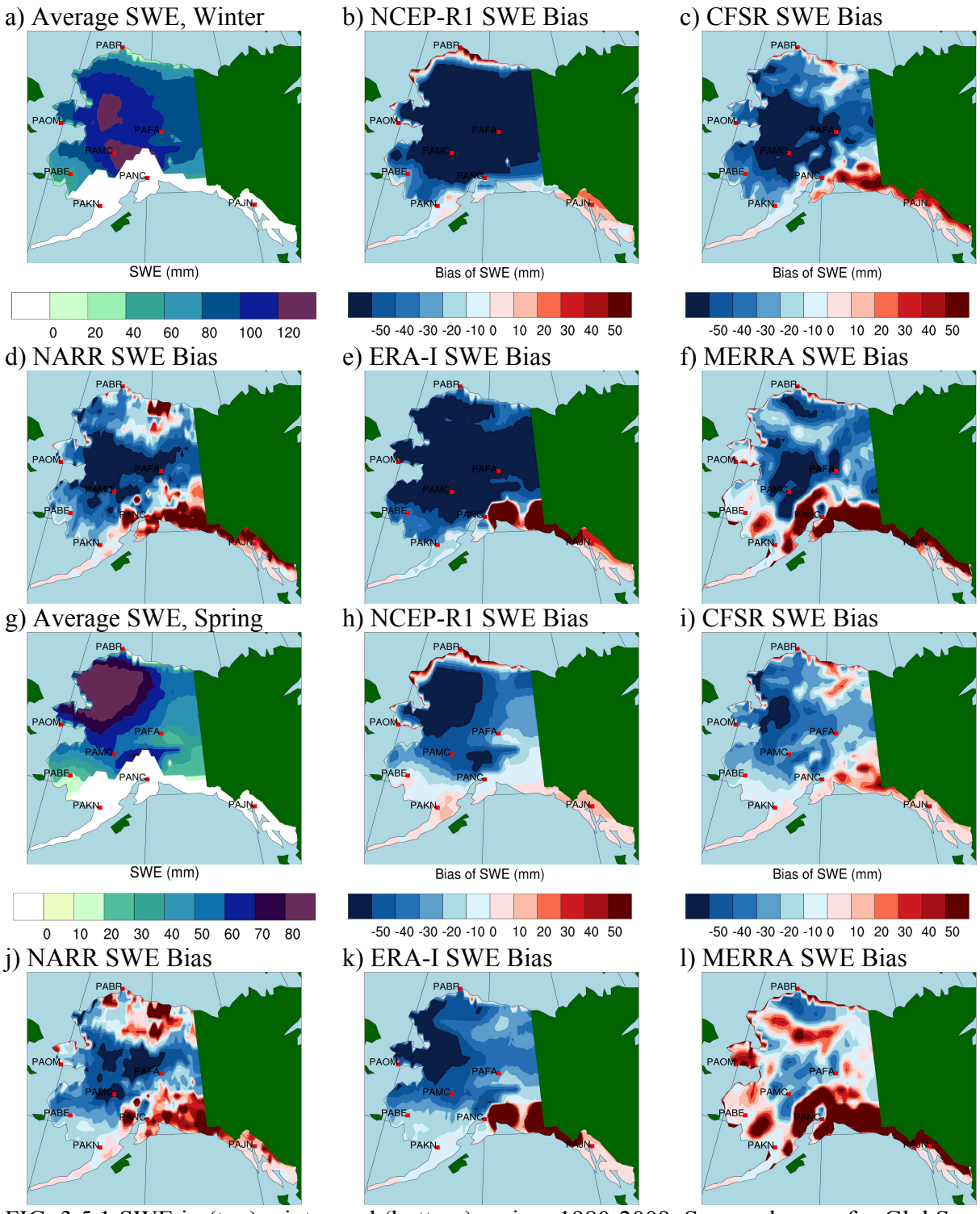

FIG. 3.5.1 SWE in (top) winter and (bottom) spring, 1980-2009. Seasonal mean for GlobSnow v2.0 is in the top left (a,g), followed by model bias (b-f, h-l). The area shaded in white has been excluded from this analysis.

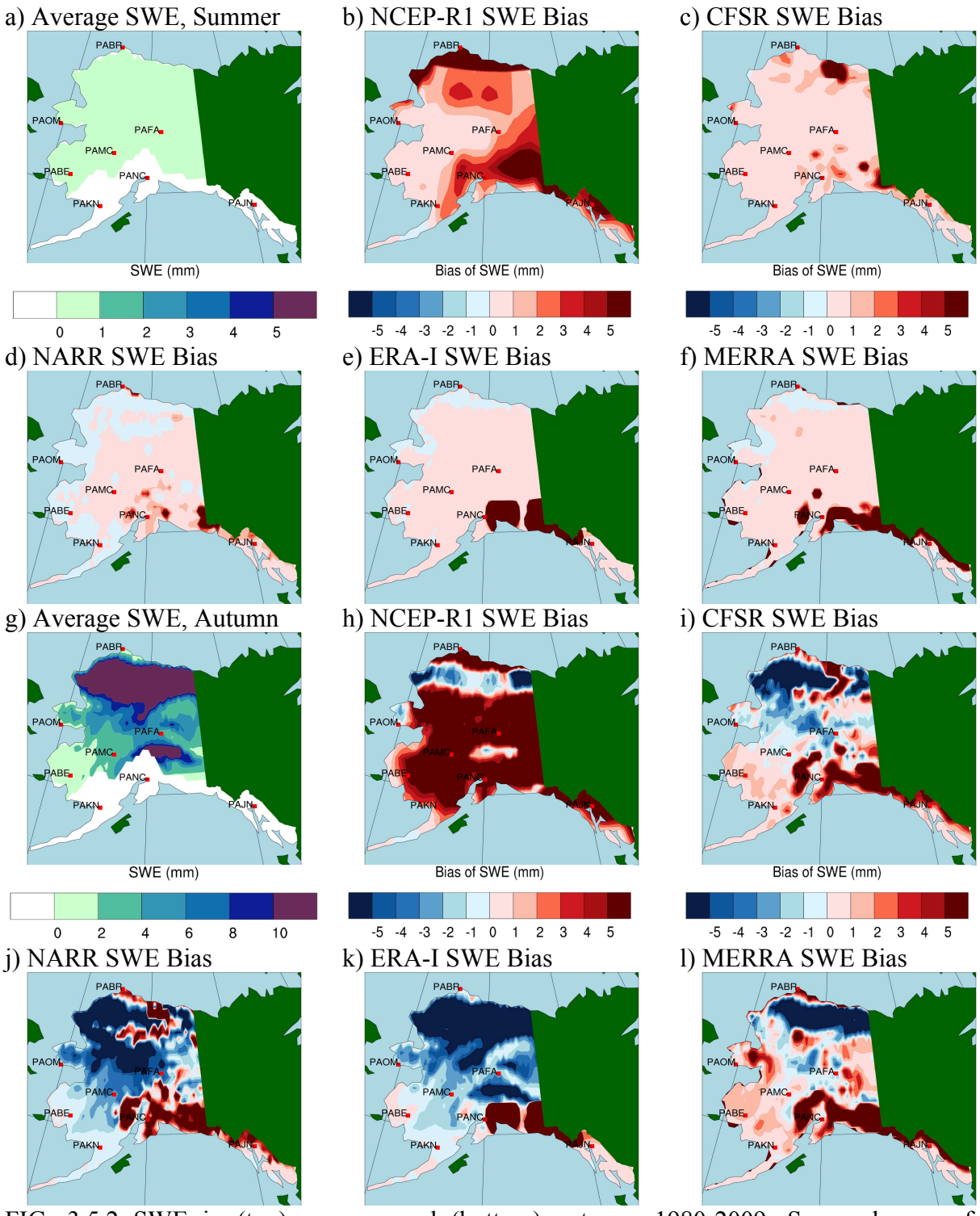

FIG. 3.5.2 SWE in (top) summer and (bottom) autumn, 1980-2009. Seasonal mean for GlobSnow v2.0 is in the top left (a,g), followed by model bias (b-f, h-l). The area shaded in white has been excluded from this analysis.

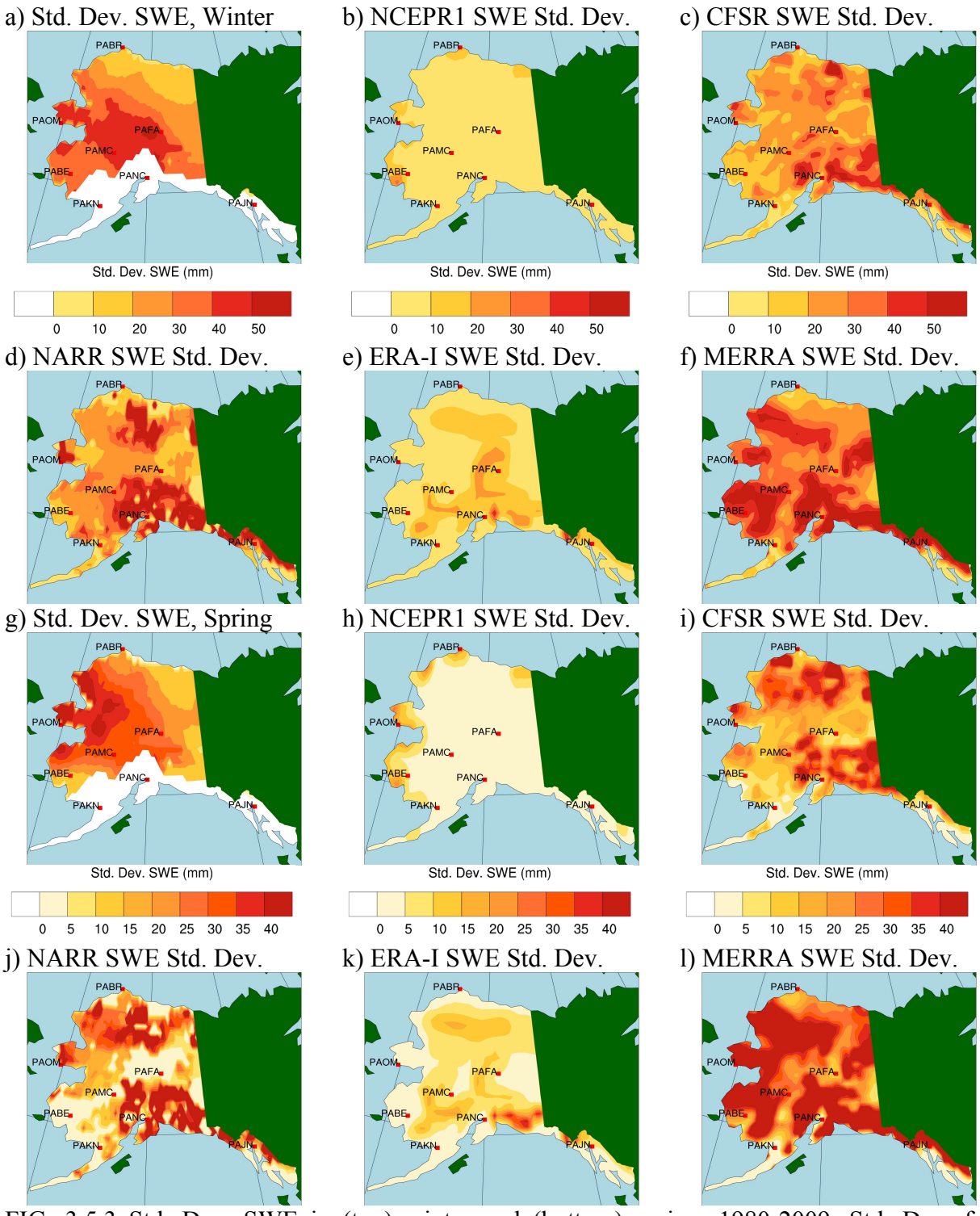

FIG. 3.5.3 Std. Dev. SWE in (top) winter and (bottom) spring, 1980-2009. Std. Dev. for GlobSnow v2.0 is in the top left (a,g), followed by model Std. Dev. (b-h, h-l). The area shaded in white has been excluded from this analysis.

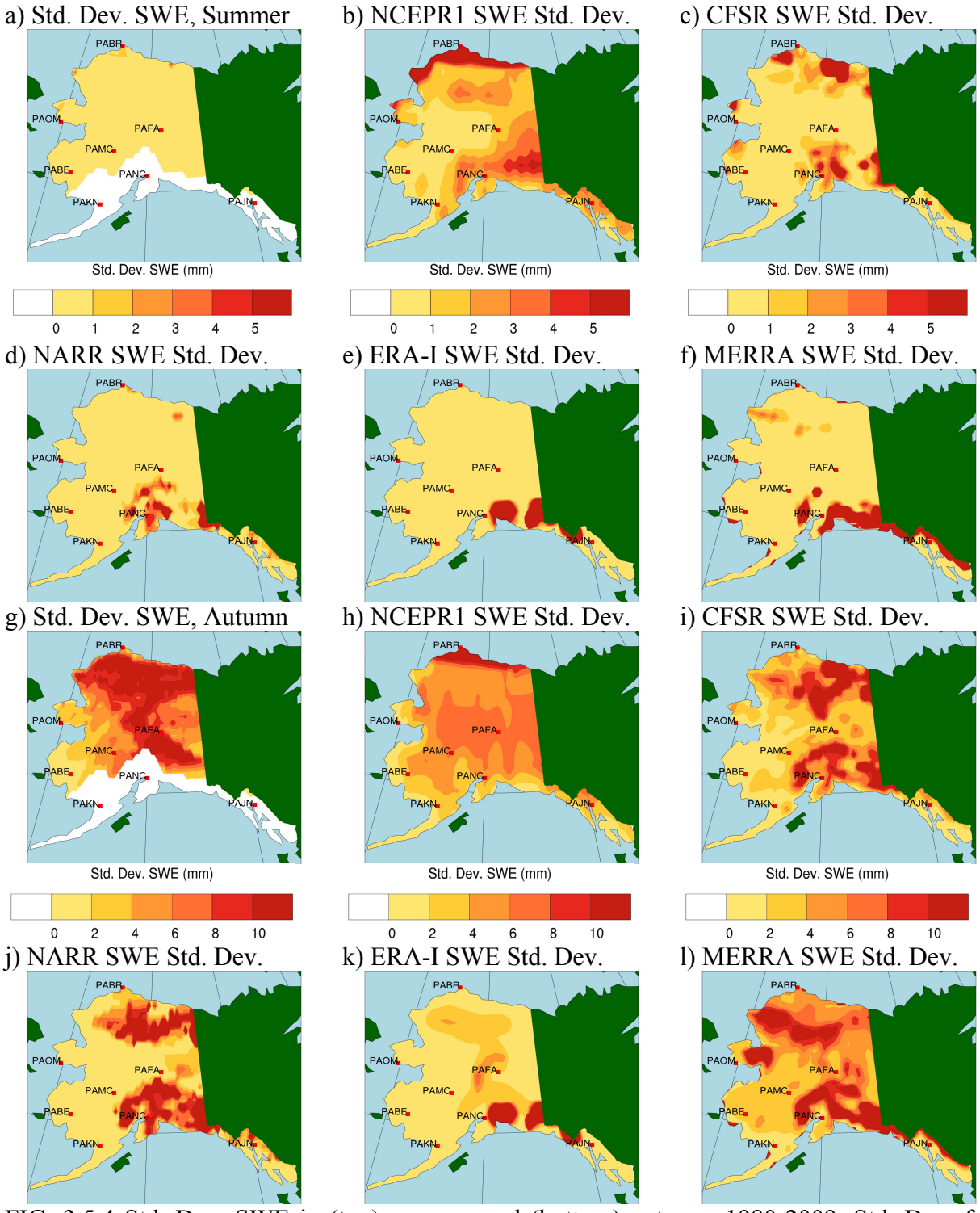

FIG. 3.5.4 Std. Dev. SWE in (top) summer and (bottom) autumn, 1980-2009. Std. Dev. for GlobSnow v2.0 is in the top left (a,g), followed by model Std. Dev. (b-f, h-l). The area shaded in white has been excluded from this analysis.

Table 3.5.1 Monthly snow-water equivalent (SE) (mm) by **climate division**. Bias (mm) (high/low) compared to GlobSnow v2.0 (GLOB). Standard deviation (SD) (mm).

	WINTER			SPRING			SUMMER			AUTUMN		
N. Slope	SE	Bias	SD	SE	Bias	SD	SE	Bias	SD	SE	Bias	SD
NCEP-R1	41.2	-40.5	3.9	41.6	-26.9	4.6	8.9	8.8	4.7	15.9	1.9	7.1
CFSR	57.2	-24.5	26.1	52.0	-16.5	31.3	3.2	3.1	7.2	10.9	-3.1	10.1
NARR	75.1	-6.6	26.3	86.4	17.9	27.7	0.0	-0.1	0.1	12.2	-1.8	5.9
ERA	33.0	-48.7	8.9	32.0	-36.5	7.8	0.1	0.0	0.1	4.6	-9.4	2.0
MERRA	53.4	-28.3	28.1	62.7	-5.8	34.6	0.2	0.1	0.6	8.9	-5.1	7.3
GLOB	81.7	N/A	18.9	68.5	N/A	21.9	0.1	N/A	0.3	14.0	N/A	10.3
W. Coast	SE	Bias	SD	SE	Bias	SD	SE	Bias	SD	SE	Bias	SD
NCEP-R1	33.3	-47.1	6.8	24.5	-28.5	7.8	0.9	0.9	1.0	7.2	4.1	3.5
CFSR	41.7	-38.7	20.1	25.1	-27.9	18.1	0.3	0.3	0.7	2.4	-0.7	2.0
NARR	45.5	-34.9	23.7	28.3	-24.7	15.9	0.0	0.0	0.0	0.2	-2.9	0.1
ERA	19.4	-61.0	4.6	12.6	-40.4	4.5	0.0	0.0	0.0	1.1	-2.0	0.5
MERRA	71.5	-8.9	41.4	66.8	13.8	43.1	0.0	0.0	0.1	4.1	1.0	5.2
GLOB	80.4	N/A	34.5	53.0	N/A	29.9	0.0	N/A	0.1	3.1	N/A	3.2
Interior	SE	Bias	SD	SE	Bias	SD	SE	Bias	SD	SE	Bias	SD
NCEP-R1	25.2	-75.2	1.0	17.8	-34.4	2.7	2.3	2.3	1.9	13.6	7.2	6.1
CFSR	59.7	-40.7	27.6	31.4	-20.8	22.9	0.5	0.5	1.0	7.0	0.6	6.0
NARR	69.2	-31.2	32.9	30.9	-21.3	21.5	0.3	0.3	0.5	5.2	-1.2	5.0
ERA	47.9	-52.5	11.7	32.7	-19.5	8.4	1.4	1.4	1.5	15.3	8.9	3.2
MERRA	73.7	-26.7	36.2	60.5	8.3	34.6	2.0	2.0	1.0	8.7	2.3	6.7
GLOB	100.4	N/A	34.0	52.2	N/A	24.6	0.0	N/A	0.0	6.4	N/A	7.7
Bristol B.	SE	Bias	SD	SE	Bias	SD	SE	Bias	SD	SE	Bias	SD
NCEP-R1	15.5	N/A	2.7	10.3	N/A	3.1	1.3	N/A	1.1	5.0	N/A	2.2
CFSR	24.7	N/A	15.8	9.2	N/A	9.2	0.2	N/A	0.3	2.5	N/A	2.5
NARR	34.3	N/A	25.1	11.5	N/A	9.8	0.1	N/A	0.2	1.5	N/A	1.5
ERA	15.6	N/A	7.3	6.1	N/A	4.3	0.0	N/A	0.0	0.6	N/A	0.4
MERRA	57.2	N/A	28.1	44.7	N/A	20.1	3.6	N/A	1.9	5.9	N/A	3.4
GLOB	N/A	N/A	N/A	N/A	N/A	N/A	N/A	N/A	N/A	N/A	N/A	N/A
C. Inlet	SE	Bias	SD	SE	Bias	SD	SE	Bias	SD	SE	Bias	SD
NCEP-R1	19.9	N/A	1.4	14.5	N/A	2.2	2.7	N/A	2.3	8.9	N/A	4.2
CFSR	58.8	N/A	33.3	26.4	N/A	24.1	1.0	N/A	2.4	6.7	N/A	6.4
NARR	98.3	N/A	48.4	52.3	N/A	35.1	1.2	N/A	3.0	7.4	N/A	8.3
ERA	66.6	N/A	16.0	49.0	N/A	7.2	33.3	N/A	2.1	37.4	N/A	6.4
MERRA	157.8	N/A	45.7	152.2	N/A	40.5	9.6	N/A	9.1	11.3	N/A	8.2
GLOB	N/A	N/A	N/A	N/A	N/A	N/A	N/A	N/A	N/A	N/A	N/A	N/A
Southeast	SE	Bias	SD	SE	Bias	SD	SE	Bias	SD	SE	Bias	SD
NCEP-R1	10.2	N/A	2.6	7.6	N/A	2.3	2.5	N/A	1.6	4.4	N/A	2.1
CFSR	25.3	N/A	18.6	9.9	N/A	10.0	0.6	N/A	0.7	2.9	N/A	2.4
NARR	39.1	N/A	29.7	20.0	N/A	19.6	0.7	N/A	1.0	2.7	N/A	3.0
ERA	60.0	N/A	7.0	53.4	N/A	5.7	48.7	N/A	3.1	50.2	N/A	3.1
MERRA	105.3	N/A	31.4	94.6	N/A	24.6	28.9	N/A	11.7	13.0	N/A	5.7
GLOB	N/A	N/A	N/A	N/A	N/A	N/A	N/A	N/A	N/A	N/A	N/A	N/A

3.6 Regional synthesis

This chapter presents gridded climate statistics of near-surface air temperature, precipitation and SWE from a suite of reanalyses both spatially and for six climate divisions across Alaska. These statistics are constructed from monthly data that has been averaged and presented seasonally. The highest resolution models typically have the lowest bias and the closest agreement with observed variability.

NARR and ERA-Interim have the lowest near-surface air temperature bias compared to observations. NCEP-R1 is markedly colder than observed, particularly in the Interior. All of the models except for NCEP-R1 have a good representation of near-surface air temperature variability; NCEP-R1 is much too high during summer and autumn.

NARR and MERRA show the lowest precipitation bias, while CFSR is consistently the wettest model. The precipitation analysis for CFSR depends heavily on the GFS forecast, which can overestimate precipitation by 45 % (Janowiak et al. 2007). NCEP-R1 has a large positive precipitation bias that is most pronounced across the Interior during summer when it shows model biases of greater than 5 cm per month. This is partially due to its cold bias because as excess humidity is added by the analysis increment into a cold atmosphere, it is forced to condense and precipitate out.

The models have positive precipitation anomalies over mainland Alaska, but have a strong negative bias for the Southeast. Over this region, the models only simulate 50 % of the observed precipitation amounts. One possible explanation for this is that because the reanalyses are unable to resolve the complex topography that dominates the Southeast climate division, they do not forecast some of the extreme precipitation values that occur observationally during an air

parcel's ascent up from the Gulf of Alaska. This underestimation by the reanalyses is reflected in the standard deviation fields where the models also have too small values.

For SWE, only Alaska north of the southern coast region is considered. NARR, CFSR, and MERRA frequently have the lowest bias. The reanalyses have negative SWE anomalies (approximately 50 % of observed) with a few exceptions. This can partially be explained by the station data that gets assimilated into the reanalyses. This data is often from a low elevation site that receives less SWE compared to the adjacent mountainous regions. ERA-Interim and NCEP-R1 underestimate SWE variability.

There is an apparent disconnect between the precipitation and SWE products. The models generally overestimate winter precipitation across northern Alaska, but also show a large negative SWE anomaly for the same locations. The temperature anomalies, which are typically small, do not help explain this finding and it remains an open research area.

Chapter 4 A station-based assessment of reanalyses for Alaska

4.1 Introduction

The regional climate in Alaska varies greatly across its landscape, as do the key climate issues such as permafrost thawing, energy security, hydrology, transportation, agricultural potential, and wildfire (Hinzman et al. 2013). However, each region in Alaska faces these and other climate issues in ways that do not necessarily overlap. Reanalyses, which are used in climate impact studies and to evaluate models that are used for future climate projection scenarios, have strengths and weaknesses that vary across space and time and these need to be documented in order to facilitate the selection of the best available data set for a given problem.

This chapter evaluates daily time series of maximum temperature (T_{max}), minimum temperature (T_{min}), precipitation (PRCP), and snow depth (SNDP) for five reanalyses (Table 2.1) at eight stations from 1979-2009. The stations included – Barrow (Section 4.2), Nome (Section 4.3), Bethel (Section 4.4), McGrath (Section 4.5), Fairbanks (Section 4.6), King Salmon (Section 4.7), Anchorage (Section 4.8), and Juneau (Section 4.9) – provide at least one point representation from all of the largest climate divisions (Bieniek et al. 2012). The reanalysis is evaluated against station data provided by the National Climate Data Center (NCDC) and its Global Summary of Day (GSOD) product. The nearest land grid cell to each station is used to represent the reanalysis data. The altitude of the stations and grid cells used for each evaluation is identified in Table 2.2.1.

The station evaluations are divided into separate sections in this chapter. Each section begins with a discussion of key results and identification of the overall model performance for the given station. The evaluation of each variable centers on a set of four plots that contain the annual cycle, standard deviation, root-mean-square-error (RMSE), and bias. All points shown in

these figures represent an average of 31 years of daily data. The annual cycle, and standard deviation plots contain six time series: NCEP-R1 (green), CFSR (red), NARR (black), ERA-Interim (blue), MERRA (lavender), and station observations (gray). These colors remain consistent throughout this chapter for ease of understanding. The bias and RMSE figures are constructed relative to station data, which means that a value of zero represents agreement with the observations. Note that no snow depth (SNDP) data is available for NCEP-R1.

Decadally-averaged annual counts of climate extreme indices are discussed next for each station and include Annual Extreme Warm Days, Annual Extreme Cold Days, Growing Season Length, and Annual Extreme Precipitation Days. These indices are based on those from the CLIMDEX project (Karl et al. 1999), however, the thresholds for these indices change by station due to the strong gradients of temperature and precipitation across Alaska and are identified on the y-axis label of each figure. For all but Growing Season Length, the thresholds for each station were chosen so that there would be approximately five to fifteen observed instances of these indices annually. Growing Season Length always represents the number of days between the fifth consecutive day when $T_{avg} > 0^{\circ}C$ and the day when $T_{min} \leq -2.2^{\circ}C$.

Following the climate extreme indices are the 31-year time series for all variables. These are included to assist reanalysis users that are only interested in a particular segment of the period included in this study. The time series can also help demonstrate the effects that changing observing systems can make in the data assimilation. These will appear as artificial jumps in the record.

The figures of each station are followed with two tables that list the best performing reanalysis models according to season and variable. This evaluation is based on seasonal-average RMSE value relative to station observations where the lowest scoring model gets ranked number

one. Note that the months included in each season are indicated by one-letter abbreviations in parentheses. The bottom table shows the seasonal-average RMSE values for all of the reanalyses according to variable. This is done to provide the reader with an understanding of how well a model performed, regardless of whether or not it is ranked number one. Each section concludes with a table that is arranged by variable and lists seasonal biases, with low biases color-coded blue and high biases in red.

The sections are self-contained, meaning that the reader can refer to one station without having read the others, and still be able to understand the key results and figures. This was done to facilitate the use of individual station evaluations to be used as a reference but leads to some repetitive text. The final section of the chapter discusses individual station results and synthesizes them to provide a coherent statewide view of reanalysis performance.

4.2 Barrow, Alaska

Barrow is located in the North Slope climate division (Bieniek et al. 2012) along the Arctic coast, dividing the Chukchi and Beaufort Seas. Barrow's coordinates are 71.28˚N, 156.78˚W, and its elevation is close to sea level. The altitude of the nearest land grid point to Barrow used for each reanalysis evaluation is identified in Table 2.2.1. An overall evaluation based on 16 possible combinations between four seasons and four climate variables, indicates that MERRA is the top model six times (Table 4.2.1). MERRA is followed by CFSR (five), NCEP-R1 and NARR (two each), and ERA-Interim (one). Model biases of all seasons and variables for Barrow are given in Table 4.2.2.

The observed mean annual cycle of daily maximum temperature (T_{max}) (see gray line, Fig. 4.2.1a) has a low temperature of -24.7˚C in late January, and a high temperature of 11.1˚C in

July. The standard deviation of T_{max} ranges from a February maximum of 9.9˚C to a June minimum of 1.8˚C (Fig. 4.2.1b). Model biases of T_{max} (Fig. 4.2.1c) are generally negative in the winter and positive in the summer. CFSR has the lowest seasonal RMSE of T_{max} (see red line, Fig. 4.2.1d), which is 1.6˚C during autumn (Table 4.2.2). CFSR also has the best representation of Annual Extreme Warm Days (Fig. 4.2.3a), which are defined as days that have a high temperature equal to or greater than 15˚C.

The observed mean annual cycle of daily minimum temperature (T_{min}) (see gray line, Fig. 4.2.1e) has a low temperature of -32.7˚C in late February, and a high temperature of 2.4˚C in July. The standard deviation of T_{min} ranges from a February maximum of 10.0˚C to a June minimum of 1.4˚C (Fig. 4.2.1f). Model biases of T_{min} (Fig. 4.2.1g) are slightly positive throughout the year, except for NCEP-R1, which shows a negative bias in autumn and winter. CFSR has the lowest seasonal RMSE of T_{min} (see red line, Fig. 4.2.1h), which is 2.6˚C during summer (Table 4.2.2). CFSR also has the best representation of Annual Extreme Cold Days (Fig. 4.2.3b), which are defined as days that have a low temperature equal to or less than -40˚C. All models except for NCEP-R1 greatly overestimate Growing Season Length at Barrow (Fig. 4.2.3d). Growing Season Length begins each year following the fifth consecutive day with an average daily temperature above freezing and terminates when T_{min} is at or below -2.2˚C.

The observed mean annual cycle of daily precipitation (PRCP) (see gray line, Fig. 4.2.2a) has a minimum of 0.02 mm in late March, and a peak near 1.5 mm in August. The standard deviation of PRCP ranges from a March minimum of 0.08 mm to a maximum above 3.0 mm in late summer (Fig. 4.2.2b). The one-day maximum standard deviation of PRCP is 9.9 mm, which is a result of one heavy-precipitation event when 12.2 mm fell on 5 Jun 1980. Model biases of PRCP (Fig. 4.2.2c) are generally positive and CFSR has the largest positive biases during all

seasons. NCEP-R1 has the lowest seasonal RMSE of PRCP (see green line, Fig. 4.2.2d), which is 0.71 mm during spring (Table 4.2.2). MERRA has the best representation of Annual Extreme Precipitation Days (Fig. 4.2.3c), which are defined as days that have an accumulated precipitation equal to or greater than 5 mm. MERRA also has the lowest seasonal RMSE values at Barrow during summer and autumn, which coincide with the wettest times of year.

The observed mean annual cycle of daily snow depth (SNDP) (see gray line, Fig. 4.2.2e) reaches a maximum of 27.6 cm in April, and melts completely by early June. Notably, MERRA keeps snow on the ground all year at Barrow. NARR and CFSR produce fictitious late-summer snow events that are seen as spikes in the time series. The standard deviation of SNDP peaks at 13.0 cm in May (Fig. 4.2.2f). Model biases of SNDP (Fig. 4.2.2g) are largely positive. ERA-Interim has the lowest seasonal RMSE of SNDP (see blue line, Fig. 4.2.2h), which is 0.9 cm during summer (Table 4.2.2).

MERRA is the top performing reanalysis data set relative to station observations at Barrow, and it does particularly well during winter. However, by retaining surface snow throughout the year, MERRA does not reliably capture summer snow depth. CFSR is the preferred reanalysis for the two temperature variables, T_{max} and T_{min}, but the worst at simulating precipitation. CFSR produces nearly twice the number of Annual Extreme Precipitation Days compared to observations. Reanalysis data users that are only interested in a particular variable or season at Barrow should refer to Tables 4.2.1 and 4.2.2 to help guide the selection of the best available data set. The 31-year time series of T_{max} (Fig. 4.2.4), T_{min} (Fig. 4.2.5), PRCP (Fig. 4.2.6), and SNDP (Fig. 4.2.7) are available for users that are primarily interested in a particular segment of the period used for this study.

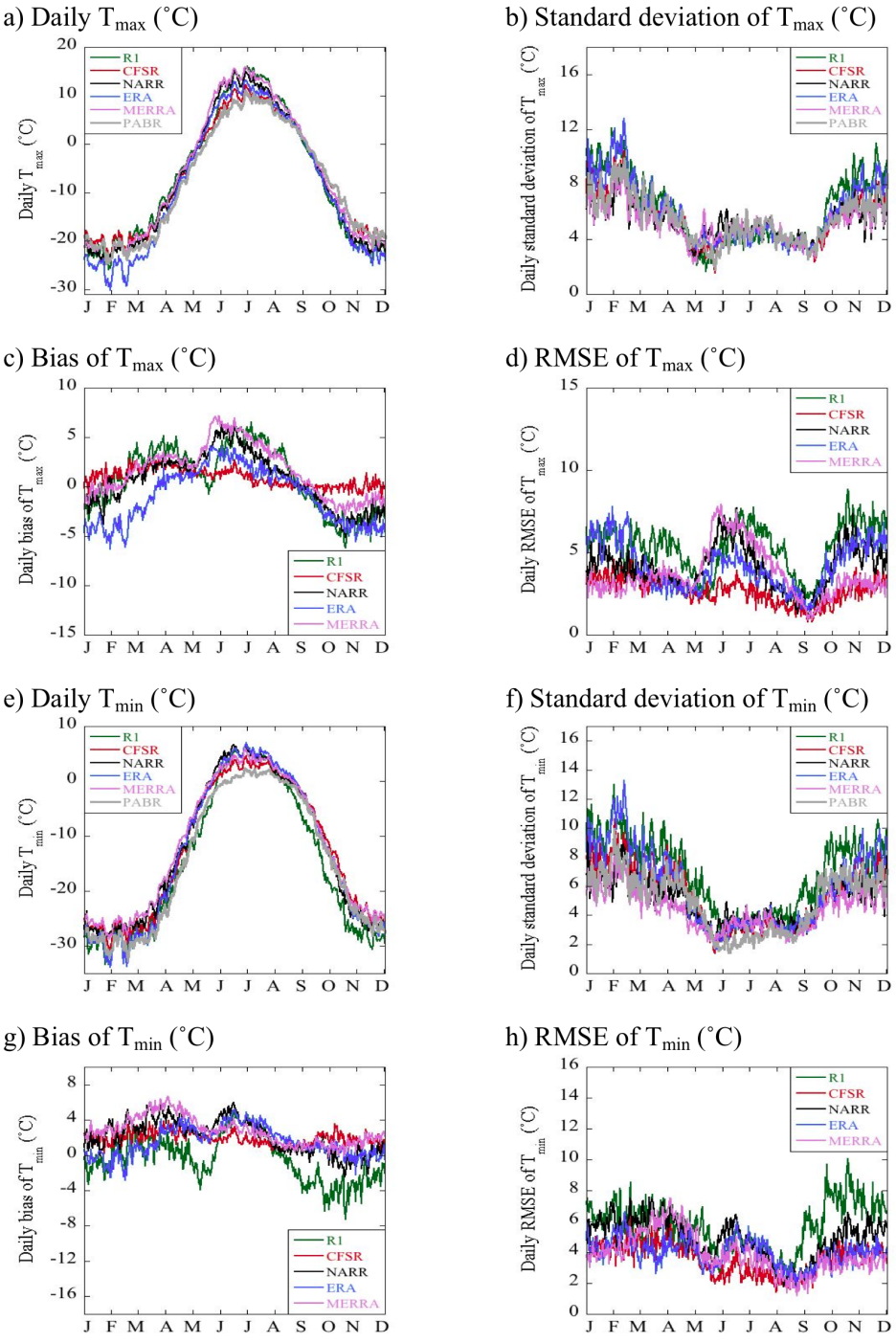

FIG. 4.2.1 Daily climate statistics of T_{max} (a-d), and T_{min} (e-h) at Barrow. The reanalyses are compared to station observations at Barrow (gray), 1979-2009.

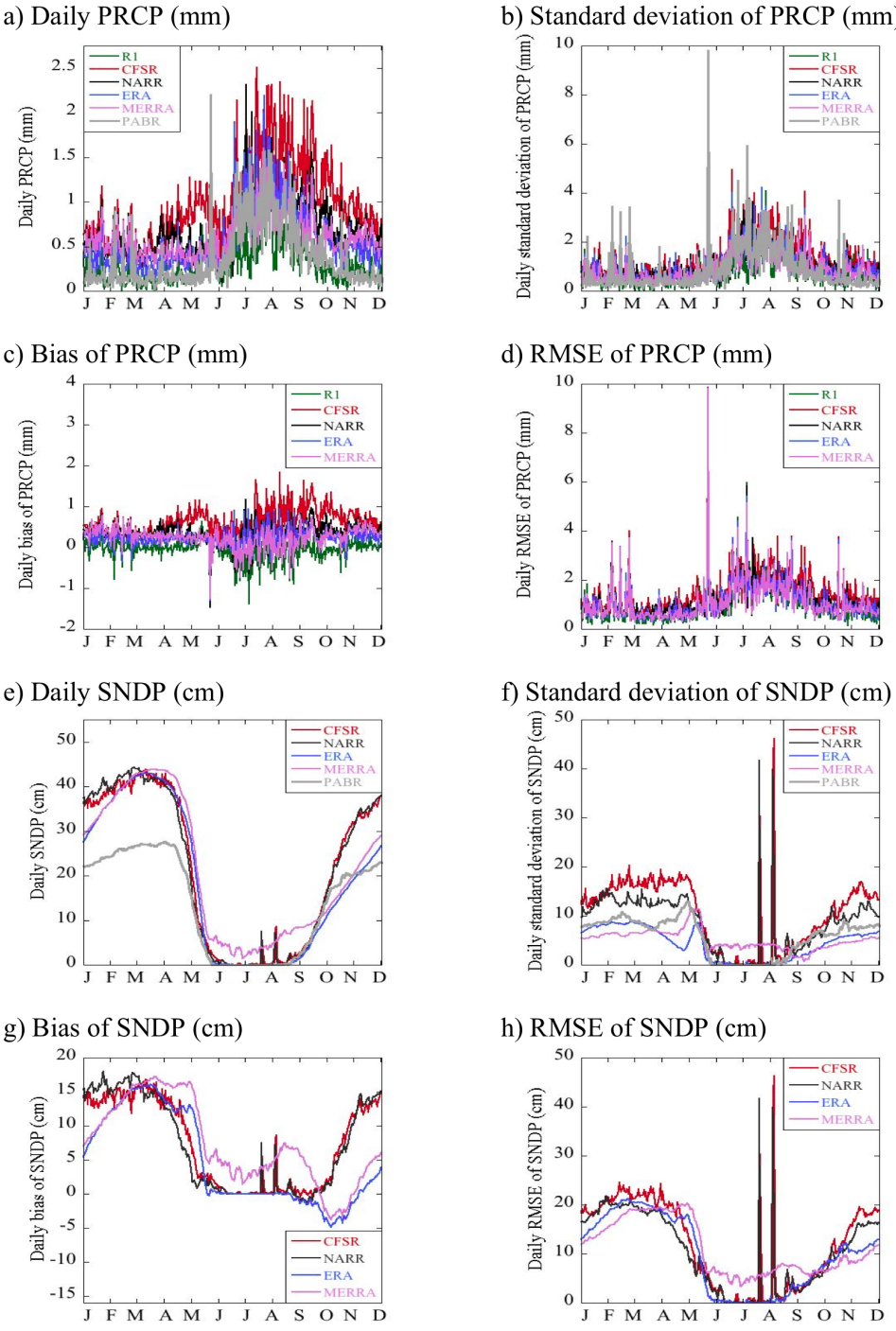

FIG. 4.2.2 Daily climate statistics of PRCP (a-d), and SNDP (e-h) at Barrow. The reanalyses are compared to station observations at Barrow (gray), 1979-2009.

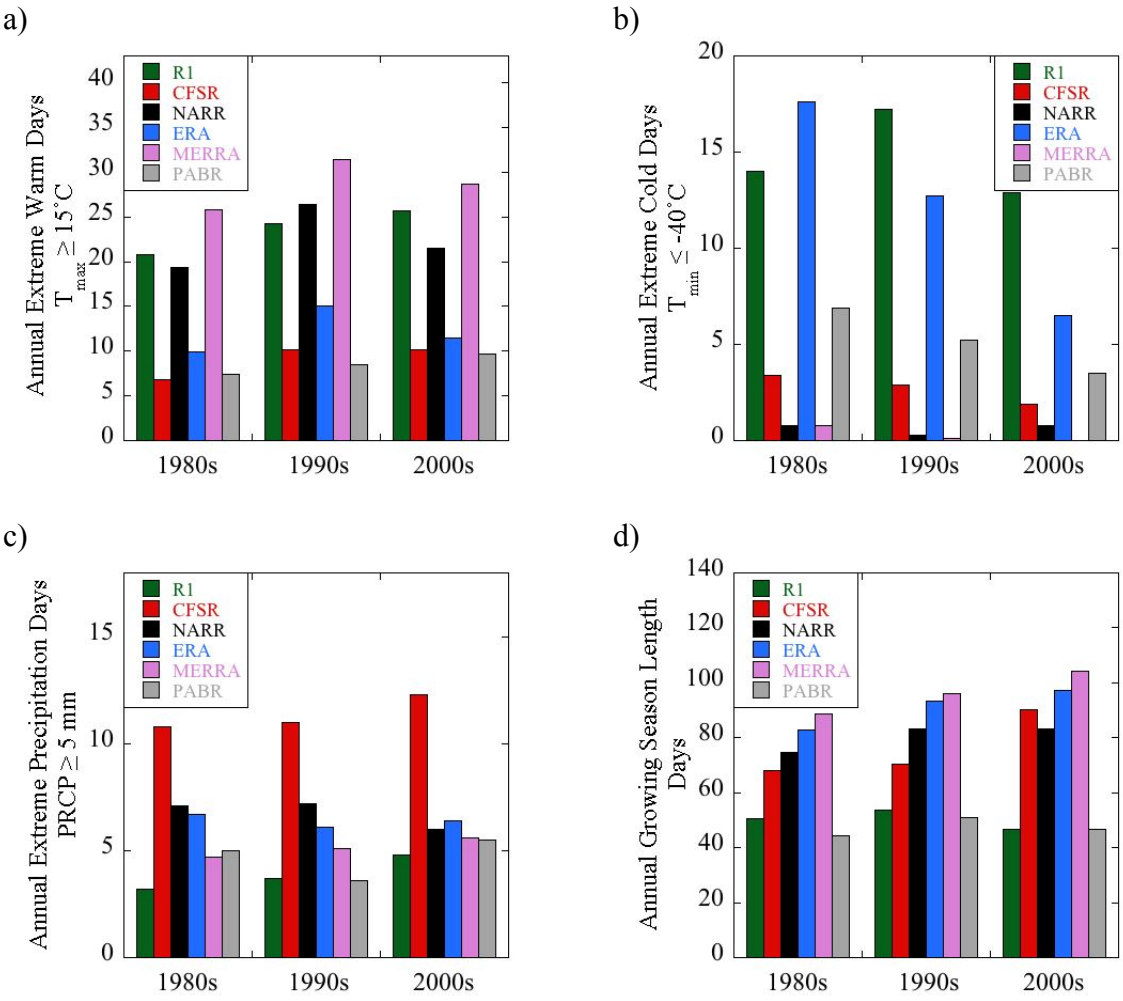

FIG. 4.2.3 Climate extreme indices at Barrow: (a) Decadal-average annual counts of Extreme Warm Days (number of days where $T_{max} \geq 15^{\circ}C$), (b) Extreme Cold Days (number of days where $T_{min} \leq -40^{\circ}C$), (c) Extreme Precipitation Days (number of days where PRCP ≥ 5 mm), (d) Growing Season Length (number of days between the fifth consecutive day when $T_{avg} > 0^{\circ}C$ and the day when $T_{min} \leq -2.2^{\circ}C$ for Barrow.

a) Monthly mean T_{max} (˚C), 1979-1983

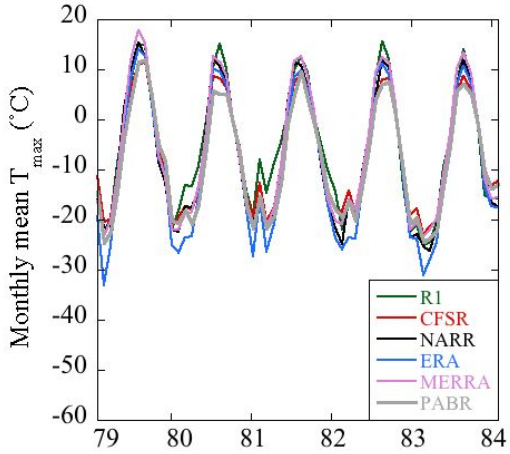

b) Monthly mean T_{max} (˚C), 1984-1988

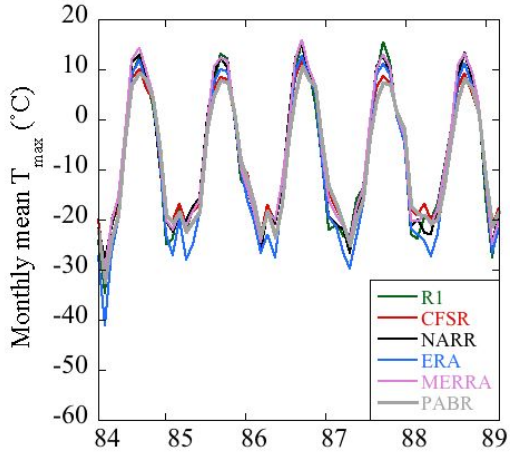

c) Monthly mean T_{max} (˚C), 1989-1993

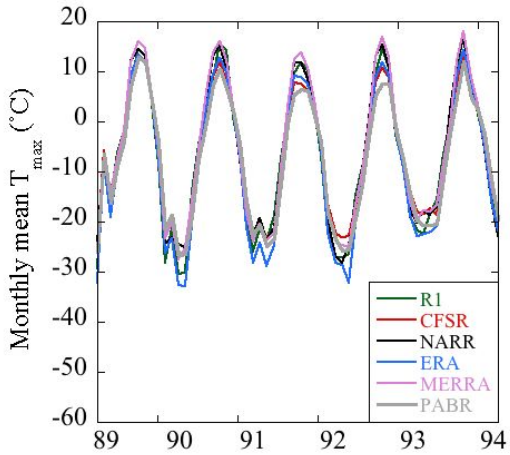

d) Monthly mean T_{max} (˚C), 1994-1998

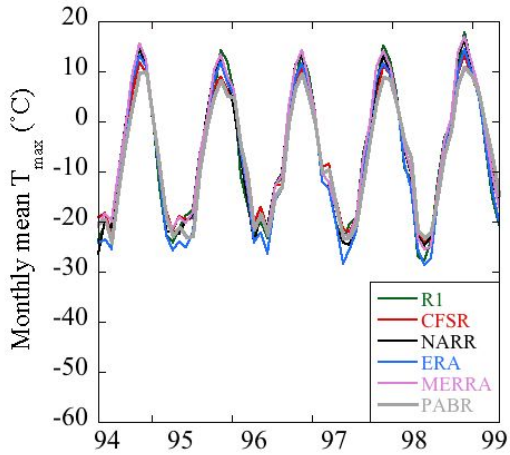

e) Monthly mean T_{max} (˚C), 1999-2003

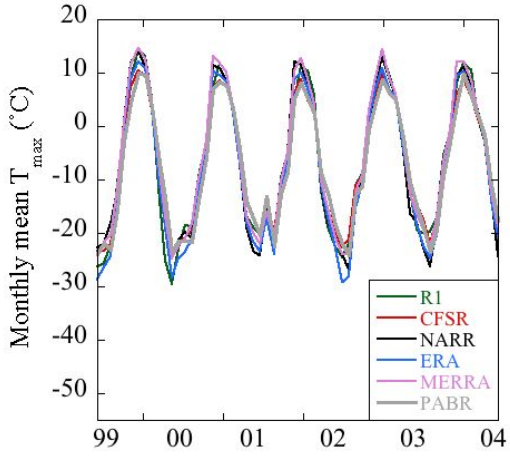

f) Monthly mean T_{max} (˚C), 2004-2009

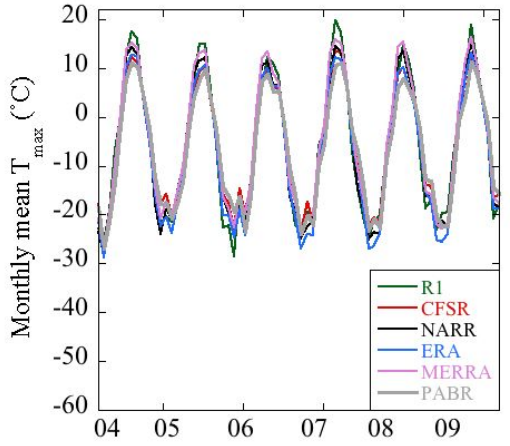

FIG. 4.2.4 Time series of monthly mean T_{max} at Barrow (gray) for a) 1979-1983, b) 1984-1988, c) 1989-1993, d) 1994-1998, e) 1999-2003, and f) 2004-2009.

a) Monthly mean T_{min} (˚C), 1979-1983

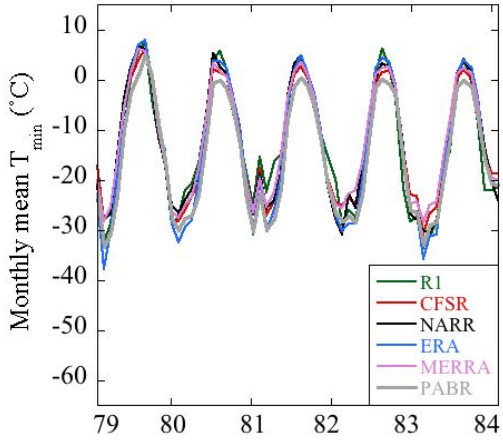

b) Monthly mean T_{min} (˚C), 1984-1988

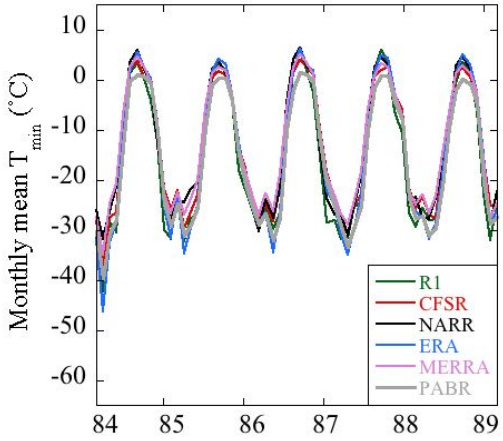

c) Monthly mean T_{min} (˚C), 1989-1993

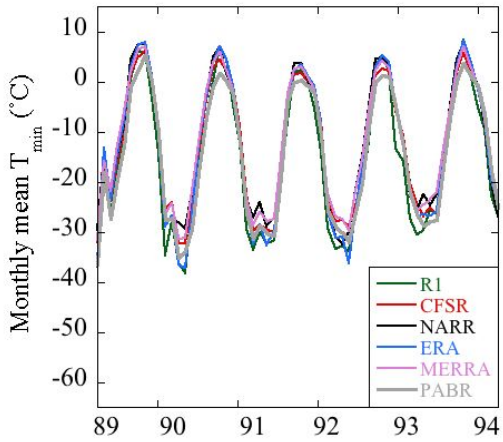

d) Monthly mean T_{min} (˚C), 1994-1998

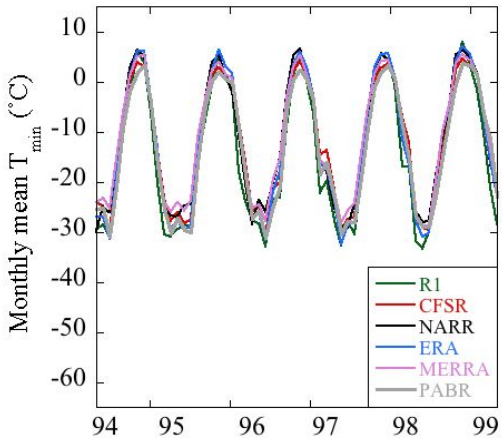

e) Monthly mean T_{min} (˚C), 1999-2003

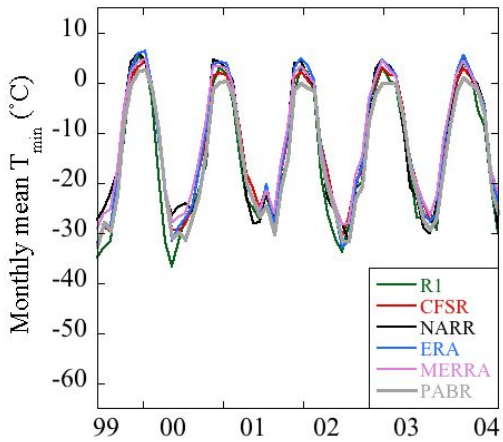

f) Monthly mean T_{min} (˚C), 2004-2009

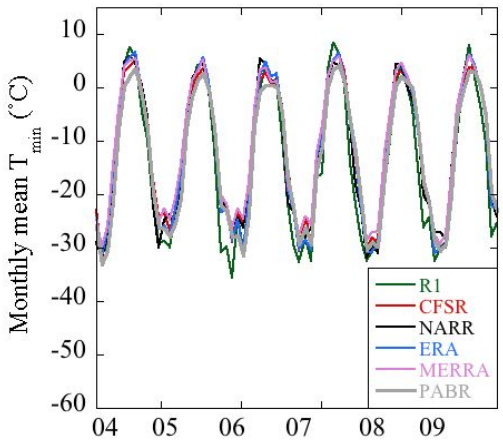

FIG. 4.2.5 Time series of monthly mean T_{min} at Barrow (gray) for a) 1979-1983, b) 1984-1988, c) 1989-1993, d) 1994-1998, e) 1999-2003, and f) 2004-2009.

a) Monthly mean PRCP (mm), 1979-1983

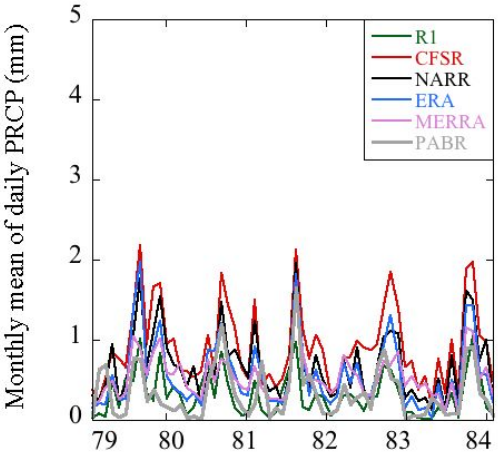

b) Monthly mean PRCP (mm), 1984-1988

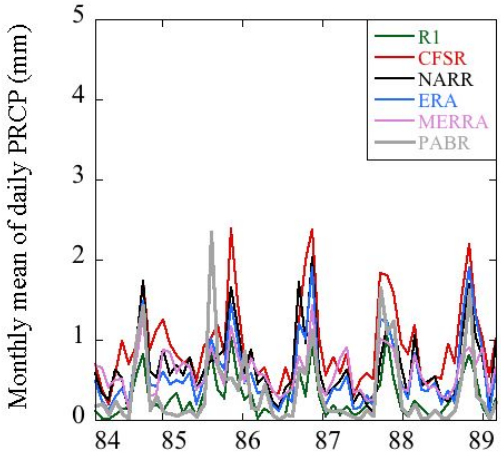

c) Monthly mean PRCP (mm), 1989-1993

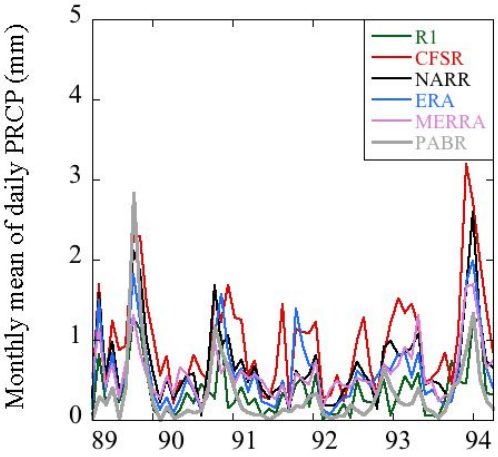

d) Monthly mean PRCP (mm), 1994-1998

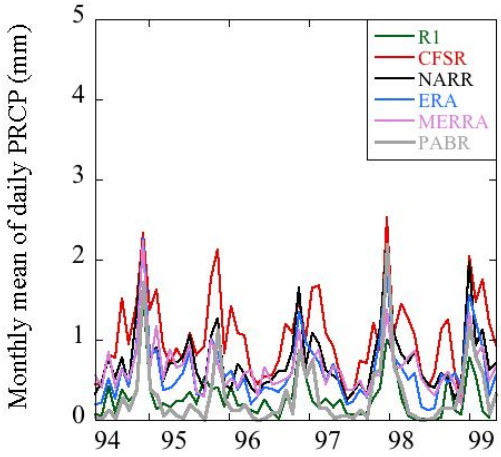

e) Monthly mean PRCP (mm), 1999-2003

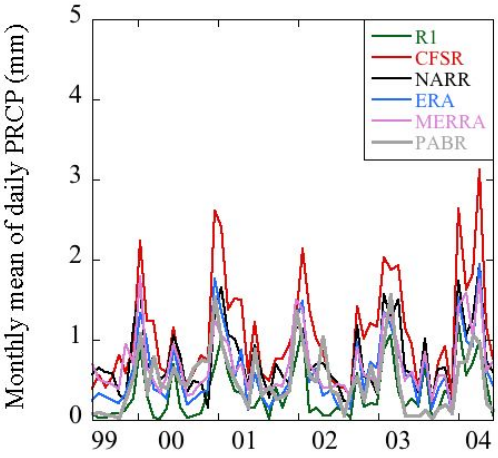

f) Monthly mean PRCP (mm), 2004-2009

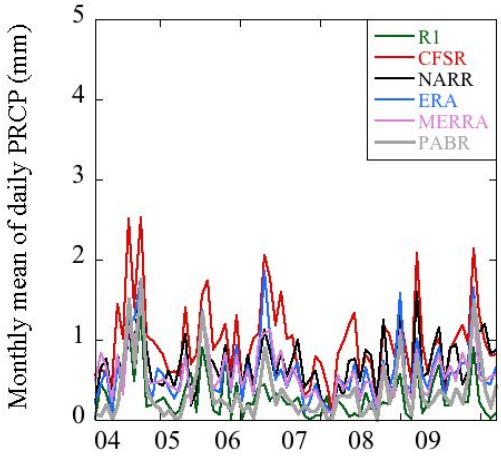

FIG. 4.2.6 Time series of monthly mean PRCP at Barrow (gray) for a) 1979-1983, b) 1984-1988, c) 1989-1993, d) 1994-1998, e) 1999-2003, and f) 2004-2009.

a) Monthly mean SNDP (cm), 1979-1983

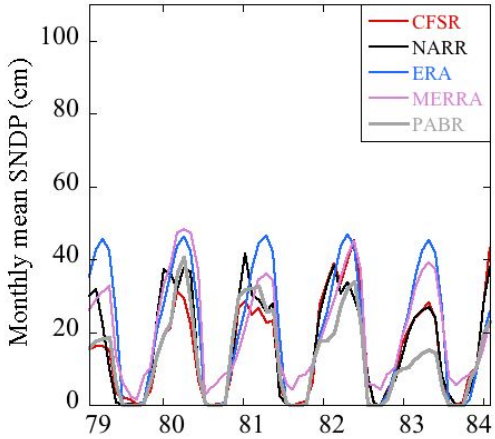

b) Monthly mean SNDP (cm), 1984-1988

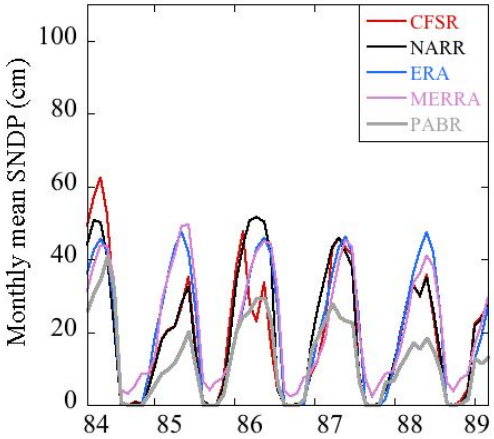

c) Monthly mean SNDP (cm), 1989-1993

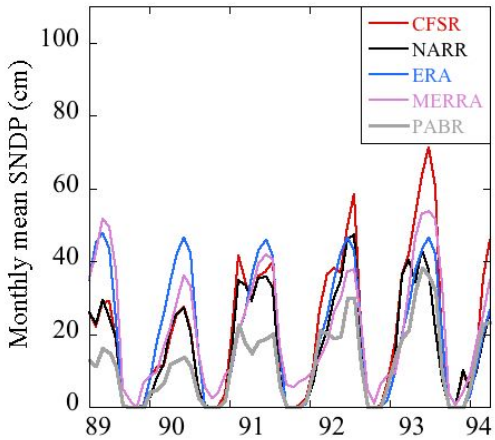

d) Monthly mean SNDP (cm), 1994-1998

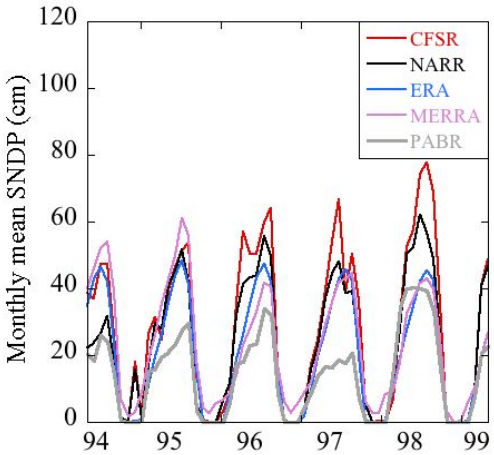

e) Monthly mean SNDP (cm), 1999-2003

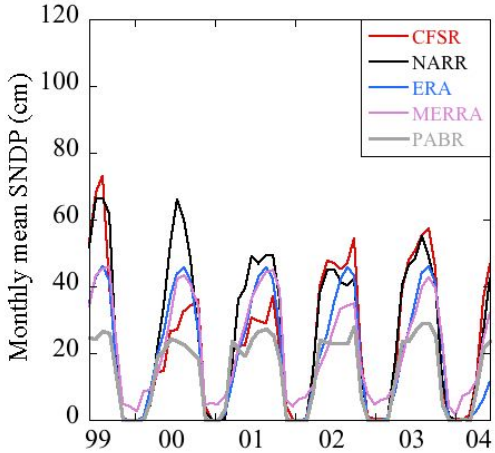

f) Monthly mean SNDP (cm), 2004-2009

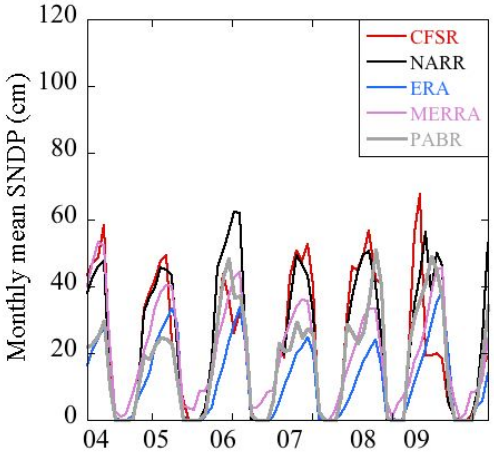

FIG. 4.2.7 Time series of monthly mean SNDP at Barrow (gray) for a) 1979-1983, b) 1984-1988, c) 1989-1993, d) 1994-1998, e) 1999-2003, and f) 2004-2009.

Table 4.2.1 Top performing reanalyses for Barrow, Alaska, 1979-2009. Performance is based on average RMSE value relative to station observations. The months included in each season are indicated by one-letter abbreviations in parentheses.

	T_{max}	T_{min}	PRCP	SNDP
WINTER (NDJFM)	MERRA	MERRA	R1	MERRA
SPRING (AM)	CFSR	CFSR	R1	NARR
SUMMER (JJA)	CFSR	CFSR	MERRA	ERA
AUTUMN (SO)	CFSR	MERRA	MERRA	NARR

Table 4.2.2 Seasonal RMSE and bias (high/low) for Barrow, Alaska, 1979-2009. Each number represents an average of daily RMSE or bias for the entire season over all 31 years. The RMSE and bias values are relative to station observations.

	WINTER		SPRING		SUMMER		AUTUMN	
T_{max} (˚C)	RMSE	Bias	RMSE	Bias	RMSE	Bias	RMSE	Bias
R1	6.3	-1.0	4.5	2.7	5.9	4.1	3.9	-1.1
CFSR	3.3	0.8	2.8	1.8	2.6	0.9	1.6	0.0
NARR	4.7	-1.3	3.5	2.4	5.0	3.7	2.7	-0.6
ERA	5.5	-3.7	3.0	1.2	4.0	2.3	2.9	-1.0
MERRA	3.1	-0.3	3.7	2.9	5.9	5.0	2.1	0.1
T_{min} (˚C)	RMSE	Bias	RMSE	Bias	RMSE	Bias	RMSE	Bias
R1	6.8	-1.2	5.8	-0.2	4.2	2.3	5.8	-2.9
CFSR	4.3	1.9	4.2	2.6	2.6	1.6	2.9	1.5
NARR	5.8	1.5	5.3	3.5	4.4	3.2	3.5	0.6
ERA	4.3	-0.1	4.2	2.8	4.2	3.4	3.1	1.1
MERRA	4.2	2.7	5.6	4.7	3.5	2.5	2.7	1.0
PRCP (mm)	RMSE	Bias	RMSE	Bias	RMSE	Bias	RMSE	Bias
R1	0.9	0.0	0.7	0.0	2.1	-0.2	1.4	-0.1
CFSR	1.3	0.5	1.1	0.7	2.4	0.6	1.9	0.9
NARR	1.1	0.4	0.9	0.4	2.1	0.2	1.5	0.4
ERA	1.0	0.2	0.7	0.2	2.1	0.2	1.5	0.3
MERRA	1.0	0.4	0.7	0.3	2.0	0.1	1.4	0.2
SNDP (cm)	RMSE	Bias	RMSE	Bias	RMSE	Bias	RMSE	Bias
CFSR	19.2	13.1	16.6	9.4	7.8	0.8	4.9	0.7
NARR	17.2	13.7	13.4	7.5	7.5	0.6	4.5	0.1
ERA	16.0	7.3	16.3	11.4	0.9	0.1	5.0	-1.6
MERRA	14.1	8.2	18.4	14.6	5.7	4.0	6.8	3.1

4.3 Nome, Alaska

Nome is located in the West Coast climate division (Bieniek et al. 2012) along the southern shore of the Seward Peninsula. Nome's coordinates are 64.51˚N, 165.44˚W, and its elevation is close to sea level. The altitude of the nearest land grid point to Nome used for each reanalysis evaluation is identified in Table 2.2.1. An overall evaluation based on 16 possible combinations between four seasons and four climate variables, indicates that NARR and MERRA are the top models five times each (Table 4.3.1). NARR and MERRA are followed by ERA-Interim (three), NCEP-R1 (two), and CFSR (one). Model biases of all seasons and variables for Nome are given in Table 4.3.2.

The observed mean annual cycle of daily maximum temperature (T_{max}) (see gray line, Fig. 4.3.1a) has a low temperature of -12.0˚C in late January, and a high temperature of 17.1˚C in July. The standard deviation of T_{max} ranges from a January maximum of 10.3˚C to an August minimum of 2.2˚C (Fig. 4.3.1b). Model biases of T_{max} (Fig. 4.3.1c) are generally negative during all seasons, except for MERRA, which has a slight positive bias during summer. MERRA has the lowest seasonal RMSE of T_{max} (see lavender line, Fig. 4.3.1d), which is 1.9˚C during autumn (Table 4.3.2). MERRA, along with CFSR, also has the best representation of Annual Extreme Warm Days (Fig. 4.3.3a), which are defined as days that have a high temperature equal to or greater than 20˚C. ERA-Interim does not produce any Annual Extreme Warm Days during the 31-year period for Nome.

The observed mean annual cycle of daily minimum temperature (T_{min}) (see gray line, Fig. 4.3.1e) has a low temperature of -22.1˚C in late January, and a high temperature of 8.9˚C in July. The standard deviation of T_{min} ranges from a February maximum of 12.0˚C to a July minimum of 2.0˚C (Fig. 4.3.1f). Model biases of T_{min} (Fig. 4.3.1g) are mixed. ERA-Interim and MERRA

have positive T_{min} biases, while NCEP-R1 and CFSR biases are negative throughout the year. NARR has low T_{min} bias throughout the year. CFSR has the lowest seasonal RMSE of T_{min} (see red line, Fig. 4.3.1h), which is 2.4˚C during summer (Table 4.3.2). The models do not represent the number of Annual Extreme Cold Days (Fig. 4.3.3b) well, which are defined as days that have a low temperature equal to or less than -30˚C. NCEP-R1 and CFSR produce too many, while NARR, ERA-Interim, and MERRA have too few. However, NCEP-R1, CFSR, and NARR do reliably estimate Growing Season Length at Nome (Fig. 4.3.3d). Growing Season Length begins each year following the fifth consecutive day with an average daily temperature above freezing and terminates when T_{min} is at or below -2.2˚C.

The observed mean annual cycle of daily precipitation (PRCP) (see gray line, Fig. 4.3.2a) has a minimum of 0.15 mm in May, and a maximum of 4.7 mm in August. The standard deviation of PRCP ranges from an April minimum of 0.40 mm to a maximum around 8.0 mm in late summer (Fig. 4.3.2b). The one-day maximum standard deviation of PRCP is 14.5 mm, which is a result of one heavy-precipitation event when 14.7 mm fell on 6 Apr 2001. Model biases of PRCP (Fig. 4.3.2c) for NARR, ERA-Interim, and MERRA are generally low. NCEP-R1 has a persistent negative PRCP bias, while CFSR has a positive one. NCEP-R1 has the lowest seasonal RMSE of PRCP (see green line, Fig. 4.3.2d), which is 1.6 mm during winter (Table 4.3.2). ERA-Interim has the best representation of Annual Extreme Precipitation Days (Fig. 4.3.3c), which are defined as days that have an accumulated precipitation equal to or greater than 10 mm. CFSR produces twice as many Annual Extreme Precipitation Days compared to observations.

The observed mean annual cycle of daily snow depth (SNDP) (see gray line, Fig. 4.3.2e) reaches a maximum of 50.1 cm in March, and melts completely by late May. The standard

deviation of SNDP peaks at 44.9 cm in March (Fig. 4.3.2f). ERA-Interim has a negative SNDP bias (Fig. 4.3.2g) during the snow season, while CFSR and NARR have large positive biases. For CFSR and NARR, these biases stem primarily from 1979-1983, when CFSR has a one-day SNDP of 929 cm, for example. Following this time period, both CFSR and NARR represent daily SNDP more accurately (Fig. 4.3.7). NARR and ERA-Interim have the lowest seasonal RMSE of SNDP (see black and blue lines, Fig. 4.3.2h), which is 0.1 cm during summer (Table 4.3.2).

NARR and MERRA are the top performing reanalysis data sets relative to station observations for Nome. NARR is the preferred reanalysis for daily T_{min}, while MERRA is for T_{max}. ERA-Interim fails to represent daily T_{max} during summer, and does not produce any Annual Extreme Warm Days. CFSR has a large positive daily PRCP bias during summer that is supported by its overestimation of Annual Extreme Precipitation Days. CFSR, along with NARR, also has a large positive SNDP bias during the snow season. Much of this discrepancy results from the period, 1979-1983, before the bias reduces substantially over the rest of the 31-year period. Reanalysis data users that are only interested in a particular variable or season at Nome should refer to Tables 4.3.1 and 4.3.2 to help guide the selection of the best available data set. The 31-year time series of T_{max} (Fig. 4.3.4), T_{min} (Fig. 4.3.5), PRCP (Fig. 4.3.6), and SNDP (Fig. 4.3.7) are available for users that are primarily interested in a particular segment of the period used for this study.

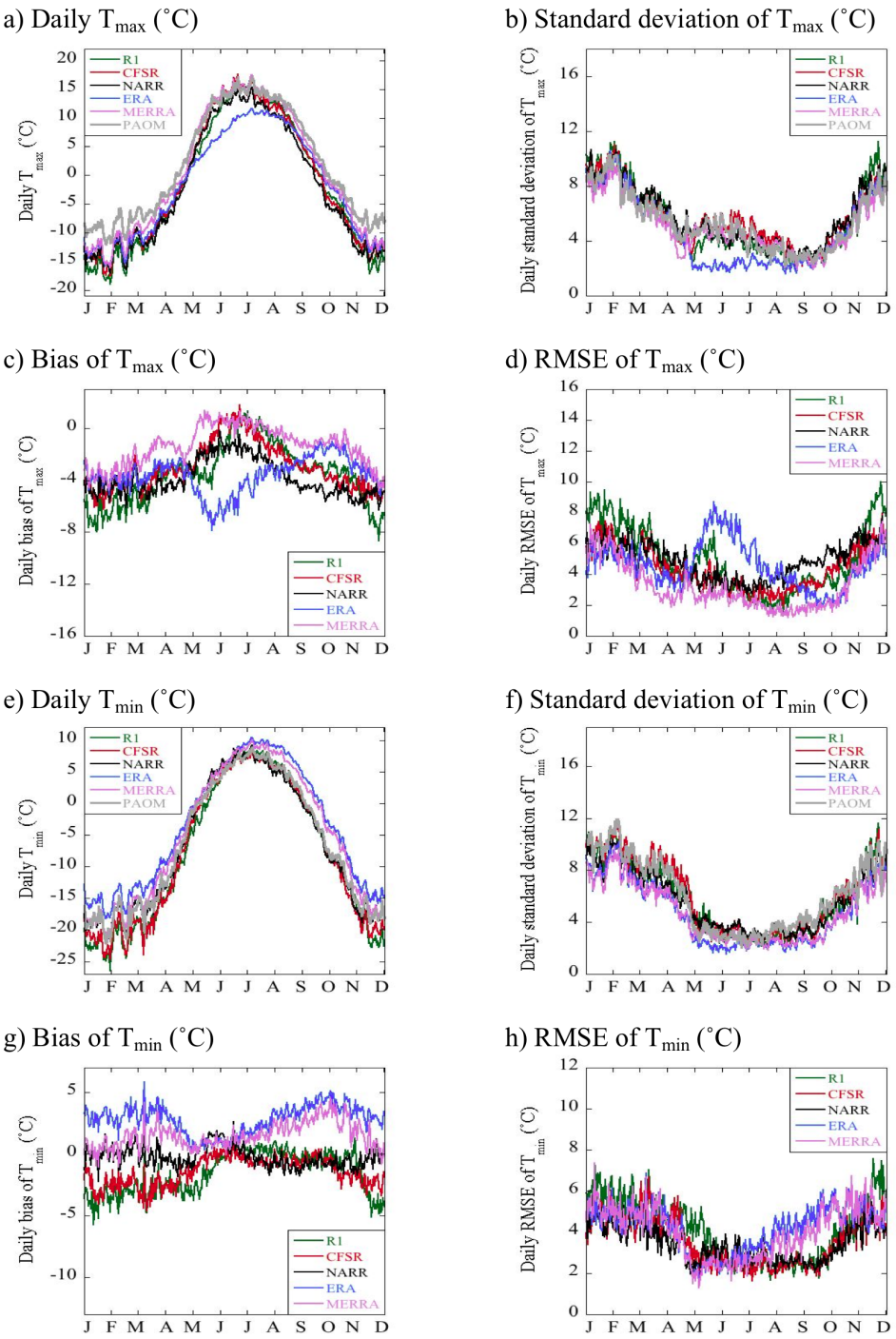

FIG. 4.3.1 Daily climate statistics of T_{max} (a-d), and T_{min} (e-h) at Nome. The reanalyses are compared to station observations at Nome (gray), 1979-2009.

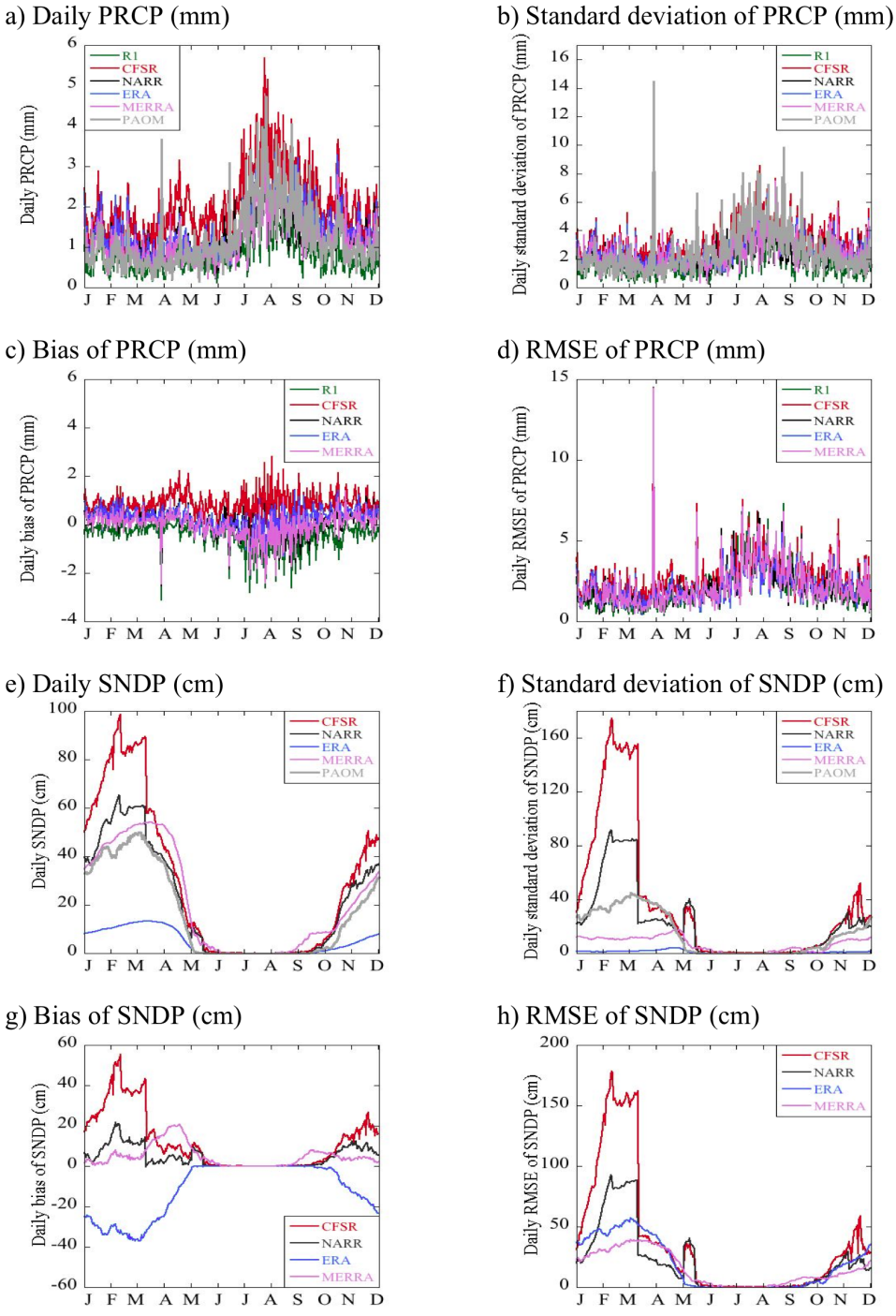

FIG. 4.3.2 Daily climate statistics of PRCP (a-d), and SNDP (e-h) at Nome. The reanalyses are compared to station observations at Nome (gray), 1979-2009.

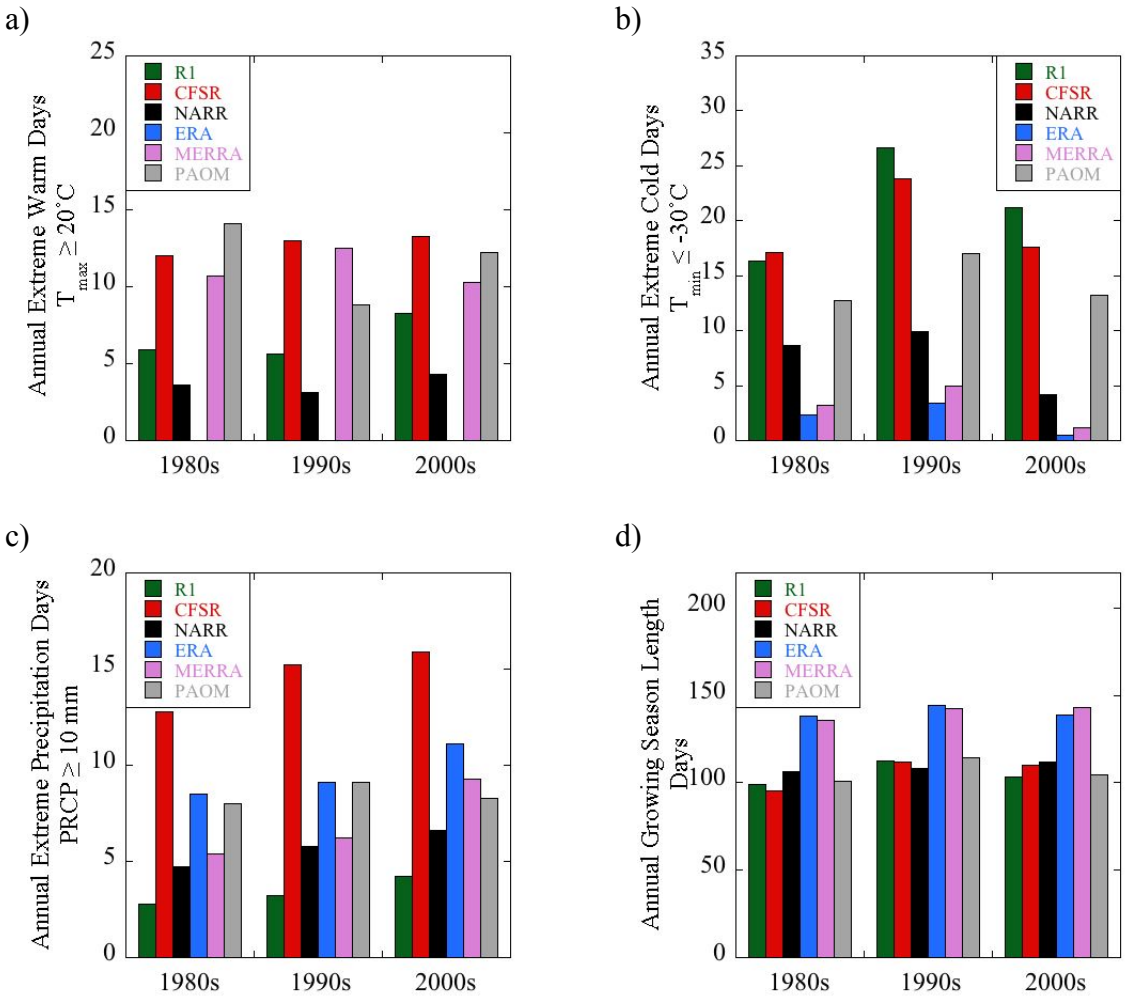

FIG. 4.3.3 Climate extreme indices at Nome: (a) Decadal-average annual counts of Extreme Warm Days (number of days where $T_{max} \geq 20^{\circ}C$), (b) Extreme Cold Days (number of days where $T_{min} \leq -30^{\circ}C$), (c) Extreme Precipitation Days (number of days where PRCP ≥ 10 mm), (d) Growing Season Length (number of days between the fifth consecutive day when $T_{avg} > 0^{\circ}C$ and the day when $T_{min} \leq -2.2^{\circ}C$ for Nome.

a) Monthly mean T_{max} (˚C), 1979-1983

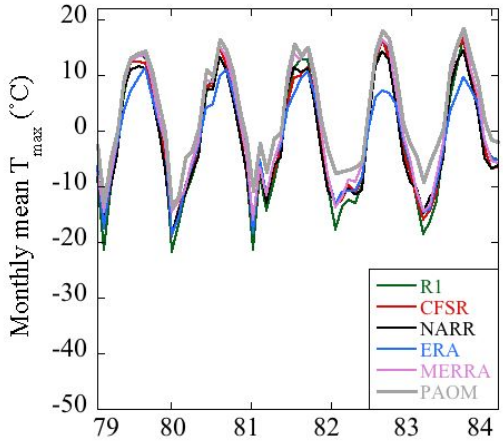

b) Monthly mean T_{max} (˚C), 1984-1988

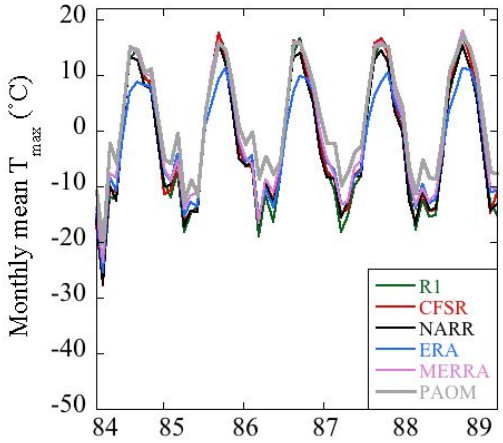

c) Monthly mean T_{max} (˚C), 1989-1993

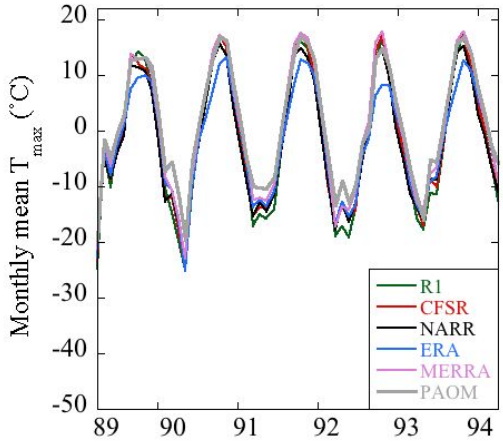

d) Monthly mean T_{max} (˚C), 1994-1998

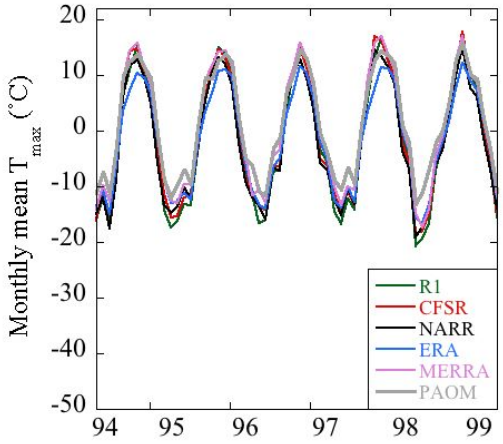

e) Monthly mean T_{max} (˚C), 1999-2003

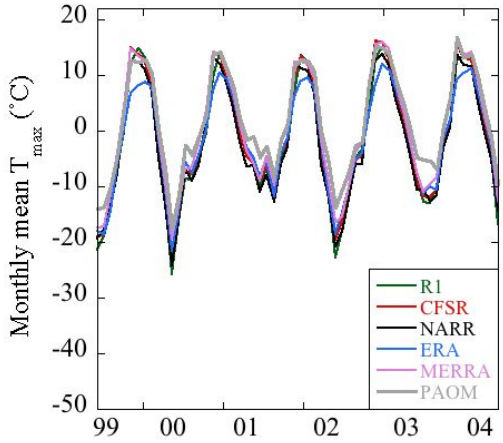

f) Monthly mean T_{max} (˚C), 2004-2009

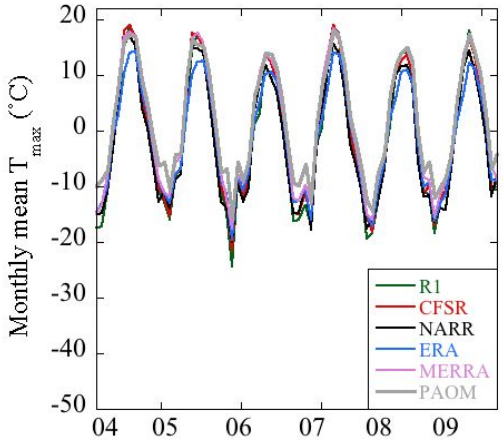

FIG. 4.3.4 Time series of monthly mean T_{max} at Nome (gray) for a) 1979-1983, b) 1984-1988, c) 1989-1993, d) 1994-1998, e) 1999-2003, and f) 2004-2009.

a) Monthly mean T_{min} (˚C), 1979-1983

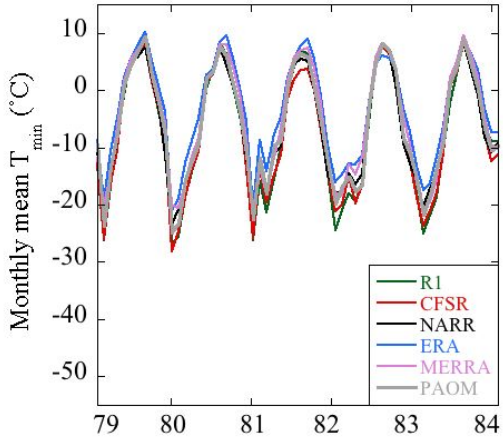

b) Monthly mean T_{min} (˚C), 1984-1988

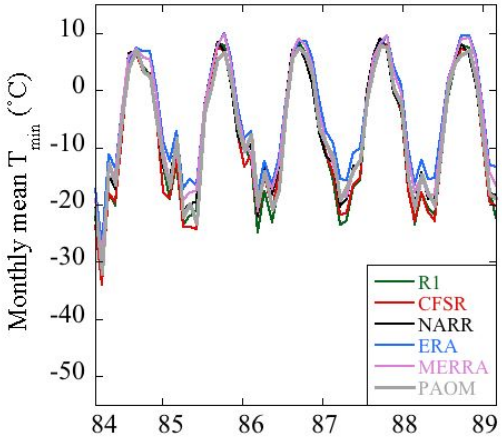

c) Monthly mean T_{min} (˚C), 1989-1993

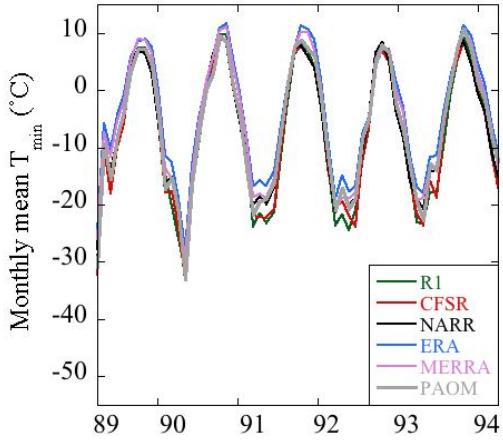

d) Monthly mean T_{min} (˚C), 1994-1998

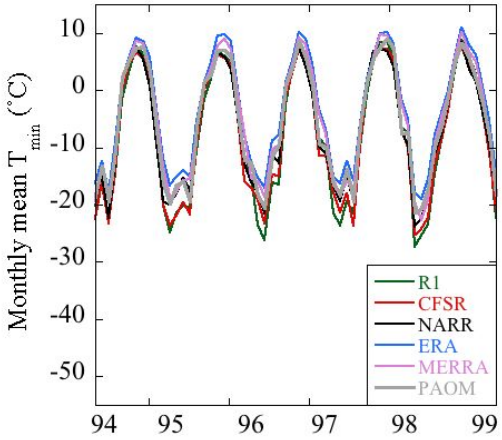

e) Monthly mean T_{min} (˚C), 1999-2003

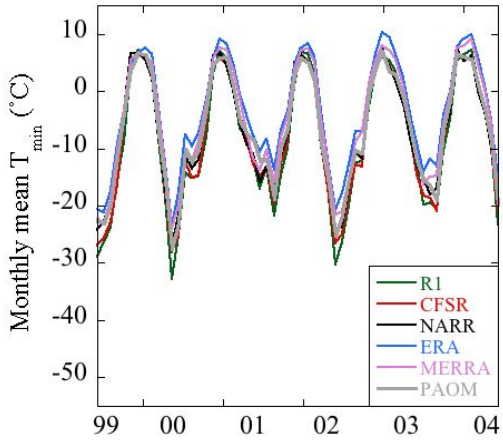

f) Monthly mean T_{min} (˚C), 2004-2009

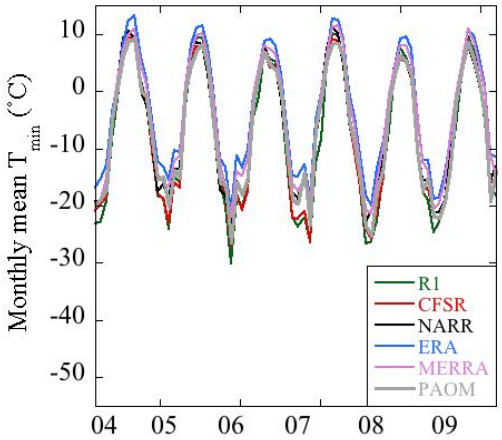

FIG. 4.3.5 Time series of monthly mean T_{min} at Nome (gray) for a) 1979-1983, b) 1984-1988, c) 1989-1993, d) 1994-1998, e) 1999-2003, and f) 2004-2009.

a) Monthly mean PRCP (mm), 1979-1983

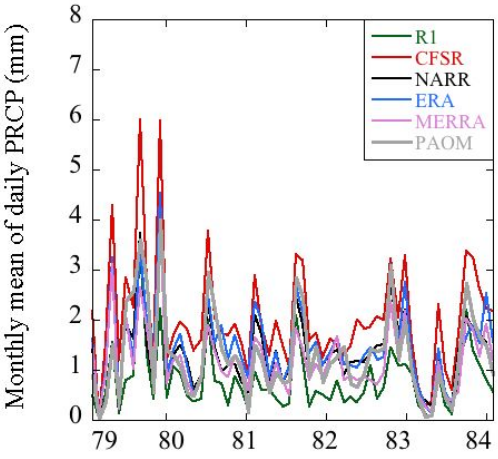

b) Monthly mean PRCP (mm), 1984-1988

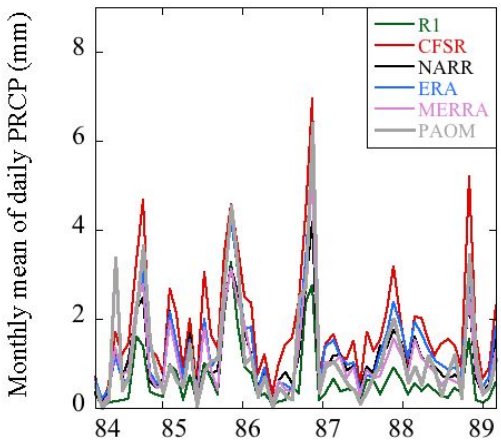

c) Monthly mean PRCP (mm), 1989-1993

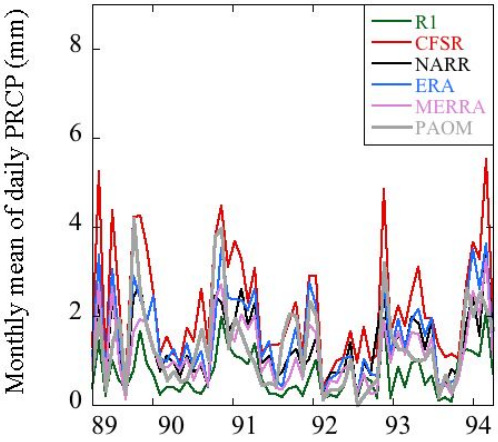

d) Monthly mean PRCP (mm), 1994-1998

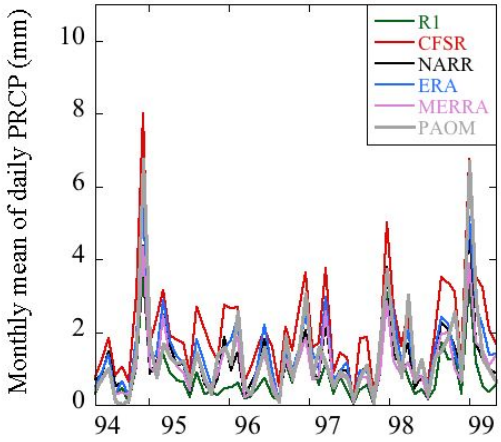

e) Monthly mean PRCP (mm), 1999-2003

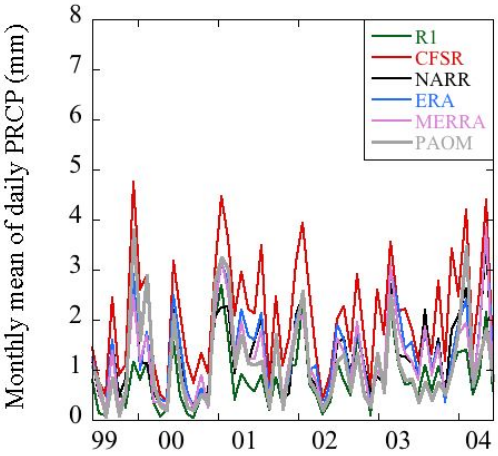

f) Monthly mean PRCP (mm), 2004-2009

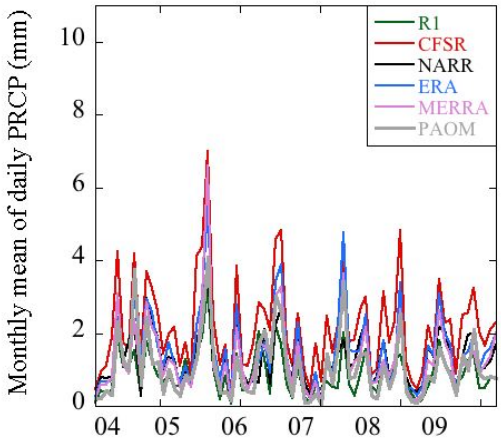

FIG. 4.3.6 Time series of monthly mean PRCP at Nome (gray) for a) 1979-1983, b) 1984-1988, c) 1989-1993, d) 1994-1998, e) 1999-2003, and f) 2004-2009.

a) Monthly mean SNDP (cm), 1979-1983

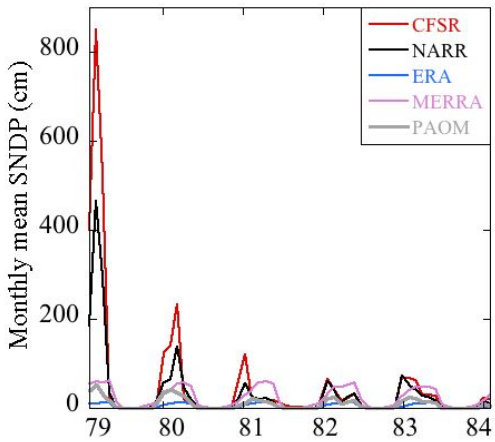

b) Monthly mean SNDP (cm), 1984-1988

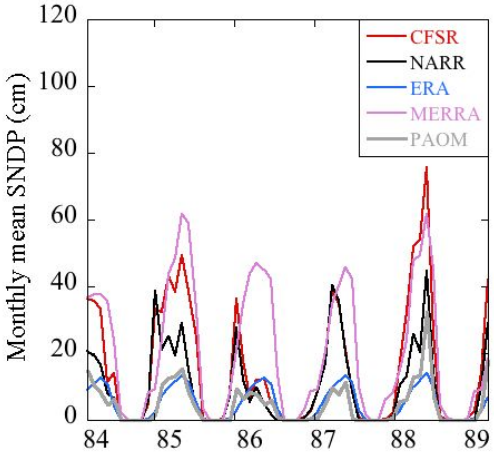

c) Monthly mean SNDP (cm), 1989-1993

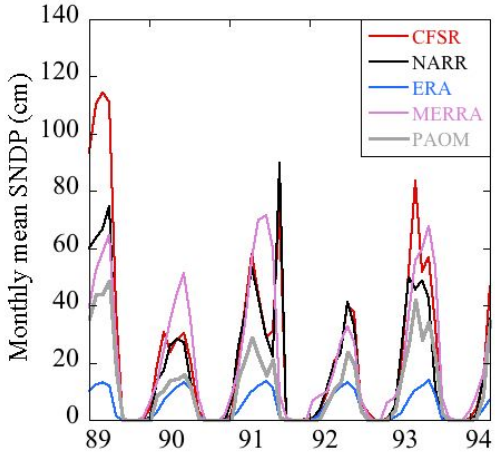

d) Monthly mean SNDP (cm), 1994-1998

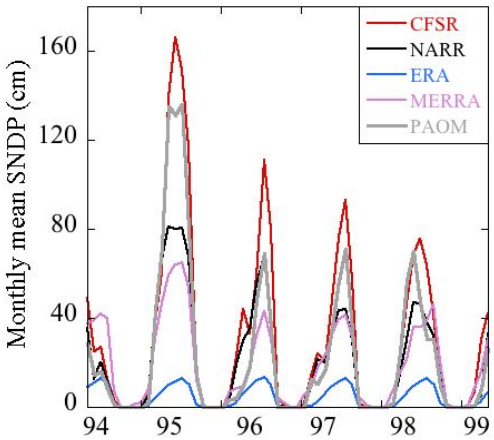

e) Monthly mean SNDP (cm), 1999-2003

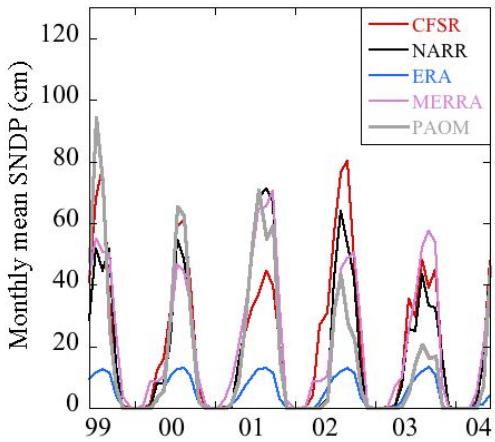

f) Monthly mean SNDP (cm), 2004-2009

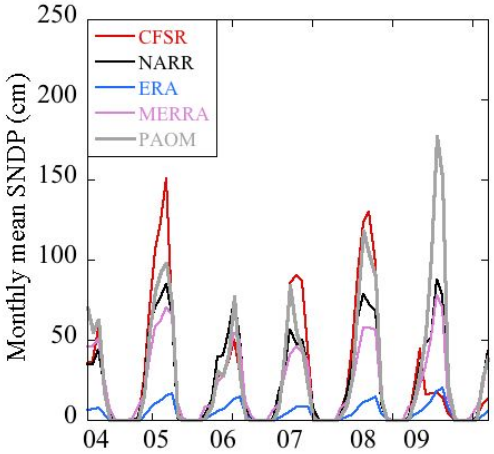

FIG. 4.3.7 Time series of monthly mean SNDP at Nome (gray) for a) 1979-1983, b) 1984-1988, c) 1989-1993, d) 1994-1998, e) 1999-2003, and f) 2004-2009.

Table 4.3.1 Top performing reanalyses for Nome, Alaska, 1979-2009. Performance is based on average RMSE value relative to station observations. The months included in each season are indicated by one-letter abbreviations in parentheses.

	T_{max}	T_{min}	PRCP	SNDP
WINTER (NDJFM)	ERA	NARR	R1	MERRA
SPRING (AM)	MERRA	NARR	R1	NARR
SUMMER (JJA)	MERRA	CFSR	MERRA	ERA
AUTUMN (SO)	MERRA	NARR	NARR	ERA

Table 4.3.2 Seasonal RMSE and bias (high/low) for Nome, Alaska, 1979-2009. Each number represents an average of daily RMSE or bias for the entire season over all 31 years. The RMSE and bias values are relative to station observations.

	WINTER		SPRING		SUMMER		AUTUMN	
T_{max} (˚C)	RMSE	Bias	RMSE	Bias	RMSE	Bias	RMSE	Bias
R1	7.1	-5.6	4.8	-3.4	3.2	-0.7	3.3	-2.8
CFSR	5.9	-4.6	4.0	-2.9	3.0	-0.4	3.6	-3.1
NARR	6.0	-4.8	4.5	-3.6	3.5	-2.0	4.9	-4.6
ERA	4.8	-3.5	4.9	-3.8	5.9	-4.8	2.9	-2.1
MERRA	4.9	-2.7	2.7	-0.9	2.3	0.3	1.9	-1.0
T_{min} (˚C)	RMSE	Bias	RMSE	Bias	RMSE	Bias	RMSE	Bias
R1	5.5	-2.8	4.6	-2.7	2.5	0.1	2.7	-0.2
CFSR	4.7	-2.4	3.8	-1.7	2.4	-0.3	2.6	-0.5
NARR	4.3	-0.2	3.1	-0.3	2.9	0.2	2.6	-0.9
ERA	4.9	3.2	3.5	1.9	3.2	1.8	4.9	4.0
MERRA	5.1	1.2	3.4	1.1	2.8	1.3	4.3	2.8
PRCP (mm)	RMSE	Bias	RMSE	Bias	RMSE	Bias	RMSE	Bias
R1	1.6	-0.2	2.5	-0.2	3.4	-0.8	2.8	-0.7
CFSR	2.4	0.8	3.1	1.0	3.6	0.8	3.1	0.9
NARR	1.8	0.3	2.5	0.2	3.2	-0.3	2.8	-0.3
ERA	2.0	0.5	2.6	0.2	3.0	-0.2	2.8	0.3
MERRA	1.9	0.2	2.6	0.1	3.2	-0.5	2.9	-0.1
SNDP (cm)	RMSE	Bias	RMSE	Bias	RMSE	Bias	RMSE	Bias
CFSR	95.5	25.4	28.7	8.0	1.2	0.3	3.3	1.3
NARR	50.4	9.0	22.4	3.9	0.1	0.0	2.8	0.6
ERA	39.0	-23.9	26.4	-10.6	0.1	0.0	2.3	-0.3
MERRA	26.6	4.5	25.7	13.3	1.8	0.4	6.1	4.3

4.4 Bethel, Alaska

Bethel is located in the West Coast climate division (Bieniek et al. 2012) in the Yukon-Kuskokwim Delta. Bethel's coordinates are 60.79˚N, 161.83˚W, and its elevation is 31 m above sea level. The altitude of the nearest land grid point to Bethel used for each reanalysis evaluation is identified in Table 2.2.1 An overall evaluation based on 16 possible combinations between four seasons and four climate variables, indicates that ERA-Interim is the top model seven times (Table 4.4.1). ERA-Interim is followed by CFSR (five), MERRA (three), NCEP-R1 (one), and NARR (zero). Model biases of all seasons and variables for Bethel are given in Table 4.4.2.

The observed mean annual cycle of daily maximum temperature (T_{max}) (see gray line, Fig. 4.4.1a) has a low temperature of -11.9˚C in late January, and a high temperature of 19.6˚C in July. The standard deviation of T_{max} ranges from a February maximum of 12.0˚C to an August minimum of 2.1˚C (Fig. 4.4.1b). Model biases of T_{max} (Fig. 4.4.1c) are generally negative. NCEP-R1 has the coldest bias during all seasons except summer when ERA-Interim has a negative bias of 2.7˚C. MERRA has the lowest seasonal RMSE of T_{max} (see lavender line, Fig. 4.4.1d), which is 1.3˚C during autumn (Table 4.4.2). ERA-Interim produces too few Annual Extreme Warm Days (Fig. 4.4.3a), which are defined as days that have a high temperature equal to or greater than 25˚C.

The observed mean annual cycle of daily minimum temperature (T_{min}) (see gray line, Fig. 4.4.1e) has a low temperature of -19.6˚C in January, and a high temperature of 10.0˚C in July. The standard deviation of T_{min} ranges from a February maximum of 11.7˚C to a July minimum of 1.7˚C (Fig. 4.4.1f). Model biases of T_{min} (Fig. 4.4.1g) are positive; ERA-Interim has the warmest bias during all seasons except summer. NCEP-R1 is the only reanalysis that has a persistently cold T_{min} bias. CFSR has the lowest seasonal RMSE of T_{min} (see red line, Fig.

4.4.1h), which is 1.9˚C during summer (Table 4.4.2). CFSR and MERRA have the best representation of the number of Annual Extreme Cold Days (Fig. 4.4.3b), which are defined as days that have a low temperature equal to or less than -30˚C. NCEP-R1 slightly underestimates Growing Season Length at Bethel (Fig. 4.4.3d), while the other models overestimate it by approximately two weeks per year. Growing Season Length begins each year following the fifth consecutive day with an average daily temperature above freezing and terminates when T_{min} is at or below -2.2˚C.

The observed mean annual cycle of daily precipitation (PRCP) (see gray line, Fig. 4.4.2a) has a minimum of 0.16 mm in April, and a maximum near 4.0 mm in August. The standard deviation of PRCP ranges from January minimum of 0.36 mm to an August maximum close to 8.0 mm (Fig. 4.4.2b). Model biases of PRCP (Fig. 4.4.2c) are generally positive throughout the year. CFSR has the largest positive PRCP biases during all seasons, which frequently exceed 1.0 mm. ERA-Interim and MERRA have the lowest seasonal RMSE of PRCP (see blue and lavender lines, Fig. 4.4.2d), which is 2.0 mm during spring (Table 4.4.2). MERRA has the best representation of Annual Extreme Precipitation Days (Fig. 4.4.3c), which are defined as days that have an accumulated precipitation equal to or greater than 10 mm. CFSR produces twice as many Annual Extreme Precipitation Days compared to observations.

The observed mean annual cycle of daily snow depth (SNDP) (see gray line, Fig. 4.4.2e) reaches a maximum of 23.8 cm in late January, and melts completely by early May. The standard deviation of SNDP peaks at 17.7 cm in February (Fig. 4.4.2f). ERA-Interim has a low SNDP bias (Fig. 4.4.2g) during the snow season, while the other models have large positive biases – MERRA and CFSR, in particular. MERRA also has a much shorter snow-free season compared

to observations. ERA-Interim has the lowest seasonal RMSE of SNDP (see blue line, Fig. 4.4.2h), which is 0.0 cm during summer (Table 4.4.2).

ERA-Interim is the top performing reanalysis data set relative to station observations for Bethel. ERA-Interim is the best model for representing daily PRCP and SNDP, however, it fails to represent Annual Extreme Warm Days during summer. CFSR is the top model for daily T_{min}, but has a large positive daily PRCP bias during summer that is consistent with the overestimation by CFSR of Annual Extreme Precipitation Days. CFSR, along with MERRA, also has a large positive SNDP bias during the snow season. MERRA is best model for T_{max}. Reanalysis data users that are only interested in a particular variable or season at Bethel should refer to Tables 4.4.1 and 4.4.2 to help guide the selection of the best available data set. The 31-year time series of T_{max} (Fig. 4.4.4), T_{min} (Fig. 4.4.5), PRCP (Fig. 4.4.6), and SNDP (Fig. 4.4.7) are available for users that are primarily interested in a particular segment of the period used for this study.

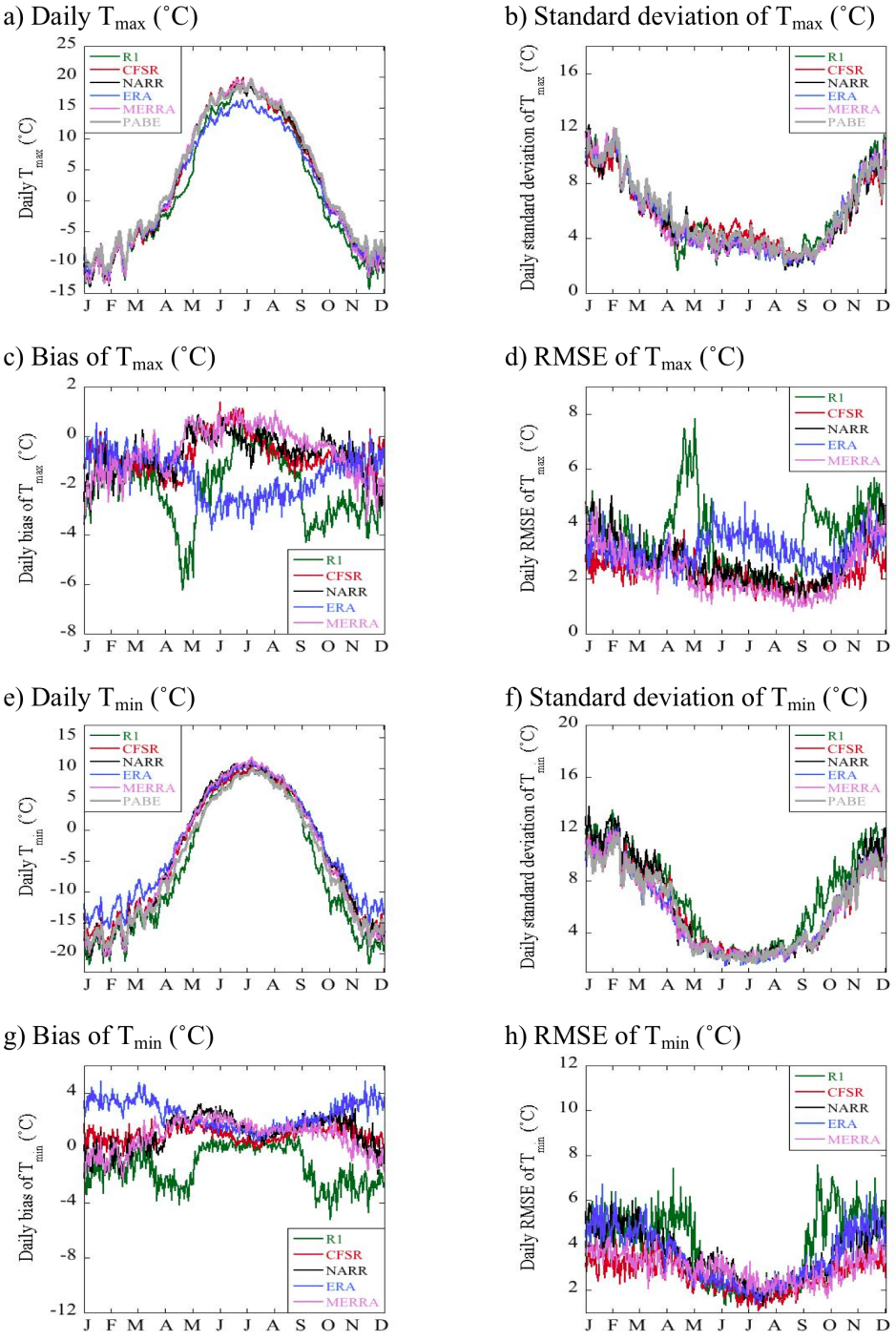

FIG. 4.4.1 Daily climate statistics of T_{max} (a-d), and T_{min} (e-h) at Bethel. The reanalyses are compared to station observations at Bethel (gray), 1979-2009.

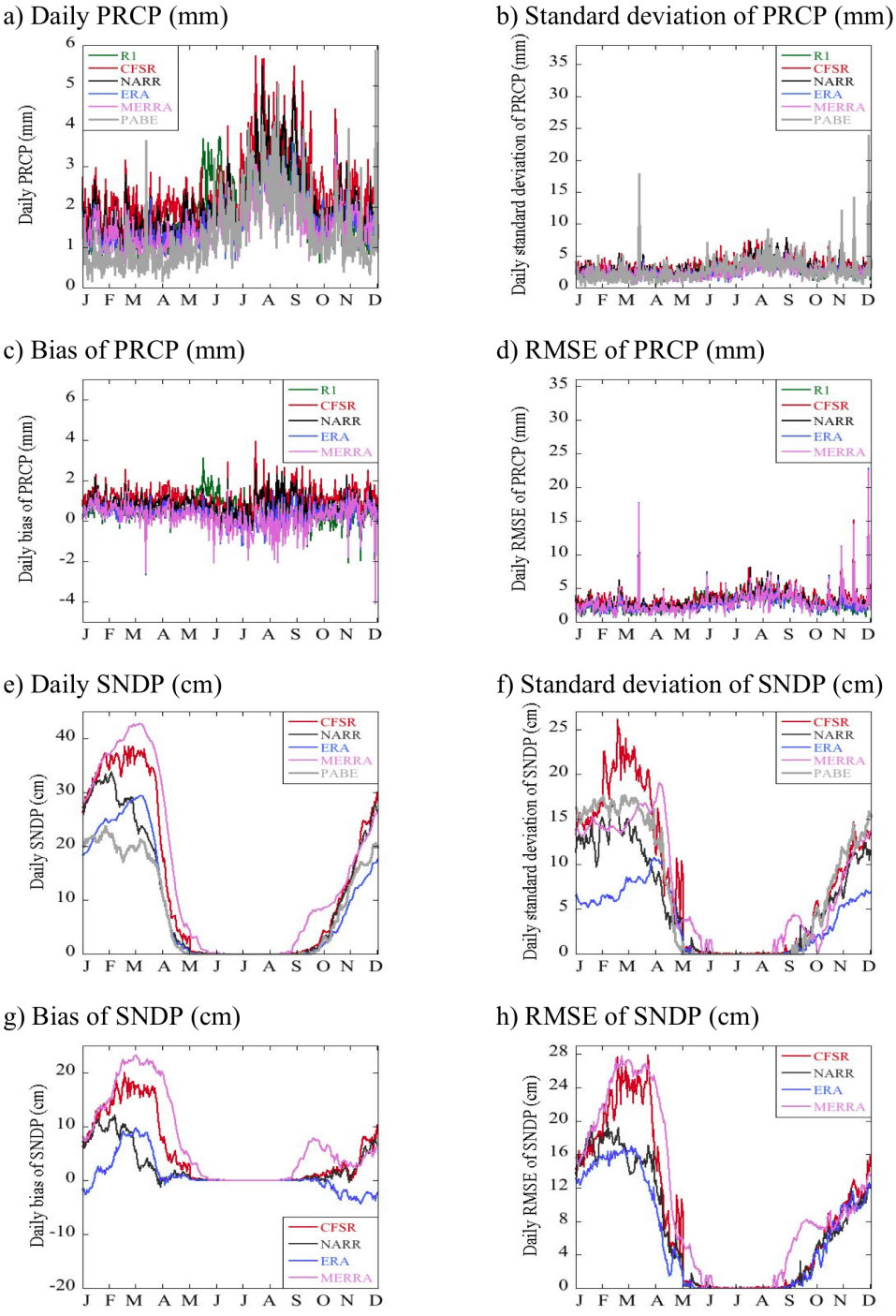

FIG. 4.4.2 Daily climate statistics of PRCP (a-d), and SNDP (e-h) at Bethel. The reanalyses are compared to station observations at Bethel (gray), 1979-2009.

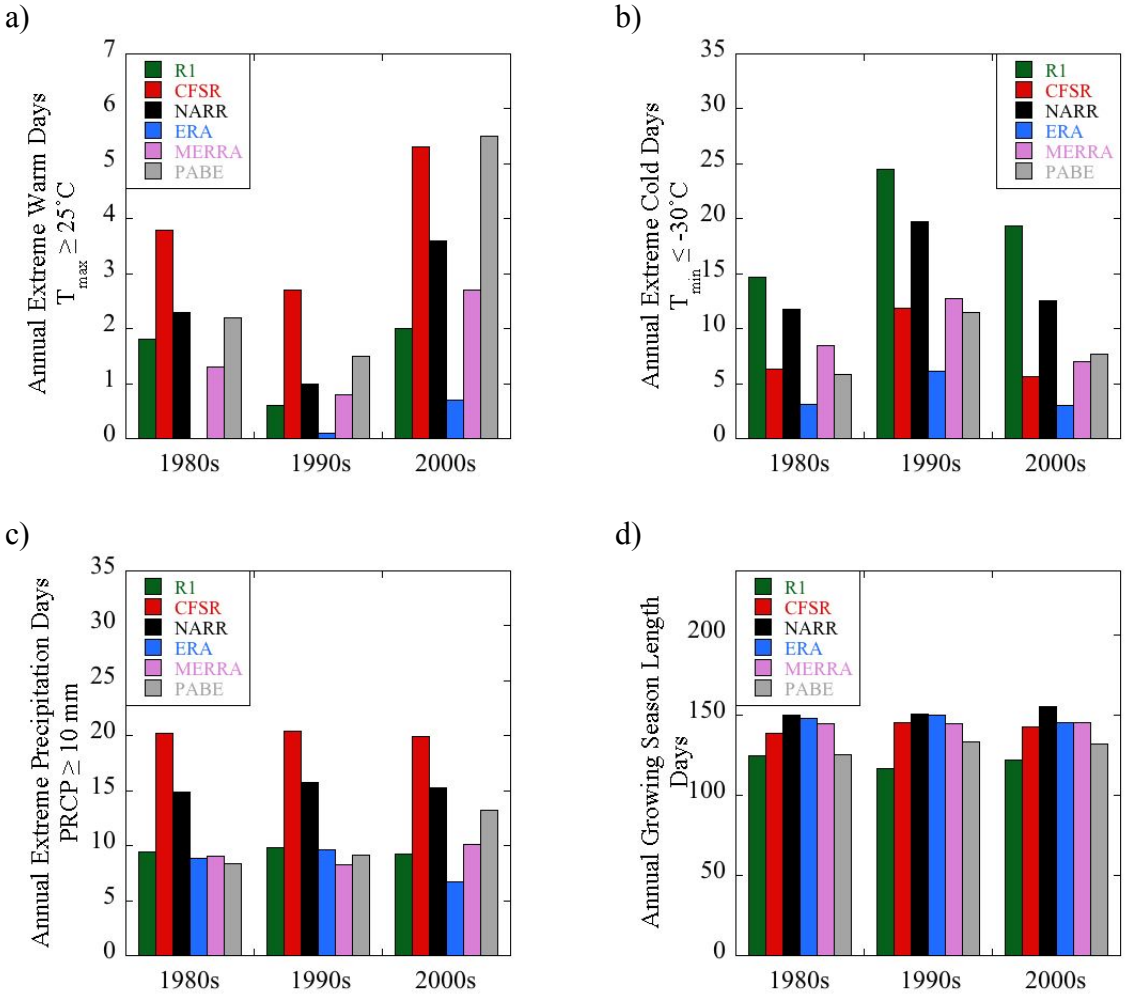

FIG 4.4.3 Climate extreme indices at Bethel: (a) Decadal-average annual counts of Extreme Warm Days (number of days where $T_{max} \geq 25^{\circ}C$), (b) Extreme Cold Days (number of days where $T_{min} \leq -30^{\circ}C$), (c) Extreme Precipitation Days (number of days where PRCP ≥ 10 mm), (d) Growing Season Length (number of days between the fifth consecutive day when $T_{avg} > 0^{\circ}C$ and the day when $T_{min} \leq -2.2^{\circ}C$ for Bethel.

a) Monthly mean T_{max} (˚C), 1979-1983

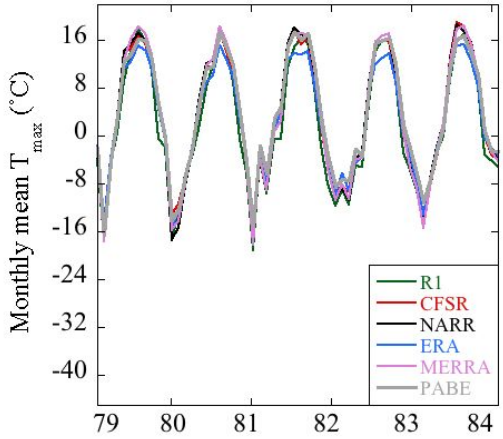

b) Monthly mean T_{max} (˚C), 1984-1988

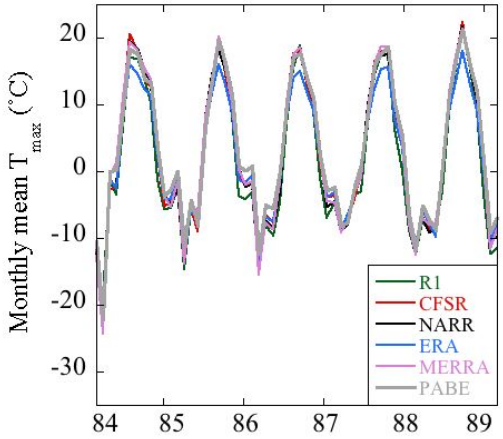

c) Monthly mean T_{max} (˚C), 1989-1993

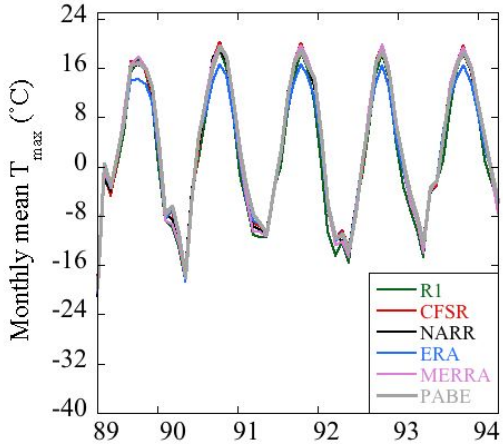

d) Monthly mean T_{max} (˚C), 1994-1998

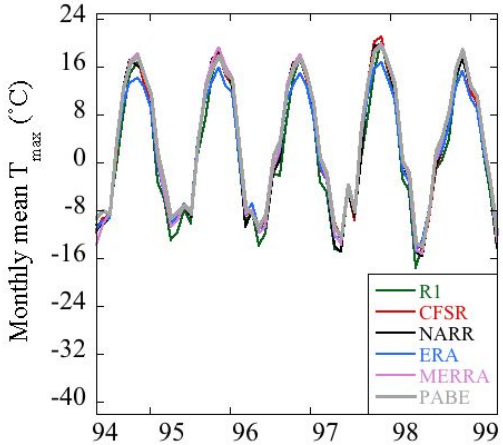

e) Monthly mean T_{max} (˚C), 1999-2003

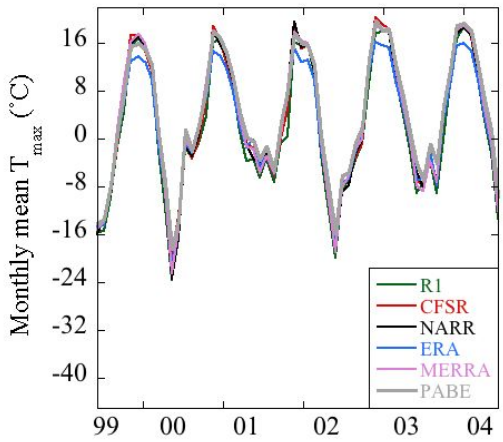

f) Monthly mean T_{max} (˚C), 2004-2009

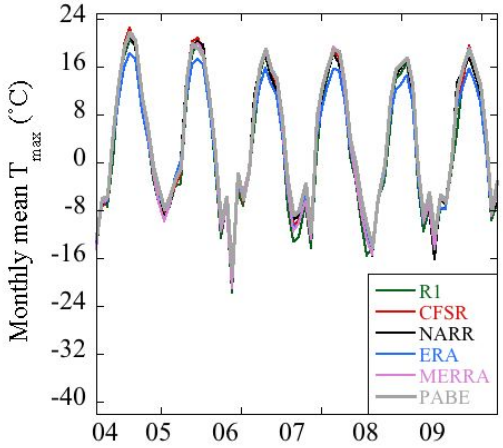

FIG. 4.4.4 Time series of monthly mean T_{max} at Bethel (gray) for a) 1979-1983, b) 1984-1988, c) 1989-1993, d) 1994-1998, e) 1999-2003, and f) 2004-2009.

a) Monthly mean T_{min} (˚C), 1979-1983

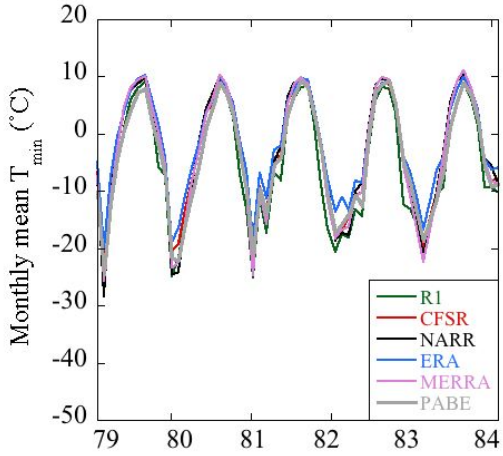

b) Monthly mean T_{min} (˚C), 1984-1988

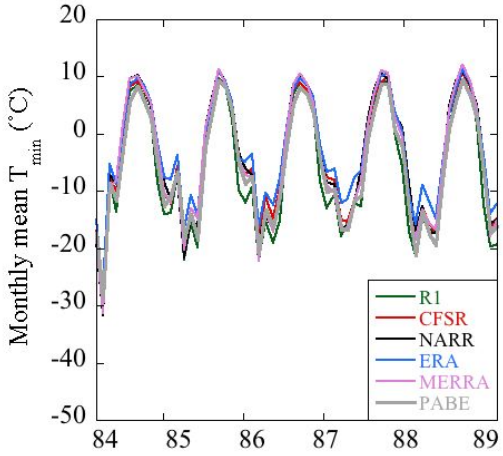

c) Monthly mean T_{min} (˚C), 1989-1993

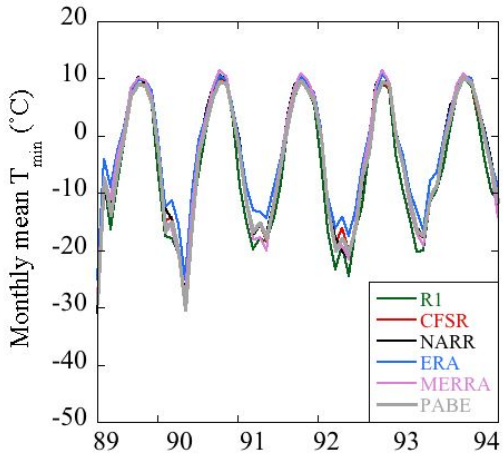

d) Monthly mean T_{min} (˚C), 1994-1998

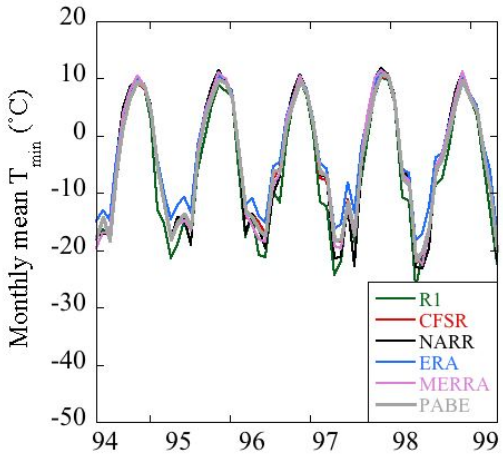

e) Monthly mean T_{min} (˚C), 1999-2003

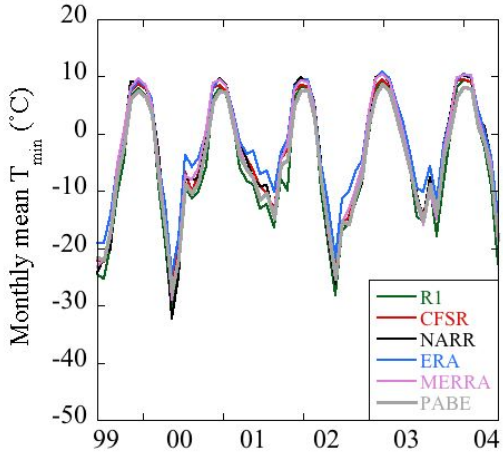

f) Monthly mean T_{min} (˚C), 2004-2009

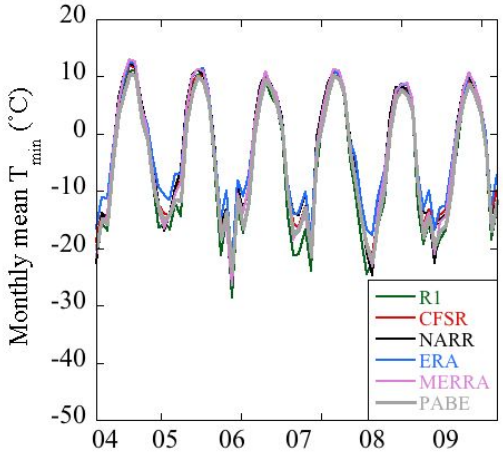

FIG. 4.4.5 Time series of monthly mean T_{min} at Bethel (gray) for a) 1979-1983, b) 1984-1988, c) 1989-1993, d) 1994-1998, e) 1999-2003, and f) 2004-2009.

a) Monthly mean PRCP (mm), 1979-1983

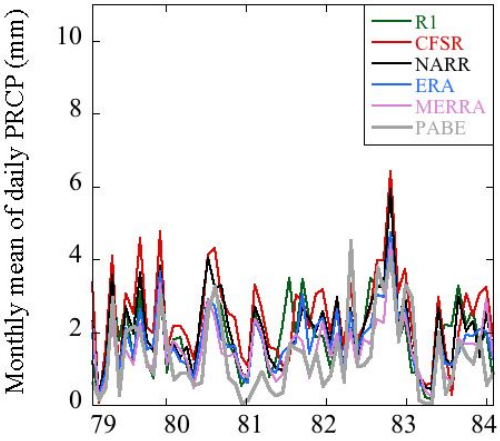

b) Monthly mean PRCP (mm), 1984-1988

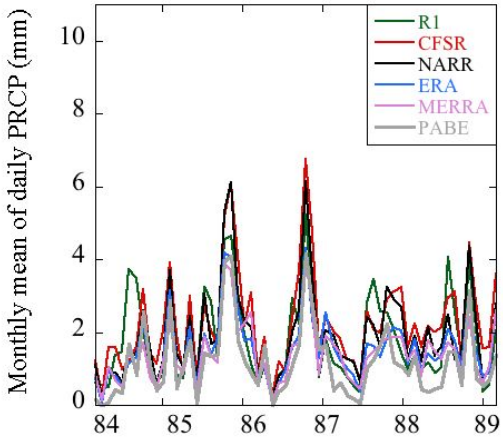

c) Monthly mean PRCP (mm), 1989-1993

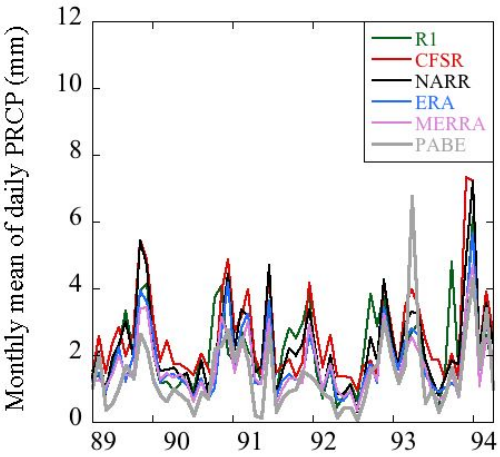

d) Monthly mean PRCP (mm), 1994-1998

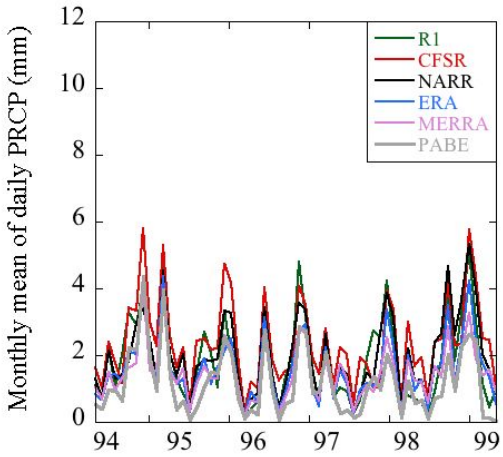

e) Monthly mean PRCP (mm), 1999-2003

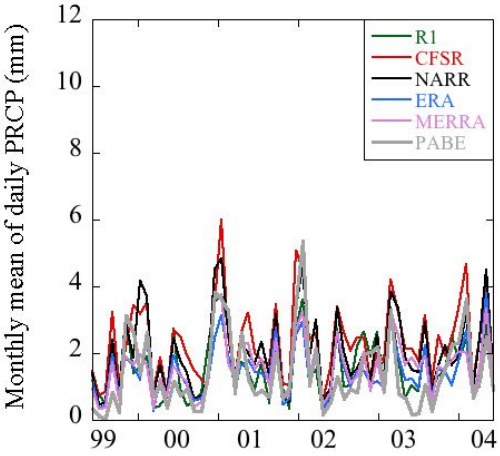

f) Monthly mean PRCP (mm), 2004-2009

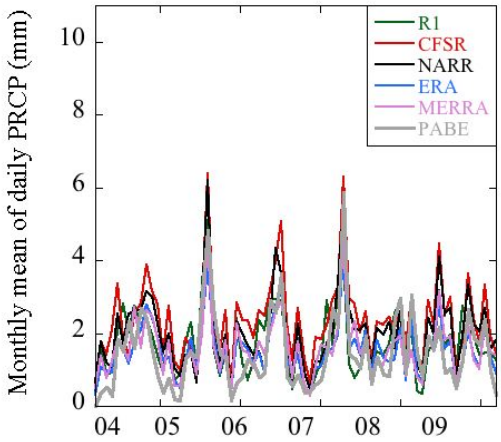

FIG. 4.4.6 Time series of monthly mean PRCP at Bethel (gray) for a) 1979-1983, b) 1984-1988, c) 1989-1993, d) 1994-1998, e) 1999-2003, and f) 2004-2009.

a) Monthly mean SNDP (cm), 1979-1983

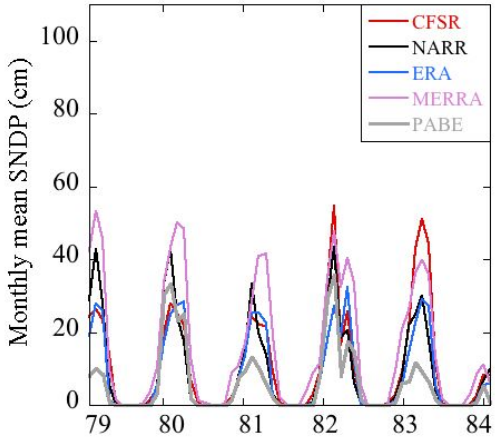

b) Monthly mean SNDP (cm), 1984-1988

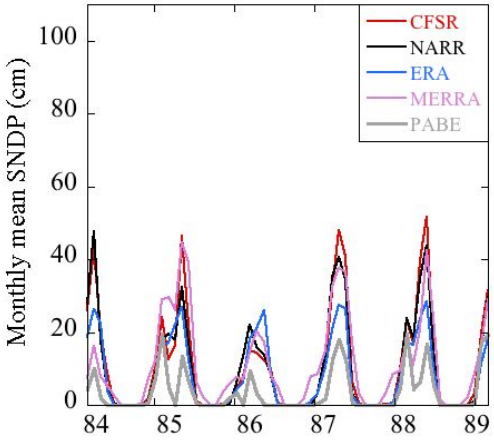

c) Monthly mean SNDP (cm), 1989-1993

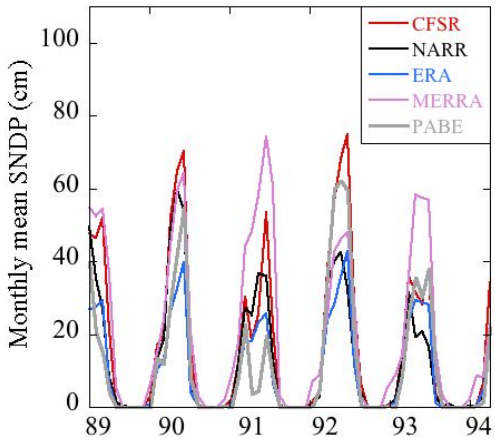

d) Monthly mean SNDP (cm), 1994-1998

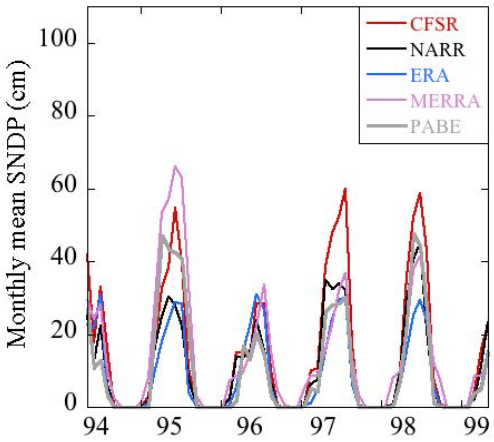

e) Monthly mean SNDP (cm), 1999-2003

f) Monthly mean SNDP (cm), 2004-2009

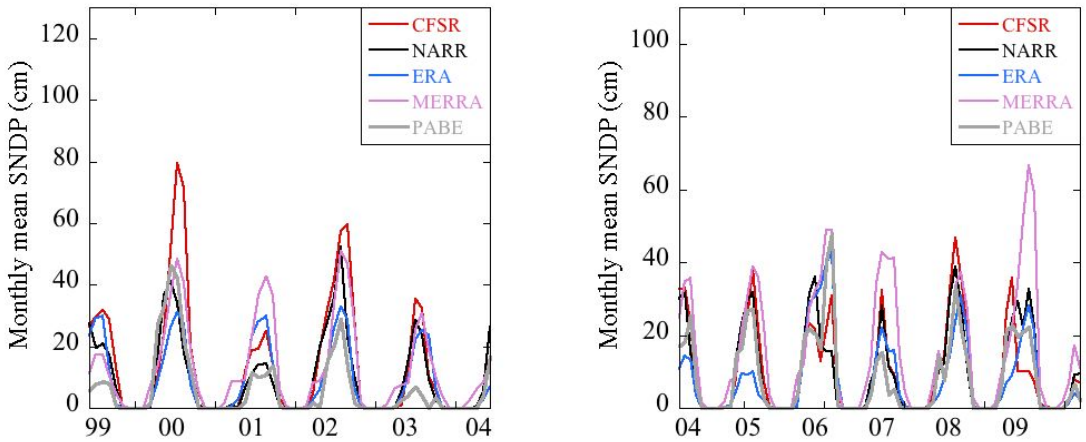

FIG. 4.4.7 Time series of monthly mean SNDP at Bethel (gray) for a) 1979-1983, b) 1984-1988, c) 1989-1993, d) 1994-1998, e) 1999-2003, and f) 2004-2009.

Table 4.4.1 Top performing reanalyses for Bethel, Alaska, 1979-2009. Performance is based on average RMSE value relative to station observations. The months included in each season are indicated by one-letter abbreviations in parentheses.

	T_{max}	T_{min}	PRCP	SNDP
WINTER (NDJFM)	CFSR	CFSR	R1	ERA
SPRING (AM)	MERRA	CFSR	ERA	ERA
SUMMER (JJA)	MERRA	CFSR	ERA	ERA
AUTUMN (SO)	MERRA	CFSR	ERA	ERA

Table 4.4.2 Seasonal RMSE and bias (high/low) for Bethel, Alaska, 1979-2009. Each number represents an average of daily RMSE or bias for the entire season over all 31 years. The RMSE and bias values are relative to station observations.

	WINTER		SPRING		SUMMER		AUTUMN	
T_{max} (˚C)	RMSE	Bias	RMSE	Bias	RMSE	Bias	RMSE	Bias
R1	3.9	-2.2	5.1	-3.5	2.3	-0.7	3.7	-2.8
CFSR	2.5	-0.9	2.6	-1.1	1.9	0.1	1.7	-1.0
NARR	3.4	-1.3	2.7	-0.5	2.1	-0.1	1.8	-0.5
ERA	3.1	-0.9	2.9	-1.5	3.5	-2.7	2.7	-1.9
MERRA	3.1	-1.4	2.3	-0.3	1.6	0.4	1.3	-0.3
T_{min} (˚C)	RMSE	Bias	RMSE	Bias	RMSE	Bias	RMSE	Bias
R1	5.1	-1.9	4.6	-2.0	2.0	0.2	4.5	-1.8
CFSR	3.3	0.8	2.8	1.3	1.9	0.7	2.3	1.3
NARR	4.7	0.1	3.5	1.9	2.5	1.6	2.9	1.8
ERA	4.8	3.4	3.3	2.3	2.2	1.3	2.9	2.0
MERRA	3.5	-0.2	3.0	1.8	2.6	1.7	2.4	1.3
PRCP (mm)	RMSE	Bias	RMSE	Bias	RMSE	Bias	RMSE	Bias
R1	3.6	0.3	2.4	0.8	3.9	0.7	3.3	0.2
CFSR	4.2	1.1	2.8	1.1	4.2	0.8	4.1	1.2
NARR	3.9	0.7	2.4	0.7	3.9	0.5	3.7	0.8
ERA	3.6	0.4	2.0	0.5	3.3	-0.1	3.2	0.2
MERRA	3.8	0.5	2.0	0.3	3.5	-0.2	3.4	0.0
SNDP (cm)	RMSE	Bias	RMSE	Bias	RMSE	Bias	RMSE	Bias
CFSR	17.7	10.2	11.0	3.9	0.1	0.0	2.2	0.5
NARR	13.9	5.7	7.8	0.5	0.1	0.0	2.3	0.2
ERA	13.0	1.7	5.7	0.5	0.0	0.0	1.8	-0.1
MERRA	18.9	12.0	15.1	9.5	0.6	0.0	5.9	4.0

4.5 McGrath, Alaska

McGrath is located in the Central Interior climate division (Bieniek et al. 2012). McGrath's coordinates are 62.96˚N, 155.61˚W, and its elevation is 102 m. The altitude of the nearest land grid point to McGrath used for each reanalysis evaluation is identified in Table 2.2.1 An overall evaluation based on 16 possible combinations between four seasons and four climate variables, indicates that MERRA is the top model seven times (Table 4.5.1). MERRA is followed by ERA-Interim (five), CFSR (three), NARR (one), and NCEP-R1 (zero). Model biases of all seasons and variables for McGrath are given in Table 4.5.2.

The observed mean annual cycle of daily maximum temperature (T_{max}) (see gray line, Fig. 4.5.1a) has a low temperature of -18.4˚C in early January, and a high temperature of 23.5˚C in July. The standard deviation of T_{max} ranges from a December maximum of 12.9˚C to an August minimum of 2.3˚C (Fig. 4.5.1b). Model biases of T_{max} (Fig. 4.5.1c) are negative, particularly in spring and autumn. NCEP-R1 has the largest cold bias during all seasons except winter. CFSR has the lowest seasonal RMSE of T_{max} (see red line, Fig. 4.5.1d), which is 2.1˚C during summer (Table 4.5.2). CFSR also has the best representation of Annual Extreme Warm Days (Fig. 4.5.3a), which are defined as days that have a high temperature equal to or greater than 25˚C.

The observed mean annual cycle of daily minimum temperature (T_{min}) (see gray line, Fig. 4.5.1e) has a low temperature of -28.9˚C in January, and a high temperature of 10.5˚C in July. The standard deviation of T_{min} ranges from a February maximum of 14.1˚C to a July minimum of 1.9˚C (Fig. 4.5.1f). Model biases of T_{min} (Fig. 4.5.1g) are generally positive, and ERA-Interim routinely has the warmest bias. The exception to this is NCEP-R1, which shows a negative bias in spring, summer, and autumn. MERRA has the lowest seasonal RMSE of T_{min} (see lavender

line, Fig. 4.5.1h), which is 2.1˚C during summer (Table 4.5.2). MERRA also has the best representation of Annual Extreme Cold Days (Fig. 4.5.3b), which are defined as days that have a low temperature equal to or less than -40˚C. The models accurately represent Growing Season Length at McGrath, (Fig. 4.5.3d), with MERRA having the best agreement with observations. Growing Season Length begins each year following the fifth consecutive day with an average daily temperature above freezing and terminates when T_{min} is at or below -2.2˚C.

The observed mean annual cycle of daily precipitation (PRCP) (see gray line, Fig. 4.5.2a) has a minimum of 0.06 mm in January, and a maximum of 4.2 mm in August. The standard deviation of PRCP ranges from a January minimum of 0.15 mm to a late summer maximum around 6.0 mm (Fig. 4.5.2b). The one-day maximum standard deviation of PRCP is 11.6 mm, which is a result of one heavy-precipitation event when 63.0 mm fell on 25 Feb 1996. Model biases of PRCP (Fig. 4.5.2c) are generally positive and NCEP-R1 and NARR have the largest positive biases, which occur during the summer. MERRA has the lowest seasonal RMSE of PRCP (see lavender line, Fig. 4.5.2d), which is 1.8 mm during spring (Table 4.5.2). MERRA and NCEP-R1 have the best representation of Annual Extreme Precipitation Days (Fig. 4.5.3c), which are defined as days that have an accumulated precipitation equal to or greater than 10 mm. ERA-Interim has the lowest seasonal RMSE values at McGrath for all seasons except for spring.

The observed mean annual cycle of daily snow depth (SNDP) (see gray line, Fig. 4.5.2e) reaches a maximum of 71.4 cm in late February, and melts completely by May. The standard deviation of SNDP peaks at 29.1 cm in March (Fig. 4.5.2f). Model biases of SNDP (Fig. 4.5.2g) are mixed. During the snow season, CFSR has a positive bias, while NARR and ERA-Interim have negative biases. MERRA has a negative SNDP bias in spring, but a positive bias in autumn that causes there to be a longer snow season overall compared to observations. ERA-Interim has

the lowest seasonal RMSE of SNDP (see blue line, Fig. 4.5.2h), which is 0.0 cm during summer (Table 4.5.2).

MERRA is the top performing reanalysis data set relative to station observations at McGrath, and it does particularly well with its representation of T_{min}. MERRA best represents Annual Extreme Cold Days, Growing Season Length, and Annual Extreme Precipitation Days. ERA-Interim has the lowest seasonal RMSE of PRCP in all seasons except for spring, and for SNDP in summer and autumn. NCEP-R1 and NARR have large positive PRCP biases in summer. Observations at McGrath show that the number of Annual Extreme Warm Days is increasing, Annual Extreme Cold Days are not, and Growing Season Length has not changed. Reanalysis data users that are only interested in a particular variable or season at McGrath should refer to Tables 4.5.1 and 4.5.2 to help guide the selection of the best available data set. The 31-year time series of T_{max} (Fig. 4.5.4), T_{min} (Fig. 4.5.5), PRCP (Fig. 4.5.6), and SNDP (Fig. 4.5.7) are available for users that are primarily interested in a particular segment of the period used for this study.

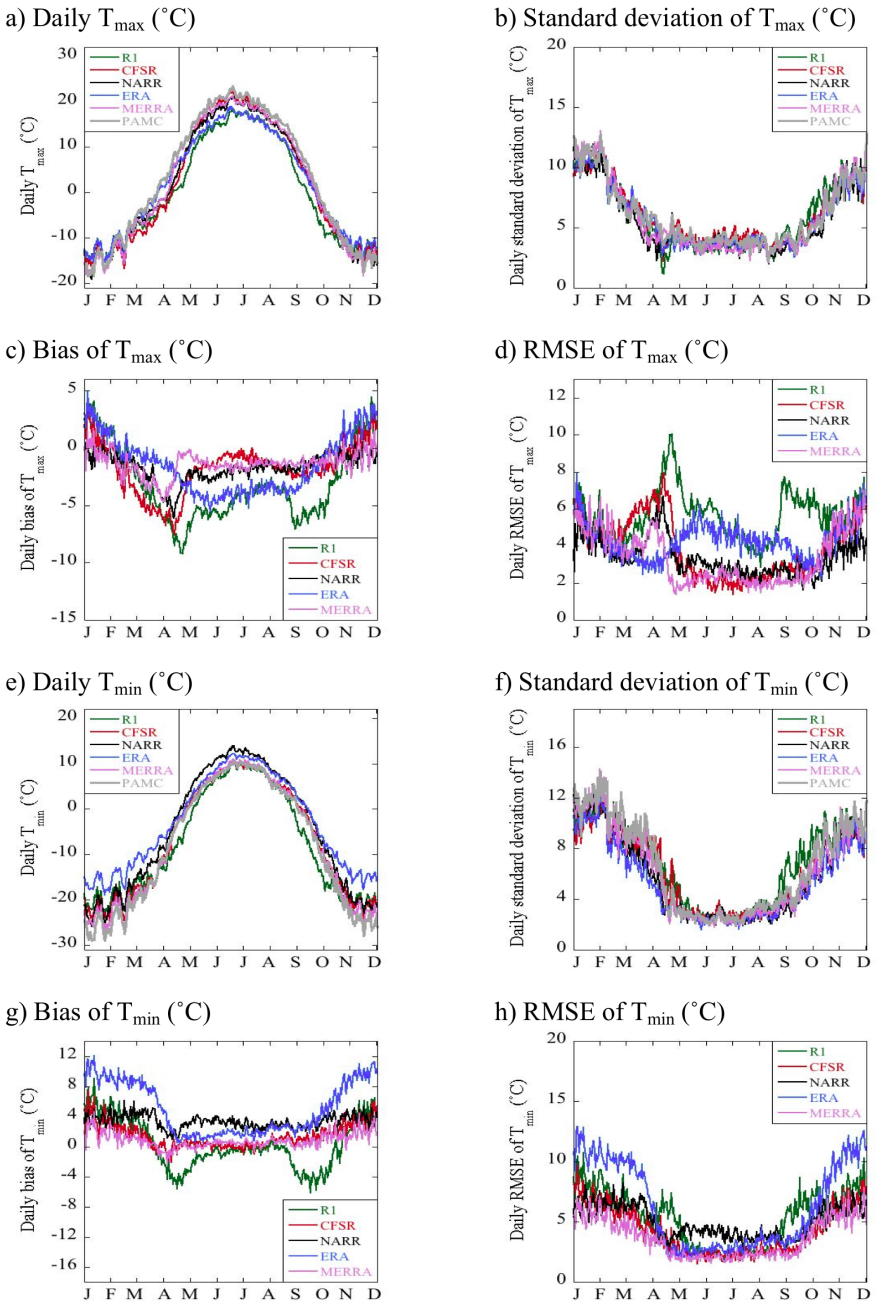

FIG. 4.5.1 Daily climate statistics of T_{max} (a-d), and T_{min} (e-h) at McGrath. The reanalyses are compared to station observations at McGrath (gray), 1979-2009.

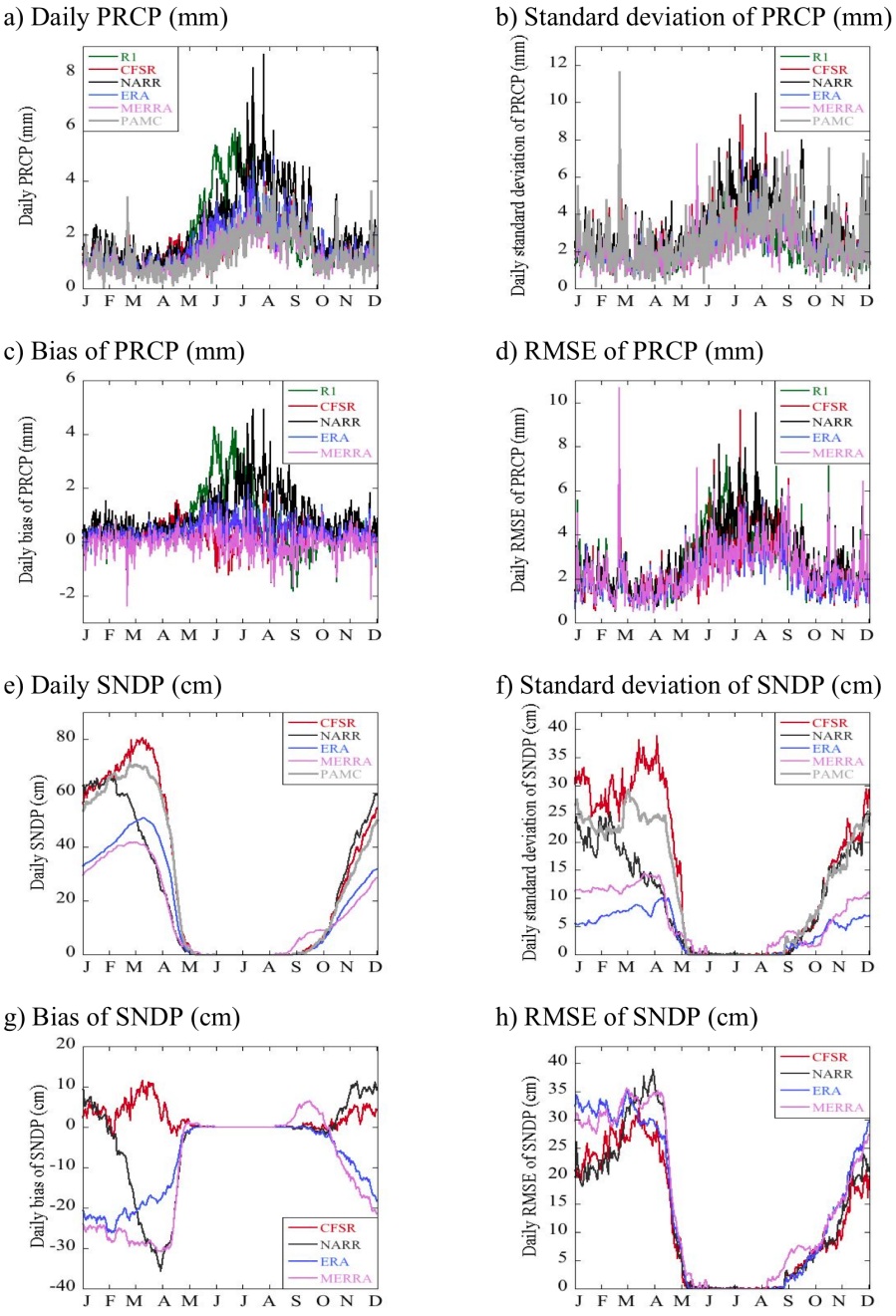

FIG. 4.5.2 Daily climate statistics of PRCP (a-d), and SNDP (e-h) at McGrath. The reanalyses are compared to station observations at McGrath (gray), 1979-2009.

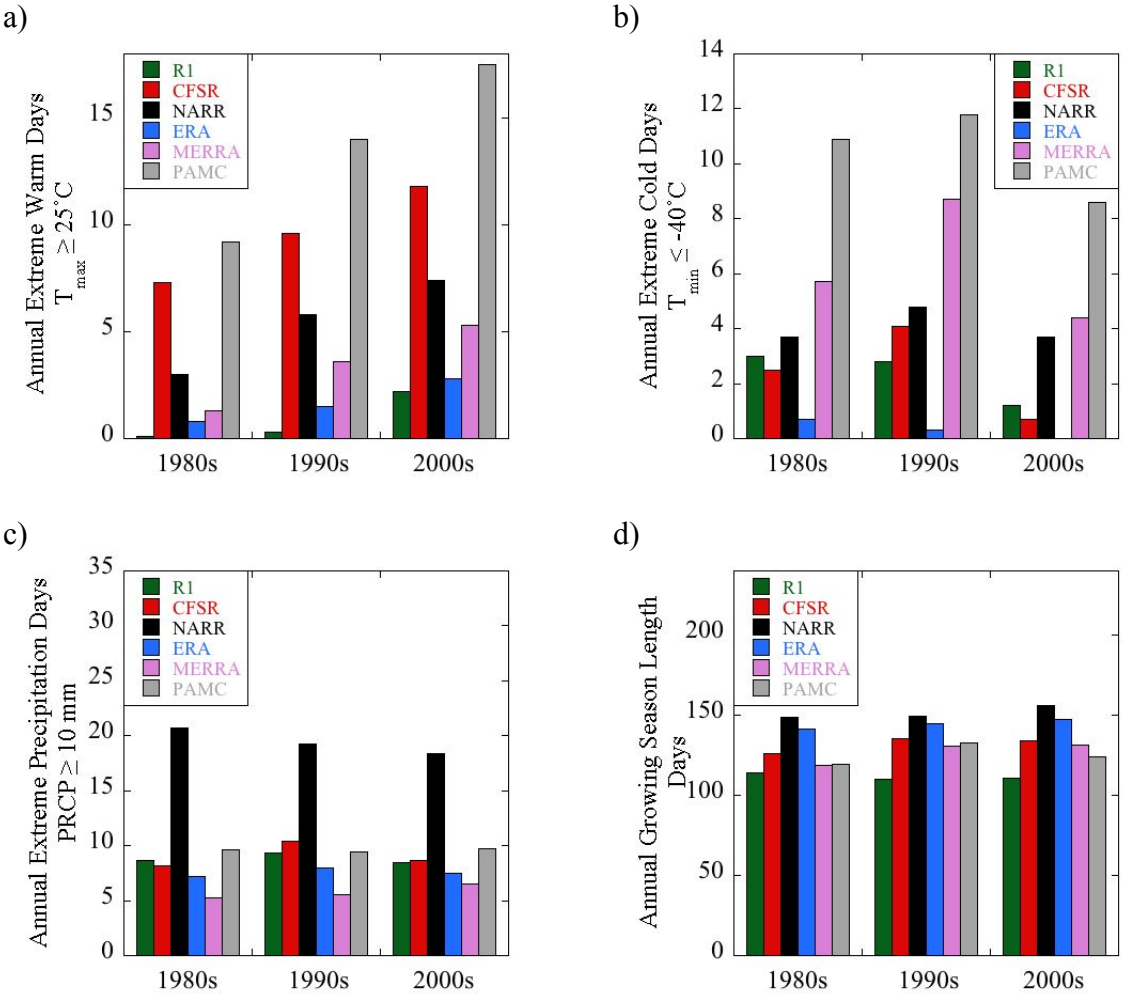

FIG. 4.5.3 Climate extreme indices at McGrath: (a) Decadal-average annual counts of Extreme Warm Days (number of days where $T_{max} \geq 25^{\circ}C$), (b) Extreme Cold Days (number of days where $T_{min} \leq -40^{\circ}C$), (c) Extreme Precipitation Days (number of days where PRCP ≥ 10 mm), (d) Growing Season Length (number of days between the fifth consecutive day when $T_{avg} > 0^{\circ}C$ and the day when $T_{min} \leq -2.2^{\circ}C$ for McGrath.

a) Monthly mean T_{max} (˚C), 1979-1983

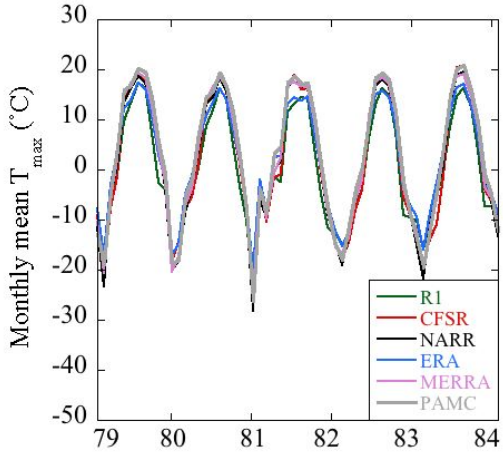

b) Monthly mean T_{max} (˚C), 1984-1988

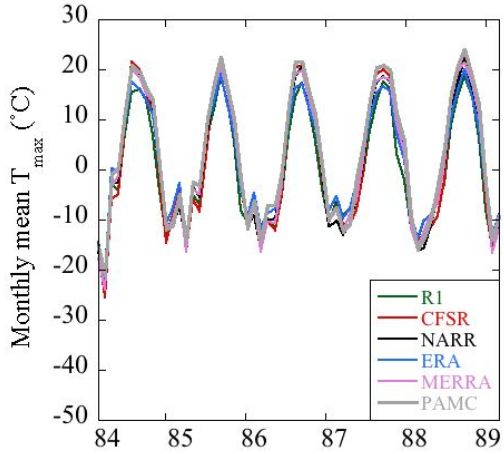

c) Monthly mean T_{max} (˚C), 1989-1993

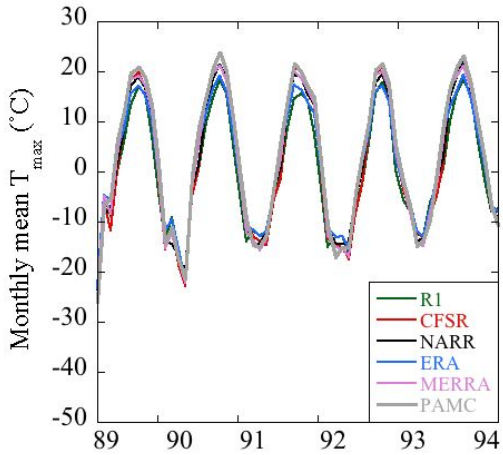

d) Monthly mean T_{max} (˚C), 1994-1998

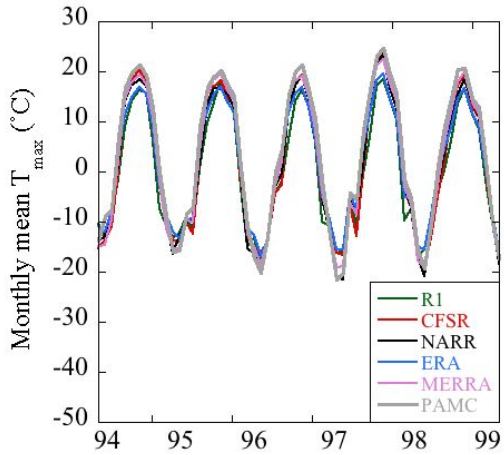

e) Monthly mean T_{max} (˚C), 1999-2003

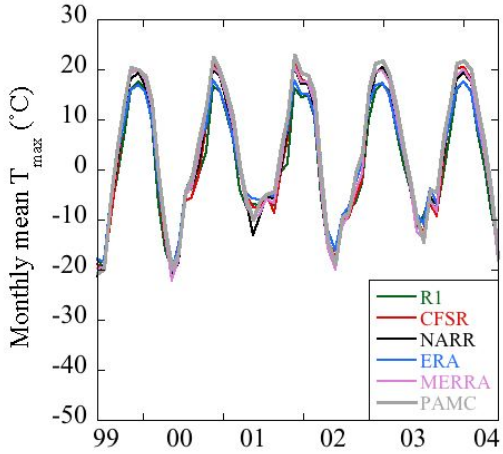

f) Monthly mean T_{max} (˚C), 2004-2009

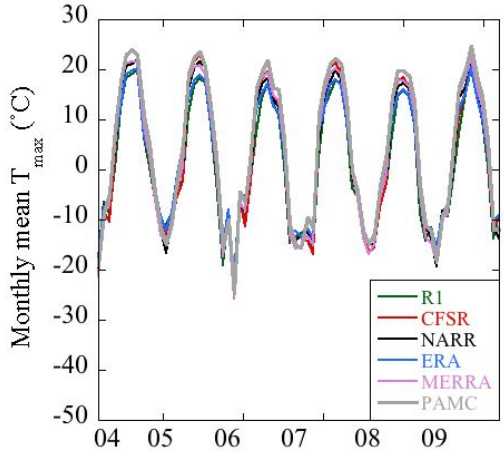

FIG. 4.5.4 Time series of monthly mean T_{max} at McGrath (gray) for a) 1979-1983, b) 1984-1988, c) 1989-1993, d) 1994-1998, e) 1999-2003, and f) 2004-2009.

a) Monthly mean T_{min} (˚C), 1979-1983

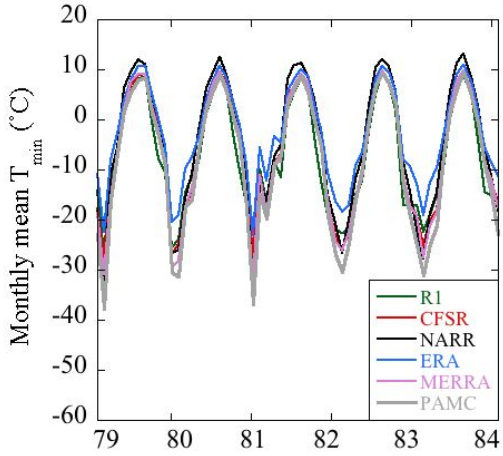

b) Monthly mean T_{min} (˚C), 1984-1988

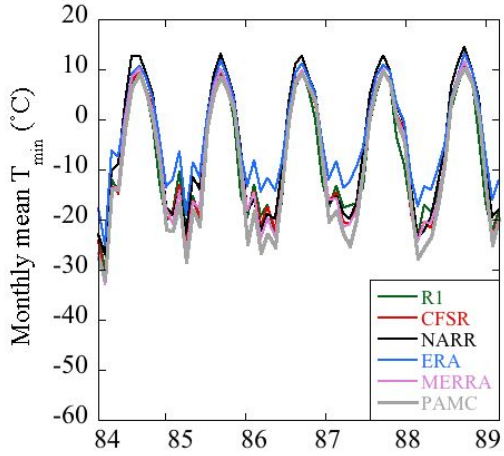

c) Monthly mean T_{min} (˚C), 1989-1993

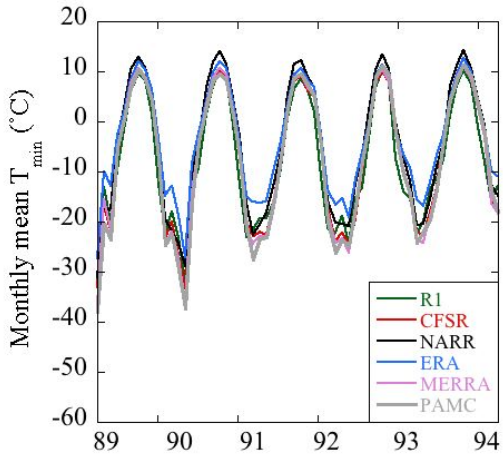

d) Monthly mean T_{min} (˚C), 1994-1998

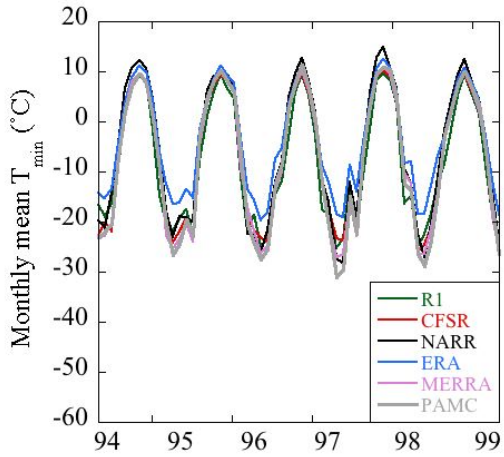

e) Monthly mean T_{min} (˚C), 1999-2003

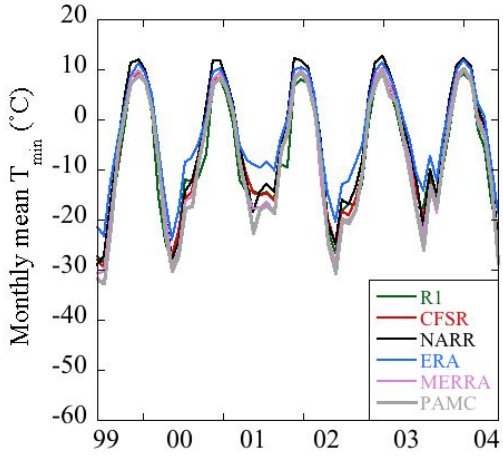

f) Monthly mean T_{min} (˚C), 2004-2009

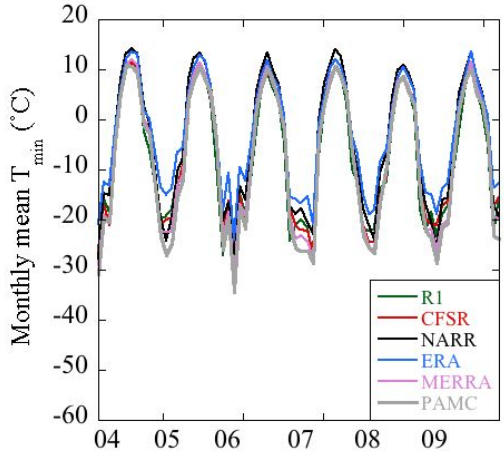

FIG. 4.5.5 Time series of monthly mean T_{min} at McGrath (gray) for a) 1979-1983, b) 1984-1988, c) 1989-1993, d) 1994-1998, e) 1999-2003, and f) 2004-2009.

a) Monthly mean PRCP (mm), 1979-1983

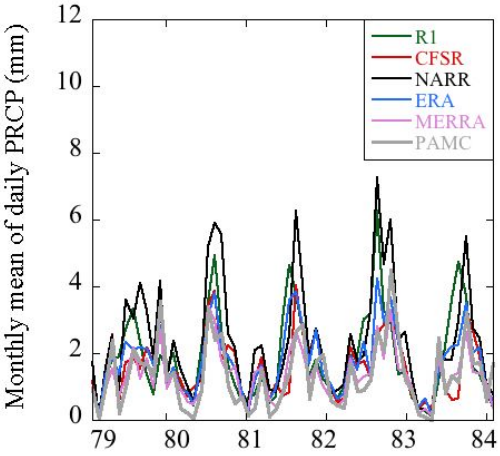

b) Monthly mean PRCP (mm), 1984-1988

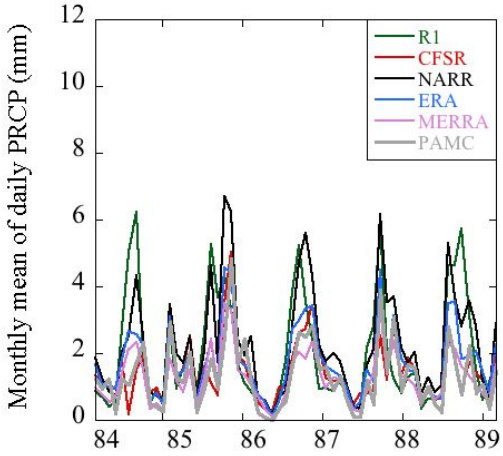

c) Monthly mean PRCP (mm), 1989-1993

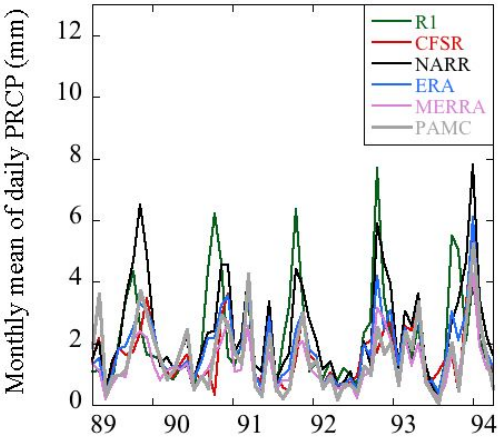

d) Monthly mean PRCP (mm), 1994-1998

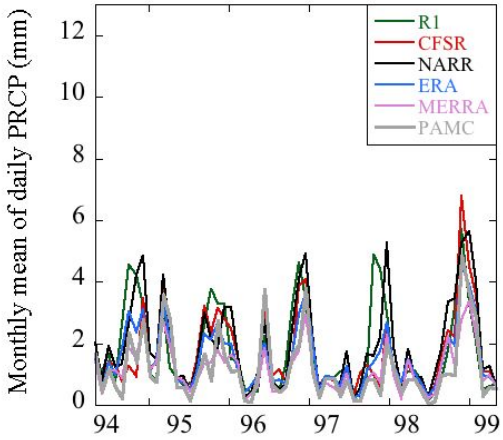

e) Monthly mean PRCP (mm), 1999-2003

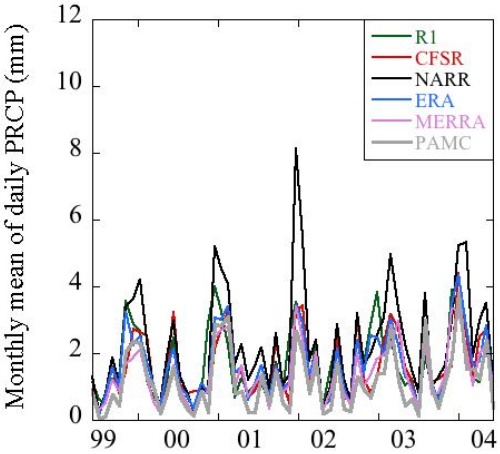

f) Monthly mean PRCP (mm), 2004-2009

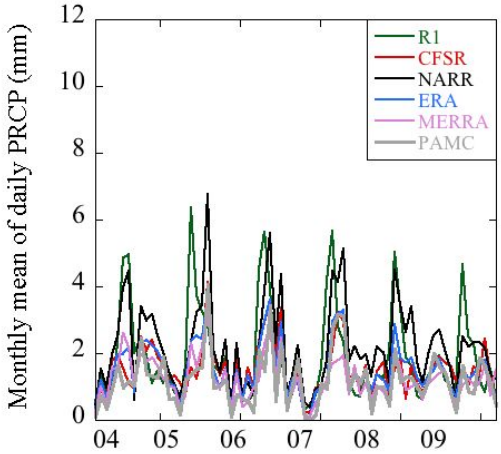

FIG. 4.5.6 Time series of monthly mean PRCP at McGrath (gray) for a) 1979-1983, b) 1984-1988, c) 1989-1993, d) 1994-1998, e) 1999-2003, and f) 2004-2009.

a) Monthly mean SNDP (cm), 1979-1983

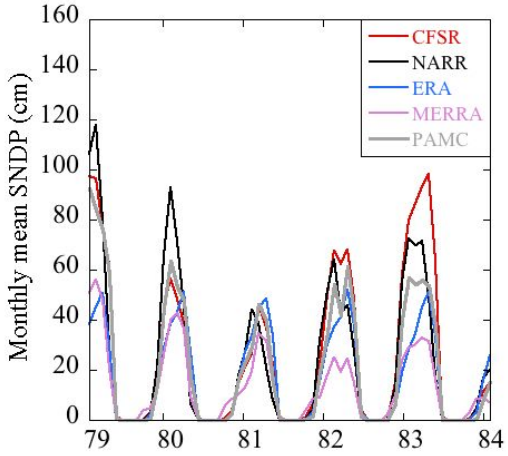

b) Monthly mean SNDP (cm), 1984-1988

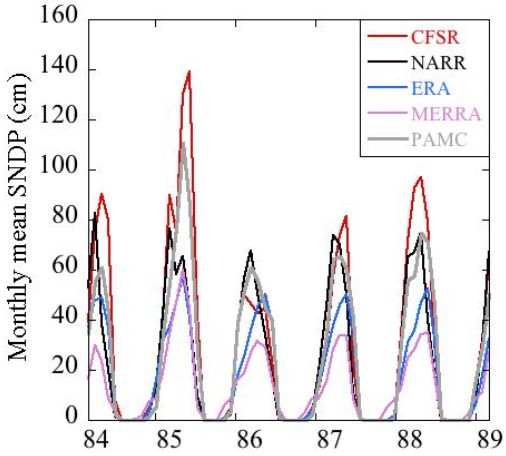

c) Monthly mean SNDP (cm), 1989-1993

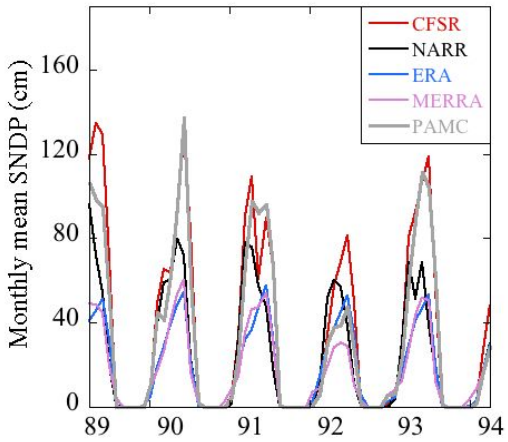

d) Monthly mean SNDP (cm), 1994-1998

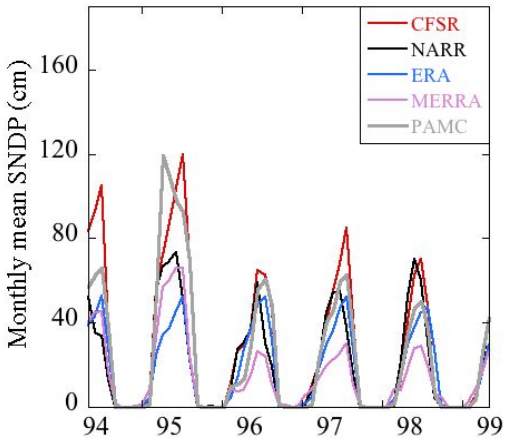

e) Monthly mean SNDP (cm), 1999-2003

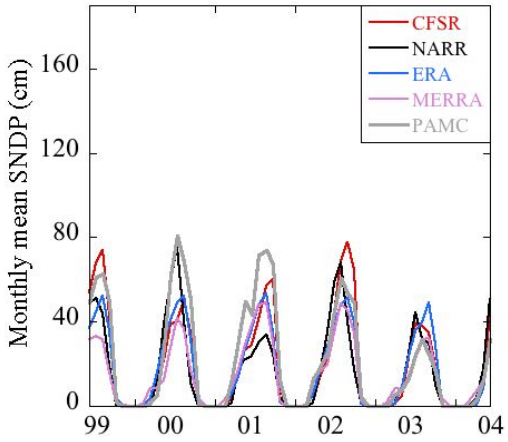

f) Monthly mean SNDP (cm), 2004-2009

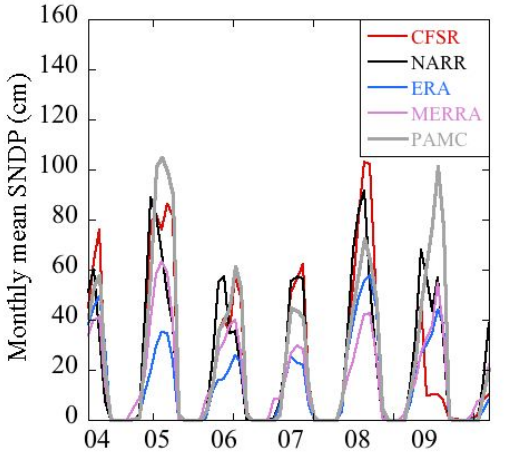

FIG. 4.5.7 Time series of monthly mean SNDP at McGrath (gray) for a) 1979-1983, b) 1984-1988, c) 1989-1993, d) 1994-1998, e) 1999-2003, and f) 2004-2009.

Table 4.5.1 Top performing reanalyses for McGrath, Alaska, 1979-2009. Performance is based on average RMSE value relative to station observations. The months included in each season are indicated by one-letter abbreviations in parentheses.

	T_{max}	T_{min}	PRCP	SNDP
WINTER (NDJFM)	NARR	MERRA	ERA	CFSR
SPRING (AM)	MERRA	MERRA	MERRA	CFSR
SUMMER (JJA)	CFSR	MERRA	ERA	ERA
AUTUMN (SO)	MERRA	MERRA	ERA	ERA

Table 4.5.2 Seasonal RMSE and bias (high/low) for McGrath, Alaska, 1979-2009. Each number represents an average of daily RMSE or bias for the entire season over all 31 years. The RMSE and bias values are relative to station observations.

	WINTER		SPRING		SUMMER		AUTUMN	
T_{max} (˚C)	RMSE	Bias	RMSE	Bias	RMSE	Bias	RMSE	Bias
R1	5.5	-0.3	7.4	-6.6	4.9	-4.4	6.2	-5.3
CFSR	5.0	-1.0	5.3	-4.3	2.1	-1.0	2.8	-2.1
NARR	3.9	-0.9	4.3	-3.5	2.8	-2.0	2.5	-1.4
ERA	4.7	1.0	3.9	-2.8	4.7	-3.9	3.7	-2.6
MERRA	4.8	-1.1	3.4	-1.9	2.2	-1.5	2.3	-1.3
T_{min} (˚C)	RMSE	Bias	RMSE	Bias	RMSE	Bias	RMSE	Bias
R1	7.4	3.4	5.1	-2.8	2.4	-0.5	5.6	-3.1
CFSR	6.4	2.8	3.5	0.1	2.3	0.2	3.1	1.1
NARR	6.3	4.0	4.3	2.6	4.0	3.0	4.0	2.8
ERA	10.2	8.8	4.1	2.2	2.9	1.8	4.3	3.0
MERRA	5.3	1.5	2.8	-0.4	2.1	0.5	3.0	0.6
PRCP (mm)	RMSE	Bias	RMSE	Bias	RMSE	Bias	RMSE	Bias
R1	2.3	0.1	2.2	0.6	4.6	1.9	3.2	-0.2
CFSR	2.1	0.2	2.1	0.5	3.8	0.1	3.1	0.5
NARR	2.4	0.5	2.1	0.7	4.8	1.8	3.6	1.1
ERA	2.1	0.1	1.8	0.4	3.3	0.6	2.8	0.4
MERRA	2.3	-0.1	1.8	0.1	3.3	0.0	3.1	-0.1
SNDP (cm)	RMSE	Bias	RMSE	Bias	RMSE	Bias	RMSE	Bias
CFSR	21.8	4.3	17.1	1.5	0.1	0.0	4.1	0.1
NARR	22.6	-2.4	22.8	-14.0	0.1	0.0	3.9	-0.4
ERA	27.4	-16.8	19.2	-7.6	0.0	0.0	3.7	-0.6
MERRA	26.9	-21.2	22.8	-13.0	0.5	0.0	6.0	3.2

4.6 Fairbanks, Alaska

Fairbanks is located in the Southeast Interior climate division (Bieniek et al. 2012), between the Yukon River to the north and the Alaska Range further south. Fairbanks's coordinates are 64.80˚N, 147.88˚W, and its elevation is 132 m. The altitude of the nearest land grid point to Fairbanks used for each reanalysis evaluation is identified in Table 2.2.1. An overall evaluation based on 16 possible combinations between four seasons and four climate variables, indicates that NARR is the top model six times (Table 4.6.1). NARR is followed by MERRA (five), ERA-Interim (three), CFSR (two) and NCEP-R1 (zero). Model biases of all seasons and variables for Fairbanks are given in Table 4.6.2.

The observed mean annual cycle of daily maximum temperature (T_{max}) (see gray line, Fig. 4.6.1a) has a low temperature of -18.7˚C in January, and a high temperature of 25.1˚C in July. The standard deviation of T_{max} ranges from a February maximum of 12.8˚C to an early September minimum of 2.7˚C (Fig. 4.6.1b). NCEP-R1 and ERA-Interim show strong negative T_{max} biases (Fig. 4.6.1c), particularly from spring through autumn, while the other models have smaller, yet still cold biases. NARR has the lowest seasonal RMSE of T_{max} (see black line, Fig. 4.6.1d), which is 2.4˚C during summer and autumn (Table 4.6.2). NARR, along with CFSR, also has the best representation of Annual Extreme Warm Days (Fig. 4.6.3a), which are defined as days that have a high temperature equal to or greater than 25˚C.

The observed mean annual cycle of daily minimum temperature (T_{min}) (see gray line, Fig. 4.6.1e) has a low temperature of -30.1˚C in January, and a high temperature of 12.1˚C in July. The standard deviation of T_{min} ranges from a February maximum of 11.9˚C to a July minimum of 1.8˚C (Fig. 4.6.1f). Model biases of T_{min} (Fig. 4.6.1g) are positive during winter. Both NCEP-R1 and MERRA show negative biases in spring, which return in autumn. NARR has the warmest

bias during all seasons for Fairbanks except winter. ERA-Interim and MERRA have the lowest seasonal RMSE of T_{min} (see blue and lavender lines, Fig. 4.6.1h), which is 2.0˚C during summer (Table 4.6.2). MERRA has the best representation of Annual Extreme Cold Days (Fig. 4.6.3b), which are defined as days that have a low temperature equal to or less than -40˚C. All models capture Growing Season Length at Fairbanks (Fig. 4.6.3d), with ERA-Interim and MERRA the best. This is notable because both ERA-Interim and MERRA underestimate the number of Annual Extreme Warm Days. Growing Season Length begins each year following the fifth consecutive day with an average daily temperature above freezing and terminates when T_{min} is at or below -2.2˚C.

The observed mean annual cycle of daily precipitation (PRCP) (see gray line, Fig. 4.6.2a) has a minimum of 0.03 mm in April, and a maximum of 3.5 mm in July. The standard deviation of PRCP ranges from an April minimum of 0.10 mm to a summer maximum near 7.0 mm (Fig. 4.6.2b). The one-day maximum standard deviation of PRCP is 9.6, which is a result of one heavy-precipitation event when 17.5 mm fell on 17 Dec 1984. Model biases of PRCP (Fig. 4.6.2c) are positive, and NCEP-R1 has the wettest biases during all seasons, particularly in summer. NARR has the lowest seasonal RMSE of PRCP (see black line, Fig. 4.6.2d), which is 1.3 mm during winter (Table 4.6.2). ERA-Interim and MERRA have the best representation of Annual Extreme Precipitation Days (Fig. 4.6.3c), which are defined as days that have an accumulated precipitation equal to or greater than 10 mm. NCEP-R1 produces twice as many of these heavy-precipitation days compared to observations and displays an increasing trend from the 1980s to the 2000s. MERRA has the lowest seasonal RMSE values for Fairbanks during summer, which coincides with the wettest time of year.

The observed mean annual cycle of daily snow depth (SNDP) (see gray line, Fig. 4.6.2e) reaches a maximum of 53.6 cm in March, and melts completely by early May. The standard deviation of SNDP peaks at 25.2 cm in April (Fig. 4.6.2f). Model biases of SNDP (Fig. 4.6.2g) are largely negative for all the reanalysis models, while NARR has the largest negative bias in winter and spring. MERRA is the exception with positive SNDP biases in spring and autumn, which indicates a longer snow season for Fairbanks compared to observations. ERA-Interim has the lowest seasonal RMSE of SNDP (see blue line, Fig. 4.6.2h), which is 0.1 cm during summer (Table 4.6.2).

NARR is the top performing reanalysis data set relative to station observations at Fairbanks, and it does particularly well at capturing daily T_{max}. However, NARR struggles with spring SNDP at Fairbanks by melting it away too quickly, which results in a pronounced negative SNDP bias. MERRA is the preferred reanalysis during winter for SNDP and T_{min}. MERRA is among the best or has the best representation of Annual Extreme Cold Days, Annual Extreme Precipitation Days, and Growing Season Length at Fairbanks. NCEP-R1 produces nearly twice the number of Annual Extreme Precipitation Days compared to observations. Reanalysis data users that are only interested in a particular variable or season at Fairbanks should refer to Tables 4.6.1 and 4.6.2 to help guide the selection of the best available data set. The 31-year time series of T_{max} (Fig. 4.6.4), T_{min} (Fig. 4.6.5), PRCP (Fig. 4.6.6), and SNDP (Fig. 4.6.7) are available for users that are primarily interested in a particular segment of the period used for this study.

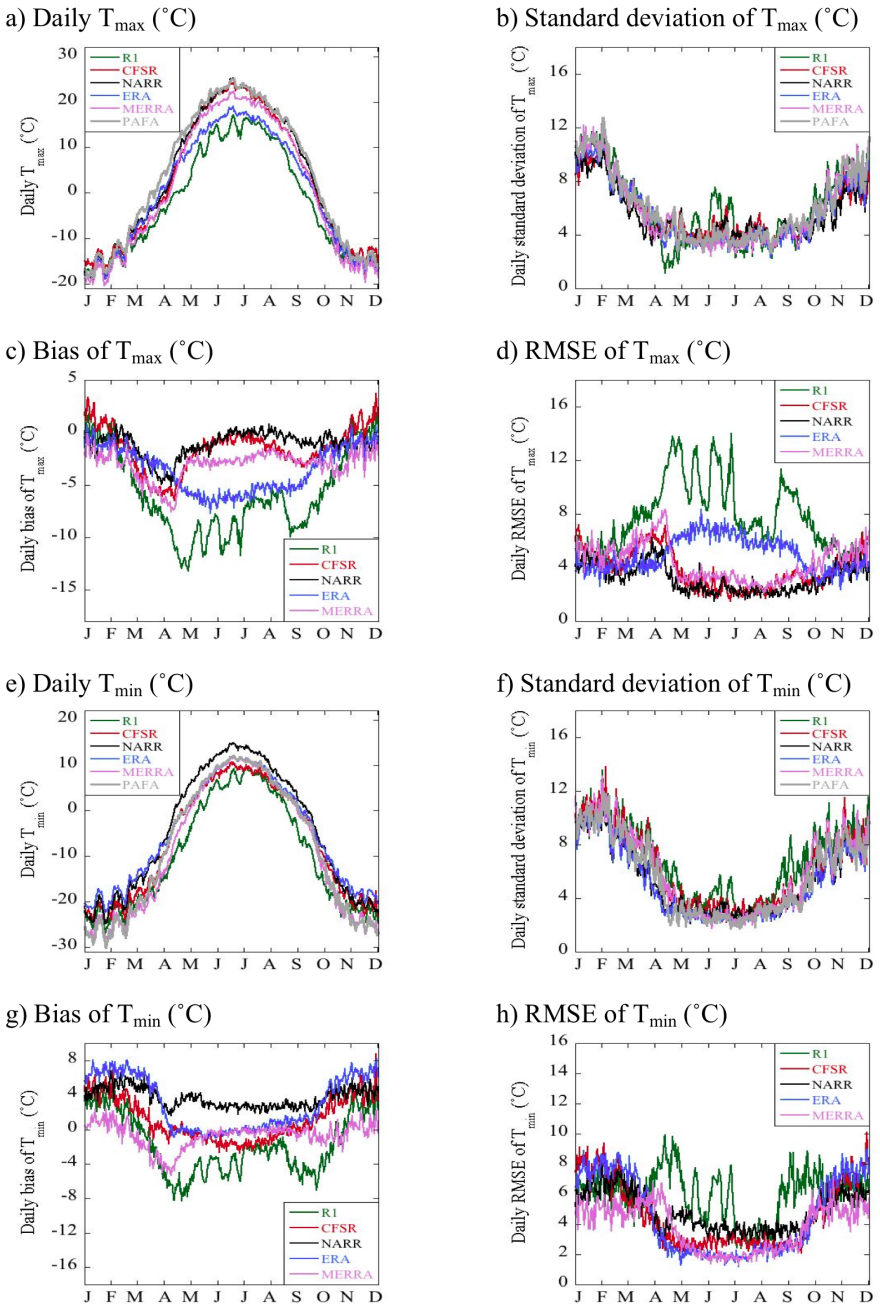

FIG. 4.6.1 Daily climate statistics of T_{max} (a-d), and T_{min} (e-h) at Fairbanks. The reanalyses are compared to station observations at Fairbanks (gray), 1979-2009.

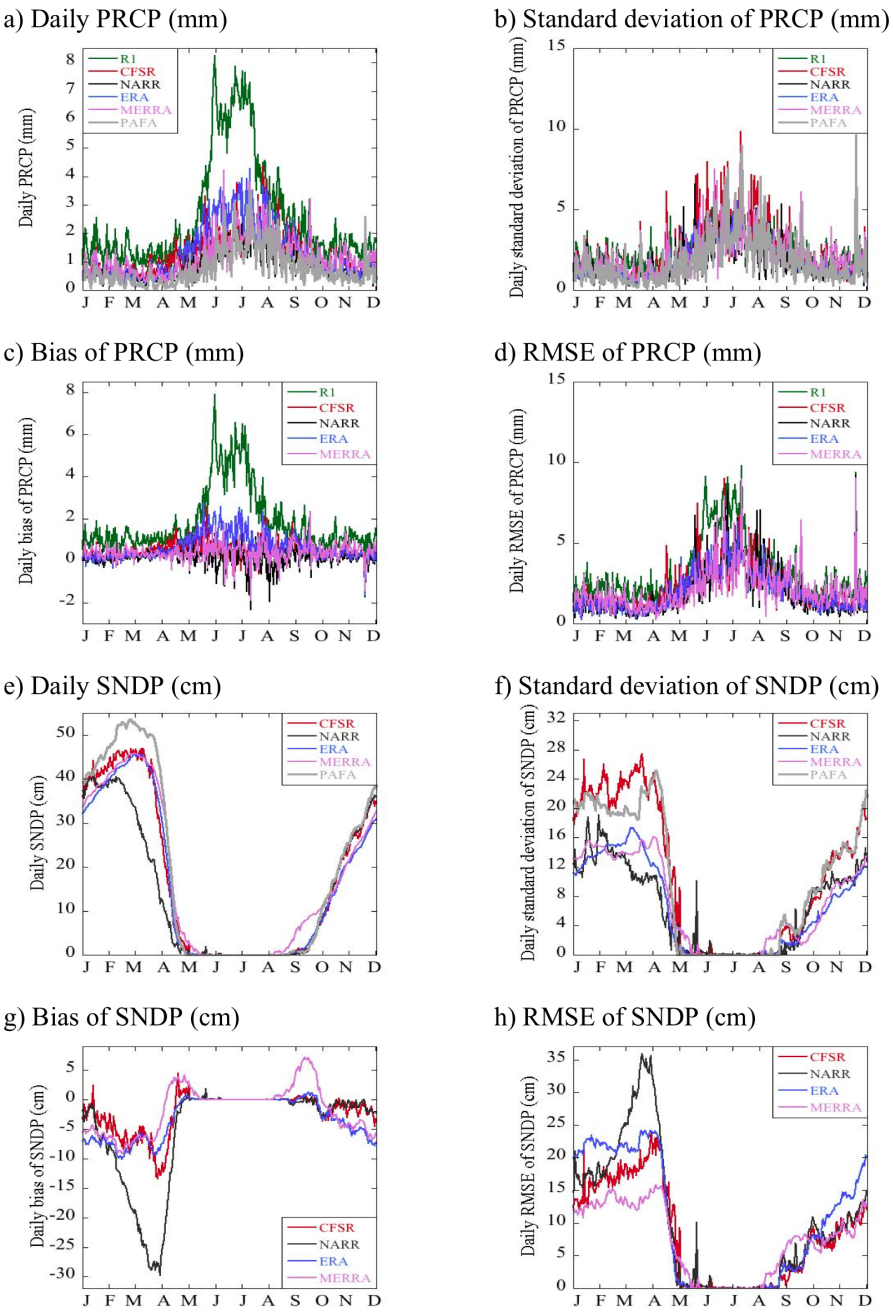

FIG. 4.6.2 Daily climate statistics of PRCP (a-d), and SNDP (e-h) at Fairbanks. The reanalyses are compared to station observations at Fairbanks (gray), 1979-2009.

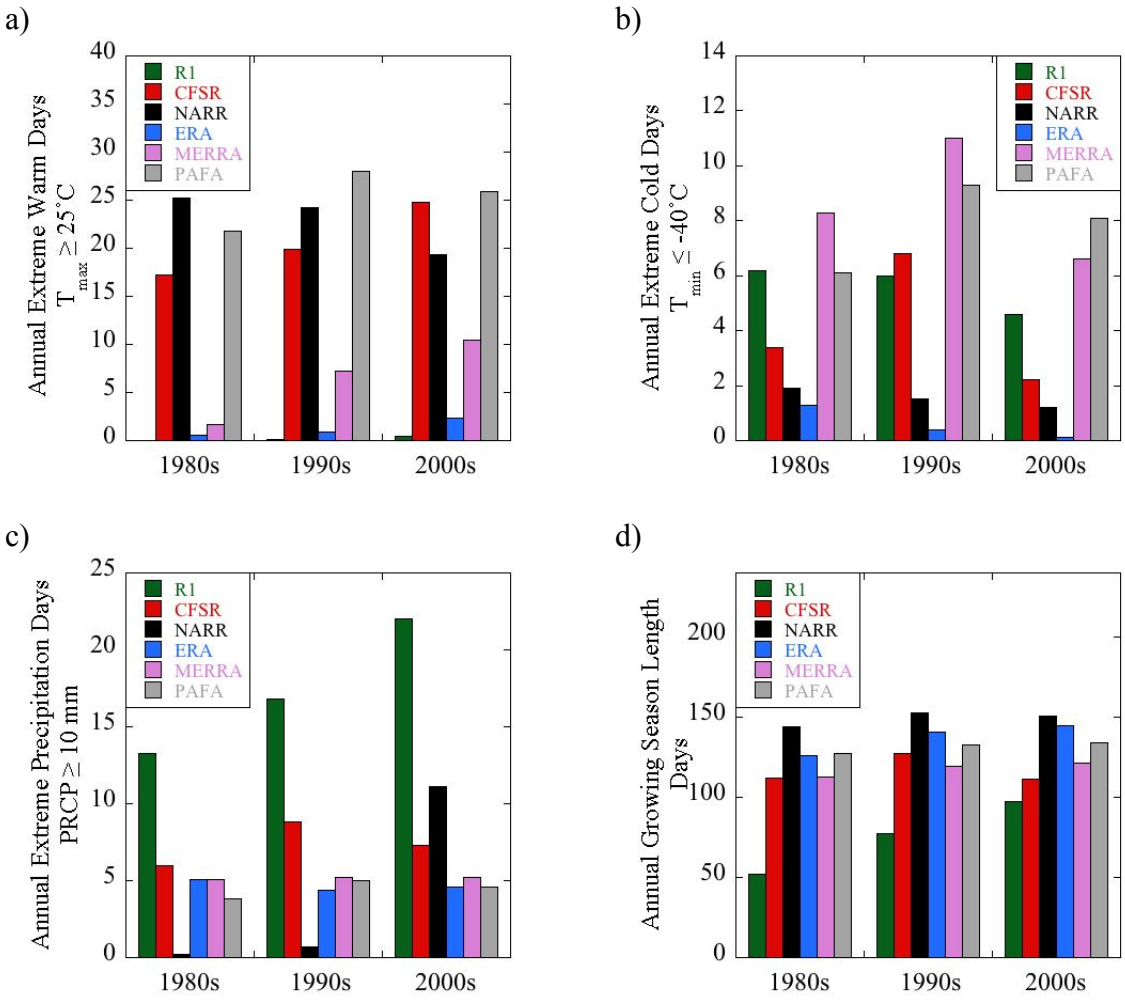

FIG. 4.6.3 Climate extreme indices at Fairbanks: (a) Decadal-average annual counts of Extreme Warm Days (number of days where $T_{max} \geq 25^{\circ}C$), (b) Extreme Cold Days (number of days where $T_{min} \leq -40^{\circ}C$), (c) Extreme Precipitation Days (number of days where PRCP ≥ 10 mm), (d) Growing Season Length (number of days between the fifth consecutive day when $T_{avg} > 0^{\circ}C$ and the day when $T_{min} \leq -2.2^{\circ}C$ for Fairbanks.

a) Monthly mean T_{max} (˚C), 1979-1983

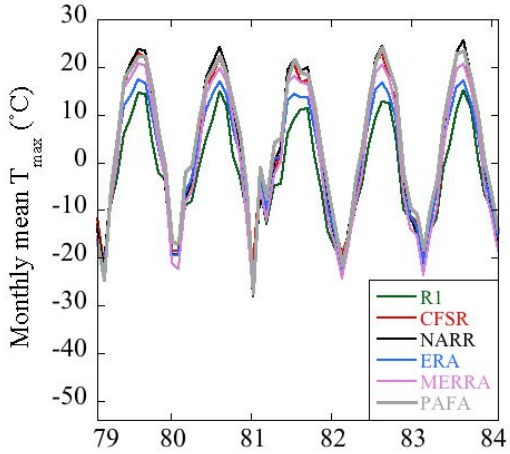

b) Monthly mean T_{max} (˚C), 1984-1988

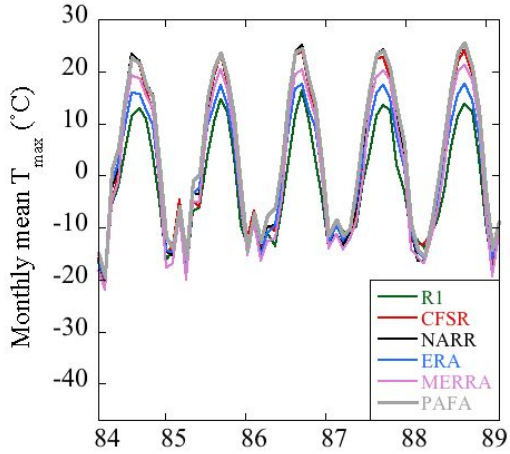

c) Monthly mean T_{max} (˚C), 1989-1993

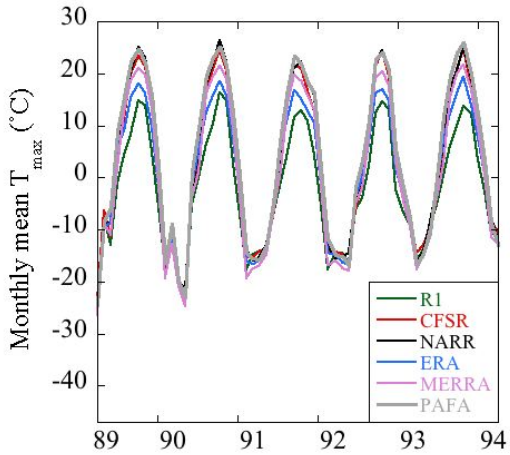

d) Monthly mean T_{max} (˚C), 1994-1998

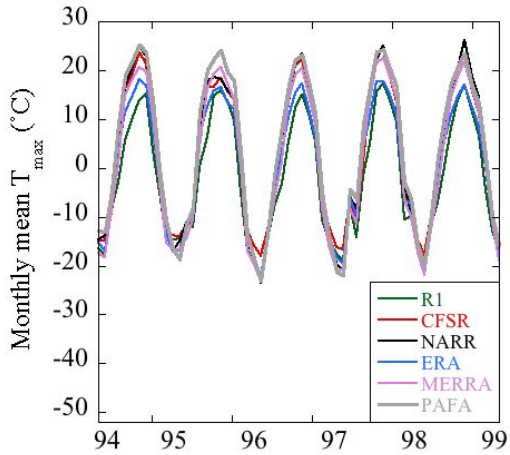

e) Monthly mean T_{max} (˚C), 1999-2003

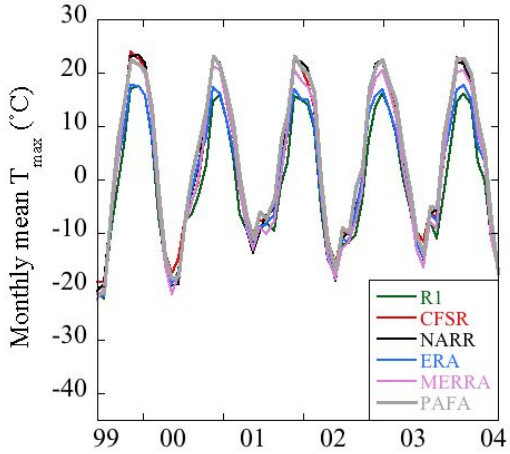

f) Monthly mean T_{max} (˚C), 2004-2009

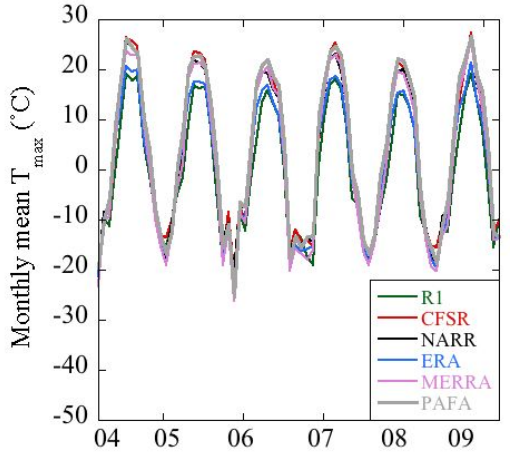

FIG. 4.6.4 Time series of monthly mean T_{max} at Fairbanks (gray) for a) 1979-1983, b) 1984-1988, c) 1989-1993, d) 1994-1998, e) 1999-2003, and f) 2004-2009.

a) Monthly mean T_{min} (˚C), 1979-1983

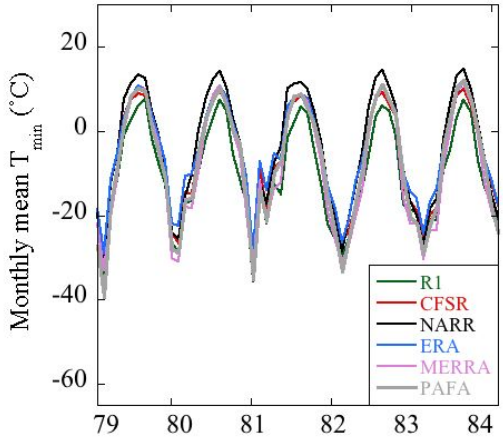

b) Monthly mean T_{min} (˚C), 1984-1988

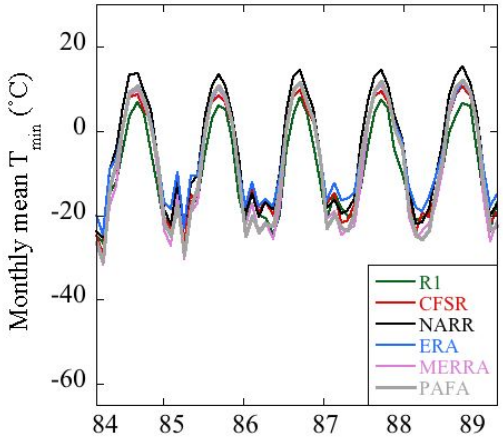

c) Monthly mean T_{min} (˚C), 1989-1993

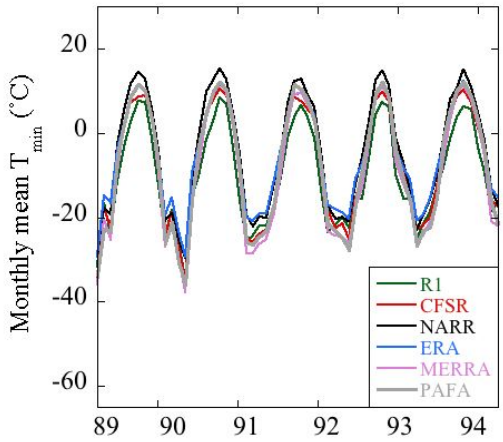

d) Monthly mean T_{min} (˚C), 1994-1998

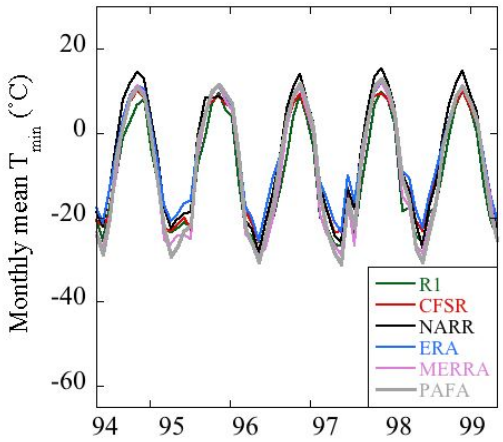

e) Monthly mean T_{min} (˚C), 1999-2003

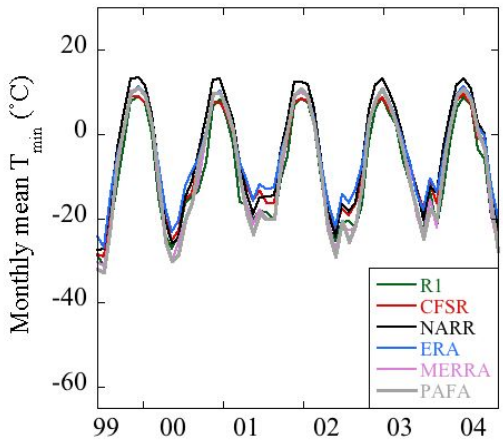

f) Monthly mean T_{min} (˚C), 2004-2009

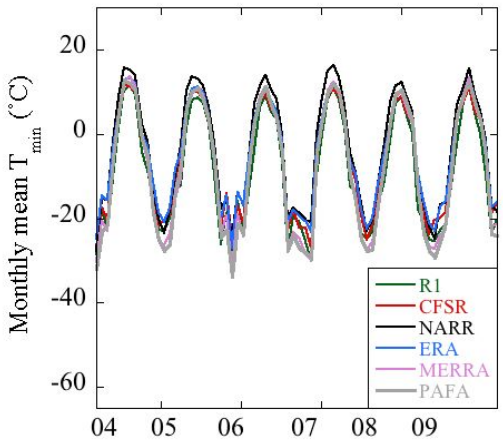

FIG. 4.6.5 Time series of monthly mean T_{min} at Fairbanks (gray) for a) 1979-1983, b) 1984-1988, c) 1989-1993, d) 1994-1998, e) 1999-2003, and f) 2004-2009.

a) Monthly mean PRCP (mm), 1979-1983

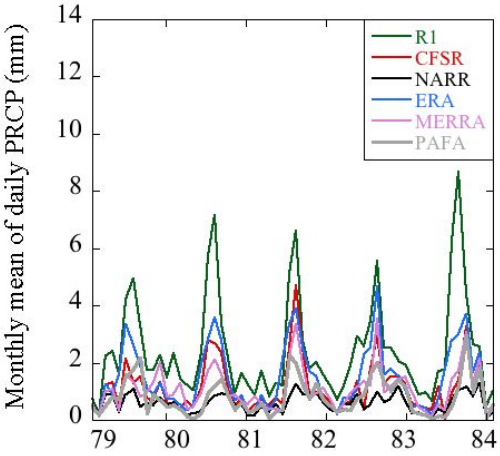

b) Monthly mean PRCP (mm), 1984-1988

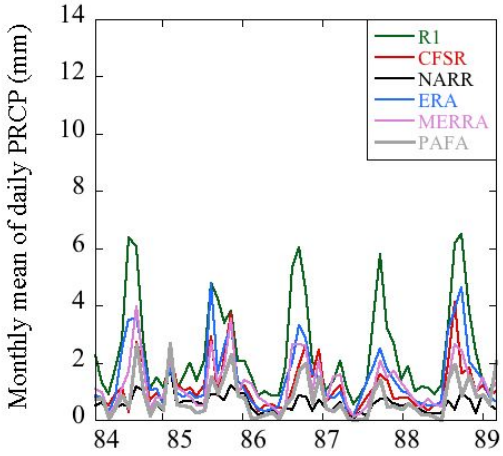

c) Monthly mean PRCP (mm), 1989-1993

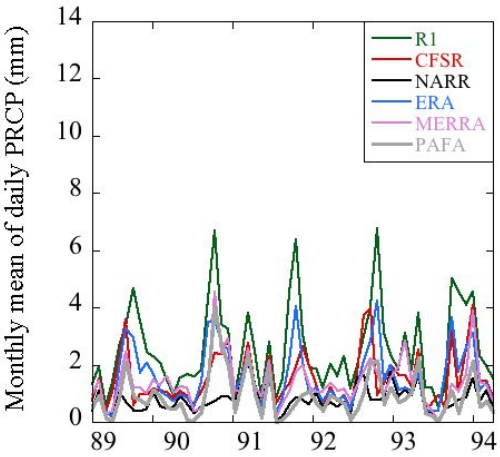

d) Monthly mean PRCP (mm), 1994-1998

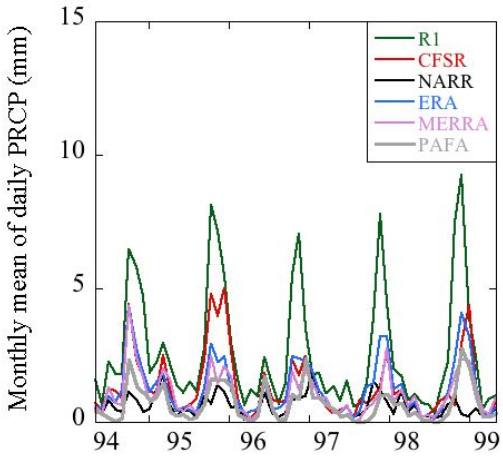

e) Monthly mean PRCP (mm), 1999-2003

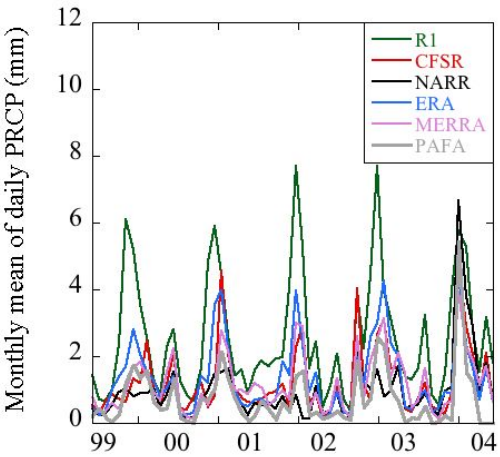

f) Monthly mean PRCP (mm), 2004-2009

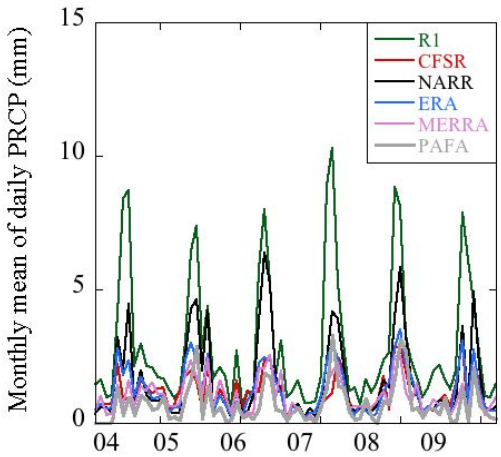

FIG. 4.6.6 Time series of monthly mean of PRCP at Fairbanks (gray) for a) 1979-1983, b) 1984-1988, c) 1989-1993, d) 1994-1998, e) 1999-2003, and f) 2004-2009.

a) Monthly mean SNDP (cm), 1979-1983

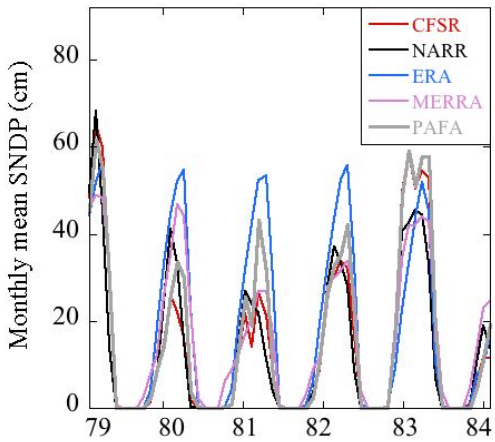

b) Monthly mean SNDP (cm), 1984-1988

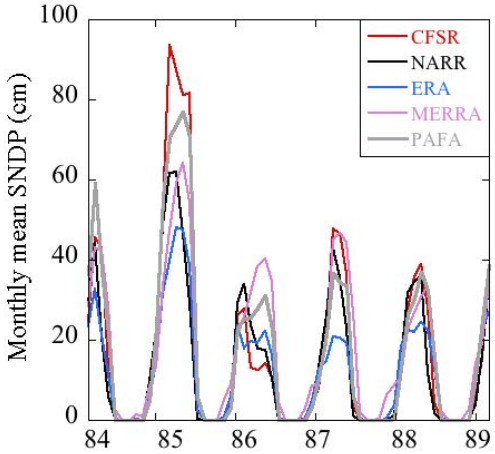

c) Monthly mean SNDP (cm), 1989-1993

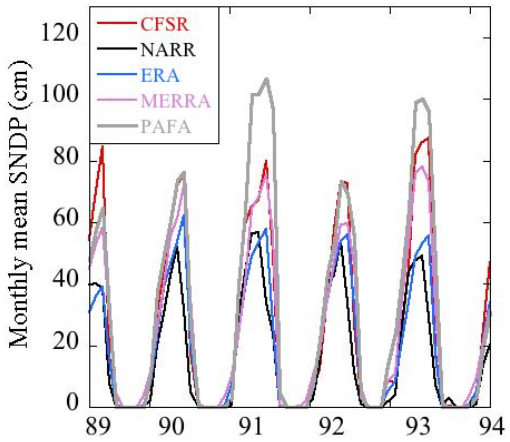

d) Monthly mean SNDP (cm), 1994-1998

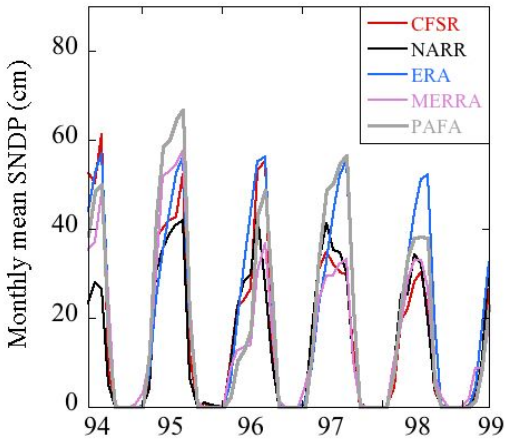

e) Monthly mean SNDP (cm), 1999-2003

f) Monthly mean SNDP (cm), 2004-2009

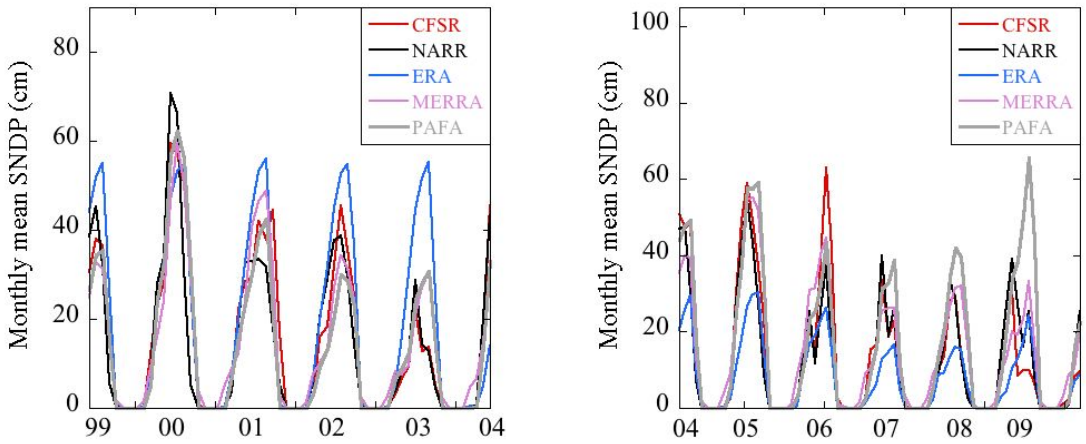

FIG. 4.6.7 Time series of monthly mean SNDP at Fairbanks (gray) for a) 1979-1983, b) 1984-1988, c) 1989-1993, d) 1994-1998, e) 1999-2003, and f) 2004-2009.

Table 4.6.1 Top performing reanalyses for Fairbanks, Alaska, 1979-2009. Performance is based on average RMSE value relative to station observations. The months included in each season are indicated by one-letter abbreviations in parentheses.

	T_{max}	T_{min}	PRCP	SNDP
WINTER (NDJFM)	NARR	MERRA	NARR	MERRA
SPRING (AM)	NARR	ERA	NARR	MERRA
SUMMER (JJA)	NARR	MERRA	MERRA	ERA
AUTUMN (SO)	NARR	CFSR	ERA	CFSR

Table 4.6.2 Seasonal RMSE and bias (high/low) for Fairbanks, Alaska, 1979-2009. Each number represents an average of daily RMSE or bias for the entire season over all 31 years. The RMSE and bias values are relative to station observations.

	WINTER		SPRING		SUMMER		AUTUMN	
T_{max} (˚C)	RMSE	Bias	RMSE	Bias	RMSE	Bias	RMSE	Bias
R1	5.9	-2.2	11.0	-10.3	9.1	-8.0	8.4	-7.4
CFSR	4.8	-0.6	4.9	-3.9	2.4	-0.9	3.1	-2.3
NARR	3.9	-1.1	3.8	-2.7	2.4	-0.3	2.4	-0.7
ERA	4.0	-1.4	5.6	-4.9	6.4	-5.9	4.9	-4.0
MERRA	5.3	-2.9	5.5	-4.6	3.1	-2.5	3.5	-2.8
T_{min} (˚C)	RMSE	Bias	RMSE	Bias	RMSE	Bias	RMSE	Bias
R1	6.3	1.6	7.4	-5.7	4.8	-3.3	6.5	-4.2
CFSR	7.0	3.6	3.3	-0.3	2.9	-1.5	3.3	0.6
NARR	6.2	4.7	4.4	3.2	3.6	2.6	4.0	2.9
ERA	7.4	6.4	2.9	0.4	2.0	-0.1	3.3	1.7
MERRA	5.0	-0.2	4.4	-2.7	2.0	-0.3	3.5	-0.6
PRCP (mm)	RMSE	Bias	RMSE	Bias	RMSE	Bias	RMSE	Bias
R1	2.3	1.0	2.5	1.4	6.1	3.9	2.9	1.3
CFSR	1.5	0.3	2.1	0.7	4.1	0.6	2.2	0.5
NARR	1.3	0.1	1.6	0.3	4.1	0.0	2.1	0.2
ERA	1.4	0.2	2.0	0.8	3.7	1.2	2.1	0.6
MERRA	1.8	0.4	1.5	0.3	3.5	0.4	2.5	0.4
SNDP (cm)	RMSE	Bias	RMSE	Bias	RMSE	Bias	RMSE	Bias
CFSR	14.1	-3.7	14.4	-3.2	0.2	0.0	4.3	-0.5
NARR	18.6	-8.3	18.6	-8.6	1.1	0.1	5.5	-0.7
ERA	19.1	-6.5	14.6	-2.6	0.1	0.0	4.4	-0.3
MERRA	11.6	-5.7	10.4	0.8	0.5	0.0	6.3	3.1

4.7 King Salmon, Alaska

King Salmon is located in the Bristol Bay climate division (Bieniek et al. 2012) along the Alaska Peninsula. King Salmon's coordinates are 58.68˚N, 156.66˚W, and its elevation is 20 m above sea level. The altitude of the nearest land grid point to King Salmon used for each reanalysis evaluation is identified in Table 2.2.1. An overall evaluation based on 16 possible combinations between four seasons and four climate variables, indicates that CFSR is the top model seven times (Table 4.7.1). CFSR is followed by ERA-Interim (four), MERRA (three), and NCEP-R1 and NARR (one each). Model biases of all seasons and variables for King Salmon are given in Table 4.7.2.

The observed mean annual cycle of daily maximum temperature (T_{max}) (see gray line, Fig. 4.7.1a) has a low temperature of -6.0˚C in January, and a high temperature of 19.5˚C in July. The standard deviation of T_{max} ranges from a February maximum of 11.5˚C to a September minimum of 1.7˚C (Fig. 4.7.1b). Model biases of T_{max} (Fig. 4.7.1c) are negative. NCEP-R1 has the coldest bias during spring and summer, while ERA-Interim is the coldest in autumn and winter. MERRA has the lowest seasonal RMSE of T_{max} (see lavender line, Fig. 4.7.1d), which is 1.7˚C during autumn (Table 4.7.2). MERRA, and CFSR have the best representation of Annual Extreme Warm Days (Fig. 4.7.3a), which are defined as days that have a high temperature equal to or greater than 25˚C. The number of Annual Extreme Warm Days increased from the 1980s to the 2000s for King Salmon.

The observed mean annual cycle of daily minimum temperature (T_{min}) (see gray line, Fig. 4.7.1e) has a low temperature of -15.9˚C in December, and a high temperature of 9.2˚C in August. The standard deviation of T_{min} ranges from a January maximum of 13.2˚C to a June minimum of 1.6˚C (Fig. 4.7.1f). Model biases of T_{min} (Fig. 4.7.1g) are positive. NARR has the

warmest bias during spring and autumn, while NCEP-R1 is the warmest during winter, and ERA-Interim is in summer. CFSR has the lowest seasonal RMSE of T_{min} (see red line, Fig. 4.7.1h), which is 2.3˚C during summer (Table 4.7.2). CFSR best represents the number of Annual Extreme Cold Days (Fig. 4.7.3b), which are defined as days that have a low temperature equal to or less than -30˚C. The other models have too few Annual Extreme Cold Days. All of the reanalysis models overestimate Growing Season Length at King Salmon (Fig. 4.7.3d) by approximately three weeks each year. Growing Season Length begins each year following the fifth consecutive day with an average daily temperature above freezing and terminates when T_{min} is at or below -2.2˚C.

The observed mean annual cycle of daily precipitation (PRCP) (see gray line, Fig. 4.7.2a) has a minimum of 0.17 mm in April, and a maximum of 4.7 mm in August. The standard deviation of PRCP (Fig. 4.7.2b) ranges from a March minimum of 0.34 mm to an August peak near 5.0 mm. The one-day maximum standard deviation of PRCP is 7.6 cm, which is the result of one heavy-precipitation event when 15.0 mm fell on 18 May 2009. Model biases of PRCP (Fig. 4.7.2c) are positive throughout the year. NARR has the highest PRCP bias during all seasons. CFSR has the lowest seasonal RMSE of PRCP (see red line, Fig. 4.7.2d), which is 2.7 mm during spring (Table 4.7.2). CFSR also has the best representation of Annual Extreme Precipitation Days (Fig. 4.7.3c), which are defined as days that have an accumulated precipitation equal to or greater than 10 mm. The other models have too many Annual Extreme Precipitation Days for King Salmon.

The observed mean annual cycle of daily snow depth (SNDP) (see gray line, Fig. 4.7.2e) reaches a maximum of 8.4 cm in December, and melts completely by April. The standard deviation of SNDP peaks at 11.7 cm in January (Fig. 4.7.2f). The models have a positive SNDP

bias (Fig. 4.7.2g) during the snow season. ERA-Interim has the lowest bias while MERRA has the highest. MERRA also has a longer snow season compared to observations. ERA-Interim has the lowest seasonal RMSE of SNDP (see blue line, Fig. 4.7.2h), which is 0.0 cm during summer (Table 4.7.2).

CFSR is the top performing reanalysis data set relative to station observations for King Salmon. CFSR reliably produces the number of Annual Extreme Warm Days, Annual Extreme Cold Days, and Annual Extreme Precipitation Days for King Salmon. ERA-Interim is the preferred reanalysis data set for daily SNDP, but not for T_{max} because it has a negative T_{max} bias for most of the year. MERRA is the worst performing model for daily SNDP and produces a long snow season compared to observations. Reanalysis data users that are only interested in a particular variable or season at King Salmon should refer to Tables 4.7.1 and 4.7.2 to help guide the selection of the best available data set. The 31-year time series of T_{max} (Fig. 4.7.4), T_{min} (Fig. 4.7.5), PRCP (Fig. 4.7.6), and SNDP (Fig. 4.7.7) are available for users that are primarily interested in a particular segment of the period used for this study.

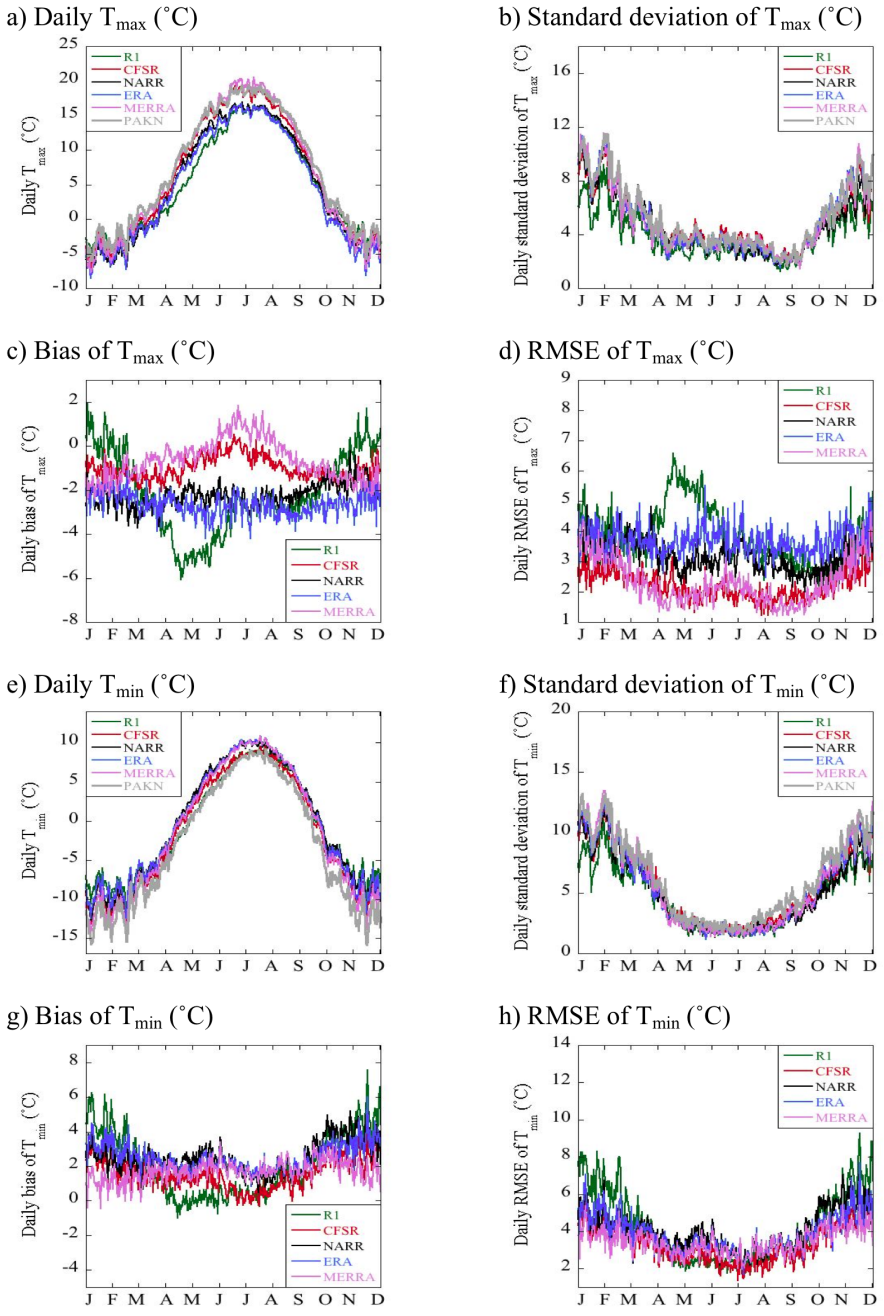

FIG. 4.7.1 Daily climate statistics of T_{max} (a-d), and T_{min} (e-h) at King Salmon. The reanalyses are compared to station observations at King Salmon (gray), 1979-2009.

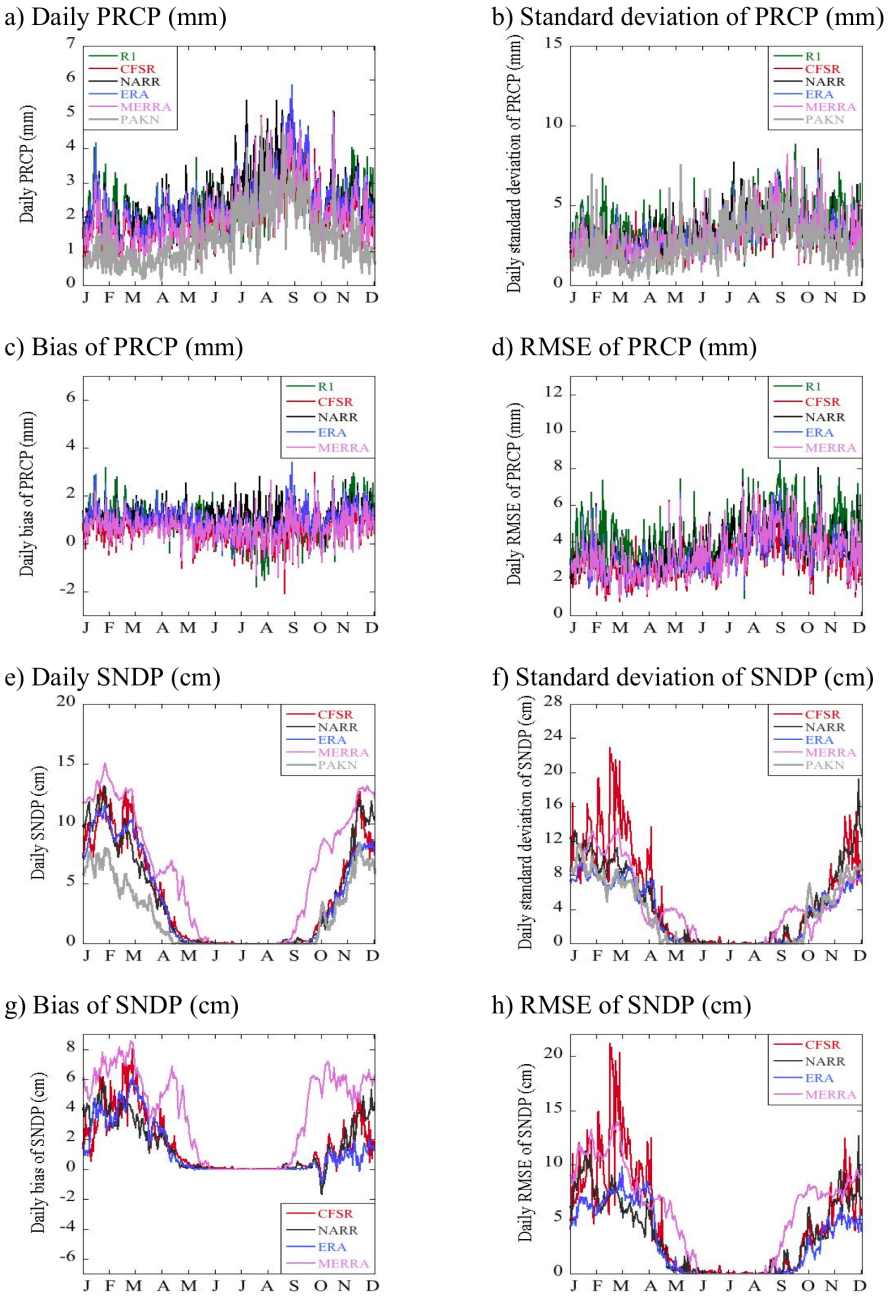

FIG. 4.7.2 Daily climate statistics of PRCP (a-d), and SNDP (e-h) at King Salmon. The reanalyses are compared to station observations at King Salmon (gray), 1979-2009.

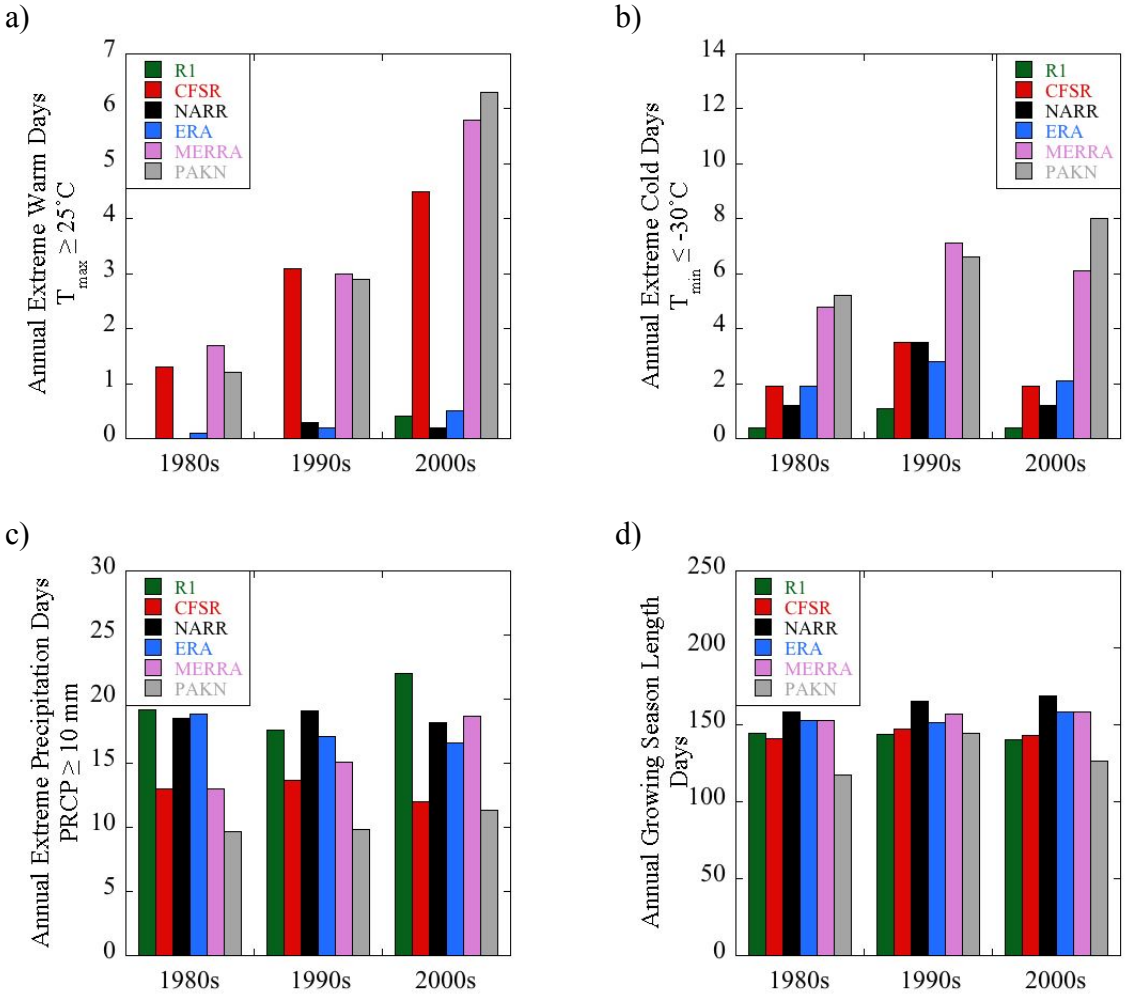

FIG. 4.7.3 Climate extreme indices at King Salmon: (a) Decadal-average annual counts of Extreme Warm Days (number of days where $T_{max} \geq 25^{\circ}C$), (b) Extreme Cold Days (number of days where $T_{min} \leq -30^{\circ}C$), (c) Extreme Precipitation Days (number of days where PRCP ≥ 10 mm), (d) Growing Season Length (number of days between the fifth consecutive day when $T_{avg} > 0^{\circ}C$ and the day when $T_{min} \leq -2.2^{\circ}C$ for King Salmon.

a) Monthly mean T_{max} (˚C), 1979-1983

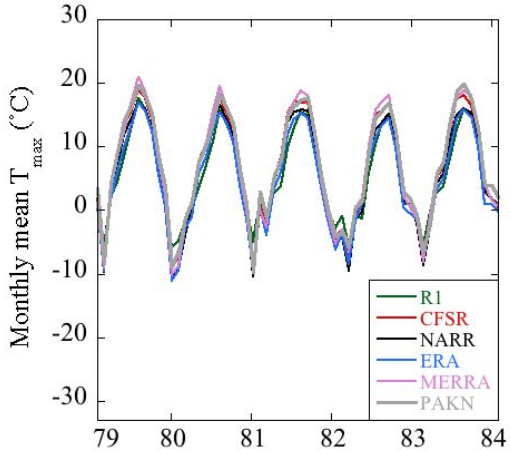

b) Monthly mean T_{max} (˚C), 1984-1988

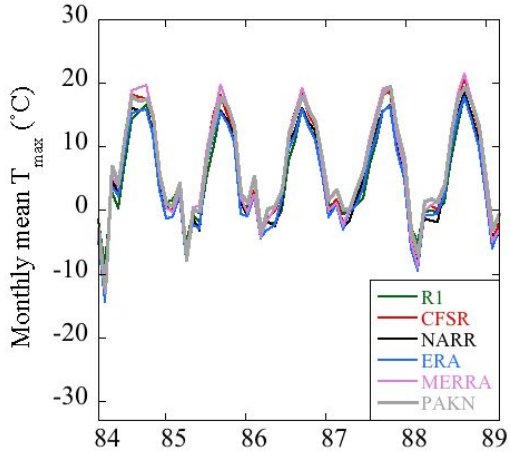

c) Monthly mean T_{max} (˚C), 1989-1993

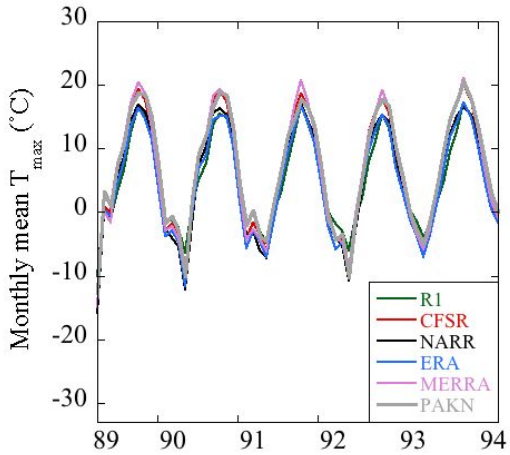

d) Monthly mean T_{max} (˚C), 1994-1998

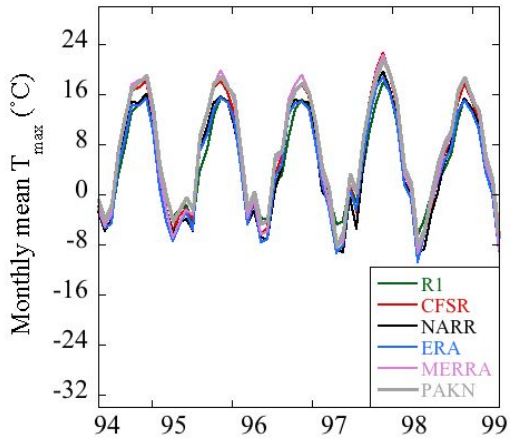

e) Monthly mean T_{max} (˚C), 1999-2003

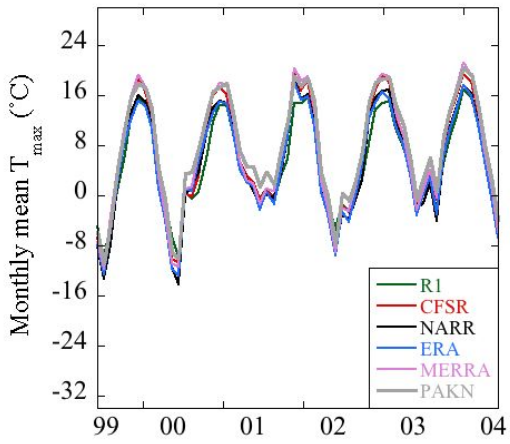

f) Monthly mean T_{max} (˚C), 2004-2009

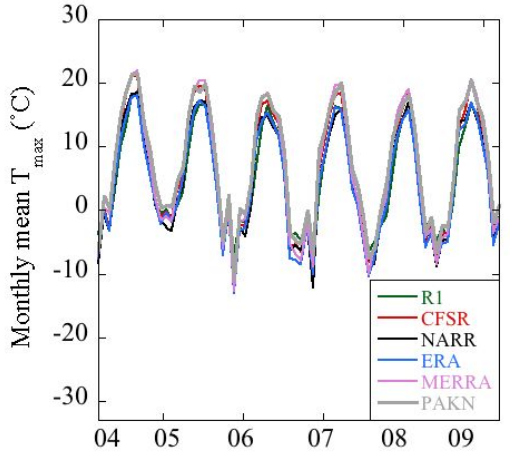

FIG. 4.7.4 Time series of monthly mean T_{max} at King Salmon (gray) for a) 1979-1983, b) 1984-1988, c) 1989-1993, d) 1994-1998, e) 1999-2003, and f) 2004-2009.

a) Monthly mean T_{min} (˚C), 1979-1983

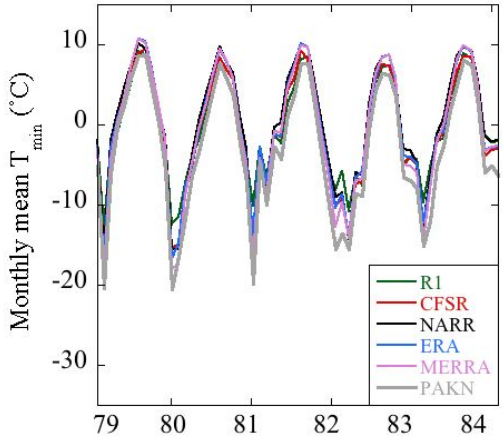

b) Monthly mean T_{min} (˚C), 1984-1988

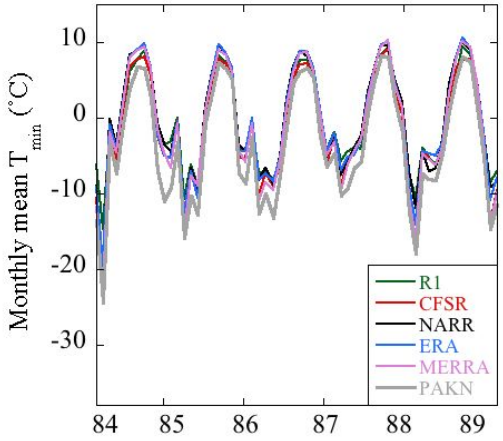

c) Monthly mean T_{min} (˚C), 1989-1993

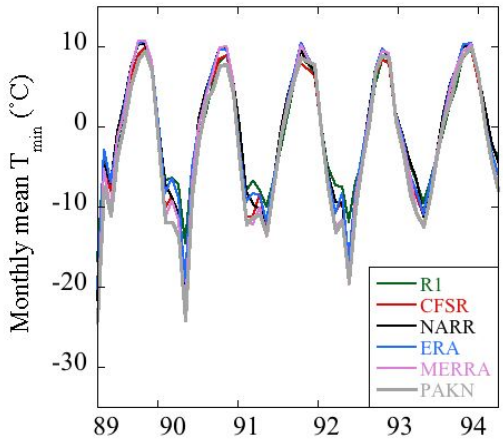

d) Monthly mean T_{min} (˚C), 1994-1998

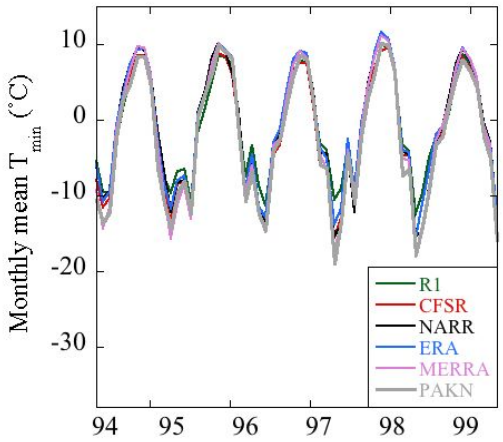

e) Monthly mean T_{min} (˚C), 1999-2003

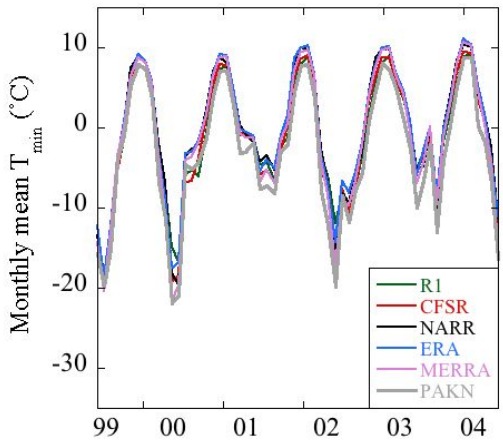

f) Monthly mean T_{min} (˚C), 2004-2009

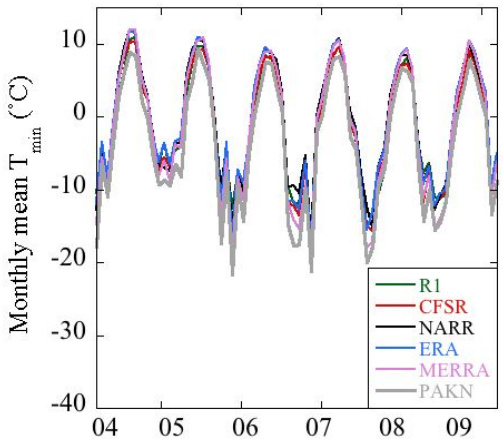

FIG. 4.7.5 Time series of monthly mean T_{min} at King Salmon (gray) for a) 1979-1983, b) 1984-1988, c) 1989-1993, d) 1994-1998, e) 1999-2003, and f) 2004-2009.

a) Monthly mean PRCP (mm), 1979-1983

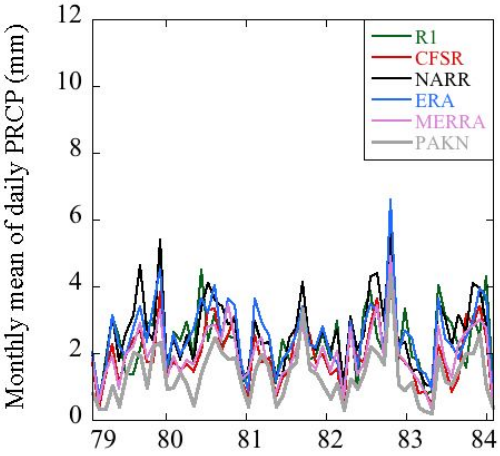

b) Monthly mean PRCP (mm), 1984-1988

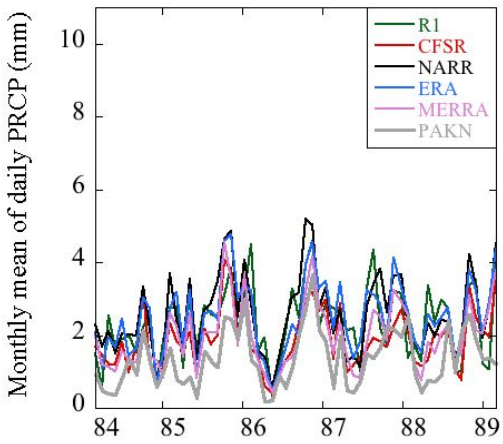

c) Monthly mean PRCP (mm), 1989-1993

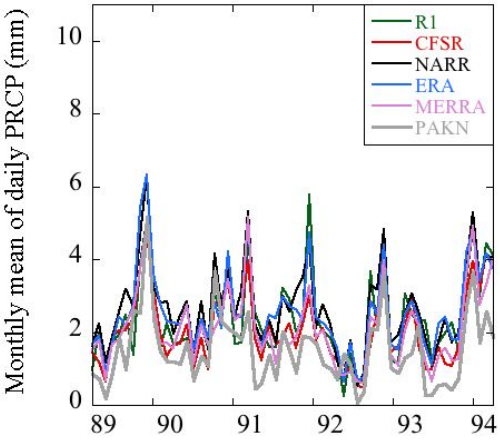

d) Monthly mean PRCP (mm), 1994-1998

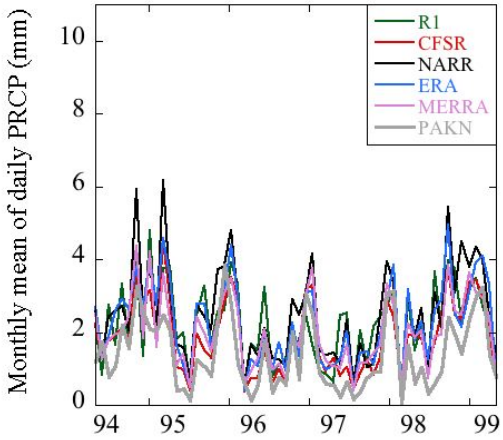

e) Monthly mean PRCP (mm), 1999-2003

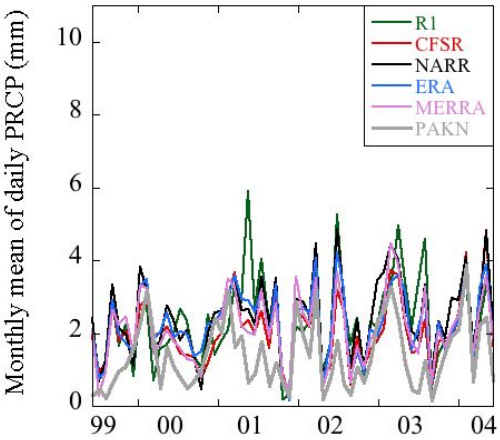

f) Monthly mean PRCP (mm), 2004-2009

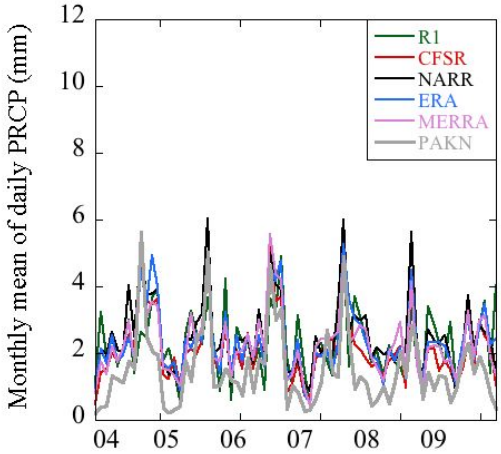

FIG. 4.7.6 Time series of monthly mean PRCP at King Salmon (gray) for a) 1979-1983, b) 1984-1988, c) 1989-1993, d) 1994-1998, e) 1999-2003, and f) 2004-2009.

a) Monthly mean SNDP (cm), 1979-1983

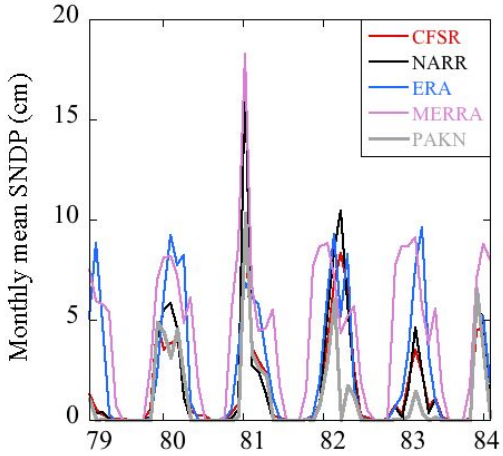

b) Monthly mean SNDP (cm), 1984-1988

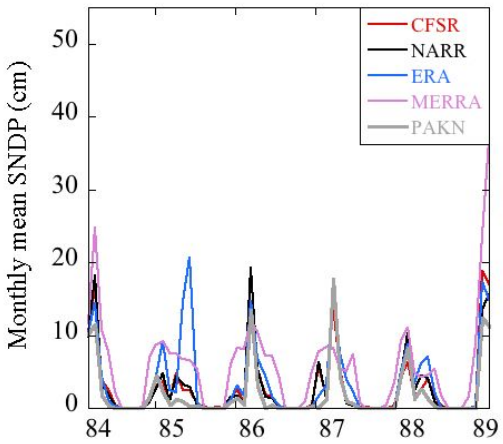

c) Monthly mean SNDP (cm), 1989-1993

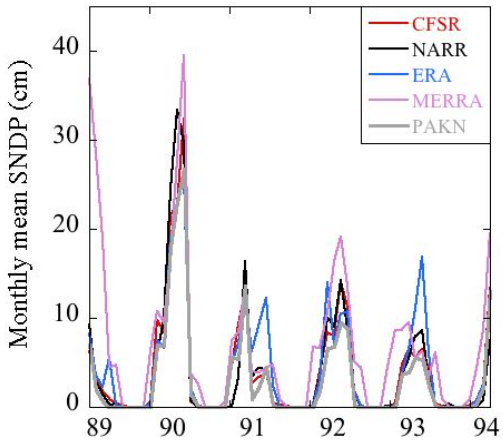

d) Monthly mean SNDP (cm), 1994-1998

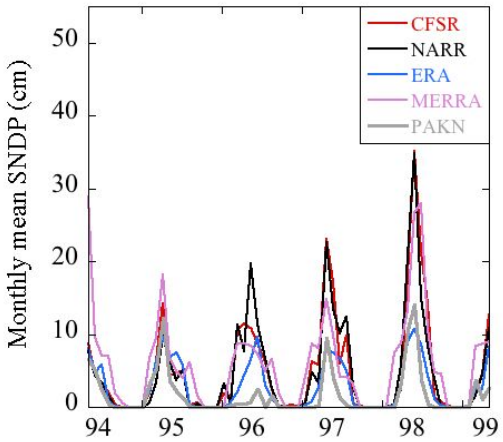

e) Monthly mean SNDP (cm), 1999-2003

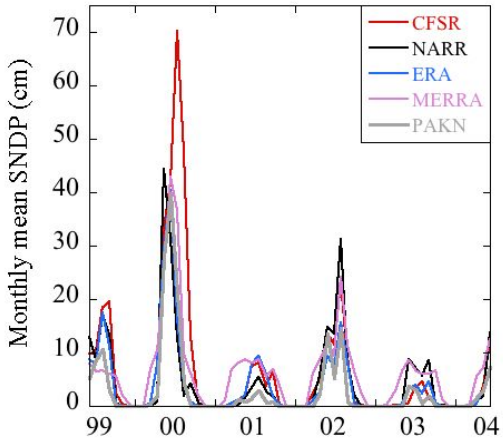

f) Monthly mean SNDP (cm), 2004-2009

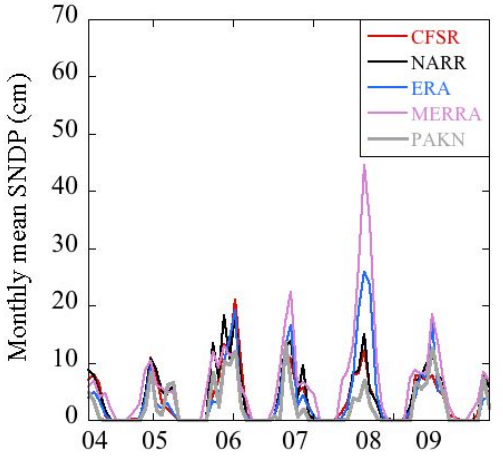

FIG. 4.7.7 Time series of monthly mean SNDP at King Salmon (gray) for a) 1979-1983, b) 1984-1988, c) 1989-1993, d) 1994-1998, e) 1999-2003, and f) 2004-2009.

Table 4.7.1 Top performing reanalyses for King Salmon, Alaska, 1979-2009. Performance is based on average RMSE value relative to station observations. The months included in each season are indicated by one-letter abbreviations in parentheses.

	T_{max}	T_{min}	PRCP	SNDP
WINTER (NDJFM)	CFSR	MERRA	CFSR	ERA
SPRING (AM)	MERRA	R1	CFSR	NARR
SUMMER (JJA)	CFSR	CFSR	ERA	ERA
AUTUMN (SO)	MERRA	CFSR	CFSR	ERA

Table 4.7.2 Seasonal RMSE and bias (high/low) for King Salmon, Alaska, 1979-2009. Each number represents an average of daily RMSE or bias for the entire season over all 31 years. The RMSE and bias values are relative to station observations.

	WINTER		SPRING		SUMMER		AUTUMN	
T_{max} (˚C)	RMSE	Bias	RMSE	Bias	RMSE	Bias	RMSE	Bias
R1	3.8	-0.5	5.3	-4.7	3.9	-3.2	2.9	-2.3
CFSR	2.6	-1.3	2.1	-1.0	1.9	-0.4	1.9	-1.3
NARR	3.5	-2.2	3.1	-2.3	3.1	-2.4	2.7	-2.0
ERA	3.9	-2.4	3.6	-2.8	3.8	-2.8	3.5	-3.0
MERRA	3.0	-1.4	1.8	-0.4	2.1	0.6	1.7	-0.8
T_{min} (˚C)	RMSE	Bias	RMSE	Bias	RMSE	Bias	RMSE	Bias
R1	6.3	3.8	2.8	0.2	2.4	0.4	3.7	2.1
CFSR	4.3	2.1	2.8	1.3	2.3	0.7	3.0	1.5
NARR	5.0	3.0	3.5	2.3	3.2	1.9	4.0	2.6
ERA	4.9	3.1	3.2	2.0	3.1	2.0	3.6	2.4
MERRA	4.0	1.4	3.0	1.7	3.0	1.8	3.5	2.1
PRCP (mm)	RMSE	Bias	RMSE	Bias	RMSE	Bias	RMSE	Bias
R1	4.4	1.2	3.6	1.0	4.4	0.4	5.4	0.5
CFSR	2.9	0.7	2.7	0.6	3.7	0.3	3.9	0.5
NARR	3.4	1.2	3.2	1.1	4.2	1.1	4.4	1.0
ERA	3.3	1.2	2.9	1.1	3.5	0.6	4.4	1.0
MERRA	3.2	0.8	2.8	0.7	3.9	0.5	4.6	0.6
SNDP (cm)	RMSE	Bias	RMSE	Bias	RMSE	Bias	RMSE	Bias
CFSR	9.6	3.2	4.6	1.2	0.2	0.0	1.9	0.2
NARR	7.0	3.1	2.9	0.8	0.1	0.0	2.1	0.0
ERA	5.9	2.6	4.0	0.9	0.0	0.0	1.1	0.0
MERRA	9.7	6.1	5.5	3.8	0.5	0.0	5.2	3.0

4.8 Anchorage, Alaska

Anchorage is located in the Cook Inlet climate division (Bieniek et al. 2012) with the Alaska Range located to the north and the Gulf of Alaska to the south. Anchorage's coordinates are 61.17˚N, 150.03˚W, and its elevation is 37 m above sea level. The altitude of the nearest land grid point to Anchorage used for each reanalysis evaluation is identified in Table 2.2.1. An overall evaluation based on 16 possible combinations between four seasons and four climate variables, indicates that MERRA is the top model seven times (Table 4.8.1). MERRA is followed by ERA-Interim (five), NCEP-R1 (two), and CFSR and NARR (one each). Model biases of all seasons and variables for Anchorage are given in Table 4.8.3.

The observed mean annual cycle of daily maximum temperature (T_{max}) (see gray line, Fig. 4.8.1a) has a low temperature of -5.6˚C in late January, and a high temperature of 20.0˚C in July. The standard deviation of T_{max} ranges from a February maximum of 8.4˚C to a September minimum of 1.4˚C (Fig. 4.8.1b). Model biases of T_{max} (Fig. 4.8.1c) are mixed. MERRA has low bias throughout the year. NARR and CFSR have generally negative biases (≤ 2˚C) for much of year, while ERA-Interim and NCEP-R1 have larger negative T_{max} biases (> 4˚C), particularly during spring and autumn. MERRA has the lowest seasonal RMSE of T_{max} (see lavender line, Fig. 4.8.1d), which is 1.8˚C during summer and autumn (Table 4.8.2). NARR has the best representation of Annual Extreme Warm Days (Fig. 4.8.3a), which are defined as days that have a high temperature equal to or greater than 20˚C. MERRA and CFSR produce too many Annual Extreme Warm Days, while ERA-Interim and NCEP-R1 have too few.

The observed mean annual cycle of daily minimum temperature (T_{min}) (see gray line, Fig. 4.8.1e) has a low temperature of -13.8˚C in January, and a high temperature of 12.0˚C in July. The standard deviation of T_{min} ranges from a February maximum of 9.1˚C to a July minimum of

1.3˚C (Fig. 4.8.1f). ERA-Interim and MERRA have low T_{min} biases (Fig. 4.8.1g) throughout the year. NARR has a slightly positive bias, particularly during spring and autumn. CFSR has negative biases especially during winter, and NCEP-R1 has even larger negative biases (> 5˚C), particularly in spring. MERRA has the lowest seasonal RMSE of T_{min} (see lavender line, Fig. 4.8.1h), which is 1.9˚C during summer (Table 4.8.2). MERRA, along with ERA-Interim and NARR, has the best representation of Annual Extreme Cold Days (Fig. 4.8.3b), which are defined as days that have a low temperature equal to or less than -25˚C. CFSR produces nearly twice as many Annual Extreme Cold Days, while NCEP-R1 has about five times as many compared to observations. The models reliably estimate Growing Season Length at Anchorage (Fig. 4.8.3d) except for NCEP-R1, which has much too short of a growing season. Growing Season Length begins each year following the fifth consecutive day with an average daily temperature above freezing and terminates when T_{min} is at or below -2.2˚C.

The observed mean annual cycle of daily precipitation (PRCP) (see gray line, Fig. 4.8.2a) has a minimum of 0.06 mm in April, and a maximum of 6.9 mm in August. The standard deviation of PRCP ranges from an April minimum of 0.20 mm to an August maximum of 18.9 mm (Fig. 4.8.2b). Model biases of PRCP (Fig. 4.8.2c) are slightly positive for much of the year, and are larger during summer. NARR and ERA-Interim have the wettest biases during all seasons for Anchorage. NCEP-R1 has the lowest seasonal RMSE of PRCP (see green line, Fig. 4.8.2d), which is 2.6 mm during spring (Table 4.8.2). NCEP-R1 also has the best representation of Annual Extreme Precipitation Days (Fig. 4.8.3c), which are defined as days that have an accumulated precipitation equal to or greater than 10 mm. The other models produce twice as many Annual Extreme Precipitation Days compared to observations.

The observed mean annual cycle of daily snow depth (SNDP) (see gray line, Fig. 4.8.2e) reaches a maximum of 29.3 cm in early March, and melts completely by late April. The standard deviation of SNDP peaks at 25.3 cm in March (Fig. 4.8.2f). CFSR has a positive SNDP bias (Fig. 4.8.2g) throughout the snow season that exceeds 20 cm in February. ERA-Interim has a smaller, but still positive SNDP bias. NARR has small positive biases, except during spring when it has a negative SNDP bias. MERRA generally has a low SNDP bias. MERRA also has the lowest seasonal RMSE of SNDP (see lavender line, Fig. 4.8.2h), which is 0.0 cm during summer (Table 4.8.2).

MERRA is the top performing reanalysis data set relative to station observations for Anchorage. MERRA is the preferred reanalysis for daily T_{max}, which is supported by its representation of Annual Extreme Warm Days. MERRA also routinely has the lowest RMSE of daily SNDP. ERA-Interim is the top model for estimating daily $T_{min,}$ however, it consistently has a large negative T_{max} bias (> 4˚C). NCEP-R1 frequently has the lowest bias of daily PRCP that is reflected by its estimation of Annual Extreme Precipitation Days. However, NCEP-R1 fails to represent daily T_{min}, and it produces nearly five times as many Annual Extreme Cold Days compared to observations. Reanalysis data users that are only interested in a particular variable or season at Anchorage should refer to Tables 4.8.1 and 4.8.2 to help guide the selection of the best available data set. The 31-year time series of T_{max} (Fig. 4.8.4), T_{min} (Fig. 4.8.5), PRCP (Fig. 4.8.6), and SNDP (Fig. 4.8.7) are available for users that are primarily interested in a particular segment of the period used for this study.

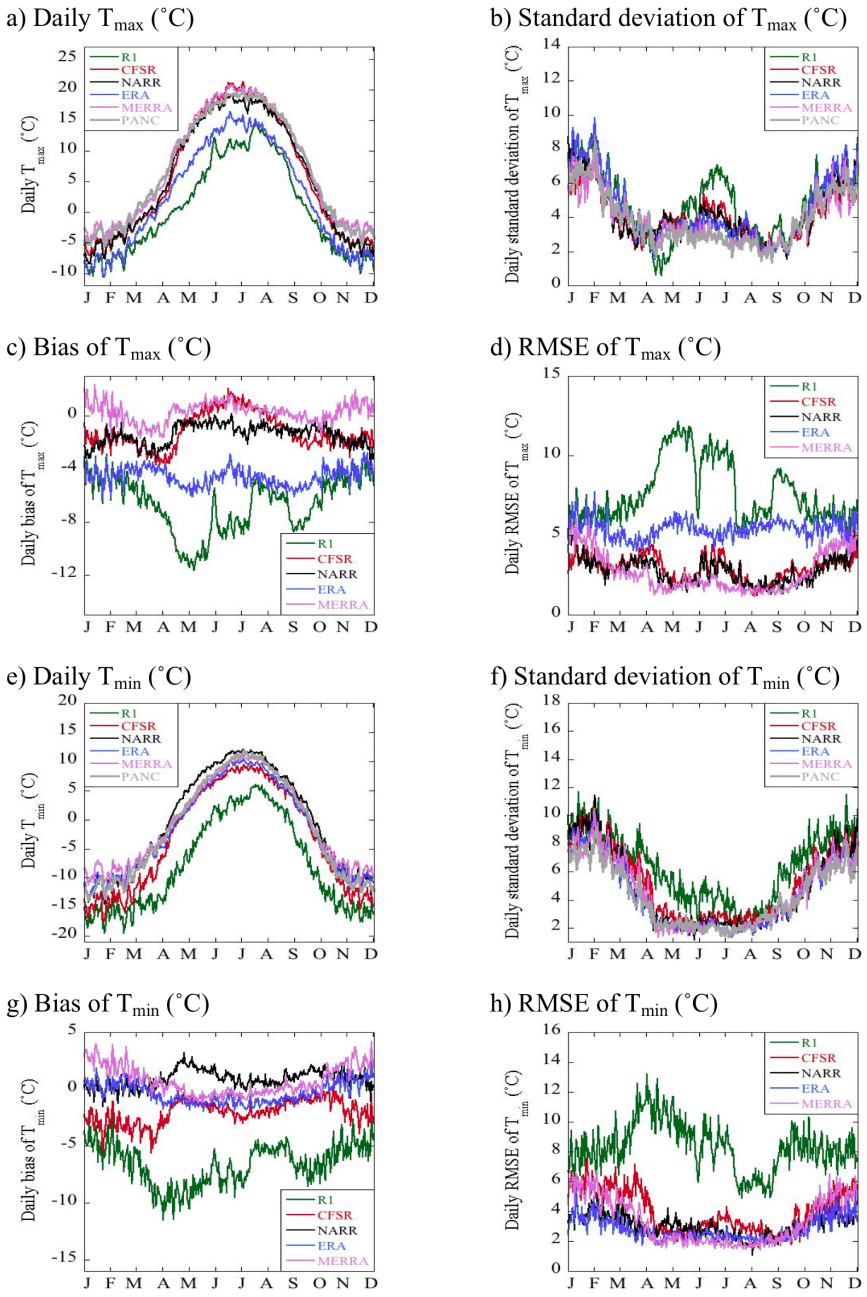

FIG. 4.8.1 Daily climate statistics of T_{max} (a-d), and T_{min} (e-h) at Anchorage. The reanalyses are compared to station observations at Anchorage (gray), 1979-2009.

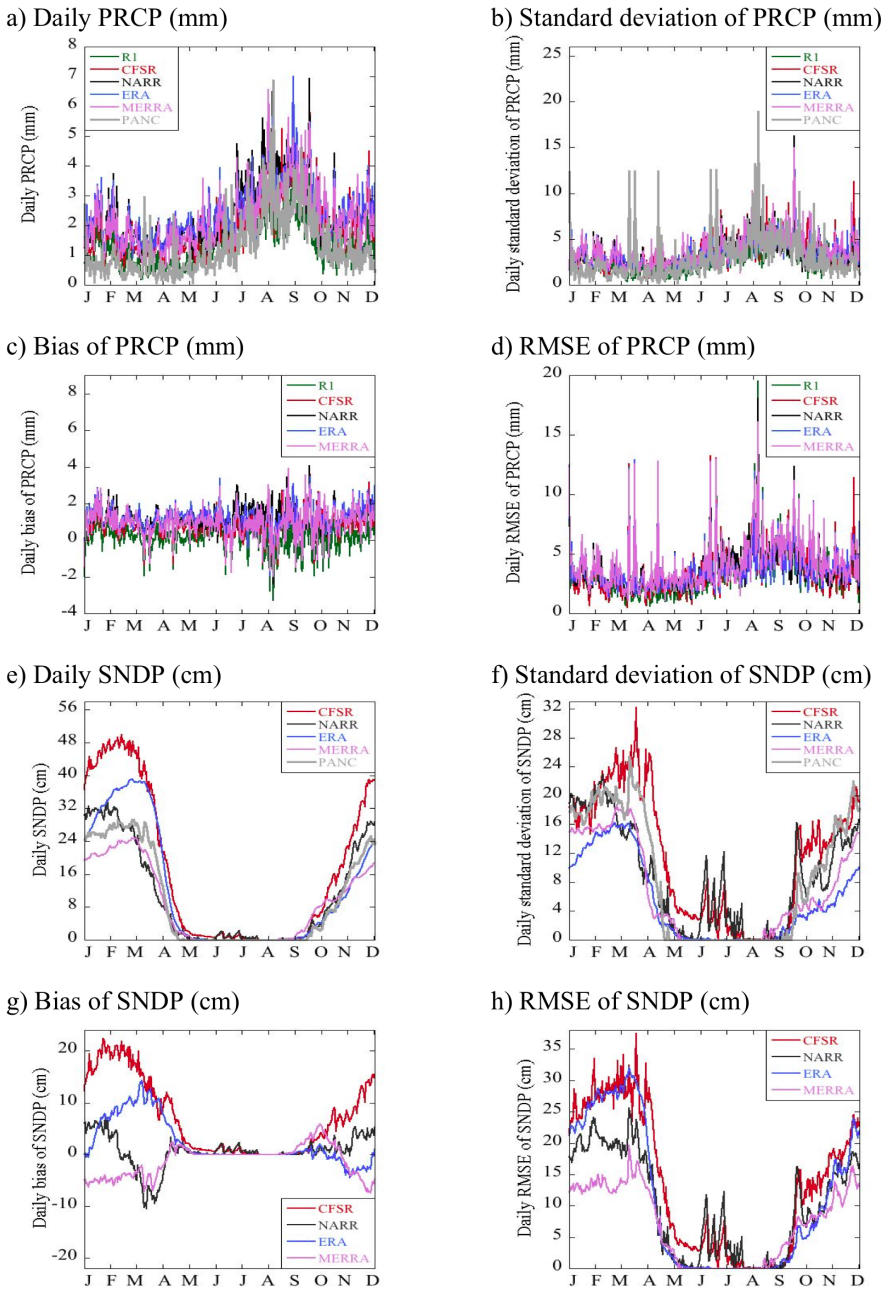

FIG. 4.8.2 Daily climate statistics of PRCP (a-d), and SNDP (e-h) at Anchorage. The reanalyses are compared to station observations at Anchorage (gray), 1979-2009.

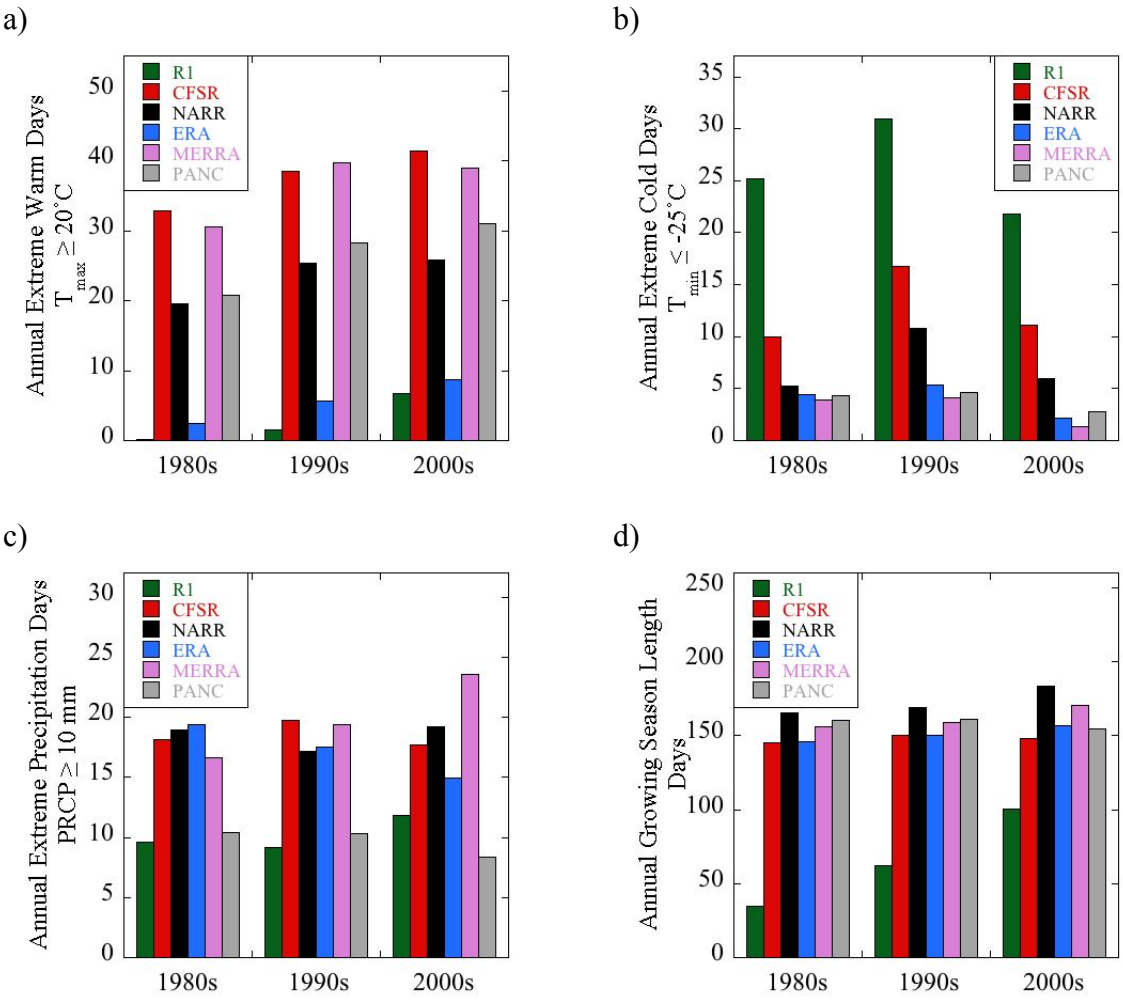

FIG. 4.8.3 Climate extreme indices at Anchorage: (a) Decadal-average annual counts of Extreme Warm Days (number of days where $T_{max} \geq 20^{\circ}C$), (b) Extreme Cold Days (number of days where $T_{min} \leq -25^{\circ}C$), (c) Extreme Precipitation Days (number of days where PRCP ≥ 10 mm), (d) Growing Season Length (number of days between the fifth consecutive day when $T_{avg} > 0^{\circ}C$ and the day when $T_{min} \leq -2.2^{\circ}C$ for Anchorage.

a) Monthly mean T_{max} (˚C), 1979-1983

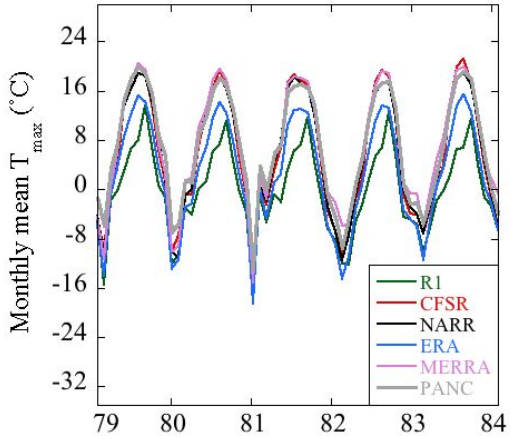

b) Monthly mean T_{max} (˚C), 1984-1988

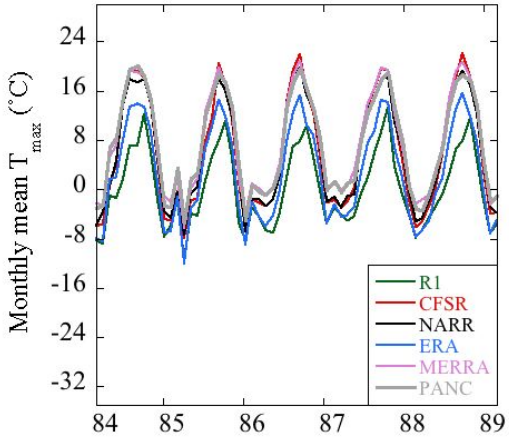

c) Monthly mean T_{max} (˚C), 1989-1993

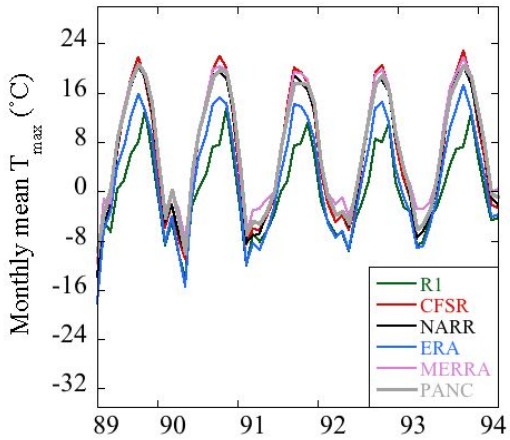

d) Monthly mean T_{max} (˚C), 1994-1998

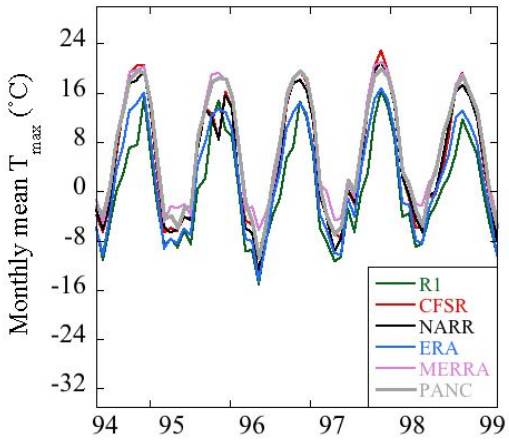

e) Monthly mean T_{max} (˚C), 1999-2003

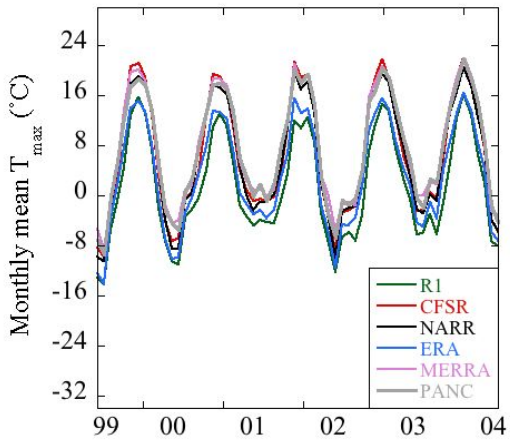

f) Monthly mean T_{max} (˚C), 2004-2009

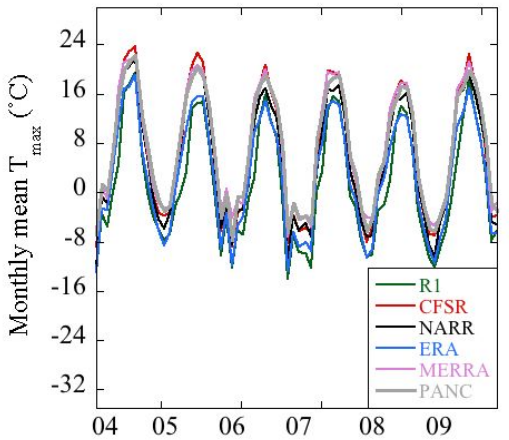

FIG. 4.8.4 Time series of monthly mean T_{max} at Anchorage (gray) for a) 1979-1983, b) 1984-1988, c) 1989-1993, d) 1994-1998, e) 1999-2003, and f) 2004-2009.

a) Monthly mean T_{min} (˚C), 1979-1983

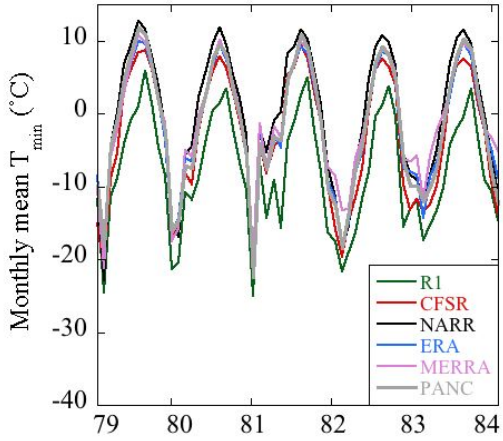

b) Monthly mean T_{min} (˚C), 1984-1988

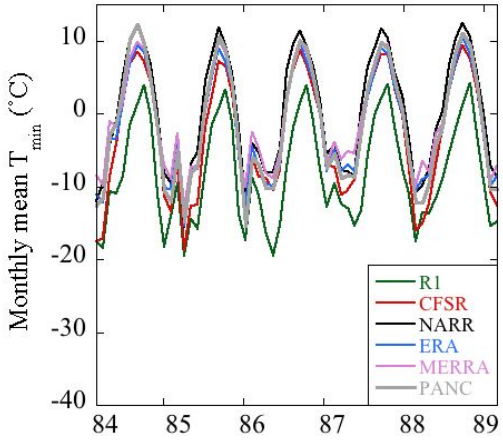

c) Monthly mean T_{min} (˚C), 1989-1993

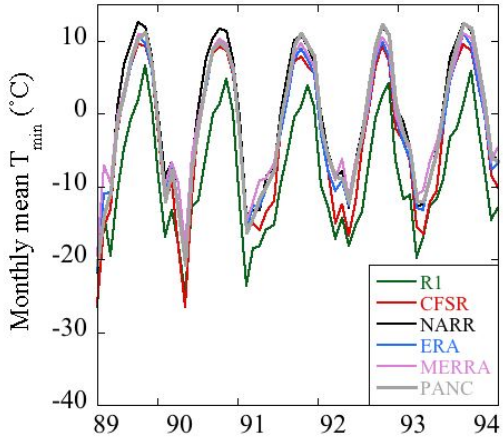

d) Monthly mean T_{min} (˚C), 1994-1998

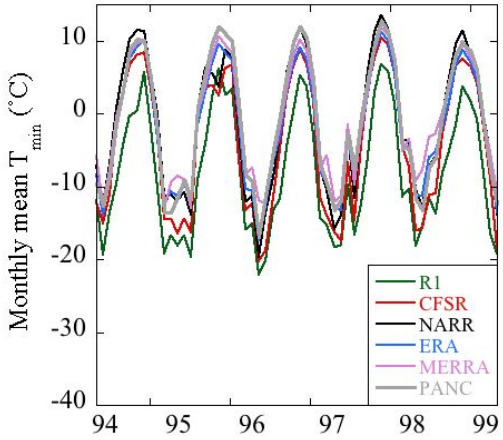

e) Monthly mean T_{min} (˚C), 1999-2003

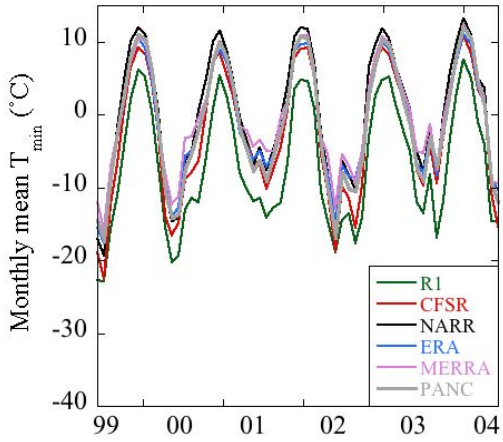

f) Monthly mean T_{min} (˚C), 2004-2009

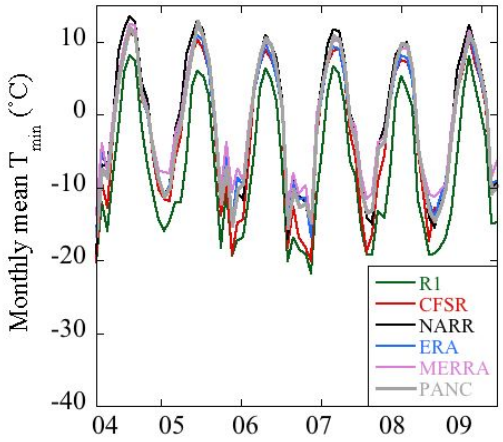

FIG. 4.8.5 Time series of monthly mean T_{min} at Anchorage (gray) for a) 1979-1983, b) 1984-1988, c) 1989-1993, d) 1994-1998, e) 1999-2003, and f) 2004-2009.

a) Monthly mean PRCP (mm), 1979-1983

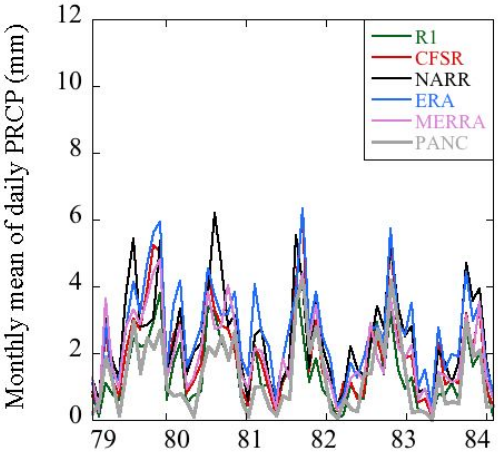

b) Monthly mean PRCP (mm), 1984-1988

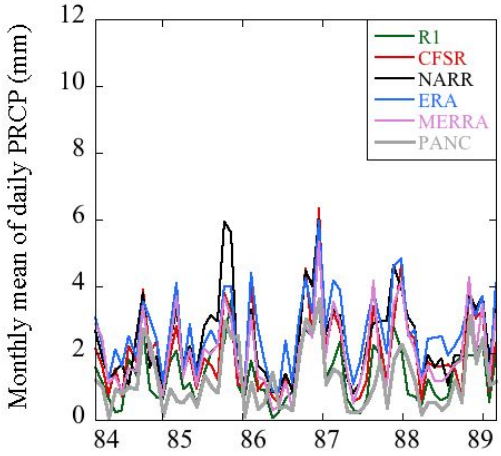

c) Monthly mean PRCP (mm), 1989-1993

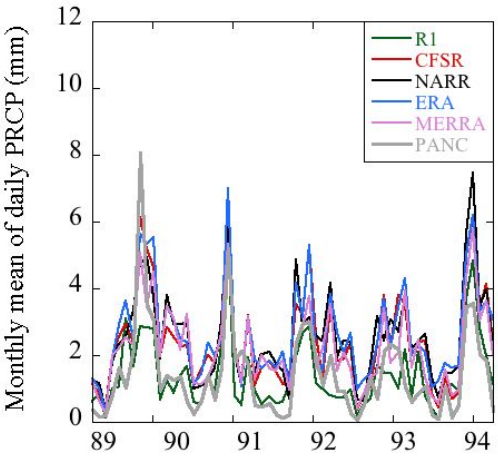

d) Monthly mean PRCP (mm), 1994-1998

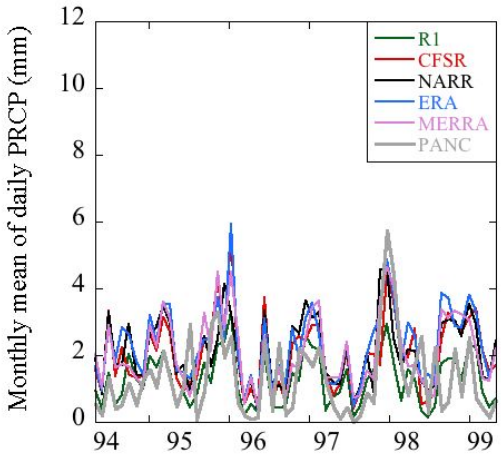

e) Monthly mean PRCP (mm), 1999-2003

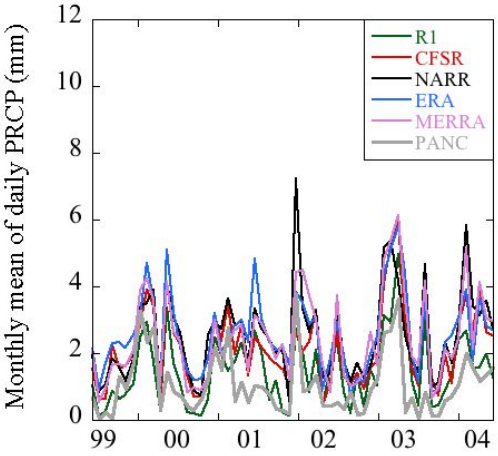

f) Monthly mean PRCP (mm), 2004-2009

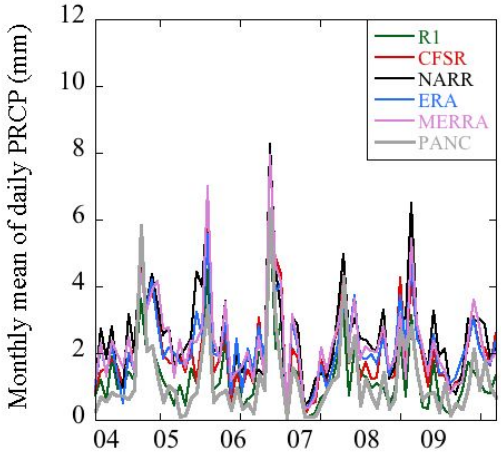

FIG. 4.8.6 Time series of monthly mean PRCP at Anchorage (gray) for a) 1979-1983, b) 1984-1988, c) 1989-1993, d) 1994-1998, e) 1999-2003, and f) 2004-2009.

a) Monthly mean SNDP (cm), 1979-1983

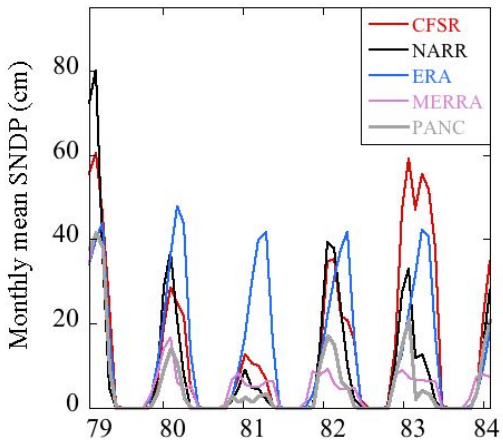

b) Monthly mean SNDP (cm), 1984-1988

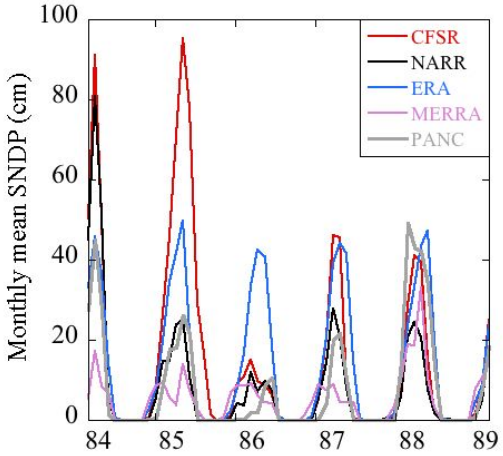

c) Monthly mean SNDP (cm), 1989-1993

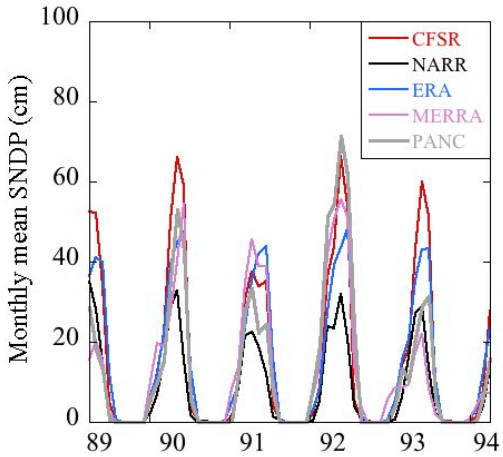

d) Monthly mean SNDP (cm), 1994-1998

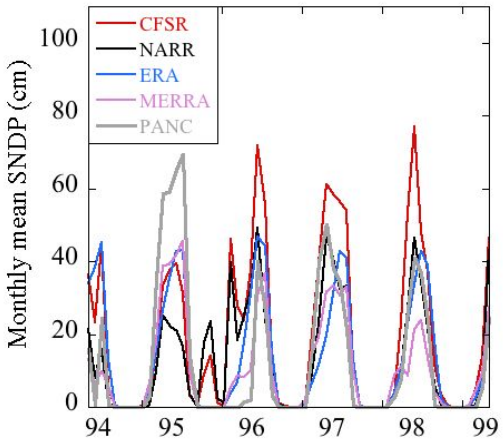

e) Monthly mean SNDP (cm), 1999-2003

f) Monthly mean SNDP (cm), 2004-2009

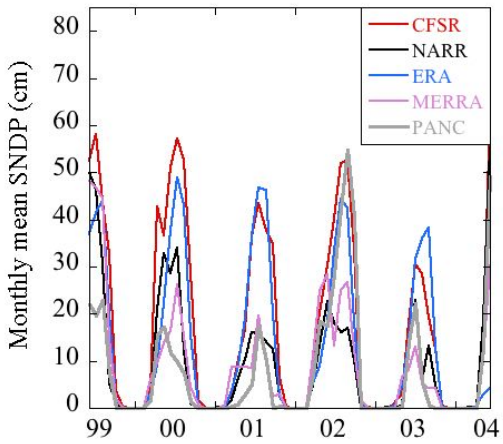

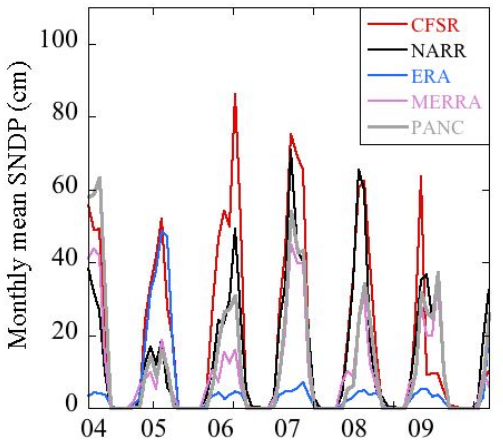

FIG. 4.8.7 Time series of monthly mean SNDP at Anchorage (gray) for a) 1979-1983, b) 1984-1988, c) 1989-1993, d) 1994-1998, e) 1999-2003, and f) 2004-2009.

Table 4.8.1 Top performing reanalyses for Anchorage, Alaska, 1979-2009. Performance is based on average RMSE value relative to station observations. The months included in each season are indicated by one-letter abbreviations in parentheses.

	T_{max}	T_{min}	PRCP	SNDP
WINTER (NDJFM)	CFSR	ERA	R1	MERRA
SPRING (AM)	MERRA	ERA	R1	MERRA
SUMMER (JJA)	MERRA	MERRA	ERA	MERRA
AUTUMN (SO)	MERRA	ERA	NARR	ERA

Table 4.8.2 Seasonal RMSE and bias (high/low) for Anchorage, Alaska, 1979-2009. Each number represents an average of daily RMSE or bias for the entire season over all 31 years. The RMSE and bias values are relative to station observations.

	WINTER		SPRING		SUMMER		AUTUMN	
T_{max} (˚C)	RMSE	Bias	RMSE	Bias	RMSE	Bias	RMSE	Bias
R1	6.4	-5.0	10.0	-9.5	8.8	-7.4	7.6	-7.1
CFSR	3.3	-1.9	3.1	-1.6	2.8	0.7	2.4	-1.6
NARR	3.4	-2.0	2.6	-1.3	2.5	-0.8	2.1	-1.1
ERA	5.5	-4.2	5.4	-5.0	5.2	-4.6	5.6	-5.2
MERRA	4.0	0.2	2.0	0.1	1.8	0.7	1.8	-0.1
T_{min} (˚C)	RMSE	Bias	RMSE	Bias	RMSE	Bias	RMSE	Bias
R1	8.2	-5.5	10.6	-9.3	7.7	-6.7	7.8	-6.4
CFSR	5.3	-2.6	3.4	-1.7	3.1	-2.0	2.9	-1.0
NARR	3.7	0.5	2.9	1.6	2.5	0.9	2.6	1.3
ERA	3.5	0.5	2.4	-1.1	2.3	-1.2	2.3	-0.6
MERRA	5.0	2.0	2.4	-0.1	1.9	-0.4	2.5	0.2
PRCP (mm)	RMSE	Bias	RMSE	Bias	RMSE	Bias	RMSE	Bias
R1	3.4	0.2	2.6	0.1	4.8	0.1	5.1	-0.1
CFSR	3.6	0.9	3.0	0.8	4.9	0.7	5.1	1.1
NARR	3.8	1.2	3.1	1.0	5.1	1.2	5.0	1.2
ERA	4.0	1.3	3.0	1.2	4.5	1.1	5.1	1.3
MERRA	4.2	1.1	3.4	0.9	5.0	0.7	6.0	1.0
SNDP (cm)	RMSE	Bias	RMSE	Bias	RMSE	Bias	RMSE	Bias
CFSR	24.3	14.2	16.1	5.3	3.1	0.5	7.6	1.3
NARR	18.0	1.2	9.5	-0.6	4.2	0.5	6.7	0.5
ERA	23.0	3.9	11.5	3.4	0.1	0.0	3.3	0.4
MERRA	12.8	-3.7	7.6	0.0	0.0	0.0	4.9	2.2

4.9 Juneau, Alaska

Juneau is located in the Southeast climate division (Bieniek et al. 2012) in the Alaskan Panhandle. Juneau's coordinates are 58.36˚N, 134.56˚W, and its elevation is close to sea level. The altitude of the nearest land grid point to Juneau used for each reanalysis evaluation is identified in Table 2.2.1. An overall evaluation based on 16 possible combinations between four seasons and four climate variables, indicates that MERRA is the top model seven times (Table 4.9.1). MERRA is followed by NARR (five), ERA-Interim (four), and CFSR and NCEP-R1 (zero). Model biases of all seasons and variables for Juneau are given in Table 4.9.2.

The observed mean annual cycle of daily maximum temperature (T_{max}) (see gray line, Fig. 4.9.1a) has a low temperature of -0.5˚C in early January, and a high temperature of 20.1˚C in August. The standard deviation of T_{max} ranges from a January maximum of 5.8˚C to a September minimum of 1.3˚C (Fig. 4.9.1b). Model biases of T_{max} (Fig. 4.9.1c) are generally negative, except for MERRA, which has low bias throughout the year. NCEP-R1 has the largest negative T_{max} bias, which exceeds 8.0˚C in spring. MERRA has the lowest seasonal RMSE of T_{max} (see lavender line, Fig. 4.9.1d), which is 1.7˚C during autumn (Table 4.9.2). MERRA also has the best representation of Annual Extreme Warm Days (Fig. 4.9.3a), which are defined as days that have a high temperature equal to or greater than 25˚C. The other models produce far too few Annual Extreme Warm Days during the 31-year period for Juneau.

The observed mean annual cycle of daily minimum temperature (T_{min}) (see gray line, Fig. 4.9.1e) has a low temperature of -6.6˚C in January, and a high temperature of 10.7˚C in late July. The standard deviation of T_{min} ranges from a January maximum of 7.6˚C to a July minimum of 1.0˚C (Fig. 4.9.1f). ERA-Interim, NARR, and MERRA have positive T_{min} biases (Fig. 4.9.1g) throughout the year of 1.0˚C, 1.5˚C, and 2.0˚C, respectively. CFSR has a persistent negative T_{min}

bias of around 2˚C, and NCEP-R1 has even colder biases that range from 2-5˚C. ERA-Interim has the lowest seasonal RMSE of T_{min} (see blue line, Fig. 4.9.1h), which is 2.0˚C during summer (Table 4.9.2). NARR has the best representation of Annual Extreme Cold Days (Fig. 4.9.3b), which are defined as days that have a low temperature equal to or less than -20˚C. NCEP-R1 and CFSR produce nearly four times as many Annual Extreme Cold Days compared to observations. The models reliably estimate Growing Season Length at Juneau (Fig. 4.9.3d), except for NCEP-R1, which has too short of a growing season. However, NCEP-R1 has shown improvement from the 1980s to the 2000s. Growing Season Length begins each year following the fifth consecutive day with an average daily temperature above freezing and terminates when T_{min} is at or below -2.2˚C.

The observed mean annual cycle of daily precipitation (PRCP) (see gray line, Fig. 4.9.2a) has a minimum of 0.90 mm in May, and a maximum of 10.9 mm in October. The standard deviation of PRCP ranges from a May minimum of 1.6 mm to a November maximum of 19.2 mm (Fig. 4.9.2b). Model biases of PRCP (Fig. 4.9.2c) are generally positive, except for autumn when NARR has a negative bias of up to 5 mm. The highest positive PRCP biases also occur in autumn when CFSR has daily biases that exceed 10 mm. CFSR has the highest PRCP bias during all seasons. MERRA has the lowest seasonal RMSE of PRCP (see lavender line, Fig. 4.9.2d), which is 4.9 mm during spring (Table 4.9.2). The models represent Annual Extreme Precipitation Days (Fig. 4.9.3c) well, except for ERA-Interim, which has close to two times the number of days and CFSR, which has nearly four times as many compared to observations. Annual Extreme Precipitation Days are defined as days that have an accumulated precipitation equal to or greater than 25 mm for Juneau.

The observed mean annual cycle of daily snow depth (SNDP) (see gray line, Fig. 4.9.2e) reaches a maximum of 17.6 cm in late January, and melts completely by early April. The standard deviation of SNDP peaks at 21.9 cm in January (Fig. 4.9.2f). NARR has low SNDP bias (Fig. 4.9.2g) during the snow season, while CFSR, MERRA, and ERA-Interim have positive biases that reach as high as 20 cm, 10 cm, and 5 cm, respectively. MERRA has the lowest seasonal RMSE of SNDP (see lavender line, Fig. 4.9.2h), which is 0.0 cm during summer (Table 4.9.2).

MERRA is the top performing reanalysis data set relative to station observations for Juneau. MERRA is the preferred reanalysis for daily T_{max}, which is supported by its reliable representation of Annual Extreme Warm Days. MERRA also best predicts daily PRCP, and has the lowest seasonal RMSE of PRCP, which is during spring. NARR is the top model for estimating daily T_{min} for Juneau, and it has the closest number of Annual Extreme Cold Days compared to observations. NCEP-R1 fails to represent daily T_{max} and T_{min} because it consistently has negative biases of 5-10˚C. Similarly, CFSR does not accurately model daily PRCP and SNDP for Juneau. CFSR has four times as many Annual Extreme Precipitation Days compared to observations and has SNDP biases greater than 20 cm in February. Reanalysis data users that are only interested in a particular variable or season at Juneau should refer to Tables 4.9.1 and 4.9.2 to help guide the selection of the best available data set. The 31-year time series of T_{max} (Fig. 4.9.4), T_{min} (Fig. 4.9.5), PRCP (Fig. 4.9.6), and SNDP (Fig. 4.9.7) are available for users that are primarily interested in a particular segment of the period used for this study.

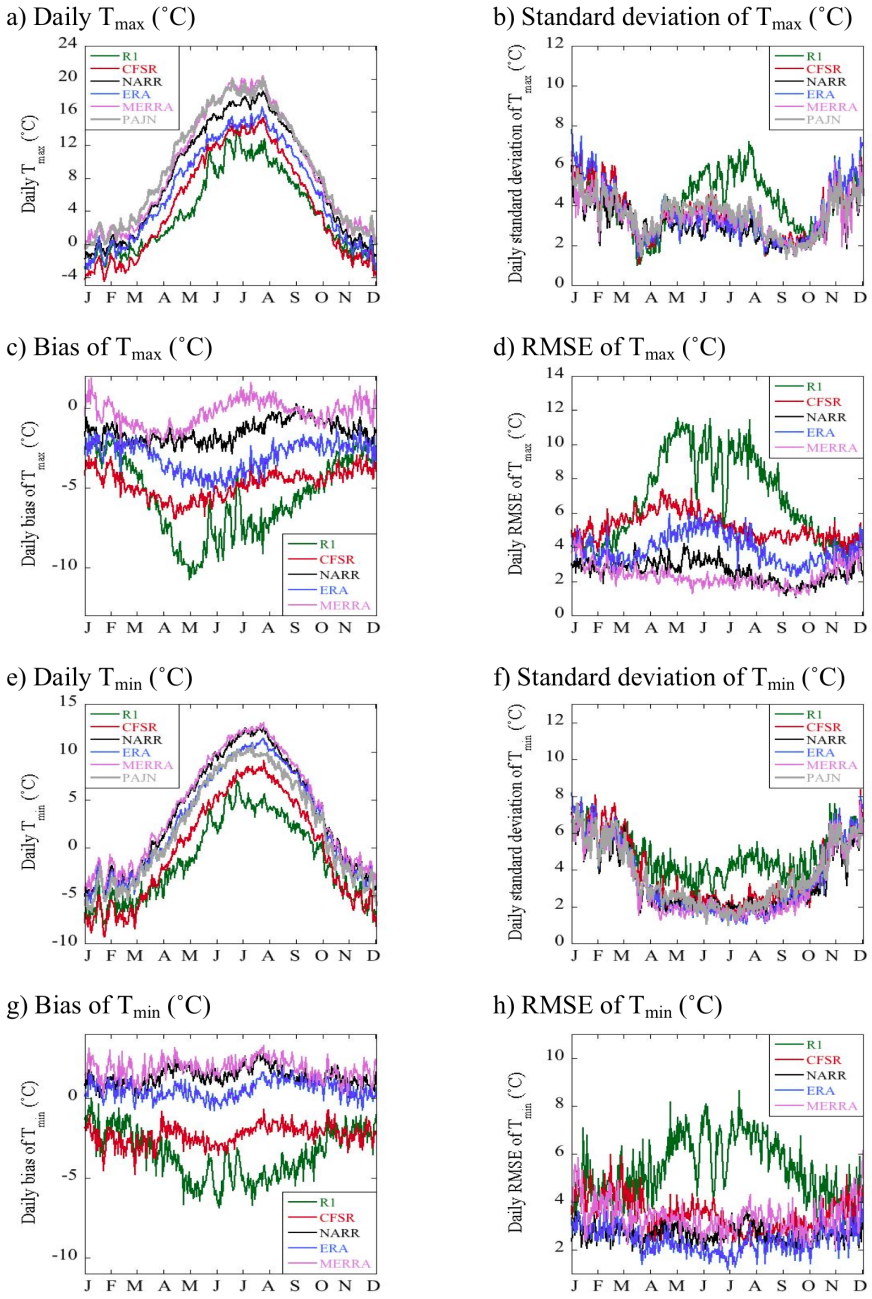

FIG. 4.9.1 Daily climate statistics of T_{max} (a-d), and T_{min} (e-h) at Juneau. The reanalyses are compared to station observations at Juneau (gray), 1979-2009.

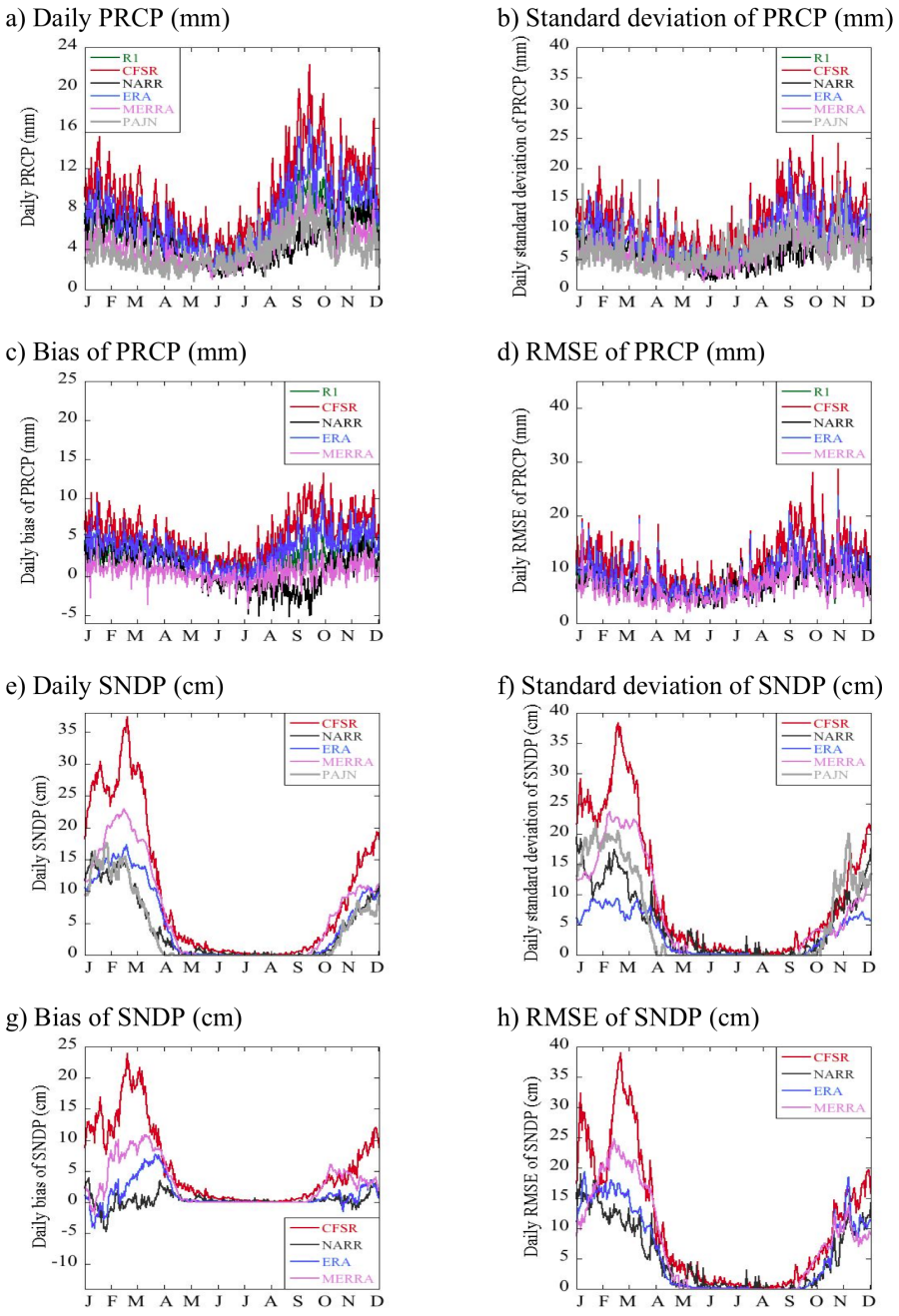

FIG. 4.9.2 Daily climate statistics of PRCP (a-d), and SNDP (e-h) at Juneau. The reanalyses are compared to station observations at Juneau (gray), 1979-2009.

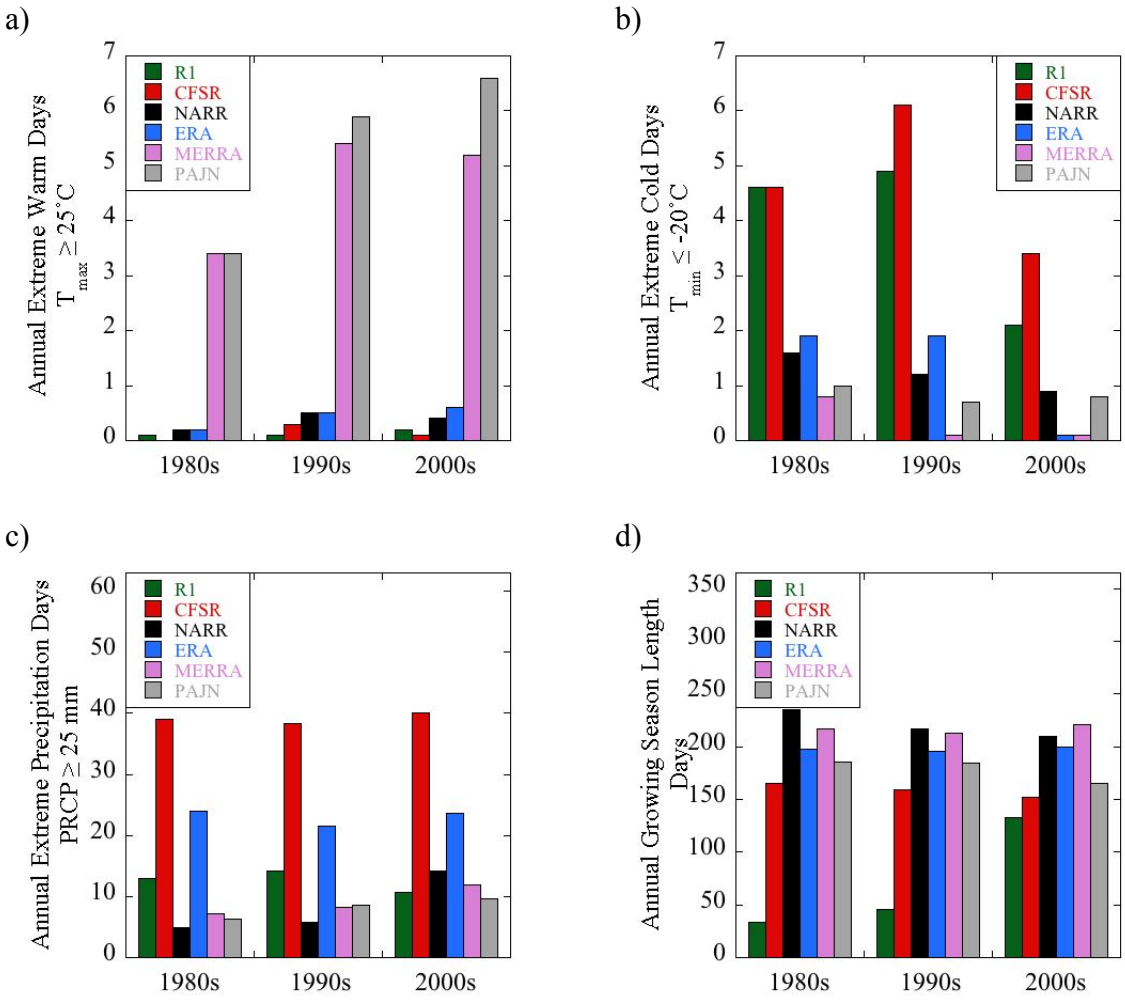

FIG. 4.9.3 Climate extreme indices at Juneau: (a) Decadal-average annual counts of Extreme Warm Days (number of days where $T_{max} \geq 25^{\circ}C$), (b) Extreme Cold Days (number of days where $T_{min} \leq -20^{\circ}C$), (c) Extreme Precipitation Days (number of days where PRCP ≥ 25 mm), (d) Growing Season Length (number of days between the fifth consecutive day when $T_{avg} > 0^{\circ}C$ and the day when $T_{min} \leq -2.2^{\circ}C$ for Juneau.

a) Monthly mean T_{max} (˚C), 1979-1983

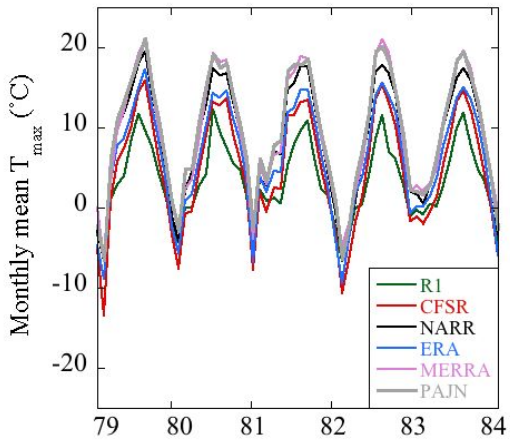

b) Monthly mean T_{max} (˚C), 1984-1988

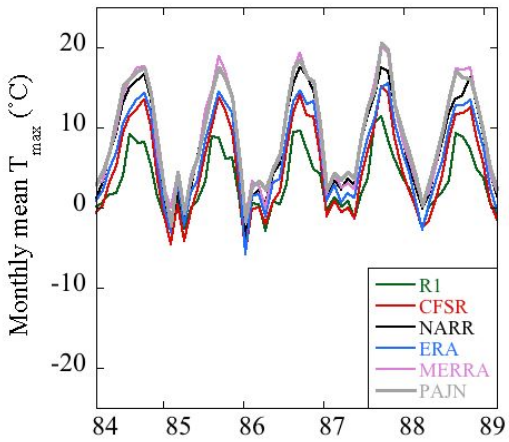

c) Monthly mean T_{max} (˚C), 1989-1993

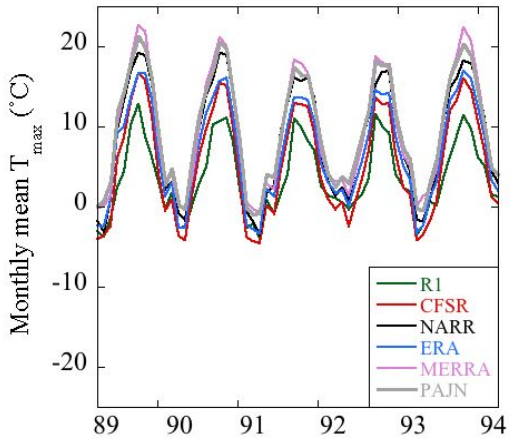

d) Monthly mean T_{max} (˚C), 1994-1998

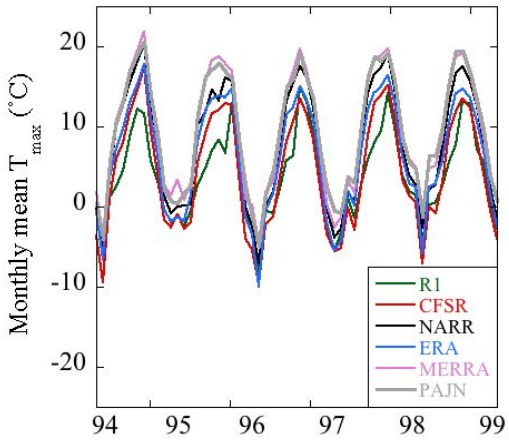

e) Monthly mean T_{max} (˚C), 1999-2003

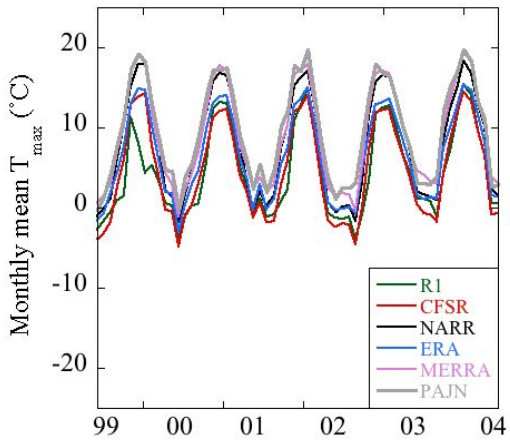

f) Monthly mean T_{max} (˚C), 2004-2009

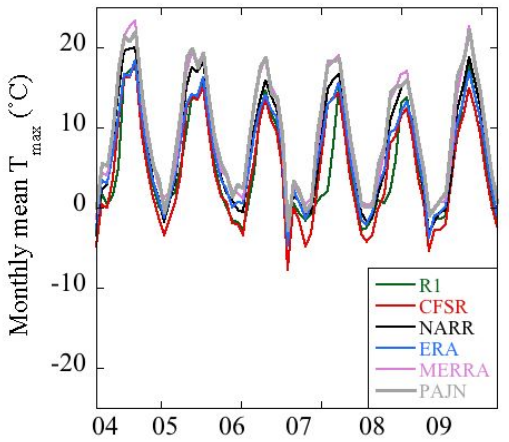

FIG. 4.9.4 Time series of monthly mean T_{max} at Juneau (gray) for a) 1979-1983, b) 1984-1988, c) 1989-1993, d) 1994-1998, e) 1999-2003, and f) 2004-2009.

a) Monthly mean T_{min} (˚C), 1979-1983

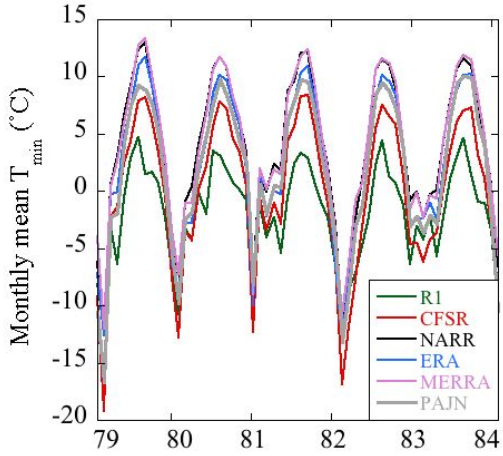

b) Monthly mean T_{min} (˚C), 1984-1988

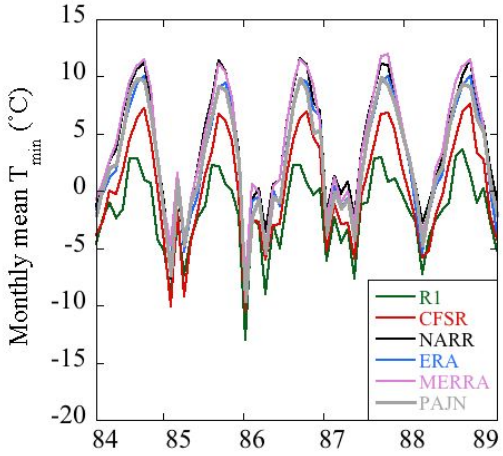

c) Monthly mean T_{min} (˚C), 1989-1993

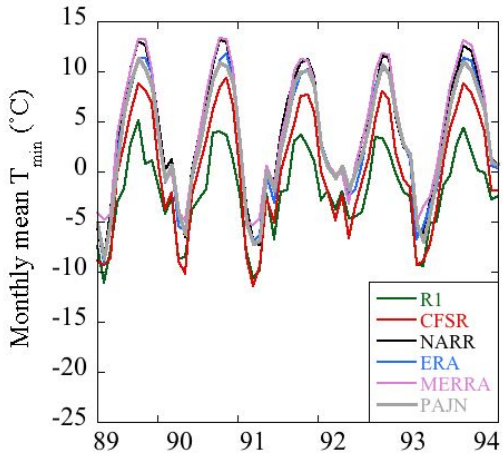

d) Monthly mean T_{min} (˚C), 1994-1998

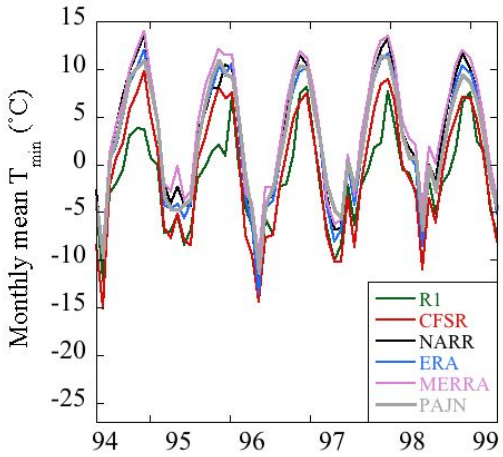

e) Monthly mean T_{min} (˚C), 1999-2003

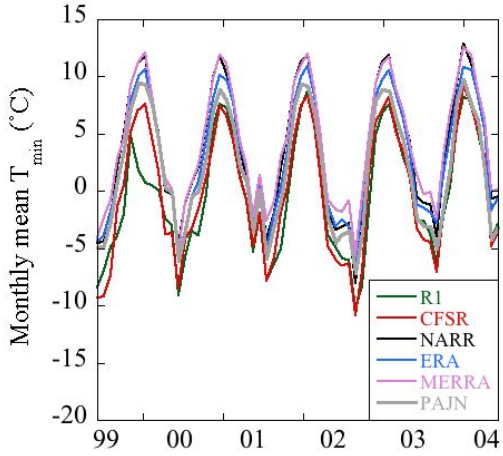

f) Monthly mean T_{min} (˚C), 2004-2009

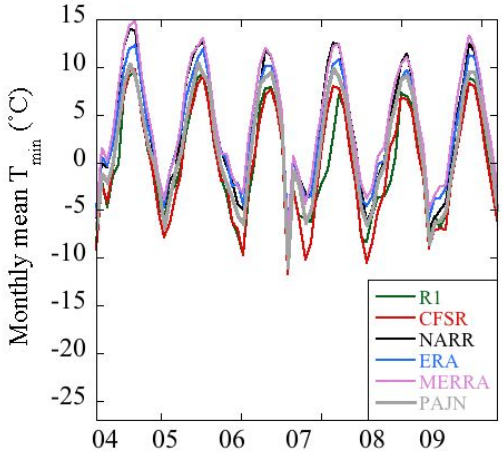

FIG. 4.9.5 Time series of monthly mean T_{min} at Juneau (gray) for a) 1979-1983, b) 1984-1988, c) 1989-1993, d) 1994-1998, e) 1999-2003, and f) 2004-2009.

a) Monthly mean PRCP (mm), 1979-1983

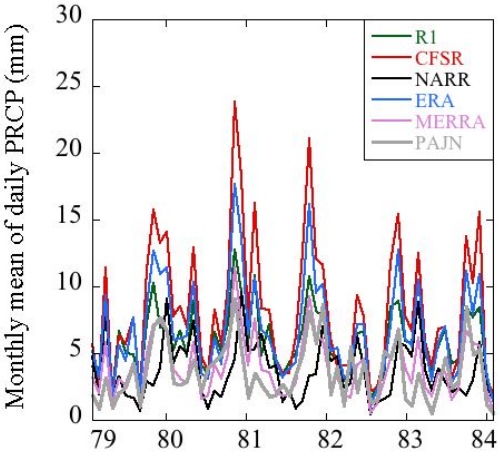

b) Monthly mean PRCP (mm), 1984-1988

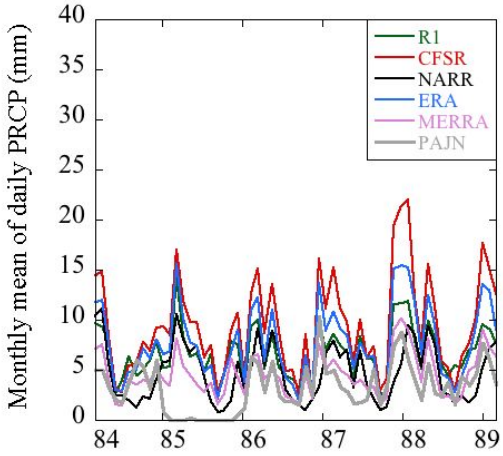

c) Monthly mean PRCP (mm), 1989-1993

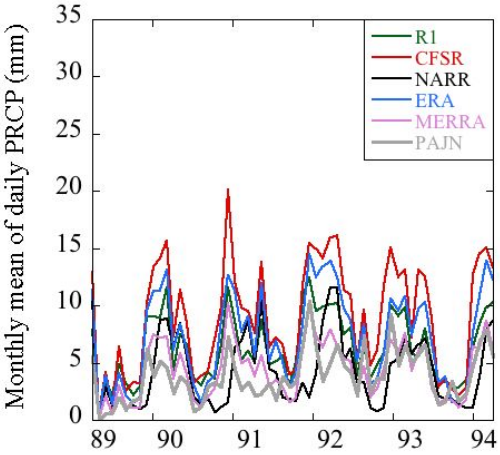

d) Monthly mean PRCP (mm), 1994-1998

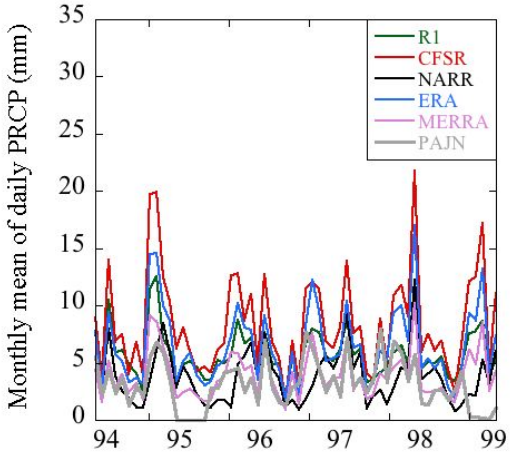

e) Monthly mean PRCP (mm), 1999-2003

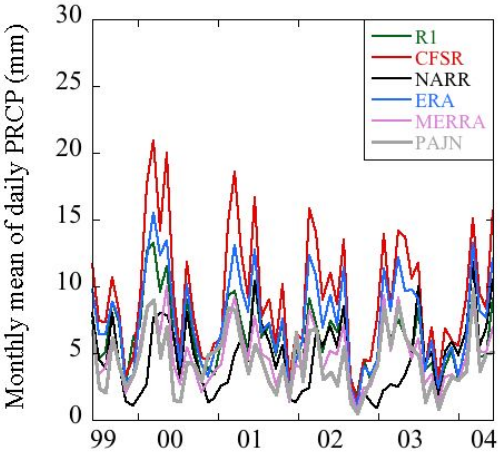

f) Monthly mean PRCP (mm), 2004-2009

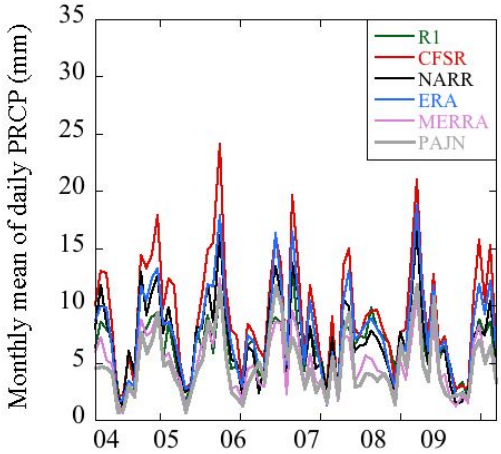

FIG. 4.9.6 Time series of monthly mean PRCP at Juneau (gray) for a) 1979-1983, b) 1984-1988, c) 1989-1993, d) 1994-1998, e) 1999-2003, and f) 2004-2009.

a) Monthly mean SNDP (cm), 1979-1983

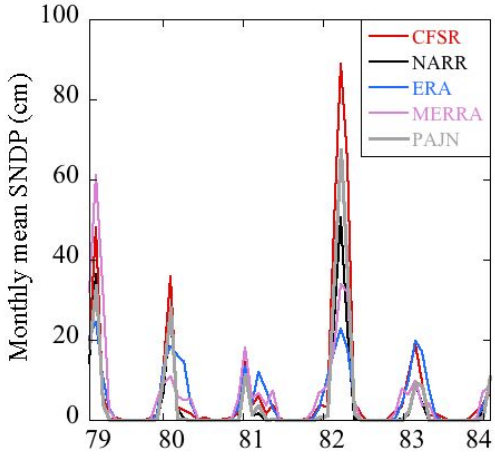

b) Monthly mean SNDP (cm), 1984-1988

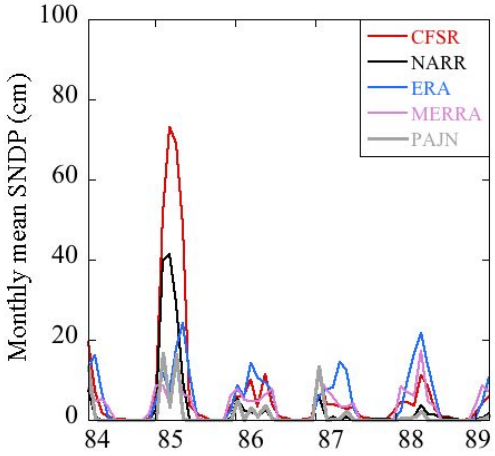

c) Monthly mean SNDP (cm), 1989-1993

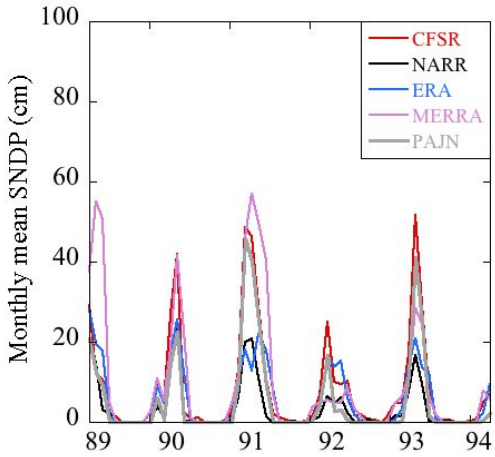

d) Monthly mean SNDP (cm), 1994-1998

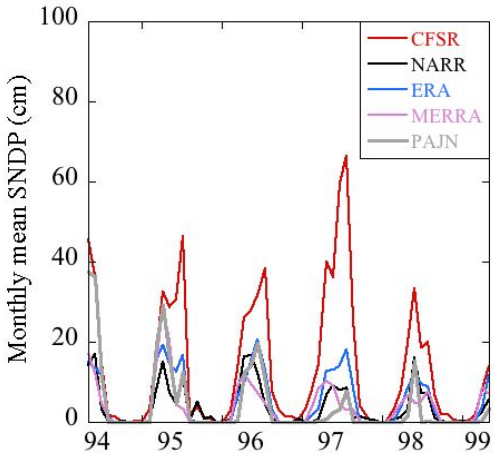

e) Monthly mean SNDP (cm), 1999-2003

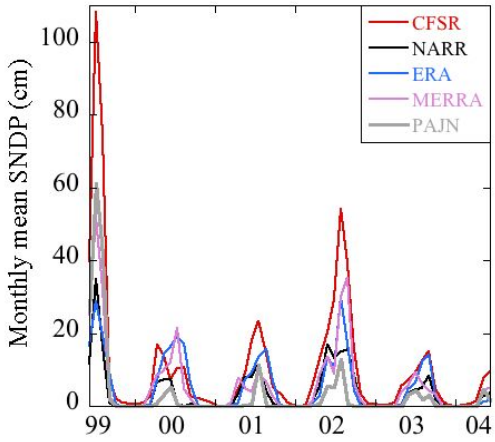

f) Monthly mean SNDP (cm), 2004-2009

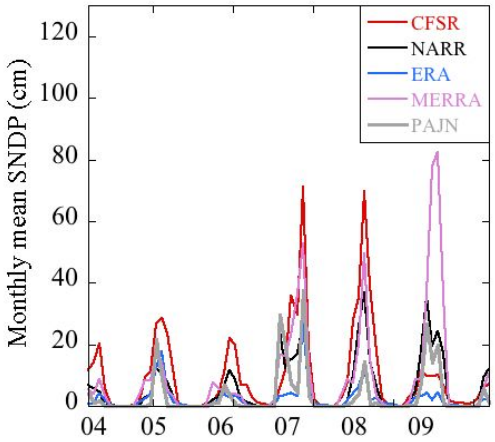

FIG. 4.9.7 Time series of monthly mean SNDP at Juneau (gray) for a) 1979-1983, b) 1984-1988, c) 1989-1993, d) 1994-1998, e) 1999-2003, and f) 2004-2009.

Table 4.9.1 Top performing reanalyses for Juneau, Alaska, 1979-2009. Performance is based on average RMSE value relative to station observations. The months included in each season are indicated by one-letter abbreviations in parentheses.

	T_{max}	T_{min}	PRCP	SNDP
WINTER (NDJFM)	NARR	NARR	MERRA	NARR
SPRING (AM)	MERRA	ERA	MERRA	NARR
SUMMER (JJA)	MERRA	ERA	MERRA	MERRA
AUTUMN (SO)	MERRA	ERA	NARR	ERA

Table 4.9.2 Seasonal RMSE and bias (high/low) for Juneau, Alaska, 1979-2009. Each number represents an average of daily RMSE or bias for the entire season over all 31 years. The RMSE and bias values are relative to station observations.

	WINTER		SPRING		SUMMER		AUTUMN	
T_{max} (˚C)	RMSE	Bias	RMSE	Bias	RMSE	Bias	RMSE	Bias
R1	4.5	-3.3	9.6	-8.8	9.2	-7.4	6.5	-5.5
CFSR	4.9	-4.3	6.4	-6.0	5.3	-4.9	4.7	-4.4
NARR	2.7	-1.6	3.1	-2.0	2.8	-1.5	1.8	-0.6
ERA	3.7	-2.4	4.6	-4.0	4.7	-3.9	2.9	-2.3
MERRA	2.9	-0.3	2.3	-1.2	2.0	0.3	1.7	-0.4
T_{min} (˚C)	RMSE	Bias	RMSE	Bias	RMSE	Bias	RMSE	Bias
R1	4.5	-2.1	6.0	-4.6	6.6	-5.0	5.5	-3.9
CFSR	4.1	-2.5	3.3	-2.3	3.2	-2.3	2.9	-1.9
NARR	2.7	0.9	2.8	1.7	2.8	1.8	2.4	1.3
ERA	2.8	0.4	2.2	0.3	2.0	0.5	2.2	1.0
MERRA	3.8	1.5	3.3	2.1	3.1	2.2	3.1	1.8
PRCP (mm)	RMSE	Bias	RMSE	Bias	RMSE	Bias	RMSE	Bias
R1	9.0	3.0	6.6	2.5	6.9	1.0	10.8	2.2
CFSR	13.0	6.4	8.1	3.4	8.7	2.3	16.3	7.7
NARR	8.6	2.9	5.3	1.1	6.7	-1.2	9.5	-1.2
ERA	10.5	4.6	6.7	2.4	7.0	1.0	12.4	4.8
MERRA	7.5	1.2	4.9	0.4	6.3	-0.4	9.5	0.6
SNDP (cm)	RMSE	Bias	RMSE	Bias	RMSE	Bias	RMSE	Bias
CFSR	22.0	11.4	7.7	3.6	1.0	0.4	2.9	1.3
NARR	11.3	0.1	4.2	1.0	0.7	0.1	0.9	0.1
ERA	13.3	1.8	4.2	1.8	0.2	0.0	0.9	0.2
MERRA	15.7	5.3	7.0	2.3	0.0	0.0	2.8	1.0

4.10 Conclusions

4.10.1 Summary of model performance

An overall evaluation based on 128 possible combinations between eight stations, four seasons, and four climate variables indicates that MERRA is the top model 43 times (Table 4.10.1). MERRA is followed by ERA-Interim (32), CFSR (24), NARR (21), and NCEP-R1 (8).

The statewide-observed mean annual cycle of daily maximum temperature (T_{max}) has a low temperature of -24.7˚C in January for Barrow, and a high temperature of 25.1˚C in July for Fairbanks (Table 4.10.2). The standard deviation of T_{max} ranges from a December maximum of 12.9˚C for McGrath to a September minimum of 1.3˚C for Juneau (Table 4.10.2). MERRA has the lowest seasonal-average RMSE of T_{max} 17 times compared to CFSR (8), NARR (6), ERA-Interim (1), and NCEP-R1 (0) (Table 4.10.3). The top-performing model during summer frequently has the best representation of Annual Extreme Warm Days and in no case does the number one model rank any lower than third for this extreme index.

The statewide-observed mean annual cycle of daily minimum temperature (T_{min}) has a low temperature of -32.7˚C in February for Barrow, and a high temperature of 12.1˚C in July for Fairbanks (Table 4.10.4). The standard deviation of T_{min} ranges from a February maximum of 14.1˚C for McGrath to a July minimum of 1.0˚C for Juneau (Table 4.10.4). The annual range of standard deviation for daily T_{min} is greater than it is for T_{max}; the winter has higher values while the summer has lower ones compared to T_{max}. The lowest standard deviation of T_{max} occurs later in summer than for T_{min}. MERRA and CFSR have the lowest seasonal-average RMSE of T_{min} 10 times each compared to ERA-Interim (7), NARR (4), and NCEP-R1 (1) (Table 4.10.5). The top-performing model during winter frequently has the best representation of Annual Extreme Cold Days.

The statewide-observed mean annual cycle of daily precipitation (PRCP) has a minimum of 0.02 mm in March for Barrow, and a maximum of 10.9 mm in October for Juneau (Table 4.10.6). The standard deviation of PRCP ranges from a March minimum of 0.08 mm for Barrow to an autumn peak above 15.0 mm for Juneau (Table 4.10.6). The lowest average daily PRCP occurs in late winter and spring, as does the lowest standard deviation of daily PRCP. ERA-Interim has the lowest seasonal-average RMSE of PRCP 9 times compared to MERRA (8), NCEP-R1 (7), NARR (5), and CFSR (3) (Table 4.10.7). The top-performing model during summer frequently has the best representation of Annual Extreme Precipitation Days and in no case does the number one model rank any lower than third for this extreme index.

The statewide-observed mean annual cycle of snow depth (SNDP) has a maximum of 71.4 cm in February for McGrath (Table 4.10.8). Latest-recorded spring melt-out dates range from April for King Salmon, Anchorage, and Juneau to June for Barrow. The highest standard deviation of SNDP is 44.9 cm in March for Nome. The annual highest standard deviation of SNDP always coincides with or follows the highest average daily SNDP. ERA-Interim has the lowest seasonal-average RMSE of SNDP 15 times compared to MERRA (8), NARR (6), and CFSR (3) (Table 4.10.9).

4.10.2 Generalizations of biases

The reanalysis models tend to dampen the diurnal cycle of temperature throughout the year; biases of T_{max} are generally negative while T_{min} biases are positive. NCEP-R1 typically has the largest negative temperature bias, which is most pronounced when the altitude of the NCEP-R1 grid cell is much higher (> 400 m) than the station (see Table 2.2.1). This occurs for

Anchorage, Fairbanks, and Juneau. ERA-Interim has similar issues for these stations; however, its nearest land grid cells have altitudes closer to the stations.

The reanalysis models generally have positive daily PRCP biases. CFSR has the highest PRCP bias during all seasons for Barrow, Nome, Bethel, and Juneau. Its last-place ranking of statewide model performance for daily PRCP reflects this. NARR shows a transition from a high PRCP bias for western stations (e.g. Bethel, McGrath, and King Salmon) to a dry bias for Juneau in southeast Alaska. This is due to differences in the data assimilation. For Alaska, NARR does not assimilate precipitation observations and the subsequent precipitation analysis is entirely model derived. The background model in NARR has a wet bias. For Canada, precipitation observations are assimilated prior to December 2002, and these help to constrain the overactive forecast model. NCEP-R1 performs well except for the Interior stations where it has a positive bias, which is highest during summer. This is due to the cold bias that NCEP-R1 has. As excess humidity in incorporated during each analysis cycle, it is done so in an unrealistically cold atmosphere and subsequently condenses and precipitates back out.

Model biases of daily SNDP are positive across Alaska except for the Interior stations of McGrath and Fairbanks. At these stations, the models have a negative SNDP bias in spring, which indicates an early snowmelt. The exception to this is MERRA, which has a long snow season for all northern and western stations. MERRA keeps snow on the ground all year long for Barrow. CFSR and NARR have a tendency to produce summer snow events that show up as spikes in the time series of average daily SNDP. This is most pronounced for Barrow, and Anchorage, but is seen to a lesser extent at Juneau. CFSR and NARR also produce extremely high SNDP biases from 1979-1983 for Nome; however, these disappear in the later time period.

Table 4.10.1 Counts of top performances by five reanalysis models for eight stations across Alaska, 1979-2009. Performance is based on seasonal-average RMSE value compared to station observations for four daily climate variables, which include maximum temperature (T_{max}), minimum temperature (T_{min}), precipitation (PRCP), and snow depth (SNDP).

	R1	**CFSR**	**NARR**	**ERA**	**MERRA**
Barrow	2	5	2	1	6
Nome	2	1	5	3	5
Bethel	1	5	0	7	3
McGrath	0	3	1	5	7
Fairbanks	0	2	6	3	5
King Salmon	1	7	1	4	3
Anchorage	2	1	1	5	7
Juneau	0	0	5	4	7
Total	**8**	**24**	**21**	**32**	**43**

Table 4.10.2 Highest and lowest values of climatological (31-year mean) daily T_{max} (˚C) and standard deviation of T_{max} (˚C). The table identifies the climatological extremes in mean daily values, extremes in standard deviation, and the month in which they occur.

	Highest Average (˚C)	**Lowest Average (˚C)**	**Highest Std. Dev. (˚C)**	**Lowest Std. Dev. (˚C)**
Barrow	11.1 (Jul)	-24.7 (Jan)	9.9 (Feb)	1.8 (Jun)
Nome	17.1 (Jul)	-12.0 (Jan)	10.3 (Jan)	2.2 (Aug)
Bethel	19.6 (Jul)	-11.9 (Jan)	12.0 (Feb)	2.1 (Aug)
McGrath	23.5 (Jul)	-18.4 (Jan)	12.9 (Dec)	2.3 (Aug)
Fairbanks	25.1 (Jul)	-18.7 (Jan)	12.8 (Feb)	2.7 (Sep)
King Salmon	19.5 (Jul)	-6.0 (Jan)	11.5 (Feb)	1.7 (Sep)
Anchorage	20.0 (Jul)	-5.6 (Jan)	8.4 (Feb)	1.4 (Sep)
Juneau	20.1 (Aug)	-0.5 (Jan)	5.8 (Jan)	1.3 (Sep)

Table 4.10.3 Top performing reanalysis models for daily T_{max} according to season for eight stations across Alaska, 1979-2009. Performance is based on seasonal-average RMSE value relative to station observations.

	Winter (NDJFM)	**Spring (AM)**	**Summer (JJA)**	**Autumn (SO)**
Barrow	MERRA	CFSR	CFSR	CFSR
Nome	ERA	MERRA	MERRA	MERRA
Bethel	CFSR	MERRA	MERRA	MERRA
McGrath	NARR	MERRA	CFSR	MERRA
Fairbanks	NARR	NARR	NARR	NARR
King Salmon	CFSR	MERRA	CFSR	MERRA
Anchorage	CFSR	MERRA	MERRA	MERRA
Juneau	NARR	MERRA	MERRA	MERRA

Table 4.10.4 Highest and lowest values of climatological (31-year mean) daily T_{min} (˚C) and standard deviation of T_{min} (˚C). The table identifies the climatological extremes in mean daily values, extremes in standard deviation, and the month in which they occur.

	Highest Average (˚C)	**Lowest Average (˚C)**	**Highest Std. Dev. (˚C)**	**Lowest Std. Dev. (˚C)**
Barrow	2.4 (Jul)	-32.7 (Feb)	10.0 (Feb)	1.4 (Jun)
Nome	8.9 (Jul)	-22.1 (Jan)	12.0 (Feb)	2.0 (Jul)
Bethel	10.0 (Jul)	-19.6 (Jan)	11.7 (Feb)	1.7 (Jul)
McGrath	10.5 (Jul)	-28.9 (Jan)	14.1 (Feb)	1.9 (Jul)
Fairbanks	12.1 (Jul)	-30.1 (Jan)	11.9 (Feb)	1.8 (Jul)
King Salmon	9.2 (Aug)	-15.9 (Dec)	13.2 (Jan)	1.6 (Jun)
Anchorage	12.0 (Jul)	-13.8 (Jan)	9.1 (Feb)	1.3 (Jul)
Juneau	10.7 (Jul)	-6.6 (Jan)	7.6 (Jan)	1.0 (Jul)

Table 4.10.5 Top performing reanalysis models for daily T_{min} according to season for eight stations across Alaska, 1979-2009. Performance is based on seasonal-average RMSE value relative to station observations.

	Winter (NDJFM)	**Spring (AM)**	**Summer (JJA)**	**Autumn (SO)**
Barrow	MERRA	CFSR	CFSR	MERRA
Nome	NARR	NARR	CFSR	NARR
Bethel	CFSR	CFSR	CFSR	CFSR
McGrath	MERRA	MERRA	MERRA	MERRA
Fairbanks	MERRA	ERA	MERRA	CFSR
King Salmon	MERRA	R1	CFSR	CFSR
Anchorage	ERA	ERA	MERRA	ERA
Juneau	NARR	ERA	ERA	ERA

Table 4.10.6 Highest and lowest values of climatological (31-year mean) daily PRCP (mm) and standard deviation of PRCP (mm). The table identifies climatological extremes in mean daily values, extremes in standard deviation, and the month in which they occur.

	Highest Average (mm)	**Lowest Average (mm)**	**Highest Std. Dev. (mm)**	**Lowest Std. Dev. (mm)**
Barrow	2.2 (Jun)	0.02 (Mar)	9.9 (Jun)	0.08 (Mar)
Nome	4.7 (Aug)	0.15 (May)	14.5 (Apr)	0.40 (Apr)
Bethel	5.9 (Dec)	0.16 (Apr)	23.9 (Dec)	0.36 (Jan)
McGrath	4.2 (Aug)	0.06 (Jan)	11.6 (Feb)	0.15 (Jan)
Fairbanks	3.5 (Jul)	0.03 (Apr)	9.6 (Dec)	0.10 (Apr)
King Salmon	4.7 (Aug)	0.17 (Apr)	7.6 (May)	0.34 (Mar)
Anchorage	6.9 (Aug)	0.06 (Apr)	18.9 (Aug)	0.20 (Apr)
Juneau	10.9 (Oct)	0.90 (May)	19.2 (Nov)	1.6 (May)

Table 4.10.7 Top performing reanalysis models for daily PRCP according to season for eight stations across Alaska, 1979-2009. Performance is based on seasonal-average RMSE value relative to station observations.

	Winter (NDJFM)	**Spring (AM)**	**Summer (JJA)**	**Autumn (SO)**
Barrow	R1	R1	MERRA	MERRA
Nome	R1	R1	MERRA	NARR
Bethel	R1	ERA	ERA	ERA
McGrath	ERA	MERRA	ERA	ERA
Fairbanks	NARR	NARR	MERRA	ERA
King Salmon	CFSR	CFSR	ERA	CFSR
Anchorage	R1	R1	ERA	NARR
Juneau	MERRA	MERRA	MERRA	NARR

Table 4.10.8 Highest and lowest values of climatological (31-year mean) daily SNDP (cm) and standard deviation of SNDP (cm). These values identify the maximum and minimum of the observed annual cycle.

	Highest Average (cm)	**Latest Melt Out**	**Highest Std. Dev. (cm)**
Barrow	27.6 (Apr)	Jun	13.0 (May)
Nome	50.1 (Mar)	May	44.9 (Mar)
Bethel	23.8 (Jan)	May	17.7 (Feb)
McGrath	71.4 (Feb)	May	29.1 (Mar)
Fairbanks	53.6 (Mar)	May	25.2 (Apr)
King Salmon	8.4 (Dec)	Apr	11.7 (Jan)
Anchorage	29.3 (Mar)	Apr	25.3 (Mar)
Juneau	17.6 (Jan)	Apr	21.9 (Jan)

Table 4.10.9 Top performing reanalysis models for daily SNDP according to season for eight stations across Alaska, 1979-2009. Performance is based on seasonal-average RMSE value relative to station observations.

	Winter (NDJFM)	**Spring (AM)**	**Summer (JJA)**	**Autumn (SO)**
Barrow	MERRA	NARR	ERA	NARR
Nome	MERRA	NARR	ERA	ERA
Bethel	ERA	ERA	ERA	ERA
McGrath	CFSR	CFSR	ERA	ERA
Fairbanks	MERRA	MERRA	ERA	CFSR
King Salmon	ERA	NARR	ERA	ERA
Anchorage	MERRA	MERRA	MERRA	ERA
Juneau	NARR	NARR	MERRA	ERA

Chapter 5 Guidance for use of reanalysis in Alaska

5.1 Synthesizing the regional and station assessments

Reanalysis estimates are not equal to observations, and using them in remote regions of Alaska should be done with caution. Yet by finding consistencies between the regional and station assessments, reanalysis users can more confidently select an appropriate dataset to suit their needs. This section provides examples of when a reanalysis is both the top-performing model at a particular station as well as across the climate division in which it is located. Following these examples, are cases when this does not hold true and one model performs most reliably for a station, while a different model better captures conditions across the corresponding climate division.

MERRA is the highest-ranking model for Barrow and performs consistently well for the North Slope climate division. During winter, MERRA has the lowest RMSE of T_{max} (3.1˚C), and T_{min} (4.2˚C) at Barrow, as well as the lowest bias of 2-meter temperature (0.8˚C) on the North Slope. MERRA has the lowest RMSE of daily precipitation (2.0 mm) at Barrow in summer, and the best representation of Annual Extreme Precipitation Days (PRCP ≥ 5 mm). It also has the lowest precipitation bias (-0.1 cm) for the North Slope in autumn. The reliable representation of precipitation is consistent with the low temperature biases in MERRA, both for Barrow and the North Slope climate division.

NARR and MERRA perform the best compared to observations for Nome and the West Coast climate division. NARR does particularly well with daily T_{min} at Nome and has the lowest RMSE during winter (4.3˚C), spring (3.1˚C), and autumn (2.6˚C). Across the West Coast, NARR has the lowest 2-meter temperature bias in winter (-0.3˚C), and spring (0.1˚C). MERRA does comparably well with daily T_{max} at Nome, having the lowest RMSE in spring (2.7˚C), summer

(2.3˚C), and autumn (1.9˚C). MERRA has the closest number of Annual Extreme Warm Days at Nome when compared to observations and the lowest 2-meter temperature bias across the West Coast during autumn (-0.2˚C). NARR does best in the cooler months while MERRA is more reliable during the warm season for Nome and the West Coast climate division.

The two Interior stations are best represented by MERRA at McGrath, and by NARR at Fairbanks. MERRA is closest to observations of daily T_{min} during all seasons at McGrath and has the lowest 2-meter temperature bias during summer (-0.2˚C) for the Interior. At Fairbanks, NARR has the lowest RMSE of daily T_{max} throughout the year and the best representation of Annual Extreme Warm Days ($T_{max} \geq 25$˚C). NARR has the lowest RMSE of daily precipitation in winter (1.3 mm), and spring (1.6 mm) for Fairbanks. NARR also has the lowest bias of precipitation for the Interior during summer (-0.6 cm), and autumn (0.0 cm), while MERRA does for winter (-0.1 cm) and spring (0.4 cm). The biases in NARR and MERRA are generally comparable for the Interior, so the selection of either would be appropriate for most studies.

MERRA is the top-performing model for Anchorage, as well as for the Cook Inlet climate division, in which it is located. MERRA has the lowest RMSE of daily T_{max} during spring (2.0˚C), summer (1.8˚C), and autumn (1.8˚C). MERRA also has the lowest bias of 2-meter temperature across the Cook Inlet climate division during spring (-0.1˚C), and autumn (-0.3˚C). MERRA performs comparably to observations of daily snow depth and has the lowest RMSE during winter (12.8 cm) and spring (7.6 cm).

There are also many inconsistencies between the regional and station assessments of the reanalysis products. These discrepancies are most frequently found in the maritime climate divisions, and those that are dominated by complex topography. Both the observational datasets

and reanalyses are subject to error in these regions because of sub-grid cell changes in the land-sea mask and elevation profile.

The evaluation of the West Coast climate division is not consistent with the station-based assessment for Bethel. ERA-Interim is the top-performing model at Bethel, having the lowest RMSE values of daily precipitation during spring (2.0 mm), summer (3.3 mm), and autumn (3.2 mm), as well as for daily snow depth during all seasons. However, ERA-Interim and CFSR have the highest precipitation biases for the West Coast. For each reanalysis, these high biases are likely due to an overreliance on the forecast model, which is typically too wet. ERA-Interim also has the largest (negative) SWE bias during winter (-61.0 mm), and spring (-40.4 mm). Therefore, Bethel's station evaluation of daily precipitation and snow depth compares best with ERA-Interim and does not agree on best model choice for the monthly precipitation and SWE evaluation for the West Coast climate division.

CFSR is the top-performing model for King Salmon, but not for the Bristol Bay climate division. CFSR has the lowest RMSE of daily T_{max} during winter (2.6˚C), and summer (1.9˚C) as well as the best agreement with observations of Annual Extreme Warm Days ($T_{max} \geq 25$˚C). Yet NARR and MERRA routinely have the lowest regional biases of 2-meter temperature across Bristol Bay. CFSR has the lowest RMSE of daily precipitation in winter (2.9 mm), and spring (2.7 mm) for King Salmon, but also the second-highest precipitation bias for Bristol Bay during these same periods.

At Juneau, MERRA has the most reliable output compared to observations. MERRA has the lowest RMSE of daily T_{max} during spring (2.3˚C), summer (2.0˚C), and autumn (1.7˚C) as well as the best representation of Annual Extreme Warm Days ($T_{max} \geq 25$˚C). MERRA produces better daily precipitation analyses during all seasons for Juneau; however, MERRA has the

largest or second-largest (negative) precipitation bias for the Southeast climate division. Because of the complex topography, this region is problematic and reanalysis data should be used with caution.

These findings demonstrate that there is no particular reanalysis that consistently outperforms the others for all variables, seasons, and regions across Alaska. The user must identify what aspects of the reanalysis products are of highest importance for their particular interest. After determining the season of interest, the key region of Alaska, and important variables, the user can follow guidelines provided in the next section to make an informed decision. Section 5.2 is set up in the format of FAQs to help guide the reader with examples of how to navigate through this study to obtain the most useful information.

5.2 FAQ

This section includes general questions and application-specific examples to help guide the reader to the most appropriate parts of this study. The general questions discuss important features of the station and regional assessments. They also provide information on where to find evaluations of particular variables. These questions are followed by specific examples related to modeling of systems (e.g., glaciers and river flow) in Alaska that require climate forcing. The answers to these questions direct the reader to not only the model evaluations but also to some of the known data problems, and pitfalls associated with the reanalysis data products. The questions included follow on the next page.

- **How well do the reanalyses compare to station observations in Alaska?**
- **How well do the reanalyses compare to gridded observations in Alaska?**
- **Example 1: What should I use to force a land hydrology model in the Interior?**
- **Example 2: What should I use to force a glacier model in southern Alaska?**
- **Example 3: Do the reanalyses reliably estimate Growing Season Length?**

- **How well do the reanalyses compare to station observations in Alaska?**

Chapter 4 provides an assessment of reanalysis quality for daily maximum temperature, minimum temperature, precipitation, and snow depth at eight first-order stations across Alaska from 1979-2009. The station data is compared to the nearest corresponding land grid cell in each reanalysis without interpolation to account for topography. Figure 2.1.1 and Table 2.1.1 illustrate the differences between station elevation and the model elevation used for comparison. Chapter 4 also includes an evaluation of climate extreme indices that relate to the four variables listed above.

- **How well do the reanalyses compare to gridded observations in Alaska?**

Chapter 3 includes a spatial assessment of the reanalyses in the form of statewide maps of model bias, and standard deviation of monthly mean temperature (Section 3.3), precipitation (Section 3.4), and snow-water equivalent (Section 3.5). The model quantities are compared to gridded observations. These maps of monthly data have been averaged and are presented seasonally. All products have been re-gridded to a common 0.5˚ x 0.5˚ resolution. Model mean, bias, and standard deviation are quantified regionally by averaging over six climate divisions, and these values are provided in tabular form for each variable.

- **Example 1: What should I use to force a land hydrology model in the Interior?**

NARR consistently has the lowest precipitation bias compared to observations in the Interior climate division, followed closely by MERRA (Table 3.4.1). MERRA is the top-performing model for McGrath (Section 4.5), while NARR is for Fairbanks (Section 4.6). Section 2.3 highlights a known dataset problem associated with NARR that relates to a change in the data assimilation at the end of 2002. The resultant artificial increase in the time series of precipitation is evident in Figure 4.6.6e; however, it is not clear that this detracts from NARR's overall performance.

- **Example 2: What should I use to force a glacier model in southern Alaska?**

For daily maximum temperature and precipitation at Juneau, MERRA routinely has the lowest bias. These are important variables because glacial ice represents ice that persists throughout the year, including summer. The models typically have a cold and wet bias otherwise. This is explained by the models' overestimation of Juneau's terrain height. In the reanalyses, Juneau is too high, which causes a cold bias, and then with every increase in humidity with each analysis increment, the excess humidity is forced to condense and precipitate out.

The snow verification dataset used in this study (GlobSnow v2.0) does not provide SWE information for permanent ice locations, which means that model bias was not calculated. However, several problems in the reanalyses have been uncovered. ERA-Interim parameterizes permanent ice pixels in the model with 10,000 mm of SWE. NARR and CFSR use the same SNODEP model in their analyses that relies heavily on low-elevation stations, which are likely to have less snow than mountainous regions. NCEP-R1 has the coarsest resolution and uses the same snow cover mask from 1973 for the years 1974-1994, which affects its variability. These

considerations, which are documented in Section 2.3, suggest that MERRA is the most appropriate choice for glacier modeling in southern Alaska. Additionally, MERRA frequently has the lowest bias of monthly SWE across northern Alaska (Section 3.5).

- **Example 3: Do the reanalyses reliably estimate Growing Season Length?**

For the eight stations in this study, average Growing Season Length ranged from as short as 47.6 days at Barrow to 178.6 days at Juneau. The day count for Growing Season Length begins after the fifth consecutive day with a mean temperature above freezing and ends when the temperature is at or below -2.2˚C. At Barrow (Section 4.2), NCEP-R1 has the best representation of mean Growing Season Length (50.3 days). The other reanalyses overestimated the observed value by nearly a factor of two. NCEP-R1 is also closest to observations at Bethel (121.5 days for NCEP-R1 compared to 129.6 observed days) (Section 4.4), and King Salmon (142.6 to 130.4) (Section 4.7). CFSR performs best at Nome (106.3 days compared to 107.3 observed days) (Section 4.3), and Juneau (160.0 to 178.6) (Section 4.9). At Anchorage (Section 4.8), MERRA compares best with station observations of Growing Season Length (162.3 days compared to 159.5 observed days). In the Interior, MERRA performs best for McGrath (126.8 days compared to 125.8) (Section 4.5), while ERA-Interim does for Fairbanks (137.2 to 131.1) (Section 4.6). At both Anchorage and Fairbanks, NCEP-R1 underestimated Growing Season Length by a factor of two or more due to its summer cold bias.

5.3 Data access

Access to all of the data files used in this study will be made available at http://www.snap.uaf.edu/ once a format has been decided.

Chapter 6 Summary

The surface air temperature in Alaska has warmed more than any other place in the United States in the past century and is projected to continue climbing (Chapin et al. 2014). This is causing rapid sea-ice loss and glacial melt, which is contributing to sea-level rise - the effects of which are already being felt in the coastal communities of Alaska. The warming temperatures are also causing permafrost to thaw, and thus enabling the possible release of huge stores of carbon to the atmosphere. Warmer temperatures have shortened the snow season in Alaska, and increased the growing season. But there has also been a change in wildfire dynamics and ecosystems as a result. These are just a few of the impacts that climate change is having on Alaska.

These climate concerns highlight the need for accurate climate data assessment to help improve future modeling. For Alaska, the amount of observational data available is limited. For example, there are only 20 first order weather stations across the state. Reanalysis helps by filling in gaps in data-void areas. Reanalyses produce high spatiotemporal gridded meteorological data by assimilating past observations into a physically consistent forecast model. The reanalyses help to study past climates and provide the boundary conditions necessary to simulate future ones.

This study evaluates data from five reanalyses (NCEP-R1, NARR, CFSR, ERA-Interim, and MERRA) for Alaska from 1979-2009. A statewide view of reanalysis performance of monthly 2-meter temperature, precipitation, and snow-water equivalent for Alaska provides a spatial evaluation (Chapter 3). This evaluation includes model mean, bias, and standard deviation, which are presented by season, as well as climate division. A point analysis of daily maximum and minimum temperature, precipitation, and snow depth for eight stations in Alaska

compares nearest-neighbor reanalysis grid points with NCDC GSOD meteorological station data (Chapter 4). The 31-year averaged time series for each variable of the annual mean, standard deviation, model bias, and RMSE are included as well as related climate extremes indices. The time series for all 31 years have been included to assist users that are only interested in using certain segments of the data, and to investigate any artificial changes that may have arisen from changes to the observing systems assimilated in the reanalyses. The connection or lack of between the spatial and station evaluations provides some insight for evaluating data-sparse areas (Chapter 5).

MERRA is generally the top-performing reanalysis for Alaska; however, the results varied depending on variable, region, and season. ERA-Interim, and NARR have the lowest statewide 2-meter temperature biases. NARR and MERRA have the lowest precipitation biases, while NARR, MERRA, and CFSR performed the best for snow-water equivalent. Choosing the appropriate reanalysis is highly dependent on the user's specific needs. The higher resolution models often agreed better with observations, and this is likely due not only to increased resolution, but also to improved data assimilation, and better model physics.

A natural next step to expand this study is to include additional reanalysis datasets. For example, the Arctic System Reanalysis (Bromwich et al. 2010) and the JRA-55 (Ebita et al. 2011) from the Japanese Meteorological Agency are next-generation models; however, the data was not yet available when this project began. Another key issue is to provide evidence that using reanalysis output across observation-sparse regions is useful. For example, how well does the gridded reanalysis data correlate to comparable observational time series from nearby stations. This measure will help to increase reanalysis user confidence when selecting a dataset to best fit their application. Another step is to expand on the climate extreme indices because

extreme weather and climate if often the costliest to society. This study provides these indices for 8 stations; however, statewide maps may prove more useful.

It is necessary to conclude with a couple of cautionary notes. First, the reanalyses are often not reliable for trend analysis because of changes in the observing systems that get assimilated. These changes cause artificial shifts in the time series that can appear to show a climate change, even in the absence of any physical mechanism that would do so. Second, reanalysis estimates are not equal to observations; however, they provide invaluable information for Alaska.

Chapter 7 References

Bekryaev, R. V., I. V. Polyakov, V. A. Alexeev, 2010: Role of Polar Amplification in Long-Term Surface Air Temperature Variations and Modern Arctic Warming. *J. Climate*, **23**, 3888–3906.

Bengtsson, L., S. Hagemann, and K. I. Hodges, 2004: Can Climate Trends be Calculated from Reanalysis Data? *J. Geophys. Res*., **109**, D11111, doi:10.1029/2004JD004536.

Bieniek, P. A., U. S. Bhatt, L. A. Rundquist, S. D. Lindsey, X. Zhang, R. L. Thoman, 2011: Large-Scale Climate Controls of Interior Alaska River Ice Breakup. *J. Climate*, **24**, 286–297.

Bieniek, P. A., and Coauthors, 2012: Climate Divisions for Alaska Based on Objective Methods. *J. Appl. Meteor. Climatol.*, **51**, 1276–1289.

Bosilovich, M., 2008: NASA's Modern Era Retrospective-analysis for Research and Applications: Integrating Earth Observations. Earthzine. [Available online at http://www.earthzine.org/2008/09/26/nasas-modern-era-retrospective-analysis/.]

Bromwich, D., Y. H. Kuo, M. Serreze, J. Walsh, L. S. Bai, M. Barlage, K. Hines, and A, Slater, 2010: Arctic System Reanalysis: Call for community involvement. *EOS Trans. AGU*, **91**, 13-14.

Chapin, F. S., III, S. F. Trainor, P. Cochran, H. Huntington, C. Markon, M. McCammon, A. D. McGuire, and M. Serreze, 2014: Ch. 22: Alaska. *Climate Change impacts in the United States: The Third National Climate Assessment*, J. M. Melillo, T. C. Richmond, and G. W. Yohe, Eds., U.S. Global Change Research Program, 514-536. doi:10.7930/J00Z7150.

Cullather, R. I., M. G. Bosilovich, 2011: The Moisture Budget of the Polar Atmosphere in MERRA. *J. Climate*, **24**, 2861–2879.

Daly, C., R. P. Neilson, D. L. Phillips, 1994: A Statistical-Topographic Model for Mapping Climatological Precipitation over Mountainous Terrain. *J. Appl. Meteor.*, **33**, 140–158.

Decker, M., M. A. Brunke, Z. Wang, K. Sakaguchi, X. Zeng, M. G. Bosilovich, 2012: Evaluation of the Reanalysis Products from GSFC, NCEP, and ECMWF Using Flux Tower Observations. *J. Climate*, **25**, 1916–1944.

Dee, D. P., and Coauthors, 2011: The ERA-Interim reanalysis: configuration and performance of the data assimilation system. *Q.J.R. Meteorol. Soc*., **137**, 553–597.

Drusch, M., D. Vasiljevic, and P. Viterbo, 2004: ECMWF's Global Snow Analysis: Assessment and Revision Based on Satellite Observations. *J. Appl. Meteor.* **43**, 9, 1282–1294.

Ebita, A., and Coauthors, 2011: The Japanese 55-Year Reanalysis "JRA-55": An interim report. *SOLA*, **7**, 149–152.

Ek, M. B., K. E. Mitchell, Y. Lin, E. Rogers, P. Grunmann, V. Koren, G. Gayno, and J. D. Tarpley, 2003: Implementation of Noah land surface model advances in the National Centers for Environmental Prediction operational mesoscale Eta model, *J. Geophys. Res*., **108**, 8851, doi:10.1029/2002JD003296.

Francis, O. P., D. E. Atkinson, 2012: Synoptic Forcing of Wave States in the southeast Chukchi Sea, Alaska, at Nearshore Locations. *Nat. Hazards*, **62**, 1273-1300.

Hayhoe, K. A., 2010: A Standardized Framework for Evaluating the Skill of Regional Climate Downscaling Techniques. Dissertation. [Available online at http:// www.snap.uaf.edu/attachments/1_Hayhoe_Katharine.pdf/.]

Helfrich, S. R., D. McNamara, B. H. Ramsay, T. Baldwin and T. Kasheta, 2007: Enhancements to, and forthcoming developments in the Interactive Multisensor Snow and Ice Mapping System (IMS). *Hydrol. Process*., **21**, 1576-1586, doi:10.1002/hyp.6720.

Hill, D. F., N. Bruhis, S. Calos, A. Arendt, J. Beamer, 2014: Spatial and temporal variability of freshwater discharge into the Gulf of Alaska, *Geophys. Res. Lett*., submitted.

Hinzman, L. D., C. J. Deal, D. A. McGuire, S. H. Mernild, I. V. Polyakov, and J. E. Walsh, 2013: Trajectory of the Arctic as an integrated system. *Ecological Applications*, **23**, 1837–1868.

Janowiak, J. E., V. J. Dagostaro, V. E. Kousky, and R. J. Joyce, 2007: An Examination of Precipitation in Observations and Model Forecasts during NAME with Emphasis on the Diurnal Cycle. *J. Climate*, **20**, 1680–1692.

Kalnay, E., and Coauthors, 1996: The NCEP/NCAR 40-Year Reanalysis Project. *Bull. Amer. Meteor. Soc.*, **77**, 437–471.

Kalnay, E., 2003: *Atmospheric modeling, data assimilation, and predictability*. Cambridge University Press, 341 pp.

Karl, T. R., N. Nicholls, and A. Ghazi, 1999: CLIVAR/GCOS/WMO workshop on indices and indicators for climate extremes: Workshop summary. *Climatic Change*, **42**, 3-7.

Kistler, R., and Coauthors, 2001: The NCEP–NCAR 50–Year Reanalysis: Monthly Means CD–ROM and Documentation. *Bull. Amer. Meteor. Soc.*, **82**, 247–267.

Kleist, D. T., D. F. Parrish, J. C. Derber, R. Treadon, W. Wu, and S. Lord, 2009: Introduction of the GSI into the NCEP Global Data Assimilation System. *Wea. Forecasting*, **24**, 1691–1705.

Kopp, T. J. and R. B. Kiess, 1996: The Air Force Global Weather Central snow analysis model. Preprints, *15th Conf. on Weather Analysis and Forecasting*, Norfolk, VA, Amer. Meteor. Soc., 220-222.

Koster, R. D., M. J. Suarez, A. Ducharne, M. Stieglitz, and P. Kumar, 2000: A catchment-based approach to modeling land surface processes in a general circulation model: 1. Model structure, *J. Geophys. Res*., **105**, 24809–24822, doi:10.1029/2000JD900327.

Lindsay, R., M. Wensnahan, A. Schweiger, J. Zhang, 2014: Evaluation of Seven Different Atmospheric Reanalysis Products in the Arctic. *J. Climate*, **27**, 2588–2606.

Lorenz, C., H. Kunstmann, 2012: The Hydrological Cycle in Three State-of-the-Art Reanalyses: Intercomparison and Performance Analysis. *J. Hydrometeor*, **13**, 1397–1420.

Luojus, K., J. Pulliainen, and the GlobSnow Consortium, 2013, Global Snow Monitoring for Climate Research: Snow Water Equivalent, Finnish Meteorological Institute, Helsinki, Finland.

Mantua, N. J., S. R. Hare, Y. Zhang, J. M. Wallace, and R. C. Francis, 1997: A Pacific Interdecadal Climate Oscillation with Impacts on Salmon Production. *Bull. Amer. Meteor. Soc.*, **78**, 1069–1079.

Mernild, S., G. Liston, and C. Hiemstra, 2014: Northern Hemisphere glaciers and ice caps surface mass balance and contribution to sea-level rise. *J. Climate*. doi:10.1175/JCLI-D-13-00669.1, in press.

Mesinger, F., and Coauthors, 2006: North American Regional Reanalysis. *Bull. Amer. Meteor. Soc.*, **87**, 343–360.

Mills, C. M., J. E. Walsh, 2013: Seasonal Variation and Spatial Patterns of the Atmospheric Component of the Pacific Decadal Oscillation. *J. Climate*, **26**, 1575–1594.

Niu, X., and R. T. Pinker, 2011: Radiative Fluxes at Barrow, Alaska: A Satellite View. *J. Climate*, **24**, 5494–5505.

Parrish, D. F., and J. C. Derber, 1992: The National Meteorological Center's Spectral Statistical-Interpolation Analysis System. *Mon. Wea. Rev.*, **120**, 1747–1763.

Pickart, R. S., A. M. Macdonald, G. W. K. Moore, I. A. Renfrew, J. E. Walsh, and W. S. Kessler, 2009: Seasonal Evolution of Aleutian Low Pressure Systems: Implications for the North Pacific Subpolar Circulation. *J. Phys. Oceanogr.*, **39**, 1317–1339.

Rienecker, M. M., and Coauthors, 2011: MERRA: NASA's Modern-Era Retrospective Analysis for Research and Applications. *J. Climate*, **24**, 3624–3648.

Rodionov, S. N., J. E. Overland, N. A. Bond, 2005: The Aleutian Low and Winter Climatic Conditions in the Bering Sea. Part I: Classification. *J. Climate*, **18**, 160–177.

Ruane, A. C., 2010: NARR's Atmospheric Water Cycle Components. Part I: 20-Year Mean and Annual Interactions. *J. Hydrometeor*, **11**, 1205–1219.

Rupp, T. S., X. Chen, M. Olson, and D. A. McGuire, 2007: Sensitivity of Simulated Boreal Fire Dynamics to Uncertainties in Climate Drivers. *Earth Interact.*, **11**, 1–21.

Saha, S., and Coauthors, 2010: The NCEP Climate Forecast System Reanalysis. *Bull. Amer. Meteor. Soc.*, **91**, 1015–1057.

Shulski, M., J. Walsh, E. Stevens, and R. Thoman, 2010: Diagnosis of Extended Cold-Season Temperature Anomalies in Alaska. *Mon. Wea. Rev.*, **138**, 453–462.

Stegall, S. T., and J. Zhang, 2012: Wind Field Climatology, Changes, and Extremes in the Chukchi–Beaufort Seas and Alaska North Slope during 1979–2009. *J. Climate*, **25**, 8075–8089.

Wendler, G, and M. Shulski, 2009: A Century of Climate Change for Fairbanks, Alaska. *Arctic*, **62**, 295-300.

Xie, P., and P. A. Arkin, 1997: Global Precipitation: A 17-Year Monthly Analysis Based on Gauge Observations, Satellite Estimates, and Numerical Model Outputs. *Bull. Amer. Meteor. Soc.*, **78**, 2539–2558.

Yang, D., B. E. Goodison, J. R. Metcalfe, V. S. Golubev, R. Bates, T. Pangburn, and C. L. Hanson, 1998: Accuracy of NWS 8" Standard Nonrecording Precipitation Gauge: Results and Application of WMO Intercomparison. *J. Atmos. Oceanic Technol.*, **15**, 54–68.

Appendix

3DVAR Three-dimensional variational data assimilation
4DVAR Four-dimensional variational data assimilation
AMSR Advanced Microwave Scanning Radiometer
AMSU Advanced Microwave Sounding Unit
CFS-2 Climate Forecast System version 2
CFSR Climate Forecast System Reanalysis
CMAP CPC Merged Analysis of Precipitation
CPC Climate Prediction Center
ECMWF European Center for Medium-Range Weather Forecasting
ERA-40 ECMWF 40-year reanalysis
ERA-Interim ECMWF-Interim reanalysis
FAQ Frequently-asked question
GEOS Goddard Earth Observing Satellite
GFS Global Forecast System
GHCN Global Historical Climatology Network
GMT Greenwich Mean Time
GSI Gridpoint Statistical Interpolation
GSOD Global Summary of Day
IAU Incremental Analysis Update
IFS Integrated Forecast System
IMS Interactive Multisensor Snow and Ice Mapping System
MERRA Modern-Era Retrospective Analysis for Research and Applications
NARR North American Regional Reanalysis
NASA National Aeronautic and Space Administration
NCAR National Corporation for Atmospheric Research
NCL NCAR Command Language
NCDC National Climatic Data Center
NCEP National Centers for Environmental Prediction
NCEP-R1 NCEP-NCAR reanalysis
NESDIS National Environmental Satellite, Data and Information Service
PDO Pacific Decadal Oscillation
PRCP Precipitation
PRISM Parameter-elevations Regressions on Independent Slopes Model
RMSE Root-mean-square error
SMMR Scanning Multichannel Microwave Radiometer
SNODEP Snow depth analysis (daily) of the U.S. Air Force Weather Agency
SNDP Snow depth
SSI Spectral statistical interpolation
SSM/I Special Sensor Microwave/Imager
SST Sea-surface temperature
SWE Snow-water equivalent
T2M Monthly mean 2-m air temperature
T255 Triangular 255-waves truncation

T362 Triangular 362-waves truncation
T62 Triangular 62-waves truncation
T_{avg} Monthly average temperature
T_{max} Daily maximum 2-m air temperature
T_{min} Daily minimum 2-m air temperature.